Directed Assembly of *p*-Carboxylatocalix[4]arenes

Piotr Przemysław Cholewa

Submitted for the degree of Doctor of Philosophy

Heriot-Watt University

School of Engineering and Physical Sciences

March 2015

ABSTRACT

The research in this thesis is centred on the design and development of novel coordination polymers (CPs) constructed from *p*-carboxylatocalix[4]arenes. Two design strategies were chosen as potential methods that would enable the rational design of CPs using transition metals (TMs) as directing centres and *p*-carboxylatocalix[4]arenes as building blocks. Each strategy was based on synthesising a target motif. The selection criteria for the target motifs were: 1) to provide the directionality in which the assembly could be extended and 2) be easily reproducible for a series of TMs. The first target motif is a planar binuclear metal cluster that can be extended in all three dimensions. The second motif is a TM complex containing a chelating ligand restricting the number of binding sites in the coordination sphere available to subsequent binding of ligands. In the preliminary study, using TM(II) ion (Co, Mn, Cd), mono-*p*-carboxylatocalix[4]arenes and bipyridines, a series of 1D CPs containing the target planar molecular panel were synthesised and characterised. The application of the "directional bonding" approach resulted in formation of the target second motif, a discrete coordination complexes constructed from TM(II) ion (Mn, Cd), mono-*p*-carboxylatocalix[4]arene and 1,10-phenanthroline. In the following study it was found that the steric effects of co-ligands used and the pre-organisation of the calixarene building block have a significant influence over the assembly process, dictating the topology of formed supramolecular architectures. Utilisation of the strategy based on the "directional bonding" approach, utilisation of a di-topic di-*p*-carboxylatocalix[4]arene resulted in formation of linear 1D CPs. Through exploitation of the di-*O*-alkoxycalix[4]arene C_2 symmetry an alternative di-topic calixarenes were synthesised and used to construct spiral 1D CPs. It was also found that in certain reaction conditions these alternative di-*p*-carboxylatocalix[4]arenes assemble into discrete dimeric metal-organic calixarene capsules rather than spiral 1D CPs. In addition, it was demonstrated that di-*p*-carboxylatocalix[4]arene can also be used to synthesise 3D CPs.

I would like to dedicate this work to Krystyna Maciaszek.

ACKNOWLEDGEMENTS

I would like to thank my supervisor, Dr Scott J. Dalgarno, for the opportunity to study such an exciting area of chemistry and for his guidance, encouragement, inspiration and all the help. He has been absolutely fantastic to work with and it has been an utmost pleasure to be a part of the Supramolecular Chemistry Group.

I am very grateful to Dr Ruaraidh D. McIntosh for all the help, invaluable advices and witty anecdotes. Special thanks go to Dr Ross McLellan for all the hints and tips he has given me throughout my research. I would also like to thank all the past and present members of the Supramolecular Chemistry Group for making the lab an enjoyable place to work and for many happy memories.

I would like to thank Dr Simon J. Teat and Dr Christine M. Beavers at the Advanced Light Source in Berkeley, California, for all their hard work in collecting X-ray data.

Finally, I would like to thank my family for all the support and words of encouragement throughout my PhD.

TABLE OF CONTENTS

Chapter 1. Introduction

1.1. Design principles in metal-directed assemblies

In recent times the demand for novel solutions to everyday problems has gone hand in hand with rapid development in technology. This demand is becoming a key driving force behind targeted scientific research and this is particularly true when considering the design of porous materials (PMs). Ever since zeolites found application in industry (due to their porosity and good thermal stability), there has been a constant pursuit of the design and further improvement of PMs.[1-3] According to IUPAC notation PMs can be divided into three subcategories depending on the size of the pores: microporous (< 2 nm), mesoporous (2 - 50 nm) and macroporous (>50 nm).[4] The volume of publications focusing on the design and modification of PMs grows larger each year, with a number reporting on the application of these materials in chemistry (e.g. catalysis), biology (e.g. drug delivery), separation and gas storage.[5-8]

Amongst the design strategies that have emerged, one of the viable procedures enabling the synthesis of PMs is based on the 'directional bonding' approach. The key aspect in this approach relays on using components such as metal ions to direct assembly. The role of the metal ions is to act as 'joints' that connect lighter materials (linkers) to form extended networks. By choosing specific metal ions and terminal ligands one can control the number of linkers coordinated to the metal as well as their relative orientation, ultimately governing the connectivity and dimensionality of the network. Control can be further enhanced *via* synthetic means by pre-organising an appropriate metal complex, in which certain sites around the coordination sphere are restricted, leaving only desired positions available to undergo bond formation with functional groups of the linker.

In order to maximise the rate of bond formation between the metal ion and the linker there is a set of functional groups used which are known to form stable coordination bonds, for example pyridines. One can now find numerous examples in

the literature which illustrate how the selection of specific metal ions and di-topic linkers enables construction of networks of varying dimensionality.[9] The resulting materials are often referred to as coordination polymers (CPs).[10] One of the first CPs was reported by Vranka *et al.*, whereby they used Ag(I) ions and pyrazine to form a linear 1D chain (Fig. 1.1A).[11] Soon after that Carreck and co-workers reported a 2D grid constructed from Co(II) ions and pyrazine.[12] However, it was not until the end of the 1980s when more groups started to report successful syntheses of various CPs and the field begun to flourish.[13, 14] Utilisation of di-topic linkers is not the only method to synthesise 3D structures. One of the first examples of such a network was reported by Robson and co-workers, whereby Cu(I) ions and a tetra-topic tetrakis(4-cyanophenyl)methane assemble to form an extended 3D polymeric network (Fig. 1.1B).[15] However, achieving absolute control over the assembly process has proven somewhat difficult when using monodentate linkers. This difficulty results from a degree of flexibility in the binding of monodentate ligands within the coordination sphere and makes the assembly less predictable. As a consequence of this, the formation of undesired topologies exhibiting non-porous character is often observed.

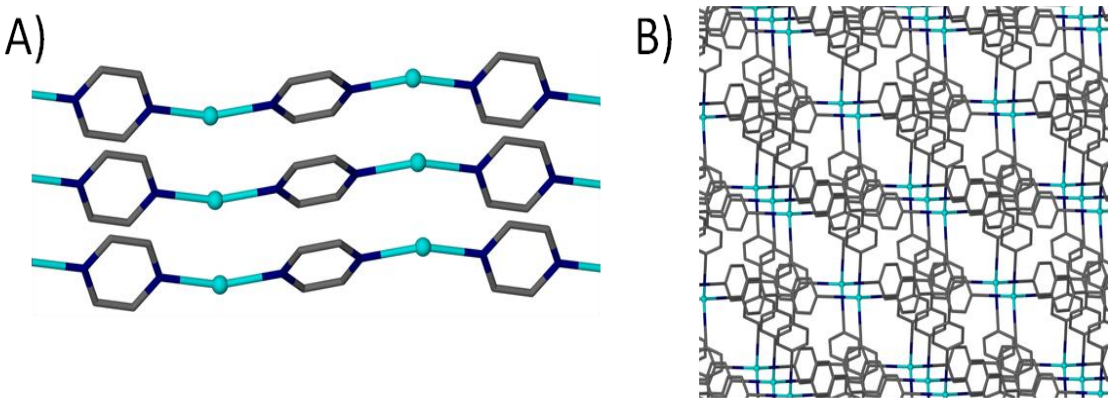

Figure 1.1. One of the early examples of (A) a 1D coordination polymer and (B) a 3D network. Hydrogen atoms omitted for clarity.[11, 15]

In order to decrease flexibility and increase control in the design of PMs, linkers with functional groups binding to the metal ion in a multidentate fashion (e.g. carboxylates and phenanthrolines) have been employed. The reason for their superiority is the higher affinity for binding metal ions (chelation), a result being that the metal ions often become locked within rigid clusters. These rigid inorganic clusters, due to their

repetitiveness in the synthesised materials, were termed secondary building units (SBUs).[16] Each SBU contains extension points through which it is connected *via* the linker to symmetry equivalent clusters. By targeting a specific SBU one can attain a cluster with extension points orientated in a desired direction, making the design and assembly of PMs more predictable. Over the years it became apparent that different framework topologies can be attained depending on the target SBU employed. These PMs are called metal-organic frameworks (MOFs), to denote the inorganic part (often the SBU), the organic linker and the high dimensionality of the material (which exhibits porosity). The most commonly occurring SBUs amongst reported MOFs are tetrahedral, octahedral and triangular prism (Fig. 1.2).[17] One of the first examples of a successfully synthesised MOF was reported by Yaghi *et al*.[18] In that report MOF-5 was synthesised using Zn(II) ions and a 1,4-benzene-di-carboxylate, and formation of tetrahedral tetranuclear SBUs linked together by rigid linkers containing chelating carboxylate groups was observed (Fig. 1.3). Ever since that discovery the field of PM research flourished where a range of different metal ions and chelate-containing linkers were successfully used to afford a variety of 3D networks.[17, 19-21]

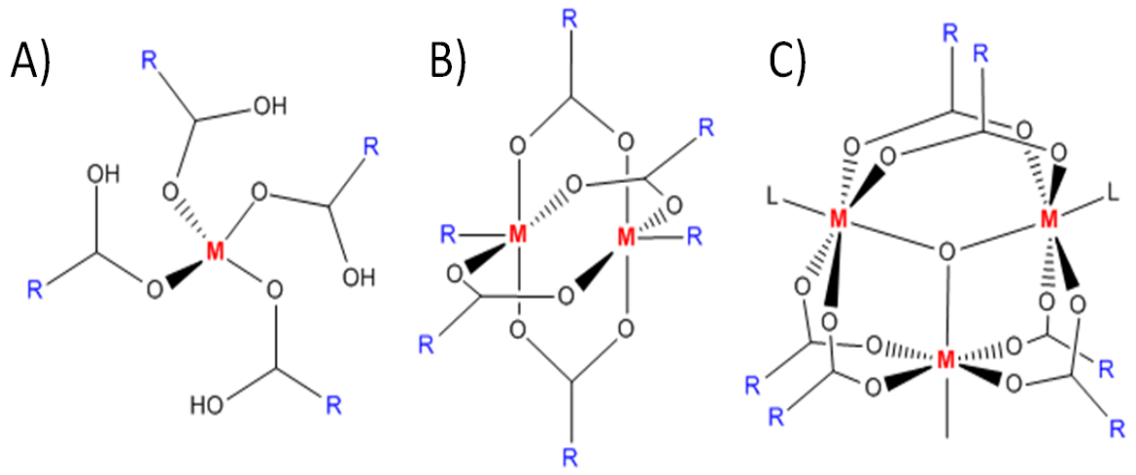

Figure 1.2. Three most commonly occurring SBUs in MOFs: (A) tetrahedral, (B) octahedral and (C) triangular prism.

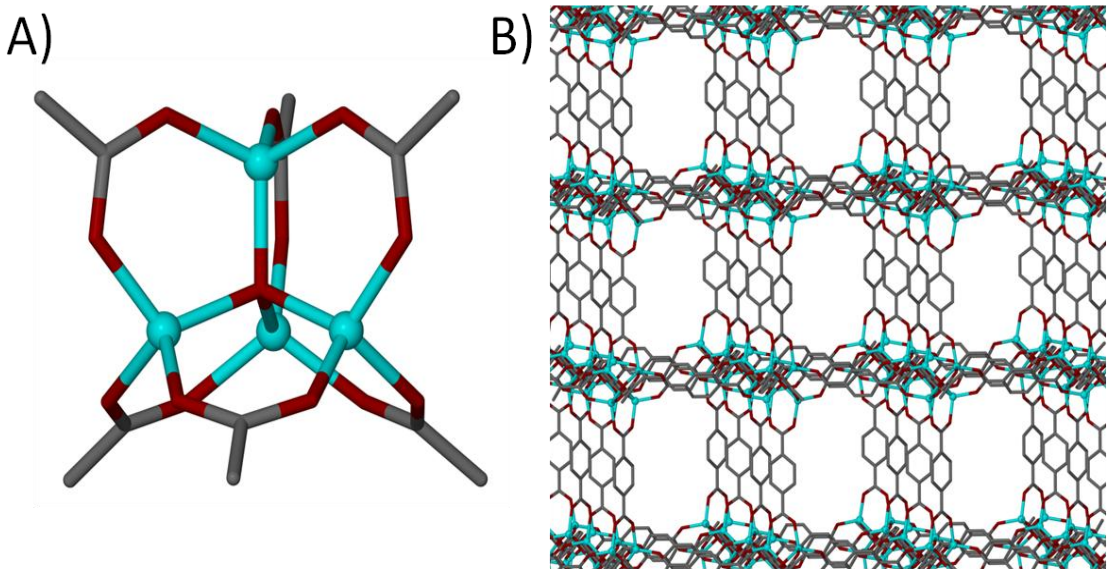

Figure 1.3. (A) An octahedral SBU and (B) an overview of the 3D connectivity in MOF-5.[18] Hydrogen atoms omitted for clarity.

Along with the growing interest in the design and construction of PMs, scientists were also interested in the design of discrete molecular containers known as metal-organic polyhedra (MOPs). Similarly, as in the case of PMs, in the course of extensive research in this field, various strategies have been established so that the scientist may rationally design and construct different MOPs. The design of MOPs started with pioneering work in which discrete 2D molecular structures relying on the 'directional bonding' approach were constructed. Early examples included the preparation of precursors based on square-planar Pt(II) and Pd(II) complexes with ligands blocking two *cis*- coordination sites, which when mixed with linear ligands such as 4,4'-bipyridine, form discrete molecular squares with four metal centres connected by the specifically chosen linker.[22] Similar concepts were applied in order to construct disparately shaped discrete 2D structures by clipping a pre-organised organic molecule to two *trans*-Pt(II) complexes. Selection of the molecular clip containing a desired angle between functional groups of the linker allows for synthesis of 2D molecular squares, triangles and hexagons (Fig. 1.4).[23, 24]

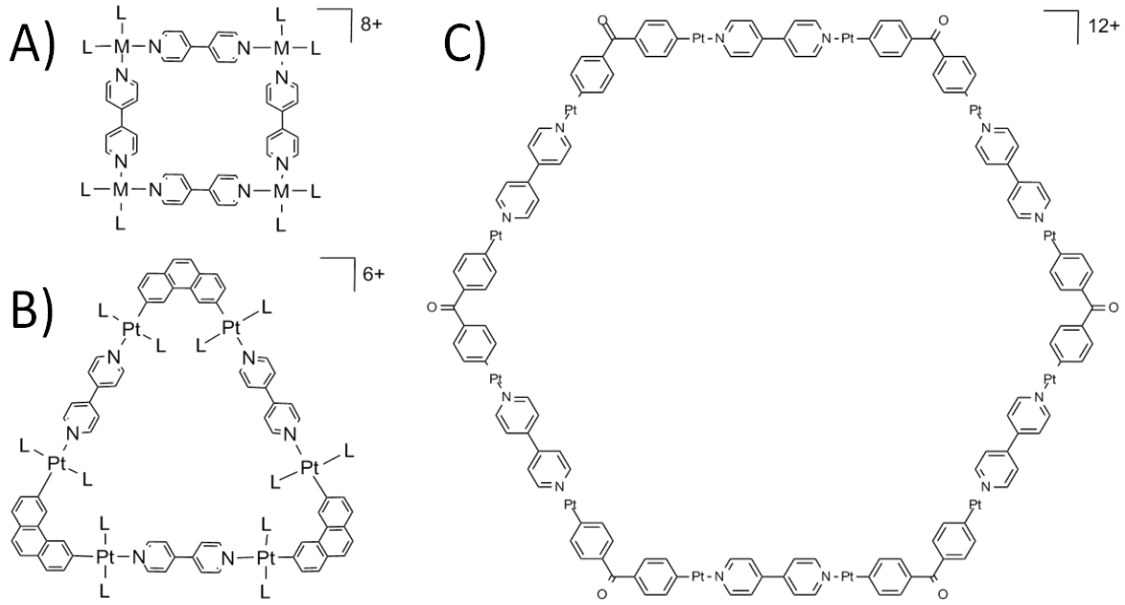

Figure 1.4. Schematic representation of a molecular (A) square, (B) triangle and (C) hexagon constructed using "directional bonding" approach. Hydrogen atoms and *trans*-Pt ligands in C omitted for clarity.[23, 24]

In order to increase the dimensionality and complexity of discrete structures one can vary the number of available binding sites on the metal and/or introduce more functional groups to the linker. By doing so when assembling pre-organised metal-containing precursors with synthetically modified linkers it is possible to construct different MOPs.[25] Given that the design of these discrete 3D structures is based on angular complementarity of all building blocks, the resulting architectures adopt thermodynamically favoured shapes. By changing the angle between the functional groups in a linker, i.e. the bite angle of the ligand coordinating to metal ions, the same metal precursor can be used to construct MOPs that differ in size. Fujita *et al.* demonstrated this by assembling Pd-based precursors with dipyridyl linkers containing a bite angle of 90˚ (Fig. 1.5A).[26] The resulting structure is constructed from six Pd(II) metal ions and twelve linkers (M_6L_{12}), and conforms to a cube. The same authors then reported that the use of a linker with a larger bite angle (127˚) results in formation of a molecular sphere possessing cuboctahedral symmetry, containing thirty six components consisting of twelve Pd-based precursors and twenty four linkers ($M_{12}L_{24}$), as shown in Figure 1.5B.[27] A further increase in the linker bite angle (135˚) yields

the thermodynamically favoured architecture which is an even larger near-spherical MOP based on a rhombicuboctahedral symmetry (Fig. 1.5C). This MOP comprises seventy two components ($M_{24}L_{48}$).[28] In principle larger MOP formation should be possible by continually increasing the bite angle (up to 180˚, when there is no curvature and 2D CPs form), but this is yet to be achieved.

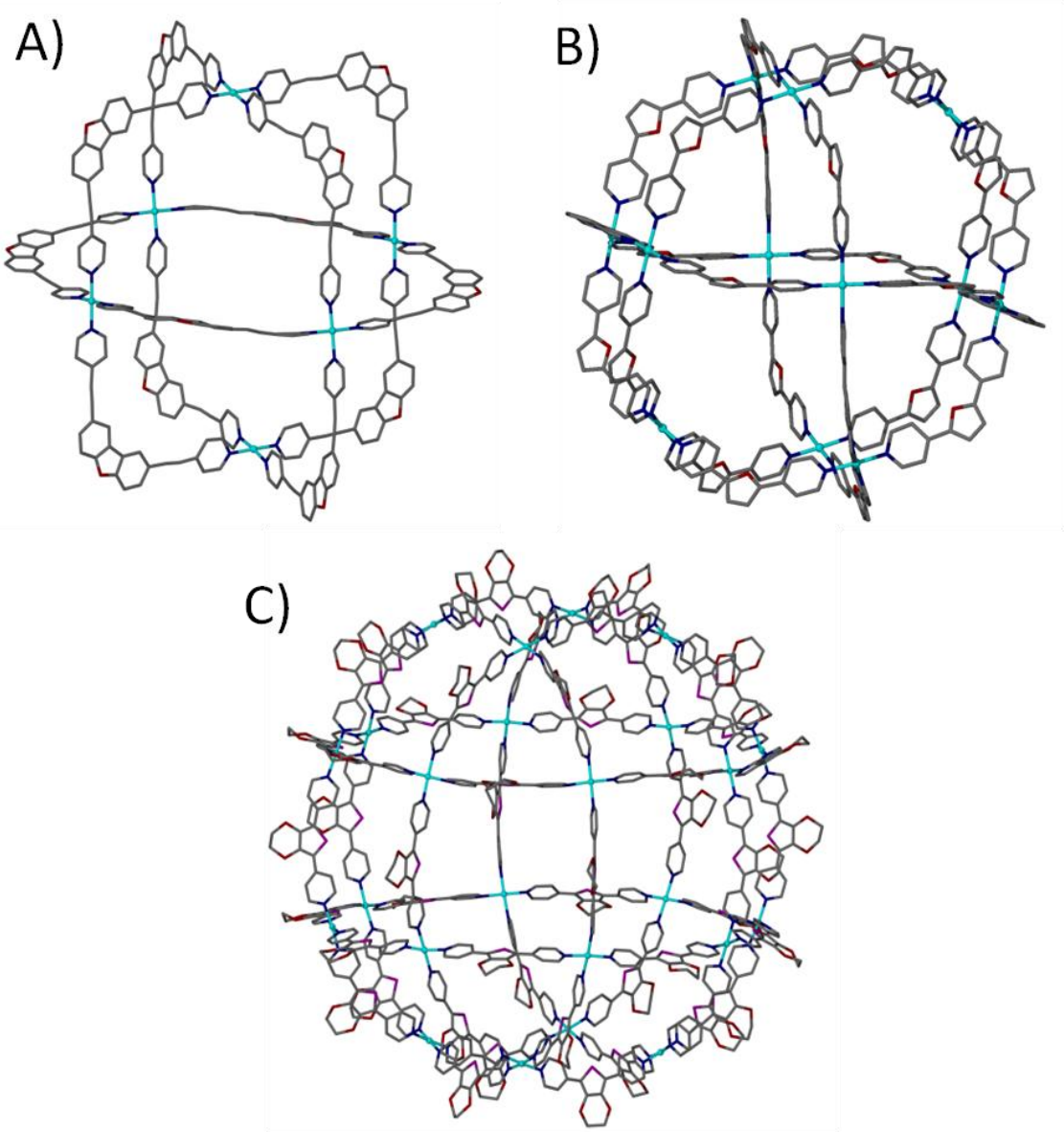

Figure 1.5. Examples of MOPs designed and constructed using the "directional bonding" approach and pre-organised di-topic linkers. MOP based on (A) cubic symmetry (linkers with a 90˚ bite angle), (B) cuboctahedral symmetry (linkers with a 127˚ bite angle) and (C) rhombicuboctahedral symmtery (linkers with a 135˚ bite angle). Hydrogen atoms and counter ions omitted for clarity.[26-28]

1.2. Macrocyclic building blocks used in metal-directed assemblies

The design of PMs and molecular capsules is not restricted to the strategies discussed above. In pursuit of versatile, curvature containing linkers, a class of molecules emerged as perfect candidates for constructing discrete molecular containers. This group of molecules consists of a variety of cyclic hosts, which due to their inherent bowl-shape, are ideal for use in the design of MOPs and metal-organic capsules (MOCs). They are synthesised *via* a condensation reaction of readily available aromatic compounds and a series of different precursors as a source of the bridging atoms. Based on the arene and reaction conditions used one can attain a series of differently sized cyclic compounds with disparate functionalities positioned across the general framework.[29] Another advantage these macrocycles possess is the relative ease with which the framework can be post-synthetically modified, allowing for additional functionalisation and directional promotion of specific interactions and/or bond formation. Further advantage of framework post-synthetic modification is that it allows for a change in the degree of flexibility of these cyclic hosts.[30] By varying the substituents and the flexibility of the macrocycle one can control the cavity size which, from the perspective of building discrete molecular containers, thereby means the internal volume of the capsule.

Amongst the macrocycles most often used in metal-directed assembly are resorcin[4]arenes and pyrogallol[4]arenes (Fig 1.6A and B respectively). Resorcin[4]arenes are synthesised by condensation of resorcinol with a chosen aldehyde and contain hydroxyl groups at the *meta* positions at the upper-rim; the *para* positions therefore remain available for synthetic modification. The resorcin[4]arene framework can be rigidified by the introduction of methylene bridges between the *meta* hydroxyl groups to afford macrocycles called cavitands. Pyrogallol[4]arenes are structural analogues to resorcin[4]arenes but with one important difference, that being the presence of an additional hydroxyl group at the *para* position. This can be beneficial in chelating to a metal centre or in directing self-assembly as highlighted below. In addition to the two macrocycles mentioned above, there is another group of cyclic hosts that have been used in metal-directed assembly; these are catechol-based cyclotricatechylenes (CTCs) and the related veratrole-based cyclotriveratrylenes (CTVs) shown in Figure 1.6C. They are made up of three arenes and possess a smaller, shallower cavity relative to the resorcin[4]arenes and pyrogallol[4]arenes. They also

contain substituents at the upper-rim that can limit the possibilities for synthetic modification. Despite this there are a number of reported synthetic pathways that enable introduction of functional groups desirable for use in directed assembly.

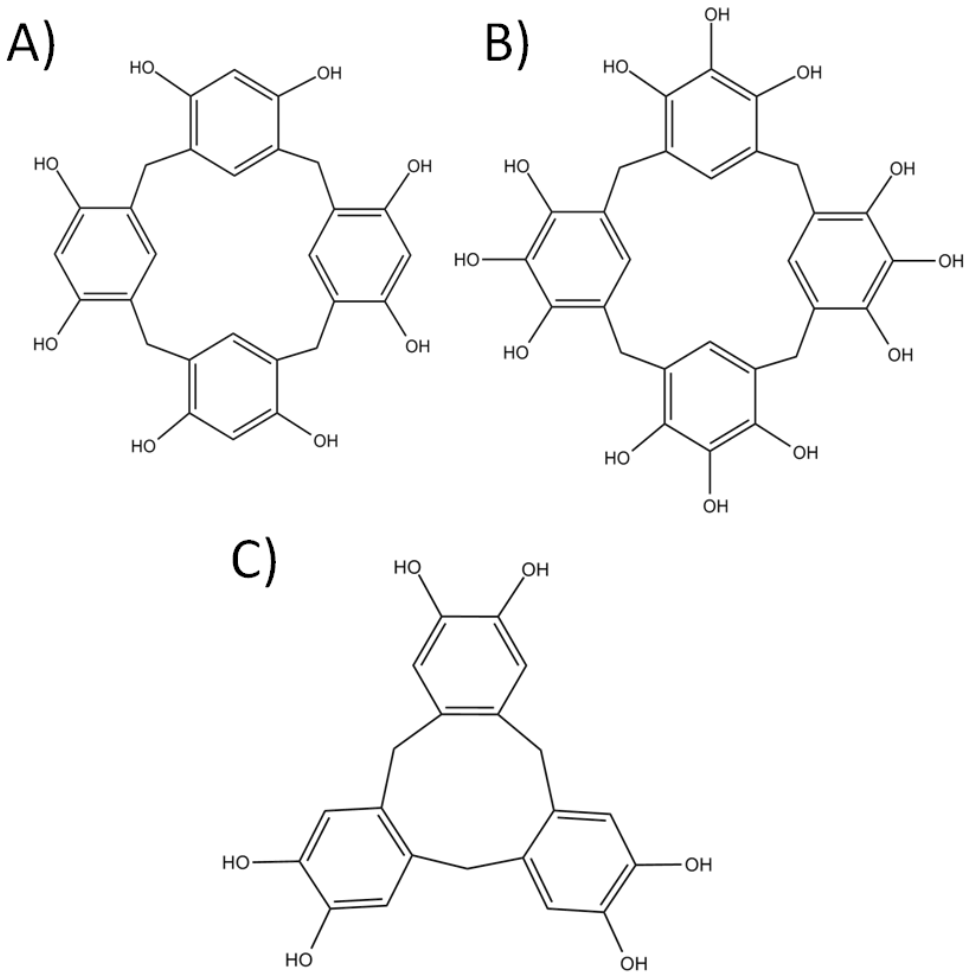

Figure 1.6. Schematic representation of the three macrocycles commonly used in construction of metal-directed assemblies: (A) resorcin[4]arene,(B) pyrogallol[4]arene and (C) cyclotricatechylene. Hydrogen atoms a part from those of hydroxyl groups are omitted for clarity.

The first utilisation of *C*-propylpyrogallol[4]arene upper-rim hydroxyl groups to construct a macrocycle-based MOC was reported by Atwood and co-workers.[31] These authors reported the formation of a large nanometre scale MOC based on an octahedral arrangement of pyrogallol[4]arene sub-units and it comprises six

macrocycles and twenty four Cu(II) ions (Fig. 1.7A). The assembly process involves removal of forty eight upper-rim hydrogens from the hydroxyl groups, with subsequent formation of ninety six new Cu–O bonds. These authors also demonstrated that when using the same pyrogallol[4]arene, but with Ga(III) instead of Cu(II) ions, it is possible to construct a MOC that is of similar size to the Cu(II)-templated analogue, but that adopts a slightly different shape as shown in Figure 1.7B.[32] The resulting MOC conforms to a disordered "rugby-ball" consisting of six pyrogallol[4]arenes and twelve Ga(III) ions. The assembly process involves removal of thirty six hydrogens from the hydroxyl groups, with subsequent formation of forty eight new Ga–O bonds. More recently it has been demonstrated that pyrogallol[4]arenes can be also utilised to construct dimeric MOCs. The formation of these requires removal of twenty four upper-rim hydroxyl groups, with subsequent binding of eight metal ions (Fig. 1.8).[33] It has been shown that these pyrogallol[4]arenes-based dimeric MOCs can be assembled from either Zn(II), Cu(II), Co(II) or Ni(II) ions.[33]

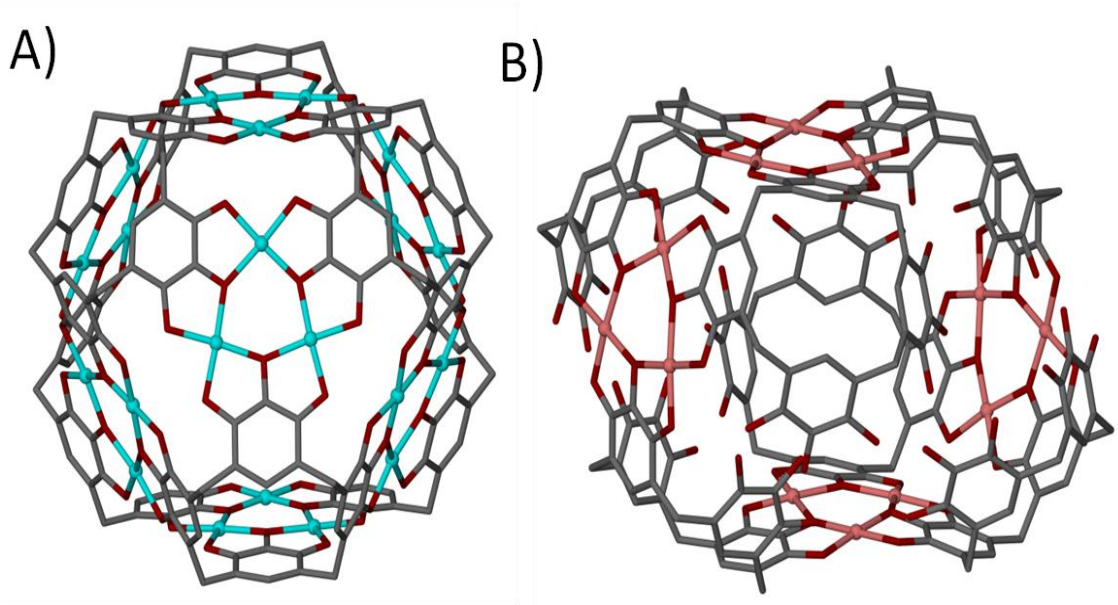

Figure 1.7. Metal-organic polyhedra constructed from six *C*-propylpyrogallol[4]arenes and either (A) twenty four Cu(II) or (B) twelve Ga(III) ions. *C*-propyl chains and hydrogen atoms are omitted for clarity.[31, 32]

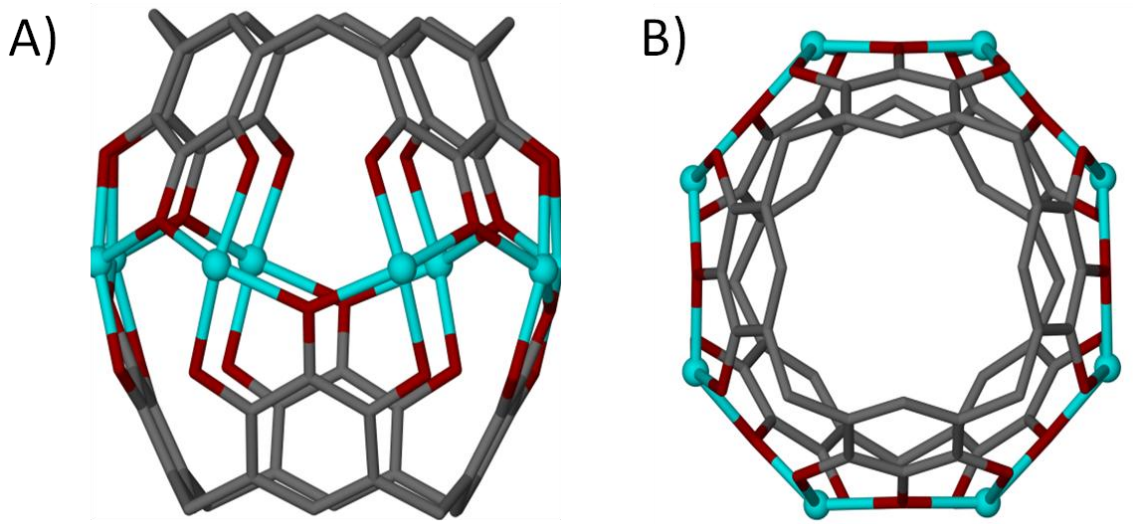

Figure 1.8. (A) and (B) Orthogonal views of a dimeric metal-organic capsule constructed from two pyrogallol[4]arenes and eight transition metal ions (Zn(II), Cu(II), Co(II) or Ni(II). Cavitand *C*-alkyl chains and hydrogen atoms are omitted for clarity.[33]

Similarly to pyrogallol[4]arenes, the functional composition of CTC upper-rim can be directly utilised in the construction of MOCs *via* deprotonation of the hydroxyl groups, followed by the introduction of a metal salt. This was demonstrated by Robson *et al.* who constructed a tetrahedral cage comprising six Cu(II) centres and four CTCs (Fig. 1.9A).[34] Although there are synthetic strategies that allow introduction of different functional groups to the CTC and CTV upper-rim, the number of reports of metal-organic capsules constructed from these macrocycles is still limited.[35-37] One of the few examples was reported by Hardie *et al.*, whereby they construct dimeric MOCs using carboxylate functionalised CTC and TM(II) ions.[38] They demonstrated that synthetically modified CTCs and Cu(II) ions assemble into a metallo-cryptophane constructed from a trinuclear Cu(II) cluster and two macrocycles (Fig 1.9B). Reaction of Co(II) ions instead of Cu(II) with the same macrocycle resulted in formation a dimeric MOC, however it is based on a complex metal cluster comprising seven Co(II) centres (Fig 1.9C).

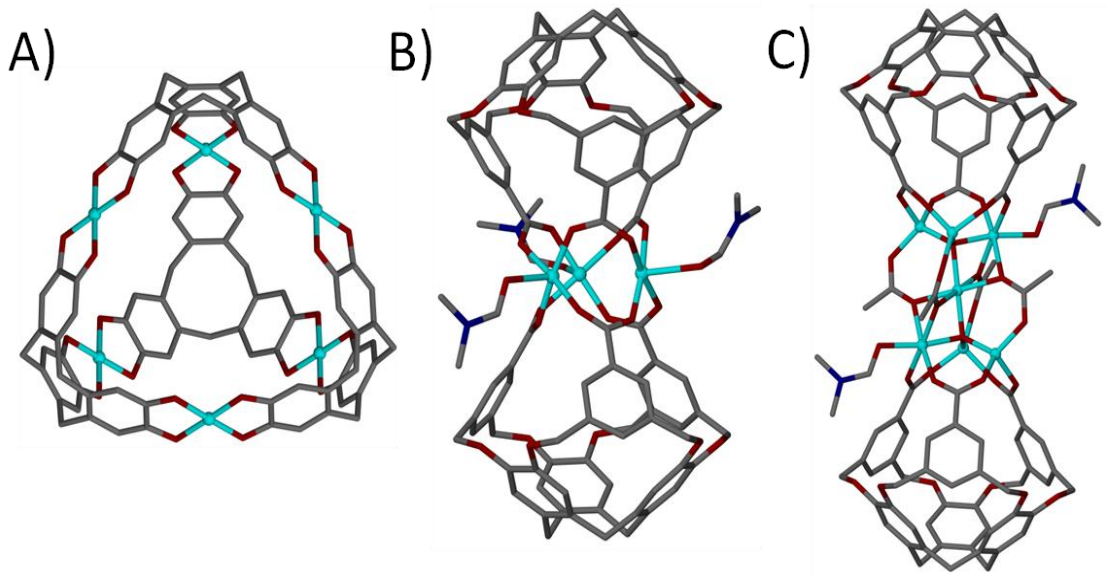

Figure 1.9. Examples of MOC constructed from CTCs and CTVs. (A) A tetrahedral cage formed from Cu(II) and CTC, (B) a dimeric MOC assembled from Cu(II) and CTVs and (C) a dimeric MOC constructed from Co(II) and CTVs. Solvent of crystallisation and hydrogen atoms are omitted for clarity.[34, 38]

With respect to general modification of the cyclic host molecule framework, an advantage resorcin[4]arenes and the related cavitands have over pyrogallol[4]arenes is the presence of vacant positions at the upper-rim. This availability allows for the introduction of functional groups such as pyridyls, nitriles, chelates (e.g. dithiocarbamates) and carboxylic acids, and their subsequent use as binding sites for metal centres. One can find literature examples in which these vacant positions are occupied by nitriles, and these ligands have subsequently been employed as monodentate ligands for coordination to *cis*-protected Pt(II) and Pd(II) ions; these afford dimeric capsules comprising two macrocycles and four metal ions (Fig. 1.10A).[39] Pyridyl functionalised cavitands have also been used to form related dimeric MOCs.[40] Furthermore, synthetic variation in the length of the upper-rim appended pyridyl moiety was shown to provide concomitant control over the volume of the resulting MOC volume.[41] Amongst the numerous upper-rim groups studied as potential metal binding sites, those that can bind in a bidentate fashion have also been explored. A cavitand functionalised at the upper-rim with a 2,2'-bipyrdine group, upon mixing with Ag(I) ions, assembles as a dimeric capsule with four metal ions, each with two chelating ligands coordinated in a tetrahedral fashion (Fig. 1.10B).[42]

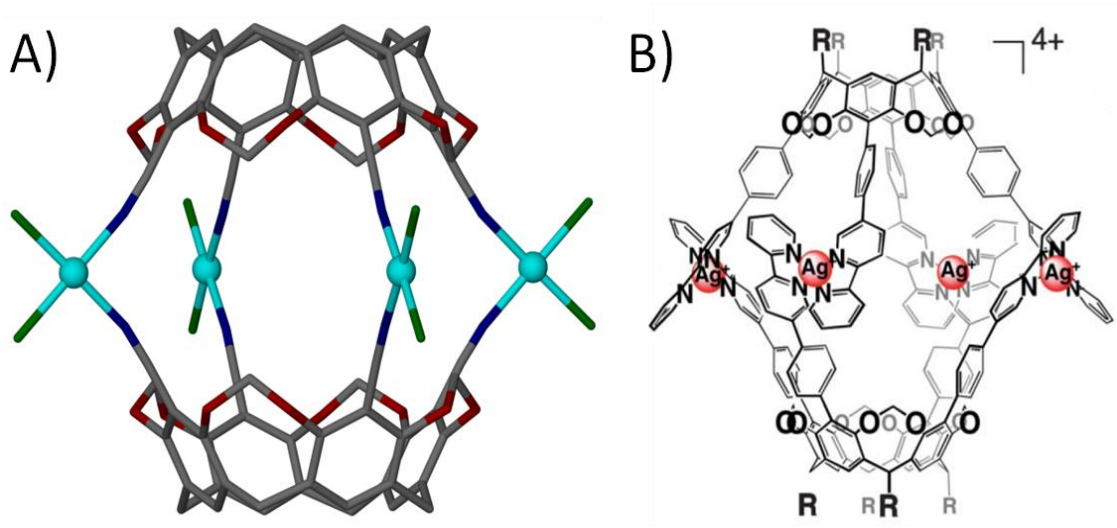

Figure 1.10. Dimeric metal-organic capsule constructed from (A) four Pt(II) / Pd(II) ions and two nitrile functionalised cavitands and (B) four Ag(I) ions and two extended cavitands.[42] 1,3-Bis(diphenylphosphino)propane in (A), cavitand *C*-alkyl chains, hydrogen atoms and counter ions in (A) and (B) are omitted for clarity.

Another functional group successfully used as a bidentate upper-rim metal binding site was a dithiocarbamate. Reaction of this cavitand with Zn(II) or Cd(II) ions afforded a trimeric capsule motif comprising six metal ions and three macrocycles (Fig. 1.11A).[43] Each of the metal centres adopt five coordinate square pyramidal geometry, with two dithiocarbamates coordinated in a square plane and a pyridine ligand occupying each axial site. By changing the metal ion template to Cu(II) the resulting assembly conforms to tetrahedral topology (Fig. 1.11B). These alternative MOPs consist of eight square planar metal centres and four cavitands. There are also a handful of examples in the literature in which cavitand containing iminodiacetate moieties at the upper-rim were utilised to construct capsules. These cavitands were found to coordinate to metal ions (Co(II) and Fe(II)) *via* iminodiacetate groups in a tridentate fashion, resulting in a dimeric MOC comprising two cavitands and four metal centres as shown in Figure 1.12A.[44] In the search of functionalised macrocycles that would enable construction of metal-directed assemblies, Holman *et al.* demonstrated that the upper-rim carboxylate functionalised cavitand can be utilised for this purpose.[45]

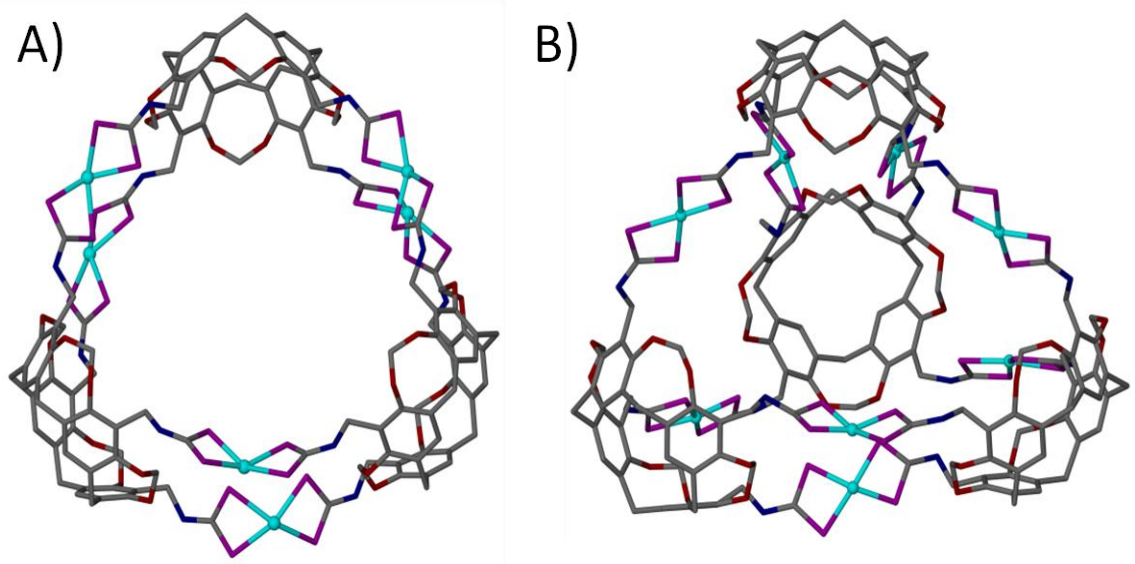

Figure 1.11. (A) Trimeric MOC constructed from six Zn(II) / Cd(II) ions and three dithiocarbamate functionalised cavitands. (B) Tetrameric MOC assembled from eight Cu(II) ions and four dithiocarbamate functionalised cavitands. Cavitand *C*-alkyl chains and hydrogen atoms are omitted for clarity.[43]

The MOC formed comprises sixteen metal centres and six cavitands, and is an another example in which the formation of an SBU dictates the outcome of assembly (Fig. 1.12B). Each of the dinuclear metal clusters formed has a three-fold symmetry and comprises two Zn(II) ions and three carboxylates that coordinate in a bridging fashion. All of the metal centres possess apical aquo ligands, two of which act as linear linkers between neighbouring capsules, producing a 1D coordination polymer of MOCs.

In addition to the MOCs constructed from cyclic hosts mentioned above, one can also find structures based on sulfonated calix[*n*]arenes (where *n* = 4,5,6 and 8).[46] These water-soluble macrocycles possess sulfonate groups at the upper-rim *para* positions *via* which they can interact with a range of organic, inorganic and hydrogen-bond donor species.[47, 48] Atwood and co-workers demonstrated that *p*-sulfonatocalix[4]arene, in the presence of pyrdine *N*-oxide and La(III) ions, form C-shaped dimers which assemble together to form molecular capsules adopting icosahedral topology.[49] Interstingly, *p*-suflonatocalix[*n*]arenes display an ability to form inclusion complexes of inclusion complexes, called 'Russian dolls', as they resemble a Matryoshka doll.[50-52] Usually such supramolecular array consists of two *p*-suflonatocalix[*n*]arene molecules encapsulating a macrocycle which is typically a

crown ether. Such second-sphere supramolecular complexation is achievable due to inclusion of a metal cation within the macrocycle.[53]

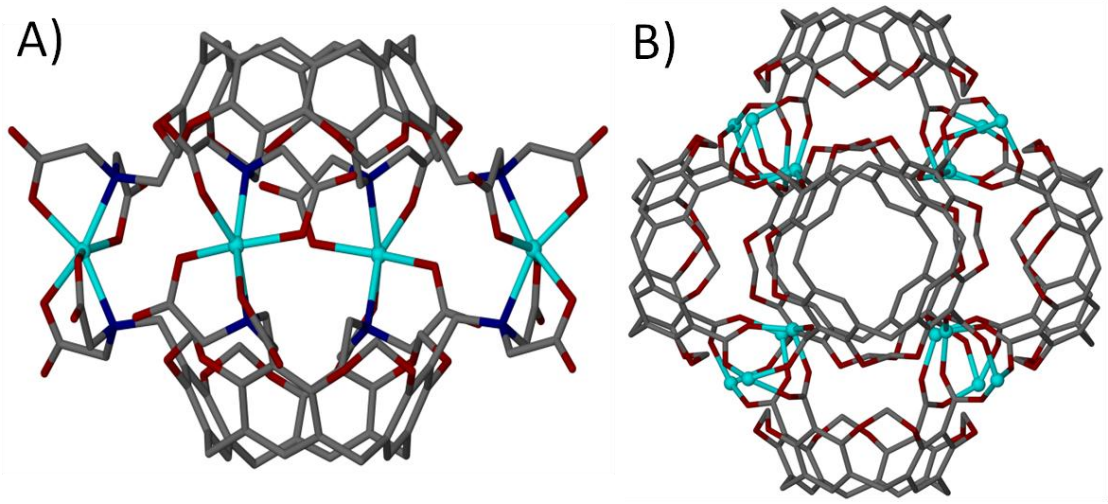

Figure 1.12. (A) Dimeric MOC constructed from four Co(II) / Fe(II) and two iminodiacetate functionalised cavitands and (B) MOP based on an octahedral symmetry constructed from sixteen metal centres and six carboxylate functionalised cavitands. Cavitand *C*-alkyl chains, hydrogen atoms and in (A) four Sr(II) counter ions are omitted for clarity.[44, 45]

1.3. *p*-Carboxylatocalixarenes as potential building blocks used in construction of assemblies.

Whilst resorcin[4]arenes and pyrogallol[4]arenes represent the most widely used macrocycles in the assembly of MOCs, amongst the number of other cyclic host exploited as building blocks, one can also find structures based on calix[4]arenes. Surprisingly, despite the number of well-established synthetic pathways enabling introduction of different functional groups to the macrocyclic framework, little has been reported on metal-directed assemblies constructed from calixarenes. Calix[4]arenes are synthesised by a condensation reaction of *p-tert*-butylphenol and formaldehyde, with subsequent de-*tert*-butylation (Fig. 1.13). It is possible to synthesise different size *p-tert*-butylcalix[*n*]arenes (TBC[*n*], [*n*] = 4 - 8), by varying the type of base, the amount of formaldehyde used with respect to *p-tert*-butylphenol, and finally the choice of the solvent to "crack" the formed polymer and the duration of the cracking.[29] Calix[4]arene contains four hydroxyl groups at the lower-rim which form H-bonding interactions that stabilise the *cone* conformation of the macrocycle.

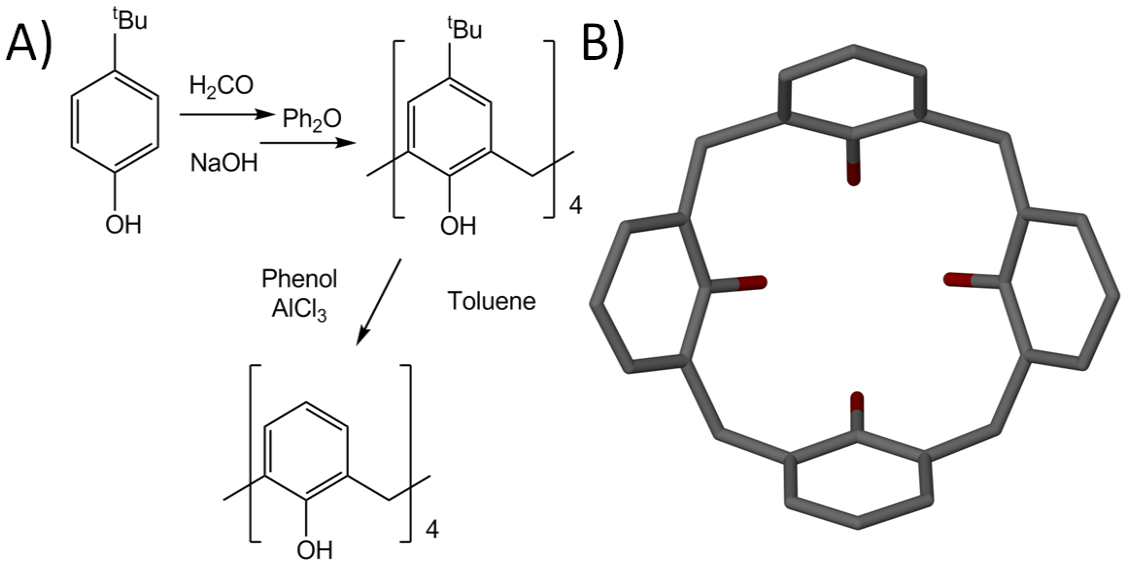

Figure 1.13. (A) Schematic of the synthesis of TBC[4] and calix[4]arenes and (B) the view of calix[4]arene.[29]

Removal of the H-bonding present at the lower rim leads to the change of the conformation from *cone* (cavity open) through *partially pinched cone* (cavity open) to a *pinched cone* (cavity closed) as shown in Figure 1.14. In the last few decades synthetic pathways have been established that allow scientists to obtain calix[4]arenes with different degree of functionalisation of the lower-rim (mono-, di-, tris- or tetra-functionalisation).[29] This provides chemists with a multitude of differently shaped macrocycles that can be utilised as building blocks. Unlike resorcin[4]arenes and pyrogallol[4]arenes, calix[4]arenes do not possess hydroxyl groups at the upper-rim. Due to the difference in reactivity between upper-rim aromatic carbon atoms the functionalisation of the upper-rim occurs at the *para* position. There are viable synthetic strategies allowing functionalisation of the *para* positions of the calix[4]arene aromatic rings, thereby allowing for introduction of different groups (e.g. halogens, sulfonato, nitro or carboxylato) or extension of the cavity (e.g. by addition of arenes). This therefore provides the supramolecular chemist access to an almost unlimited library of macrocycle-based building blocks. In addition, calixarenes have been proven to possess the ability to bind guests within their cavities, thus making the application of this group of macrocycles as building blocks in construction of PMs even more advantageous.[29] Atwood *et al.* have demonstrated that in the solid state TBC[4] and calix[4]arenes are capable of absorbing gases such as freons, methane and carbon

dioxide.[54, 55] This ability to entrap guest species within the solid has been attributed to the lattice voids generated during the formation of crystals. The formation of these interstitial lattice cavities is induced by the arrangement of inherent bowl-shaped calixarenes. Considering this ability to uptake guest species, calixarenes can be considered as highly useful building blocks for the design and construction of PMs.

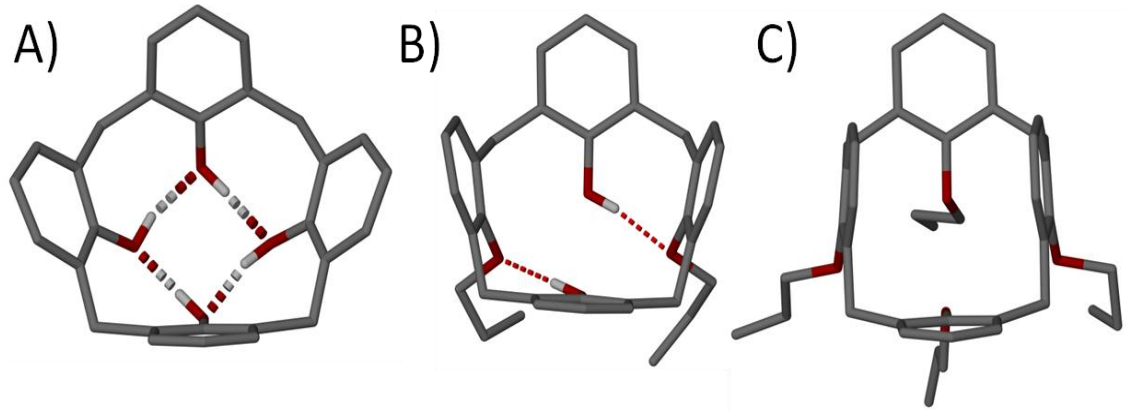

Figure 1.14. Three calixarene conformations depended on the presence of the hydrogen at the lower-rim: (A) *cone*, (B) *partially pinched cone* and (C) *pinched cone*.

When one considers the importance of the benzoate moiety in the formation of SBUs, and thus in the design and construction of MOFs and MOPs, it is surprising that little has been reported on formation of such structures with calixarenes possessing upper-rim carboxylate functionality. This is especially true given that synthetic pathways for the introduction of upper-rim carboxylic groups to the general macrocyclic framework are well established. The first of the very few examples of the use of *p*-carboxylatocalix[4]arene as building blocks in the rational design of novel supramolecular architectures that can be found in the literature is the metal-organic calixarene capsule (MOCC) constructed by Cotton and co-workers.[56] They have demonstrated that by reacting tetra-*p*-carboxylatocalix[4]arene with a pre-organised Rh(II) complex a dimeric MOCC is formed. Each capsule is constructed from two calixarenes which are fastened together by four dirhodium centres, as shown in Figure 1.15. Each dirhodium cluster comprises two formamidinates and two carboxylates, all of which bridge the two rhodium centres to form a paddlewheel structure, an SBU which (as is shown above) is very important in the synthesis of MOFs and MOPs.

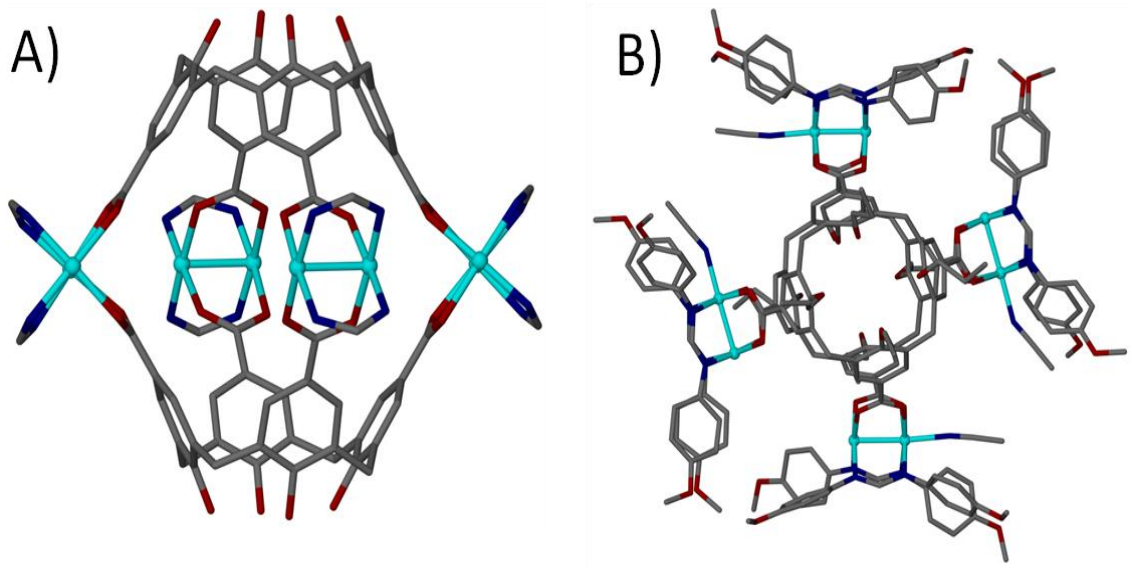

Figure 1.15. (A) and (B) Orthogonal views of a dimeric metal-organic calixarene capsule comprising four dirhodium clusters and two tetra-*p*-carboxylatocalix[4]arenes. Hydrogen atoms and part of formamidinates in (A) are omitted for clarity.[56]

It has been already shown that Fujita and co-workers successfully used angular complementarity of building blocks to rationally design and construct different Platonic solids. More recently de Mendoza *et al*. demonstrated that, through careful consideration of complementary symmetry of both metal-directing centres and organic linkers, and utilisation of the 'directional bonding' approach, it is possible to design and construct MOC using *p*-carboxylatocalixarenes.[57] This elegant and rational design concept was demonstrated by reacting a C_3-symmetric metal-directing centre (a uranyl ion, UO_2^{2+}) with a C_4-symmetric ligand (tetra-*p*-carboxylatocalix[4]arene) to produce a metal-organic calixarene capsule conforming to octahedral topology (Fig. 1.16A). The formed capsule comprises six calixarenes and eight uranyl sub-units, bearing an overall negative charge of 8^- which is counterbalanced by the presence of two fully protonated 1,4,7,10-tetraazacyclododecanes. The same strategy was employed to greatly enhance the size / volume of the capsule by using same C_3-symmetric directing centre, but with a larger C_5-symmetric ligand analogue (penta-*p*-carboxylatocalix[5]arene), as shown in Figure 1.16B. As a result of using a ligand of higher symmetry, twelve calixarenes and twenty uranyl ions form a capsule conforming to icosahedral topology with an overall negative charge of 20^- that is counterbalanced by associated pyridinium ions.

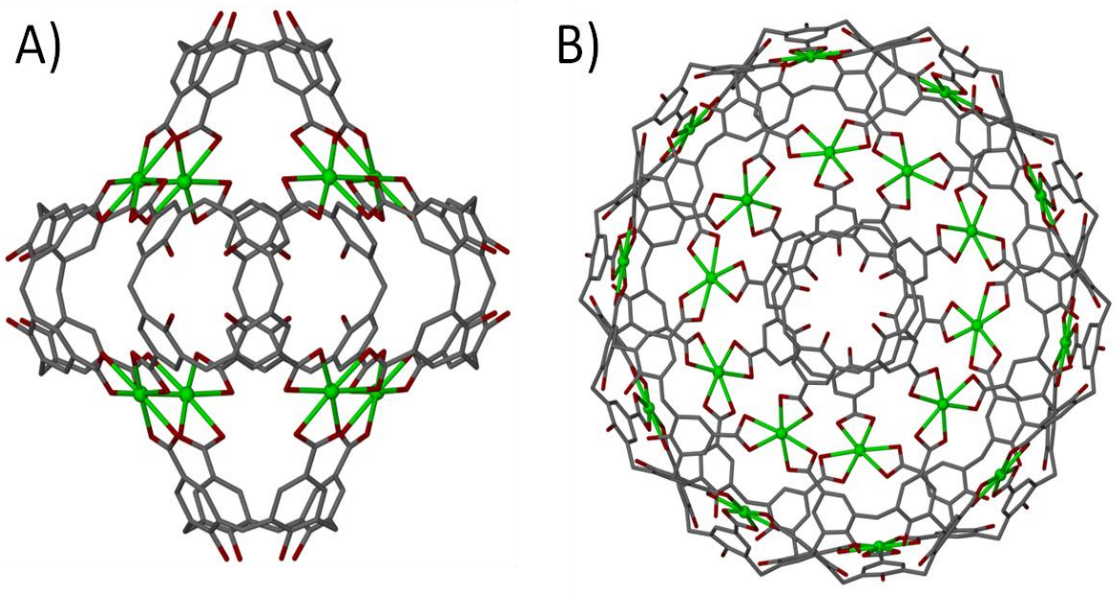

Figure 1.16. Metal-organic calixarene capsules adopting (A) octahedral and (B) icosahedral topology, both constructed using uranyl ions tetra-*p*-carboxylatocalix[4]arene and penta-*p*-carboxylatocalix[5]arene respectively. Hydrogen atoms and counter ions omitted for clarity.[57]

Surprisingly, so far very little has been reported on the use of *p*-carboxylatocalixarenes as potential building blocks for rational design of 3D PMs. Dalgarno *et al.* demonstrated how tetra-*p*-carboxylato-tetra-*O*-butoxycalix[4]arenes can be utilised to construct metal-organic calixarene nanotubes.[58] The reaction of tetra-*p*-carboxylatocalixarenes with Co(II) ions in the presence of pyridine results in formation of discrete aqua-bridged binuclear complexes, each containing two calixarenes and four pyridines (Fig. 1.17A). As a result of the relative positioning of calixarenes within the complex formed, back-to-back packing rather than bi-layer formation was observed in the solid state. This has a concomitant effect on the topological features observed in the synthesised material and results in formation of three solvent channels running along the *c* axis of the unit cell (Fig. 1.17B). The tetra-alkylation of the calixarene lower-rim results in the macrocycle adopting a *pinched-cone* conformation what precludes from any guest inclusion within the cavity. Unfortunately, the synthesised material does not possess a 3D connectivity and upon removal from mother liquor / de-solvation it loses crystallinity.

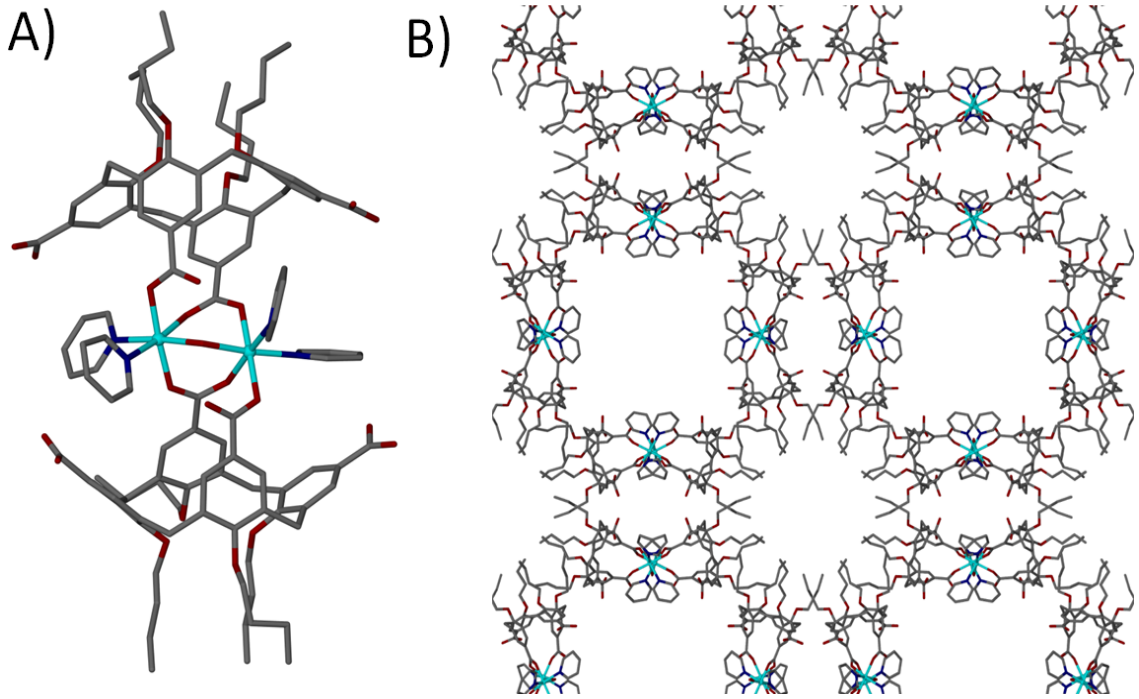

Figure 1.17. (A) Discrete aqua-bridged binuclear complex comprising two tetra-*p*-carboxylato-tetra-*O*-butoxycalix[4]arenes and four pyridines. (B) View along the *c* axis of the unit cell showing three solvent channels. Hydrogen atoms omitted for clarity.[58]

Recently Burrows *et al.* demonstrated that di-*p*-carboxylato-tetra-*O*-propoxycalix[4]arenes can be used to construct CPs.[59] The reaction of Cu(II) ions with four calixarenes leads to formation of paddle-wheel SBUs linked together to give 2D molecular sheets (Fig. 1.18A and B). Utilisation of Co(II) ions also results in formation of 2D molecular sheets, however a much more complex, rod-like metal cluster running along the *a* axis of the unit cell is formed (Fig 1.18C and D). Interestingly, they have shown that when using Cd(II) ions square SBUs form and assemble to give a 3D network instead of 2D molecular sheets (Fig 1.19). Unfortunately channels were not formed in any of the reported structures, and as a result it was not possible to gain insight into the applicability of calixarene-based 3D CPs in gas storage. Furthermore, in all three structures, as a result of the *pinched-cone* conformation of the calixarene, exclusion of solvent molecules from the cavity is observed. Thermogravimetric analysis reveals that upon removal of the coordinated solvent molecules the framework collapses and loses its crystallinity. Nevertheless, the successful synthesis of a calixarene-based 3D CP is an important step towards the utilisation of *p*-carboxylatocalixarenes in the rational design and construction of PMs.

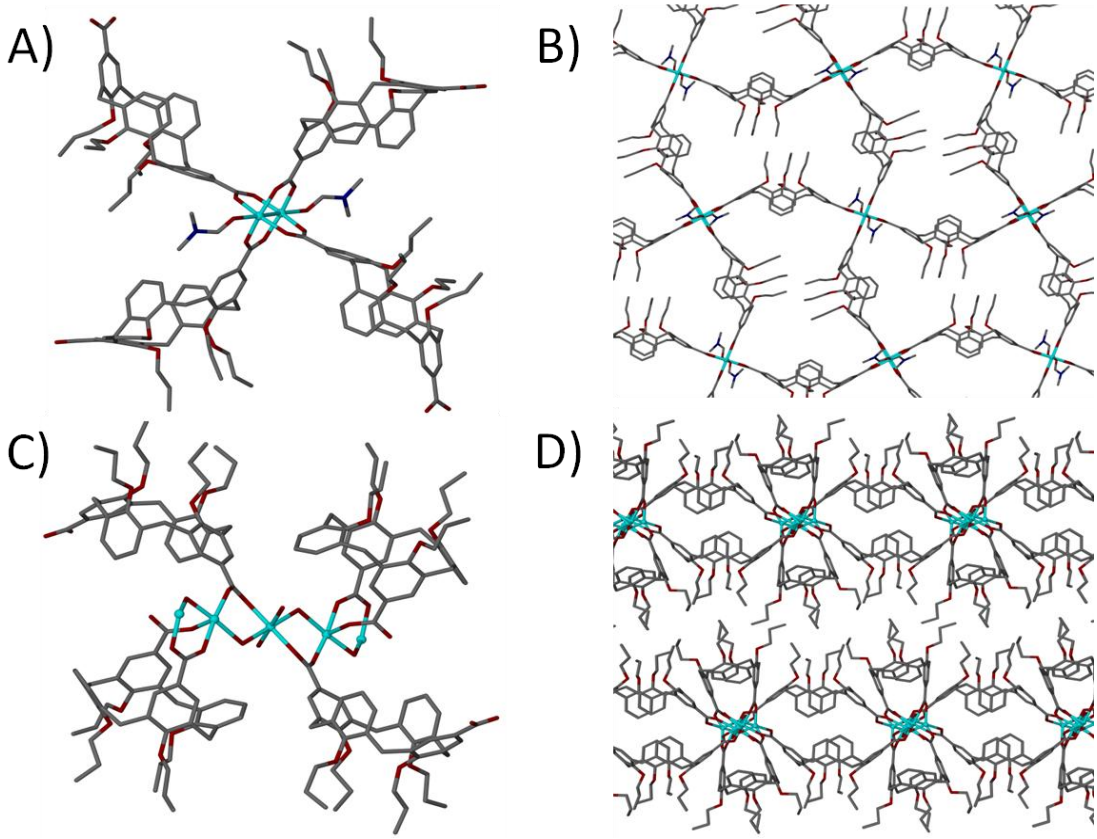

Figure 1.18. Examples of 2D CPs constructed using di-topic di-*p*-carboxylato-tetra-*O*-propoxycalix[4]arenes. (A) Cu(II) paddlewheel SBU and (B) resulting 2D molecular sheet. (C) Co(II) rod-like cluster and (D) resulting 2D molecular sheet. Hydrogen atoms and dmf of crystallisation are omitted for clarity.[41]

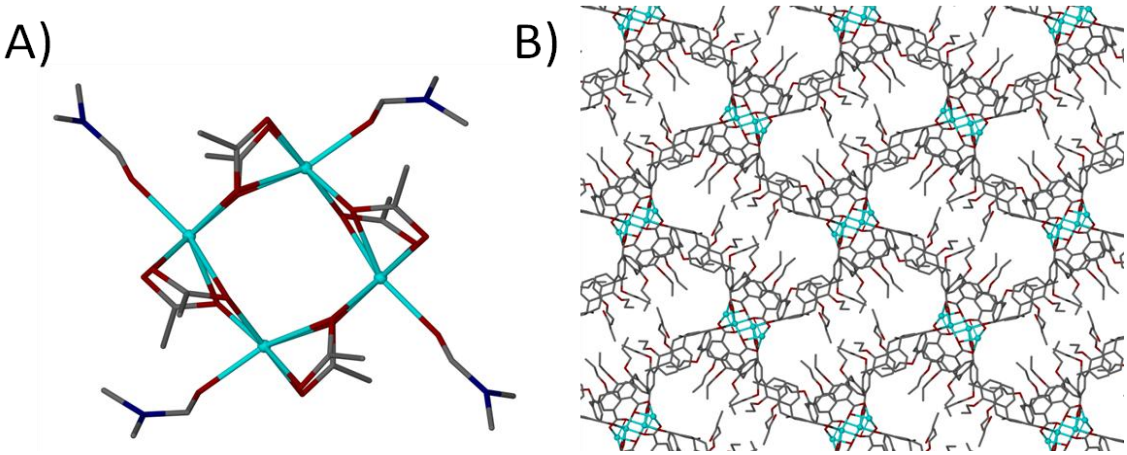

Figure 1.19. Utilisation of Cd(II) ions and di-*p*-carboxylato-tetra-*O*-propoxycalix[4]arenes results in formation of (A) square SBUs linked together to give (B) a 3D network. Hydrogen atoms and dmf of crystallisation omitted for clarity.[59]

1.4. Thesis overview

The main aim of this thesis was to utilise *p*-carboxylatocalixarenes as building blocks in the design and construction of PMs and molecular containers. A major focus was therefore to find a versatile synthetic pathway that would enable the construction of desired supramolecular architectures in a predictive and controlled fashion. Additionally, the fine-tuning of structural features in synthesised CPs and molecular containers was set as an additional criterion that the target strategy should fulfil.

Chapter 2 describes the search of target cluster motifs as potential candidates that would allow the design and construction of CPs using transition metals (TMs) as directing centres and *p*-carboxylatocalix[4]arene as building blocks. This fundamental investigation was focused on finding a motif that would provide the directionality in which the assembly could be extended and be easily reproducible for a series of TMs. As a starting point towards rational CP / PM design a planar binuclear metal cluster was selected that would allow construction of a versatile molecular panel containing TM and mono-*p*-carboxylatocalix[4]arenes. In addition, a strategy based on the "directional bonding" approach was explored as an alternative method to facilitate the construction of CPs. In order to obtain the desired directionality at the metal centre when coordinating mono-*p*-carboxylatocalix[4]arenes, 1,10-phenanthroline was selected as a chelating co-ligand in order to restrict the TM coordination sphere. The 1D CPs and discrete complexes discussed display a number of interesting features in the solid state that provided valuable insight for the remainder of the thesis.

Chapter 3 describes the study of the use of "directional bonding" approach as a method for the design of CPs. The investigation was focused on the use of different TM(II) ions, 1,10-phenanthroline as a co-ligand and *p*-carboxylatocalix[4]arene as a di-topic linker for the construction of metal-directed linear 1D CPs. Structural analysis reveals that some of the synthesised materials display markedly different solid-state packing. This variation was found to co-occur with variation in the guest residing within the calixarene cavity. In addition, the use of various 1,10-phenanthroline derivatives in the synthesis of CPs was explored. It was found that variation in this influenced inclusion of the guest within the macrocycle cavity.

In Chapter 4 it is demonstrated that, through synthetic pre-organisation of the macrocycle framework, calixarene C_2 symmetry can be utilised to construct metal-

directed supramolecular architectures different from those discussed in Chapter 3. The design strategy was based on the same approach used to synthesise linear 1D CPs, whereby *p*-carboxylatocalix[4]arenes were used as di-topic linkers, however the alternative positioning of two carboxylate groups at the upper-rim results in formation of spiral 1D CPs. Concomitantly, as a result of a different shape of formed 1D CPs different solid-state packing is observed. Further exploration of the influence of 1,10-phenanthroline derivatives on the self-assembly was also carried out.

Chapter 5 details how certain TM(II) ions (Cd and Zn), di-topic alternative *p*-carboxylatocalix[4]arenes and 1,10-phenanthroline or its derivatives assemble together to form dimeric metal-organic calixarene capsules rather than infinite spiral 1-D CPs. The investigation revealed that, depending on the TM(II) ions used, two types of dimeric capsules can be synthesised, these being either tilted or head-to-head. It is also demonstrated how utilisation of a more bulky 1,10-phenanthroline derivative results in rearrangements in the coordination sphere which induce changes to the overall shape of the formed capsules and their solid-state packing.

Finally, Chapter 6 details how a 3D CP can be synthesised when using *p*-carboxylatocalix[4]arene as a di-topic linker. The synthesised material is composed of binuclear Cd(II) SBUs and the complex CP conforms to an adamantoid topology. In addition, the outcome of the exploration of solvothermal reaction conditions is also presented.

1.5. Calixarene ligand names and corresponding numbers

Compound number	Compound name
1	*p*-*tert*-Butylcalix[4]arene / TBC[4]
2	Calix[4]arene / C[4]
3a	Tetra-*O*-propoxycalix[4]arene
3b	Tetra-*O*-butoxycalix[4]arene
3c	Tetra-*O*-pentoxycalix[4]arene
4a	*p*-Monoformyl-tetra-*O*-propoxycalix[4]arene
4b	*p*-Monoformyl-tetra-*O*-butoxycalix[4]arene
4c	*p*-Monoformyl-tetra-*O*-pentoxycalix[4]arene
5a	*p*-Monocarboxylato-tetra-*O*-propoxycalix[4]arene
5b	*p*-Monocarboxylato-tetra-*O*-butoxycalix[4]arene
5c	*p*-Monocarboxylato-tetra-*O*-pentoxycalix[4]arene
14a	Di-*O*-propoxycalix[4]arene
14b	Di-*O*-butoxycalix[4]arene
14c	Di-*O*-pentoxycalix[4]arene
15a	*p*-Diformyl-di-*O*-propoxycalix[4]arene
15b	*p*-Diformyl-di-*O*-butoxycalix[4]arene
15c	*p*-Diformyl-di-*O*-pentoxycalix[4]arene
16a	*p*-Dicarboxylato-di-*O*-propoxycalix[4]arene
16b	*p*-Dicarboxylato-di-*O*-butoxycalix[4]arene
16c	*p*-Dicarboxylato-di-*O*-pentoxycalix[4]arene
26a	Di-*O*-propoxy-di-*O*-nosylcalix[4]arene
26b	Di-*O*-butoxy-di-*O*-nosylcalix[4]arene
26c	Di-*O*-butoxy-di-*O*-nosylcalix[4]arene
27a	*p*-Di-formyl-di-*O*-propoxy-di-*O*-nosylcalix[4]arene
27b	*p*-Di-formyl-di-*O*-butoxy-di-*O*-nosylcalix[4]arene
27c	*p*-Di-formyl-di-*O*-pentoxy-di-*O*-nosylcalix[4]arene
28a	*p*-Di-carboxylato-di-*O*-propoxy-di-*O*-nosylcalix[4]arene
28b	*p*-Di-carboxylato-di-*O*-butoxy-di-*O*-nosylcalix[4]arene
28c	*p*-Di-carboxylato-di-*O*-pentoxy-di-*O*-nosylcalix[4]arene
29a	*Alt*-*p*-di-carboxylato-di-*O*-propoxycalix[4]arene
29b	*Alt*-*p*-di-carboxylato-di-*O*-butoxycalix[4]arene
29c	*Alt*-*p*-di-carboxylato-di-*O*-pentoxycalix[4]arene

1.6. Structural formulae of calixarene ligands used in this study

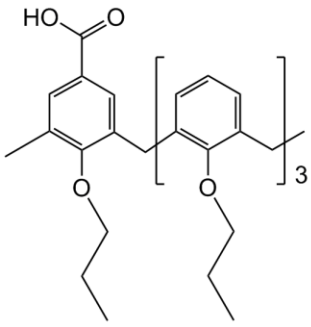

5a

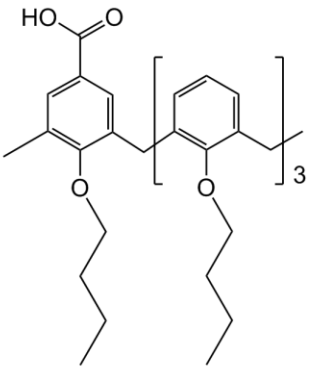

5b

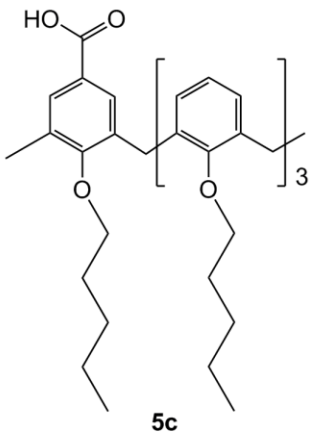

5c

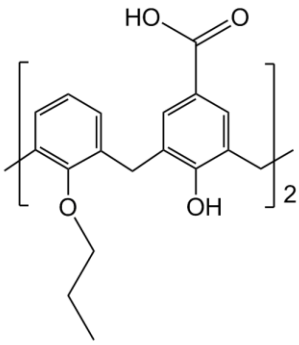

16a

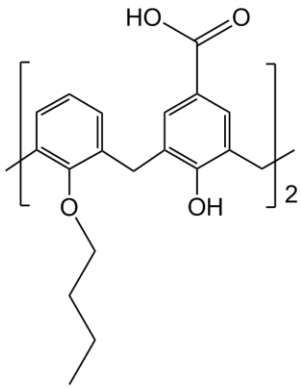

16b

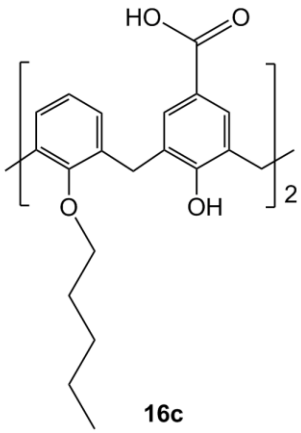

16c

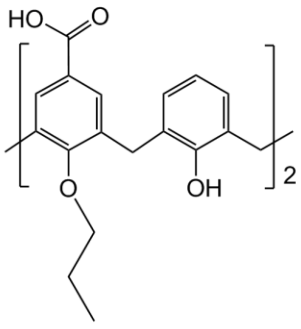

29a

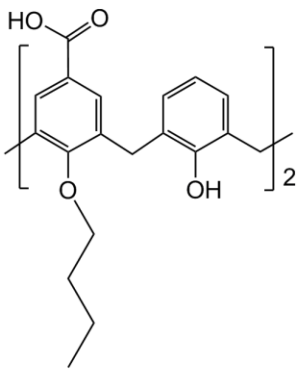

29b

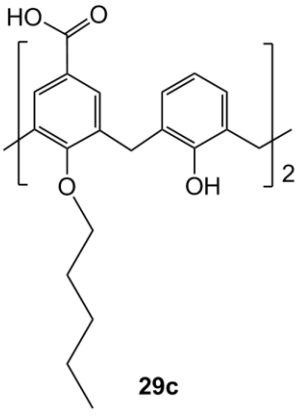

29c

1.7. References

1. R. Szostak, *Molecular Sieves: Principles of Synthesis and Identification*, Springer, **1998**.
2. M. E. Davis, *Nature*, **2002**, *417*, 813.
3. S. Kitagawa, R. Kitaura and S.-i. Noro, *Angew. Chem. Int. Ed.*, **2004**, *43*, 2334.
4. J. Rouquerol, D. Avnir, C. W. Fairbridge, D. H. Everett, J. M. Haynes, N. Pernicone, J. D. F. Ramsay, K. S. W. Sing and K. K. Unger, *Pure Appl. Chem.*, **1994**, *66*, 1739.
5. L. R. MacGillivray, *Metal-Organic Frameworks: Design and Application*, Wiley, **2010**.
6. S. R. Batten, S. M. Neville and D. R. Turner, *Coordination Polymers: Design, Analysis and Application*, RSC, **2009**.
7. J. L. C. Rowsell and O. M. Yaghi, *Angew. Chem. Int. Ed.*, **200**5, *44*, 4670.
8. J. Liu, L. Chen, H. Cui, J. Zhang, L. Zhang and C.-Y. Su, *Chem. Soc. Rev.*, **2014**, *43*, 6011.
9. D. J. Tranchemontagne, J. L. Mendoza-Cortes, M. O'Keeffe and O. M. Yaghi, *Chem. Soc. Rev.*, **2009**, *38*, 1257.
10. S. R. Batten, N. R. Champness, X.-M. Chen, J. Garcia-Martinez, S. Kitagawa, L. Ohrstrom, M. O'Keeffe, M. P. Suh and J. Reedijk, *Cryst. Eng. Commun.*, **2012**, *14*, 3001.
11. R. G. Vranka and E. L. Amma, *Inorg. Chem.*, **1966**, *5*, 1020.
12. P. W. Carreck, M. Goldstein, E. M. McPartlin and W. D. Unsworth, *J. Chem. Soc. D: Chem. Commun.*, **1971**, 1634.
13. R. W. Gable, B. F. Hoskins and R. Robson, *J. Chem. Soc., Chem. Commun.*, **1990**, 1677.
14. T. Iwamoto, S.-i. Nishikiori, T. Kitazawa and H. Yuge, *J. Chem. Soc., Dalton Trans.*, **1997**, 4127.
15. B. F. Hoskins and R. Robson, *J. Am. Chem. Soc.*, **1989**, *111*, 5962.
16. J. Kim, B. Chen, T. M. Reineke, H. Li, M. Eddaoudi, D. B. Moler, M. O'Keeffe and O. M. Yaghi, *J. Am. Chem. Soc.*, **2001**, *123*, 8239.
17. T. R. Cook, Y.-R. Zheng and P. J. Stang, *Chem. Rev.*, **2012**, *113*, 734.
18. H. Li, M. Eddaoudi, M. O'Keeffe and O. M. Yaghi, *Nature*, **1999**, *402*, 276.

19. S. L. James, *Chem. Soc. Rev.*, **2003**, *32*, 276.
20. J. L. C. Rowsell and O. M. Yaghi, *Micropor. Mesopor. Mat.*, **2004**, *73*, 3.
21. M. Eddaoudi, D. F. Sava, J. F. Eubank, K. Adil and V. Guillerm, *Chem. Soc. Rev.*, **2015**, *44*, 228.
22. M. Fujita, J. Yazaki and K. Ogura, *J. Am. Chem. Soc.*, **1990**, *112*, 5645.
23. Y. K. Kryschenko, S. R. Seidel, A. M. Arif and P. J. Stang, *J. Am. Chem. Soc.*, **2003**, *125*, 5193.
24. S. Leininger, M. Schmitz and P. J. Stang, *Org. Lett.*, **1999**, *1*, 1921.
25. R. Chakrabarty, P. S. Mukherjee and P. J. Stang, *Chem. Rev.*, **2011**, *111*, 6810.
26. K. Suzuki, M. Tominaga, M. Kawano and M. Fujita, *Chem. Commun.*, **2009**, 1638.
27. M. Tominaga, K. Suzuki, M. Kawano, T. Kusukawa, T. Ozeki, S. Sakamoto, K. Yamaguchi and M. Fujita, *Angew. Chem. Int. Ed.*, **2004**, *43*, 5621.
28. Q.-F. Sun, J. Iwasa, D. Ogawa, Y. Ishido, S. Sato, T. Ozeki, Y. Sei, K. Yamaguchi and M. Fujita, *Science*, **2010**, *328*, 1144.
29. C. D. Gutsche, *Calixarenes - An Introduction*, 2nd edn., RSC, **2008**.
30. Asfari Z., Bohmer V., Harrowfield J. and Vicens J., *Calixarenes 2001*, Kluwer Academic Publishers, Dordrecht, **2001**.
31. R. M. McKinlay, G. W. V. Cave and J. L. Atwood, *Proc. Nat. Acad. Sci USA*, **2005**, *102*, 5944.
32. R. M. McKinlay, P. K. Thallapally, G. W. V. Cave and J. L. Atwood, *Angew. Chem. Int. Ed.*, **2005**, *44*, 5733.
33. N. P. Power, S. J. Dalgarno and J. L. Atwood, *Angew. Chem. Int. Ed.*, **2007**, *46*, 8601.
34. B. F. Abrahams, B. A. Boughton, N. J. FitzGerald, J. L. Holmes and R. Robson, *Chem. Commun.*, **2011**, *47*, 7404.
35. M. J. Hardie, *Chem. Soc. Rev.*, **2010**, *39*, 516.
36. Z. Zhong, A. Ikeda, S. Shinkai, S. Sakamoto and K. Yamaguchi, *Org. Lett.*, **2001**, *3*, 1085.
37. B. F. Abrahams, N. J. FitzGerald and R. Robson, *Angew. Chem. Int. Ed.*, **2010**, 49, 2896.
38. T. K. Ronson, H. Nowell, A. Westcott and M. J. Hardie, *Chem. Commun.*, **2011**, *47*, 176.
39. P. Jacopozzi and E. Dalcanale, *Angew. Chem. Int. Ed.*, **1997**, *36*, 613.

40. L. Pirondini, F. Bertolini, B. Cantadori, F. Ugozzoli, C. Massera and E. Dalcanale, *Proc. Nat. Acad. Sci.USA*, **2002**, *99*, 4911.
41. R. Pinalli, V. Cristini, V. Sottili, S. Geremia, M. Campagnolo, A. Caneschi and E. Dalcanale, *J. Am. Chem. Soc.*, **2004**, *126*, 6516.
42. T. Haino, M. Kobayashi, M. Chikaraishi and Y. Fukazawa, *Chem. Commun.*, **2005**, 2321.
43. O. D. Fox, M. G. B. Drew and P. D. Beer, *Angew. Chem. Int. Ed.*, **2000**, *39*, 135.
44. O. D. Fox, N. K. Dalley and R. G. Harrison, *J. Am. Chem. Soc.*, **1998**, *120*, 7111.
45. O. Ugono, J. P. Moran and K. T. Holman, *Chem. Commun.*, **2008**, 1404.
46. S. J. Dalgarno, J. L. Atwood and C. L. Raston, *Chem. Commun.*, **2006**, 4567.
47. J. L. Atwood, L. J. Barbour, M. J. Hardie and C. L. Raston, *Coord. Chem. Rev.*, **2001**, *222*, 3.
48. M. J. Hardie, J. A. Johnson, C. L. Raston and H. R. Webb, *Chem. Commun.*, **2000**, 849.
49. G. W. Orr, L. J. Barbour and J. L. Atwood, *Science*, **1999**, *285*, 1049.
50. S. J. Dalgarno, J. L. Atwood and C. L. Raston, *Chem. Commun.*, **2006**, 4567.
51. A. Drljaca, M. J. Hardie and C. L. Raston, *J. Chem. Soc., Dalton Trans.*, **1999**, 3639.
52. M. J. Hardie and C. L. Raston, *J. Chem. Soc., Dalton Trans.*, **2000**, 2483.
53. S. J. Dalgarno and C. L. Raston, *Chem. Commun.*, **2002**, 2216.
54. J. L. Atwood, L. J. Barbour, A. Jerga and B. L. Schottel, *Science*, **2002**, *298*, 1000.
55. J. L. Atwood, L. J. Barbour and A. Jerga, *Angew. Chem. Int. Ed.*, **2004**, *43*, 2948.
56. F. A. Cotton, P. Lei, C. Lin, C. A. Murillo, X. Wang, S.-Y. Yu and Z.-X. Zhang, *J. Am. Chem. Soc.*, **2004**, *126*, 1518.
57. S. Pasquale, S. Sattin, E. C. Escudero-Adán, M. Martínez-Belmonte and J. de Mendoza, *Nat. Commun.*, **2012**, *3*, 785.
58. S. Kennedy, G. Karotsis, C. M. Beavers, S. J. Teat, E. K. Brechin and S. J. Dalgarno, *Angew. Chem., Int. Ed.*, **2010**, *49*, 4205.
59. S. P. Bew, A. D. Burrows, T. Duren, M. F. Mahon, P. Z. Moghadam, V. M. Sebestyen and S. Thurston, *Chem. Commun.*, **2012**, *48*, 4824.

Chapter 2. Transition metals and mono-*p*-carboxylatocalix[4]arenes: coordination complexes as target motifs

As highlighted in Chapter 1, the majority of examples in which calixarenes are utilised as building blocks in supramolecular chemistry mainly result in the formation of molecular capsules and polyhedra. This is primarily due to their inherent shape, and thus resulting orientation of functional groups around the general macrocycle framework, making them ideal candidates for the construction of such architectures. However, due to the intrinsic calixarene cavity, this group of macrocycles should potentially be very useful in the construction of various PMs that contain solvent pockets and channels. Surprisingly little has been done in this area of research so far, with very few examples of calixarene-based PMs in the literature.

In order to rationally design PMs it is important to be able to fine-tune the structural features observed in the solid state, as this enables one to control and adjust the physical and chemical properties of the material. As such the synthesis of any material has to be reliable in terms of its predictability and reproducibility; this is why the use of SBUs in the design of various PMs has proven to be so fruitful. In order to successfully exploit calixarenes as building blocks in the design of PMs, one has to develop a rational approach in which the connectivity of key components / building blocks can be controlled in a predictive manner. In theory such a strategy can be based on either a "directional bonding approach" or the use of SBUs. The use of SBUs can be a viable approach, given that the calixarene framework can be synthetically pre-organised to contain carboxylic acids, however due to the bulkiness of the macrocycle their synthesis can often prove to be somewhat difficult. This has led to a search for a target motif that would: 1) provide the directionality of some of the well-established SBUs, 2) allow the use of bulky *p*-carboxylatocalixarenes instead of simple benzoates and 3) be easily reproducible for a series of transition metals. It was therefore decided to explore a different strategy, based on the "directional bonding approach", whereby

co-ligand restriction of the transition metal coordination sphere could provide the desired directionality at the metal centre, ultimately allowing for the construction of PMs.

2.1. Coordination polymer design strategy

The Cambridge Structural Database (CSD) was used to identify a target motif which would facilitate the construction of a CP.[60] Given that *p*-carboxylatocalix[4]arenes (*p*-CO_2[4]s) have not been used extensively in the construction of CPs and PMs, a search of the database for common structural motifs was based on benzoates. The reasons for benzoate being a good candidate to be used in the search were: 1) benzoates, akin to *p*-carboxylatocalixarenes, possess a carboxylate group through which they coordinate to TMs and 2) there are numerous examples in the literature where they have been exploited as building blocks to construct CPs and MOFs.[7, 17, 61] Dalgarno and co-workers previously reported metal-directed supramolecules which, through solvent control, were assembled into metal-organic nano-tubular architectures.[58] The role of pyridine was proven to be very important as it influenced the positioning of calixarenes around the cluster core, leading to the formation of nano-tubular assemblies (Fig. 1.17). In addition to this, pyridine was also found to be involved in stabilisation of the assembly through participation in non-covalent interactions (*via* the pyridine-carboxylic acid synthon).[5] Due to the above reasons the primary search criteria for a target cluster were expanded to include pyridine.

A search of the CSD for coordination complexes containing the three target components gave 12212 hits.[1] Analysis showed that the combination of TMs, pyridine (py) and benzoates often afforded a metal-organic building block based on a binuclear TM benzoate cluster of general formula [TM_2(benzoate)$_4$(Py)$_4$] that conforms to a panel arrangement as shown in Figure 2.1. Selection of this target cluster motif was also driven by results that showed that the target panel often formed with both mono-topic (pyridines) and di-topic linkers (bi-pyridyls).[62-64] The length of di-topic linker can be readily varied whilst the structure of the molecular panel and the network / connectivity of the resulting CP remains unchanged. Examples from literature also showed that the integrity of the panel is maintained when using different TM(II) ions (eg. Co, Mn and Cd), and that formation occurs under both thermodynamic and kinetic

control. This planar binuclear metal cluster was therefore selected as a starting point towards rational CP / PM design through construction of a versatile molecular panel containing mono-*p*-carboxylatocalix[4]arenes (mono-*p*-CO_2[4]s, rather than benzoates); this gives a target motif of formula [TM_2(mono-*p*-CO_2[4])$_4$($Py)_4$].

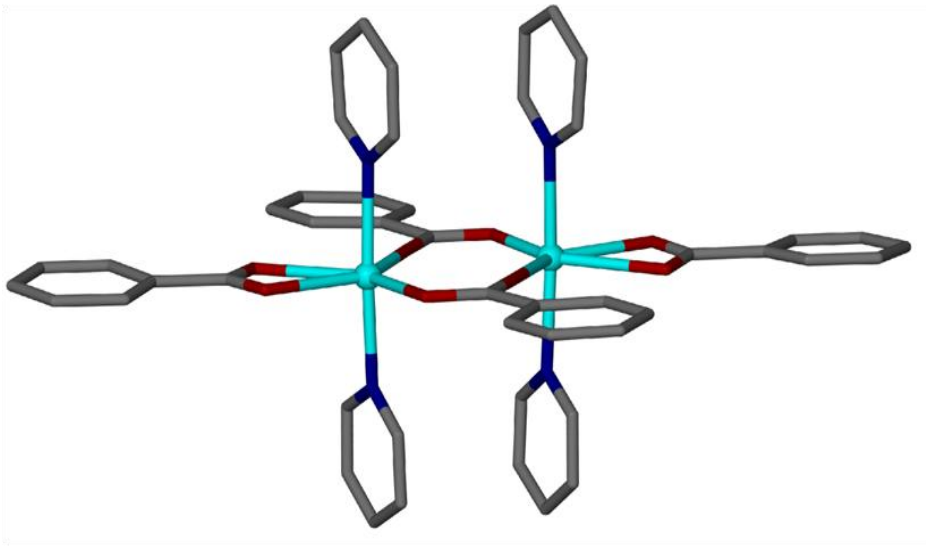

Figure 2.1 Planar binuclear metal cluster, of formula [TM_2(benzoate)$_4$($Py)_4$], chosen as a target motif for CP / PM design.

2.1.1. Synthesis of mono-p-carboxylatocalix[4]arenes

A series of mono-*p*-CO_2[4]s were synthesised according to literature procedure in order to investigate the applicability of the chosen target motif described above.[65] The general synthetic route comprised five steps as shown in Figure 2.2, with the third being a tetra-alkylation in which different chains were introduced to the calixarene lower-rim. The resulting mono-*p*-CO_2[4]s adopt a pinched-cone conformation as expected due to lower-rim tetra-alkylation; in this arrangement two distal arenes pinch whilst the remaining two splay relative to the C[4] annulus. Tetra-alkylated calixarenes with methyl and ethyl chains were excluded from the investigation due to their conformational flexibility. This arises from the fact that, with short chains present, all four aryl groups can freely rotate through the C[4] annulus. By introducing four

sufficiently large substituents at the lower-rim it is therefore possible to restrict conformational flexibility accordingly.

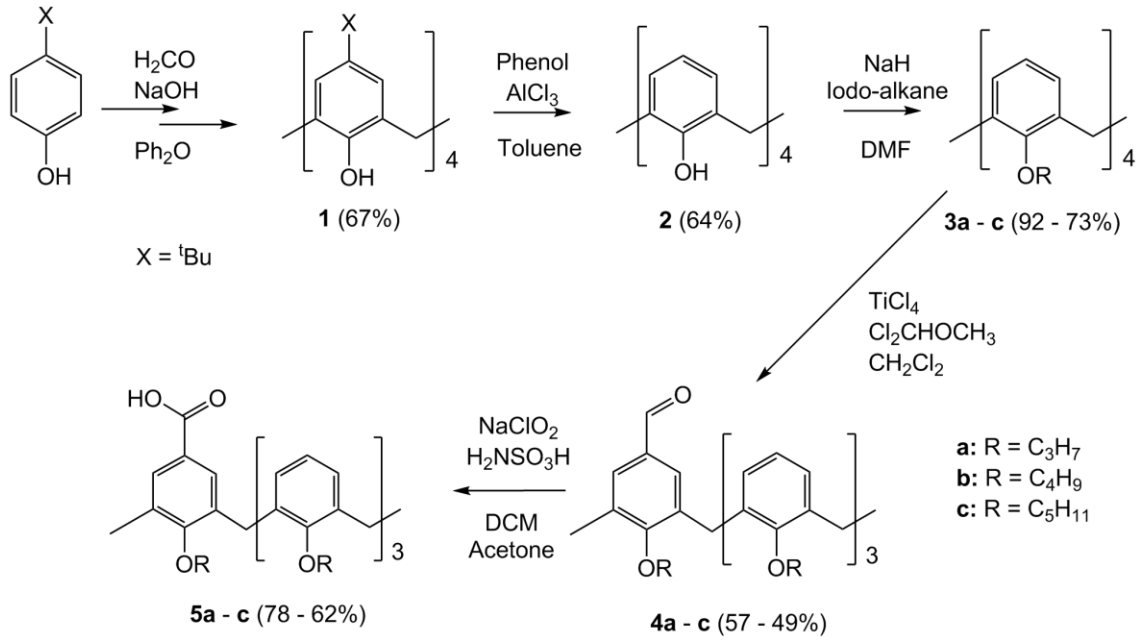

Figure 2.2 Schematic of the synthesis of mono-*p*-carboxylatocalix[4]arenes **5a - c**.

2.1.2. Proof of concept

Having synthesised a small library of mono-*p*-CO_2[4]s (**5a - c**), a series of TM(II) ions (Co, Mn and Cd) were chosen based on the examples identified in Section 2.1 above. Due to the poor solubility of mono-*p*-CO_2[4]s, and in order to aid dissolution of each macrocycle, the reaction conditions reported in the literature required minor modification. As only a handful of solvents were found to be capable of dissolving **5a - c**, dimethylformamide (dmf) became the solvent of "choice". Unfortunately, reactions of chosen TM(II) ions with mono-*p*-CO_2[4]s (**5a - c**) and pyridine in dmf did not yield crystalline material, with powder x-ray diffraction (PXRD) proving the amorphous nature of the precipitate formed. Being unable to verify whether the targeted motif was formed with pyridine, and given that the target motif could also be synthesised using a di-topic linker, pyridine was substituted for 4,4'-bpyridine (bpy), 4,4'-bpyridylethane (bpa) or 4,4'-bpyridylethene (bpe) as a co-ligand in the reaction. Ambient reactions were carried out according to a modified literature procedure in

which a dmf solution containing a mono-*p*-CO_2[4] (**5a - c**) and Co(II), Mn(II) or Cd(II) nitrate were placed in sample vials, followed by careful layering of methanolic solution containing bpy.[66] A number of the reactions incorporating **5a** returned single crystals with slow evaporation over a period of several weeks and these are summarised in Table 2.1; unfortunately all reactions involving both **5b** and **5c** were unsuccessful. All suitable samples from the study with **5a** were analysed using single crystal x-ray diffraction (SCXRD) and these are discussed below in detail.

Co-ligand	Co(II)	Mn(II)	Cd(II)
bpy	√ (**6**)	√ (**7**)	√ (**8**)
bpa	√ (**9**)	X	√ (**10**)
bpe	√ (**11**)	X	X

Table 2.1 Matrix of reactions between mono-*p*-CO_2[4] **5a,** Co(II), Mn(II) or Cd(II) nitrate, and bpy, bpa or bpe.

Structural analysis of $[Co_2(\mathbf{5a})_4(bpy)_2]\cdot 6dmf$ (**6**) revealed formation of the target molecular panel (Figure 2.3A), comprising two TM(II) ions and four mono-*p*-CO_2[4]s, with two bpys residing on either side of the near planar motif. The panel conforms to a parallelogram and has dimensions of 1.8 × 1.0 nm (measured between centroids generated from mono-*p*-CO_2[4] lower-rim oxygens), representing a large building unit / molecular panel. The crystals are in a triclinic cell and structure was solved in space group *P*-1. The unit cell parameters are a = 11.298(2) Å, b = 15.849(3) Å and c = 27.416(5) Å, and α = 89.235(3)º, β = 80.416(3)º and γ = 80.184(3)º. The asymmetric unit comprises two mono-*p*-CO_2[4]s (**5a**), one Co(II) ion and bpy, and three dmf of crystallisation. The carboxylate moiety, comprising atoms O(1)-C(29)-O(2), is coordinated to Co(1) in a chelating fashion with respective Co(1)-O(1) and Co(1)-O(2) distances of 2.204(3) Å and 2.155(3) Å. The carboxylate group located on the second mono-*p*-CO_2[4], comprising atoms O(7)-C(70)-O(8), is coordinated in a bridging fashion to Co(1) and symmetry equivalent (s.e.) Co(1)' *via* O(7) and O(8) respectively, with respective bond lengths of 2.045(3) Å and 2.040(3) Å. Symmetry expansion

shows that the panels are linked in the desired fashion *via* two bpys on either side to afford a CP chain as shown in Figure 2.3B, with N(1)-Co(1) and N(2)-Co(1)' distances of 2.116(3) Å and 2.123(3) Å respectively. Tetra-*O*-alkylation of the calixarene lower-rim generally precludes guest inclusion in the resulting mono-*p*-CO_2[4].[67] This is observed in the present structure, with all calixarenes adopting a pinched-cone conformation as shown in Figure 2.3A. Structural analysis revealed that co-crystallised dmf molecules occupy space around the panel, residing in interstitial regions between neighbouring CP chains. SCXRD analysis of [Mn_2(**5a**)$_4$(bpy)$_2$]·6dmf (**7**) and [Cd_2(**5a**)$_4$(bpy)$_2$]·6dmf (**8**) revealed that they are isostructural with **6**, proving that the target panel can be synthesised for different TM(II) ions.

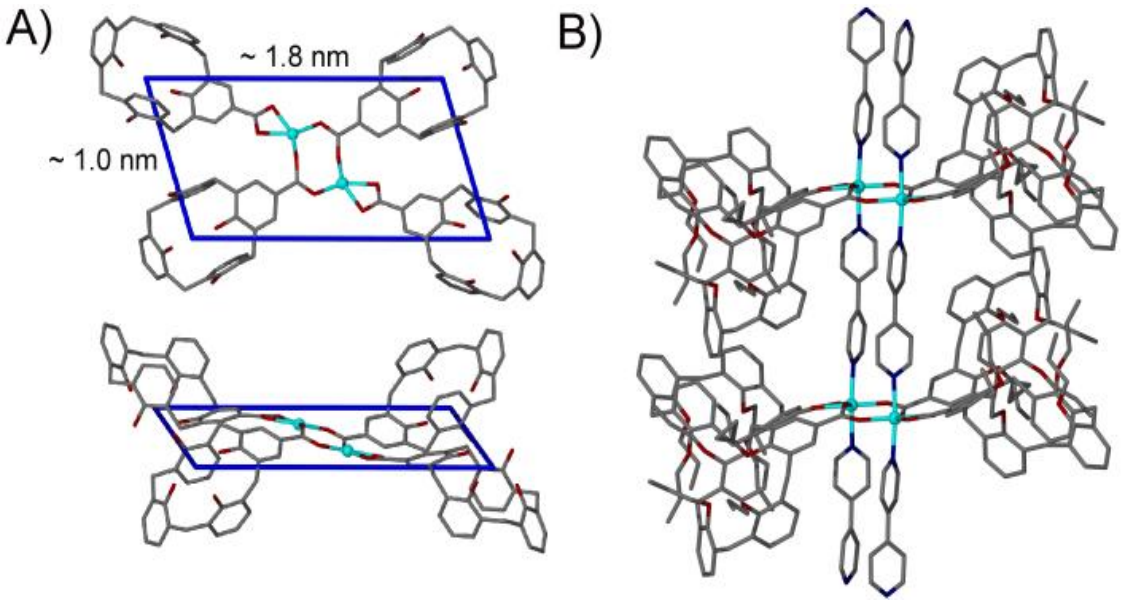

Figure 2.3 (A) Near orthogonal views of the [TM_2(**5a**)$_4$(bpy)$_2$]·6dmf molecular panel found in [Co_2(**5a**)$_4$(bpy)$_2$]·6dmf (**6**) with mono-*p*-CO_2[4] lower-rim alkyl chains omitted for clarity. (B) CP chain in the extended structure of **6**. Dmf of crystallisation and hydrogen atoms omitted for clarity in both.

After successful synthesis of the target motif using bpy in place of pyridine, the study focused on the applicability of a longer linker (bpa) for the construction of target molecular panels comprising mono-*p*-CO_2[4]s. Reaction of Co(II) ions with mono-*p*-CO_2[4] (**5a**) and bpa yielded red crystals of formula [Co_2(**5a**)$_4$(bpa)$_2$]·8dmf (**9**). The

crystals of **9** are in a triclinic cell and the structure was solved in space group *P*-1. The unit cell parameters are a = 13.0333(8) Å, b = 13.5524(7) Å and c = 27.8507(18) Å, and α = 92.526(4)º, β = 95.448(4)º and γ = 99.997(4)º. Structural analysis of **9** revealed formation of the target molecular panel (Figure 2.4A), and as observed in **6**, it comprises two Co(II) ions and four mono-*p*-CO_2[4]s, with bpa acting as a di-topic linker. The panel conforms to the expected parallelogram of dimensions of 1.8 × 1.0 nm (measured between centroids generated from mono-*p*-CO_2[4] lower-rim oxygens). The asymmetric unit contains two mono-*p*-CO_2[4]s (**5a**), one Co(II) ion, one bpa and four dmf of crystallisation. The carboxylate group, comprising atoms O(1)-C(29)-O(2), is coordinated to Co(1) in a chelating fashion with Co(1)-O(1) and Co(1)-O(2) distances of 2.162(3) Å and 2.256(3) Å respectively. The carboxylate group located at the second mono-*p*-CO_2[4], comprising atoms O(3)-C(70)-O(4), is coordinated in a bridging fashion to Co(1) and symmetry equivalent (s.e.) Co(1)' *via* O(3) and O(4), with respective bond lengths of 2.073(3) Å and 2.055(3) Å. Symmetry expansion shows that the panels are linked *via* two bpa ligands in the same fashion as in **6** (Figure 2.4B), with N(1)-Co(1) and N(2)-Co(1)' distances of 2.139(3) Å and 2.125(3) Å respectively.

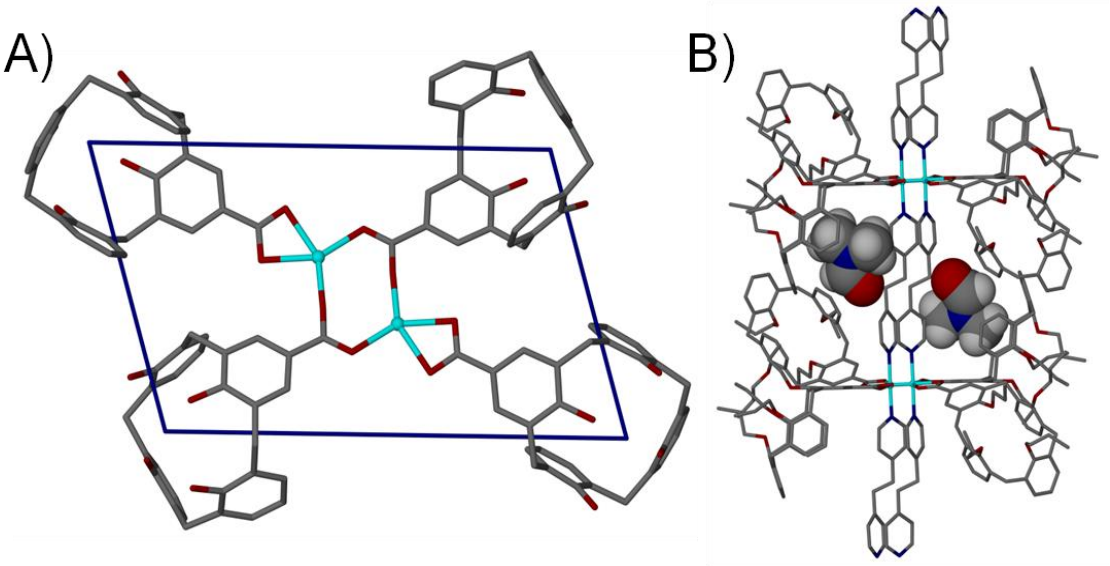

Figure 2.4 (A) View of the [Co_2(**5a**)$_4$(bpa)$_2$]·8dmf molecular panel in **9** with mono-*p*-CO_2[4] lower-rim alkyl chains omitted for clarity. (B) Extended structure of **9** showing dmf of crystallisation occupying cone conformer *p*-CO_2[4]s. Dmf shown in the space filling representation; other co-crystallised dmf molecules and hydrogen atoms omitted for clarity.

Structural analysis of **9** reveals that the panel contains two crystallographically unique mono-*p*-CO_2[4]s, both of which adopt cone rather than pinched-cone conformations. This occurs with concomitant inclusion of a co-crystallised dmf molecule in each calixarene cavity; in this arrangement typical CH···π interactions occur between hydrogen atoms of dmf methyl groups and the aromatic rings of the calixarene framework with contact distances being 2.40 Å, 2.85 Å and 3.00 Å.[68] This is particularly interesting when one considers the host-guest behaviour of *p*-^{t}Bu-calix[4]arene toward gases such as CO_2 and the potential that these molecules may hold with respect to CP / MOF construction.[55, 69] Structural analysis of $[Cd_2(\mathbf{5a})_4(bpa)_2]\cdot 8dmf$ (**10**) revealed it to be isostructural with **9**, with the molecular panel also containing two crystallographically unique mono-*p*-CO_2[4]s in the cone conformation.

Further analysis of the bpa linked CP (**9**) showed that the ditopic linkers are positioned such that, if one could substitute bpa for bpe, it may be possible to perform a single-crystal-to-single-crystal [2 + 2] photodimerisation in line with Schmidt's topochemical criteria for photochemical cycloaddition.[70] In order to investigate this, reactions were carried out using same procedure as used to synthesise **6** - **10** but using methanolic solution of bpe, yielding $[Co_2(\mathbf{5a})_4(bpe)_2]\cdot 8dmf$ (**11**). As in **6**, **9** and **10**, crystals of **11** are in a triclinic cell and the structure was also solved in space group *P*-1. The unit cell parameters are a = 12.9815(18) Å, b = 13.5780(2) Å and c = 27.7690(4)Å, and α = 93.021(4)º, β = 95.356(4)º and γ = 99.997(4)º. Structural analysis of **11** revealed formation of the target motif (Figure 2.5A), and as observed in **6** and **9**, the molecular panel comprises two Co(II) ions and four mono-*p*-CO_2[4]s (**5a**), with bpe acting as a linker between neighbouring panels. The panel also conforms to a parallelogram of similar dimensions (1.8 × 1.0 nm), measured between centroids generated from mono-*p*-CO_2[4]s lower-rim oxygens). As in **6** and **9** the asymmetric unit comprises two mono-*p*-CO_2[4]s (**5a**), one Co(II) ion, one linker (bpe) and four dmf of crystallisation. The carboxylate group, comprising atoms O(5)-C(29)-O(6), is coordinated to Co(1) in a chelating fashion with Co(1)-O(5) and Co(1)-O(6) distances of 2.156(5) Å and 2.242(5) Å respectively. The carboxylate moiety located at the second mono-*p*-CO_2[4], comprising atoms O(11)-C(110)-O(12), is coordinated in a bridging fashion to Co(1) and symmetry equivalent (s.e.) Co(1)' *via* O(11) and O(12), with respective bond lengths of 2.079(4) Å and 2.039(6) Å. Symmetry expansion

shows that the panels are linked *via* bpe linkers in the same fashion as in **6** and **9** (Figure 2.5B), with N(1)-Co(1) and N(2)-Co(1)' distances of 2.121(6) Å and 2.120(6) Å respectively. The distance between bpe alkene chains was found to be 4.0 Å which is at the extremes of the desirable topochemical criteria for [2 + 2] photodimerisation.

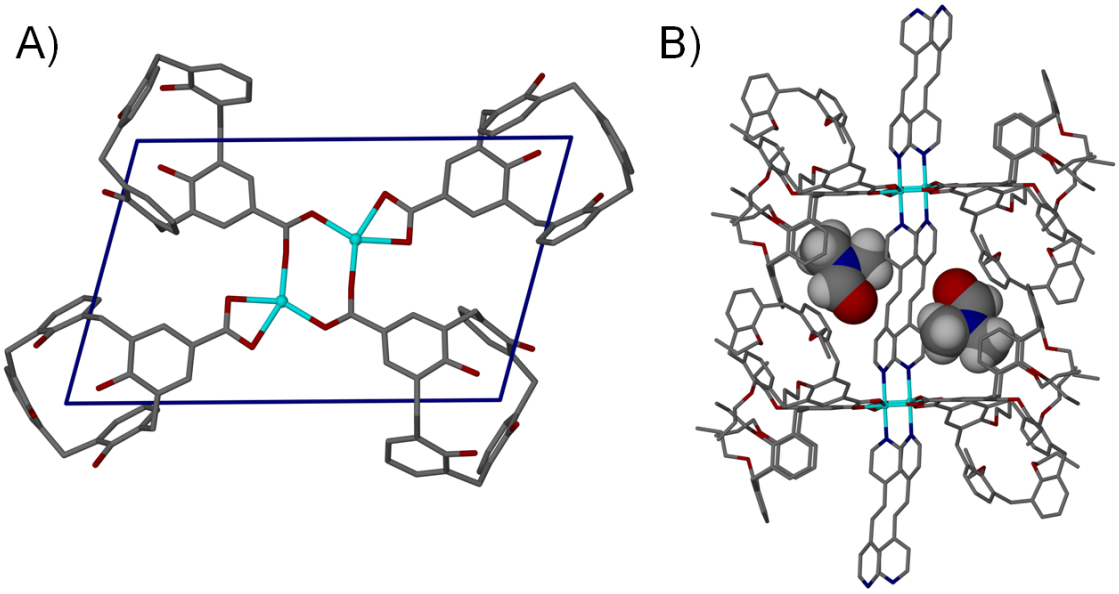

Figure 2.5 (A) View of the $[Co_2(\mathbf{5a})_4(bpe)_2]\cdot 8dmf$ molecular panel in **11** with mono-*p*-CO_2[4] lower-rim alkyl chains omitted for clarity. (B) Extended structure of **11** showing dmf of crystallisation occupying cone conformer *p*-CO_2[4]s. Dmf shown in the filling representation; other co-crystallised dmf molecules and hydrogen atoms omitted for clarity.

Although this was the case single-crystal-to-single-crystal photodimerisation was still attempted but experiments revealed that the structure remained unchanged following long exposure to UV light. As such it is clear that the distance between bpe linkers and their orientation was not optimal for photochemical cycloaddition to take place. There is a notable difference observed in the crystal packing of **6** compared to both **9** and **11**, that being the distance found between the centroids of molecular panels between two neighbouring CP chains. In **6** this distance is found to be ~1.6 nm, which is greater by ~0.3 nm than the analogous distance in both **9** and **11** (Figure 2.6). The alignment of neighbouring CP chains is necessarily dictated by the length of the linker between the molecular panels; this has a concomitant effect on the potential for interdigitation between neighbouring CP chains. In **6** the bpy linker (1.1 nm) is shorter than the bpa

and bpe linkers in **9** and **11** respectively, both of which are ~1.4 nm long. This shorter linker precludes efficient packing and causes the CPs to assemble with the significantly greater inter-chain distance.

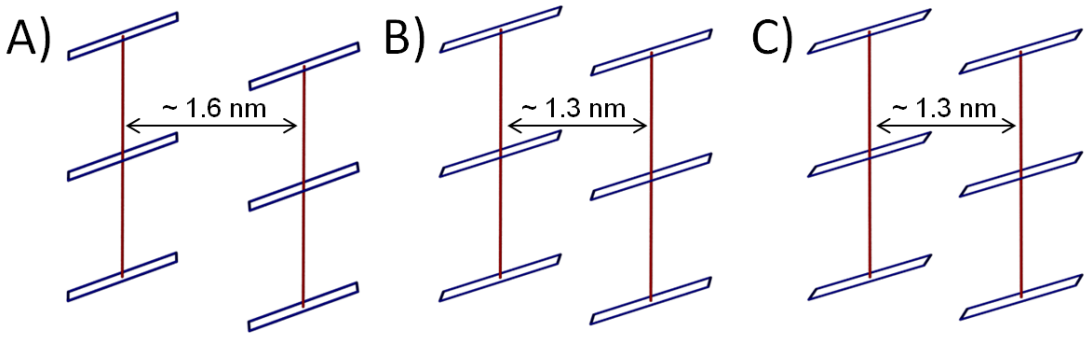

Figure 2.6 Distance between neighbouring CPs with red and blue lines representing the linker and molecular panel respectively for (A) $[Co_2(\mathbf{5a})_4(bpy)_2]\cdot 6dmf$ (**6**), (B) $[Co_2(\mathbf{5a})_4(bpa)_2]\cdot 8dmf$ (**9**), and (C) $[Co_2(\mathbf{5a})_4(bpe)_2]\cdot 8dmf$ (**11**).

In contrast, the linkers in **9** and **11** are long enough to facilitate interdigitation of calixarenes from panels of neighbouring CPs (Figure 2.7). Less efficient packing of CPs observed in **6** results in the formation of rectangular solvent-filled channels of dimensions of approximately 1.0 nm × 0.6 nm, as shown in Figure 2.6. The self-assembly of CPs with longer linkers results in a disruption of the packing observed in **6**, and rather than forming solvent channels in the solid state, the CPs align to form solvent pockets. This is an interesting feature as it provides insight into the method of controlling assembly toward the design of porous materials. For example, structures containing panels of bulky, basket-shaped organic building blocks (e.g. calixarenes) may promote the formation of solvent-filled pockets / channels, the exact nature of which may depend on the degree of interdigitation. Given these solid state structural features and the presence of solvent pockets and channels, in order to investigate their potential as gas storing materials, PXRD analyses were carried out. Unfortunately, after analysing the diffraction pattern of **6**, **9** and **11** it became evident that the filtered crystalline materials lose crystallinity upon removal from the mother liquors and drying.

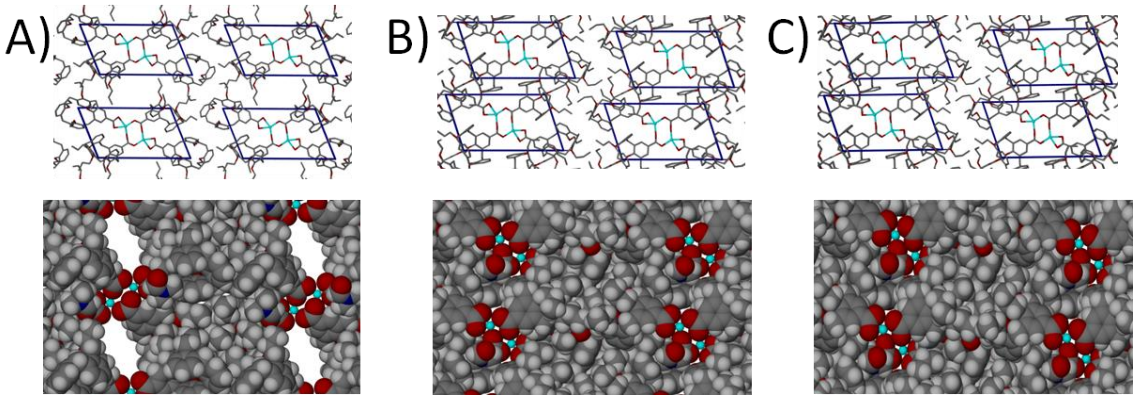

Figure 2.7 Ball and stick and space filling representation of the crystal packing along the linker axis showing solvent channels and pockets (A) $[Co_2(\mathbf{5a})_4(bpy)_2]\cdot 6dmf$ (**6**), (B) $[Co_2(\mathbf{5a})_4(bpa)_2]\cdot 8dmf$ (**9**), and (C) $[Co_2(\mathbf{5a})_4(bpe)_2]\cdot 8dmf$ (**11**). Hydrogen atoms, dmf of crystallisation, and bpy / bpa / bpe linkers omitted for clarity.

To summarise this section, a target molecular panel based on a binuclear cluster motif (Fig. 2.1) was synthesised for a series of transition metal ions using mono-*p*-carboxylatocalix[4]arene in place of benzoate. These results showed that calixarenes can be utilised not only as co-ligands in coordination chemistry, but also more importantly as building blocks in the design and construction of new CPs. When considering the network connectivity in synthesised materials, the stability of solids towards de-solvation can potentially be improved by increasing the dimensionality of the network. The following section describes the preliminary investigation of a different design strategy which is based on the 'directional bonding' approach. In this approach TM(II) ions, mono-*p*-CO_2[4]s, and chelating co-ligands are utilised in order to organise the coordination sphere and gain control over the directionality of co-ligands.

2.2. 1,10-Phenanthroline as a co-ligand in supramolecular assembly

When utilising metal ions in the rational design of supramolecular architectures, the ability to control the positioning of ligands around the coordination sphere is of primary importance. By choosing specific metal ions and terminal co-ligands one can gain control over the relative orientation of coordinated species, ultimately governing the connectivity and dimensionality of the resulting supramolecular architecture. As highlighted in Chapter 1 chemists employ various strategies to control the outcome of self-assembly, with the two most prominent being the 'directional bonding' approach and the utilisation of SBUs. The latter exploits inherent properties of multidentate ligands - their high affinity for binding metal ions (chelate effect), which can result in metal ions being locked within rigid clusters. This high affinity for binding metal ions can also be exploited in the former approach in order to restrict the number of available binding sites at a metal centre. By doing so one can then fill the remaining coordination sites with various ligands. This approach can often lead to the formation of single metal coordination complexes (rather than a binuclear molecular panel as discussed above for example), and naturally result in the formation of markedly different architectures.

An example of a chelating ligand which has been extensively used in coordination chemistry, and that recently has been used as a co-ligand in supramolecular chemistry, is 1,10-phenanthroline (phen).[71] It is a bidentate, heteroaromatic ligand, with two pre-organised nitrogen atoms positioned so as to facilitate cooperative cation binding. Phen is also rigid and planar, possessing extended conjugation, a feature that can be advantageous when using it as a co-ligand in constructing supramolecular architectures; it readily forms π-stacking interactions for example. Such structural features may be of importance as they can often help to stabilise self-assembly *via* non-covalent interactions. A search of the CSD for complexes containing a TM(II) ion, benzoate and phen showed that these components often form a common complex of general formula [TM(benzoate)$_2$(phen)(solvent)] as shown in Figure 2.7.[60] As a starting point in this investigation it was important to see whether mono-*p*-CO_2[4]s could be successfully used in place of benzoate to construct discrete structures based on this target complex. Additionally, as part of the investigation was to study the role of phen, its involvement in non-covalent interactions and its influence on the packing in the solid state.

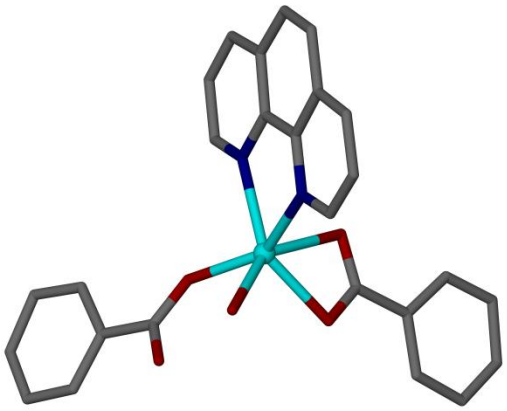

Figure 2.8 Common phen complex of general formula [TM(benzoate)$_2$(phen)(solvent)].

2.2.1. Proof of concept

This investigation began by carrying out reactions using a series of TM(II) ions, *p*-CO_2[4]s **5a-c** in place of benzoate and phen as co-ligand, with the goal being formation of discrete complexes conforming to the general formula [TM(*p*-CO_2[4])$_2$(phen)(solvent)].[72, 73] The TM(II) ions investigated were Mn, Co, Ni, Cu, Zn and Cd, however only two of the reactions from a combinatorial matrix afforded crystalline solids that were suitable for SCXRD analysis. The reactions are summarised below in Table 2.2.

	Mn(II)	**Co(II)**	**Ni(II)**	**Cu(II)**	**Zn(II)**	**Cd(II)**
5a	√	x	x	x	x	√
5b	x	x	x	x	x	x
5c	x	x	x	x	x	x

Table 2.2 Matrix of reactions between mono-*p*-CO_2[4]s **5a-c**, a series of TM(II) ions and phen to give discrete complex of formula [TM(benzoate)$_2$(phen)(solvent)].

Reaction of Mn(II) ions, mono-*p*-CO_2[4] **5a** and phen, and subsequent slow evaporation of the reaction mixture resulted in formation of diffraction quality single crystals of complex [Mn(**5a**)$_2$(phen)(H_2O)]·(dmf)$_2$ (**12**). Crystals of **12** are in a triclinic cell and the structure was solved in the space group *P*-1. The unit cell parameters are *a* = 9.6926(8) Å, *b* = 18.8194(17) Å and *c* = 24.9780(2) Å, and α = 77.167(4)º, β = 85.174(5)º and γ = 89.000(5)º. The asymmetric unit contains a coordination complex comprising one Mn(II) ion, one phen, one aquo ligand, two mono-*p*-CO_2[4]s and two dmf of crystallisation as shown in Figure 2.9. Comparison of Figures 2.8 and 2.9 shows that target complex was successfully synthesised, with phen coordinated to the Mn(1) as a chelate, with both Mn(1)-N(1) and Mn(1)-N(2) bond lengths being 2.254(4) Å. Inspection of the crystal structure reveals that the calixarene carboxylate groups are coordinated to Mn(1) in a different fashion.

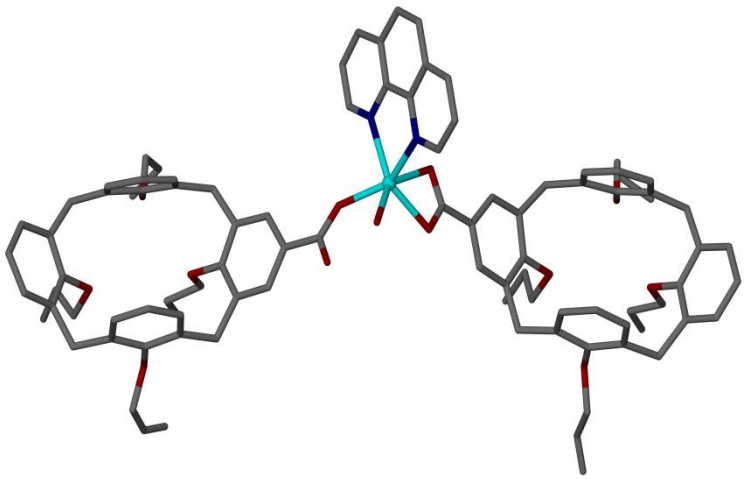

Figure 2.9 Discrete complex [Mn(**5a**)$_2$(phen)(H_2O)] (**12**). Dmf of crystallisation and hydrogen atoms omitted for clarity.

The carboxylate group comprising O(11)-C(83)-O(12) is coordinated to Mn(1) in a bidentate fashion with Mn(1)-O(11) and Mn(1)-O(12) distances of 2.347(3) Å and 2.155(3) Å respectively. The carboxylate group located on the second mono-*p*-CO_2[4], comprising atoms O(5)-C(42)-O(6), is coordinated to the Mn(1) in a monodentate fashion *via* O(5) with a bond length of 2.112(2) Å. The aquo ligand is coordinated to the metal ion *via* a Mn(1)-O(13) bond of a distance of 2.210(3) Å. Both mono-*p*-

CO_2[4]s adopt a pinched-cone conformation in the solid state as shown in Figure 2.9. This is frequently observed when utilising calixarenes possessing this 'synthesis-induced' conformation, and typically results in omission of any potential guest molecule from the restricted calixarene cavity. Symmetry expansion of the asymmetric unit shows that phens from two neighbouring discrete complexes are within a distance of 3.38 - 3.42 Å from each other (Figure 2.10), suggesting there is a π-stacking between them and affording a "non-covalent dimer". Further analysis also shows a presence of CH···π interactions between ligated phen and calixarene propyl hydrogen atoms from a neighbouring "non-covalent dimer", with C(40) hydrogen atoms and s.e. phen distances of 2.71 Å and 2.90 Å respectively. Analysis of the extended crystal structure reveals solvent channels running along the *a* axis of the unit cell (Fig. 2.11). Due to high disorder of the dmf of crystallisation they were removed with the routine SQUEEZE.[74] The presence of solvent channels occupied by co-crystallised dmf presented the possibility to explore de-solvation, solvent exchange and alternative guest storage. However, PXRD analysis revealed that single crystals lose crystallinity upon removal from the mother liquor / drying so subsequent analysis of gas sorption properties was abandoned.

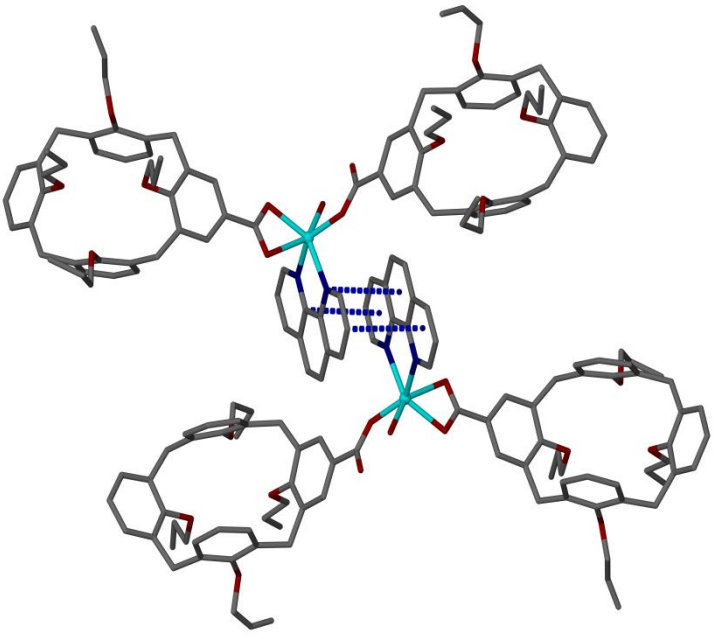

Figure 2.10 "Non-covalent dimer" with π-stacking between phens from two neighbouring discrete complexes of [Mn(**5a**)$_2$(phen)(H_2O)] (**12**) shown as dashed blue lines. Dmf of crystallisation and hydrogen atoms omitted for clarity.

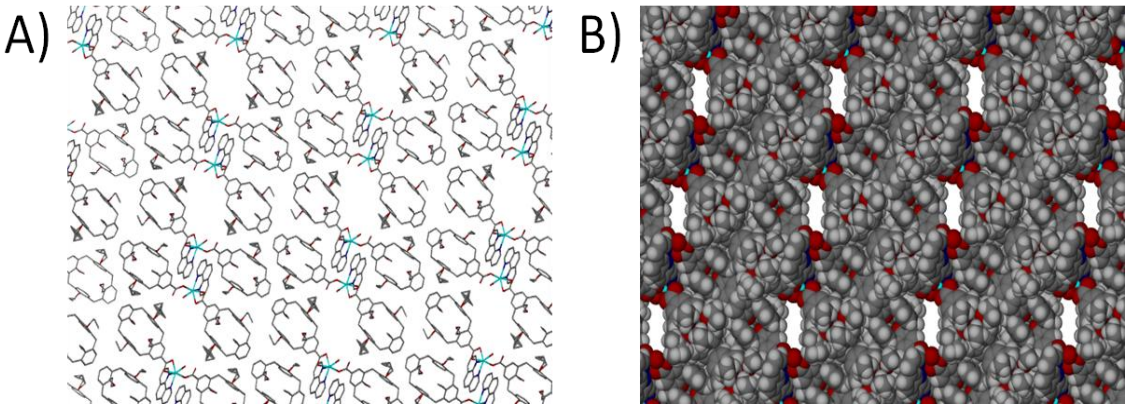

Figure 2.11 Ball and stick (A) and space filling (B) representations of solvent channels running along the axis *a* of the unit cell in [Mn(**5a**)$_2$(phen)(H$_2$O)] (**12**). Hydrogen atoms and dmf of crystallisation omitted for clarity.

A reaction carried out using the same conditions used to form **12**, but using Cd(II) in place of Mn(II) resulted in formation of diffraction quality single crystals of formula [Cd(**5a**)$_2$(phen)(dmf)]·(H$_2$O) (**13**) (Figure 2.12). The crystals of **13** are in a orthorhombic cell and the structure was solved in space group *Pbcn*. The unit cell parameters are a = 9.5285(10)Å, b = 18.7569(14)Å and c = 47.5290(4) Å which are markedly different to those of **12** (a = 9.6926(8) Å, b = 18.8194(17) Å and c = 24.9780(2) Å, and α = 77.167(4)º, β = 85.174(5)º and γ = 89.000(5)º). Structural analysis reveals formation of a discrete coordination complex, with the asymmetric unit containing one Cd(II) ion, calixarene **5a**, phen, dmf and one unbound water molecule. Due to symmetry phen, dmf and water molecule were all refined at half occupancy. The relative orientation of ligands around the Cd(II) ion in **13** was found to be markedly different to that observed in **12**. The complex comprises of one Cd(II) ion, one phen and two mono-*p*-CO$_2$[4]s, however dmf is coordinated to the metal centre in place of water. The carboxylate group comprising O(5)-C(29)-O(6) is coordinated to Cd(1) in a bidentate fashion with Cd(1)-O(5) and Cd(1)-O(6) distances of 2.379(3) Å and 2.365(4) Å respectively. As expected, phen is coordinated as a chelate with Cd(1)-N(45) and Cd(1)-N(55) bond lengths of 2.392(10) Å and 2.414(7) Å respectively. The dmf molecule is coordinated *via* the oxygen with a Cd(1)-O(7) bond length of 2.265(13) Å. The ligated mono-*p*-CO$_2$[4] adopts a pinched-cone conformation in the solid state, precluding a guest molecule from residing in the calixarene cavity, as shown in Figure

2.12. Analysis of the solid state packing in **13** showed that the relative positioning of discrete complexes with respect to each other is different to that found in **12**. The distance between phens from neighbouring complexes in **13**, being at distance of ~3.4 Å, is at the upper limit for π-stacking interactions.[75] In **13** there is significantly less overlap between phens from two neighbouring complexes compared to the overlap between phens from neighbouring complexes in **12**. The closest contact distance between propyl hydrogen atoms and phen is ~3.2 Å, indicating an absence of CH···π interactions in **13**. Extension of the asymmetric unit showed that the sold state packing in **13** is different to that observed in **12**, and results in an absence of solvent channels. Unfortunately further analysis was not carried out, as attempts to obtain a homogeneous crystalline product of **13** were unsuccessful.

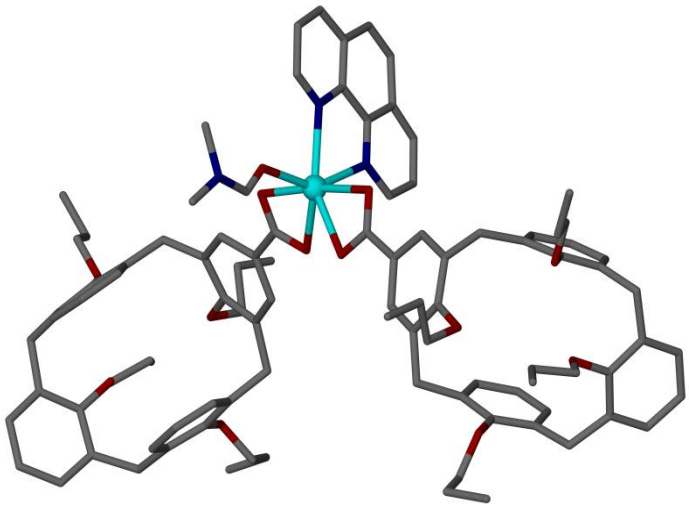

Figure 2.12 Discrete complex of [Cd(**5a**)$_2$(phen)(dmf)]·(H_2O) (**13**). Hydrogen atoms omitted for clarity.

To summarise this section, a discrete target complex (Fig. 2.8) was synthesised using mono-*p*-CO_2[4] **5a** in place of benzoate. These preliminary results showed that ligated phen can be highly beneficial when used as a co-ligand for these systems. It can be utilised to restrict the number of available coordination sites around the metal centre, ultimately helping to direct the binding of other ligands. Furthermore, thanks to its structural features, ligated phen can also participate in non-covalent interactions that help to stabilise self-assembly in the solid state.

2.3. Summary

Two target motifs / complexes were chosen from the CSD as potential candidates for the design and construction of supramolecular assemblies, one being a molecular panel and the other a discrete complex. This fundamental investigation, which focused on mono-*p*-CO_2[4]s proved that such functionalised calixarenes, with the help of carefully selected co-ligands, can be successfully utilised as building blocks in the construction of target architectures. The 1D CPs and discrete complexes synthesised here displayed a number of interesting features in the solid state that provide valuable insight for the remainder of this thesis. As such these features represent an excellent base / starting point for fine-tuning in the design and construction of a series of supramolecular assemblies.

2.4. Experimental

General experimental procedures and specifications of analytical instruments used are provided in Chapter 8.

2.4.1. Synthesis of compounds 1 - 13.

***p-tert*-Butylcalix[4]arene (1)** was synthesised according to literature procedure.[76] A solution of sodium hydroxide (0.6994 g, 17.5 mmol) dissolved in deionised water (5 mL) was added to *p-tert*-butylphenol (125.1 g, 832.8 mmol) and formaldehyde (37%, 76 mL) and the mixture was heated at reflux with stirring until a polymer formed. This mixture was then cooled to room temperature prior to the addition of toluene (500 mL) and diphenyl ether (1.0 L). The resulting mixture was heated until all toluene was removed, kept under reflux at 260ºC for 4 hours and left to cool to room temperature. Ethyl acetate (500 mL) was added and the solution stirred for 2 hours. A precipitate was collected by filtration and washed with ethyl acetate to afford 90.6 g of **1** as white crystals (yield 67%); **^{1}H NMR** (300MHz, $CDCl_3$) δ = 10.35 (s, 4 H, O<u>H</u>), 7.06 (s, 8 H, Ar<u>H</u>), 4.26 (d, *J* = 12.8 Hz, 4 H, Ar<u>C</u>H_2Ar), 3.50 (d, *J* = 11.7 Hz, 4 H, Ar<u>C</u>H_2Ar), 1.22 (s, 36 H, C(<u>C</u>H_3)$_3$).

Calix[4]arene (2) was synthesised according to literature procedure.[77] Phenol (3.785 g, 40.2 mmol) and **1** (25.0 g, 38.5 mmol) was dissolved in toluene (250 mL). Anhydrous aluminium chloride (50.7 g, 308.2 mmol) was added and the solution was stirred at room temperature under nitrogen for 3 hours. The reaction was quenched over an ice / DCM (220 mL) mixture and treated with 1M HCl (200 mL). The organic layer was separated, washed twice with deionised water and dried over $MgSO_4$. Solvent was removed under reduced pressure to afford a dark orange oily solution. Addition of diethyl ether caused precipitation of a solid which was filtered and washed with diethyl ether to give 10.57 g of **2** as pale yellow powder (yield 64%); **^{1}H NMR** (300MHz, $CDCl_3$) δ = 10.21 (s, 4 H, O<u>H</u>), 7.07 (d, *J* = 7.7 Hz, 8 H, Ar<u>H</u>), 6.83 - 6.59 (m, 4 H, Ar<u>H</u>), 4.27 (br. s., 4 H, Ar<u>CH$_2$</u>Ar), 3.57 (br. s., 4 H, Ar<u>CH$_2$</u>Ar).

Tetra-*O*-alkoxy-calix[4]arene (3a - c) was synthesised according to literature procedure.[78] Sodium hydride (60% mineral oil suspension, 1.60 g, 40.0 mmol) and **2** (2.00 g, 4.7 mmol) were dissolved in dimethylformamide (80 mL) and stirred for 10 minutes prior to the addition of the appropriate iodo-alkane (40.0 mmol). The mixture was then heated to 80ºC with stirring for 1 hours. The reaction was quenched with methanol and solvents were removed under reduced pressure. Residue was washed with deionised water and filtered. Recrystallisation from acetone gave **3a - c.**

Tetra-*O*-propoxy-calix[4]arene (3a) was obtained as white small crystals in a 92% yield; **^{1}H NMR** (300MHz, $CDCl_3$) δ = 6.64 - 6.54 (m, 12 H, Ar<u>H</u>), 4.46 (d, *J* = 13.6 Hz, 4 H, Ar<u>CH$_2$</u>Ar), 3.85 (t, *J* = 7.5 Hz, 8 H, O-<u>CH$_2$</u>-), 3.15 (d, *J* = 13.6 Hz, 4 H, Ar<u>CH$_2$</u>Ar), 1.93 (sxt, *J* = 7.5 Hz, 8 H, -<u>CH$_2$</u>-), 1.00 (t, *J* = 7.3 Hz, 12 H, -<u>CH$_3$</u>).

Tetra-*O*-butoxy-calix[4]arene (3b) was obtained as white crystals in a 76% yield; **^{1}H NMR** (300MHz, $CDCl_3$) δ = 6.64 - 6.54 (m, 12 H, Ar<u>H</u>), 4.46 (d, *J* = 13.6 Hz, 4 H, Ar<u>CH$_2$</u>Ar), 3.90 (t, *J* = 7.3 Hz, 8 H, -O-<u>CH$_2$</u>-), 3.15 (d, *J* = 13.2 Hz, 4 H, Ar<u>CH$_2$</u>Ar), 1.90 (quin, *J* = 7.5 Hz, 8 H, -<u>CH$_2$</u>-), 1.46 (sxt, *J* = 15.1 Hz, 8 H, -<u>CH$_2$</u>-CH$_3$), 1.00 (t, *J* = 7.3 Hz, 12 H, -<u>CH$_3$</u>).

Tetra-*O*-pentoxy-calix[4]arene (3c) was obtained as yellow oily residue in a 73% yield; **^{1}H NMR** (300MHz, $CDCl_3$) δ = 6.65 - 6.53 (m, 12 H, Ar<u>H</u>), 4.46 (d, *J* = 13.2 Hz,

4 H, Ar$\underline{CH_2}$Ar), 3.90 (t, *J* = 7.5 Hz, 8 H, -O-$\underline{CH_2}$-), 3.16 (d, *J* = 13.2 Hz, 4 H, Ar$\underline{CH_2}$Ar), 1.92 (quin, *J* = 7.2 Hz, 8 H, , -O-CH_2-$\underline{CH_2}$-), 1.46 (sxt, *J* = 15.1 Hz, 16 H, -$\underline{CH_2}$-$\underline{CH_2}$-CH_3), 0.95 (t, *J* = 7.3 Hz, 12 H, -$\underline{CH_3}$).

***p*-Monoformyl-tetra-*O*-alkoxy-calix[4]arene (4a - c)** was synthesised according to literature procedure.[79] The appropriate compound **3a - c** (0.98 mmol) was dissolved in dichloromethane (20.0 mL) and cooled to -10ºC. Dichloromethylmethylether (98 μL, 1.08 mmol) was added to the solution, followed by titanium tetrachloride (0.13 mL, 1.19 mmol). The resulting solution was stirred under nitrogen for 1 hour with temperature rising steadily from -10ºC to -5ºC. The reaction was quenched with deionised water (50 mL) and the organic layer was separated, washed with water and dried over Na_2SO_4. Following removal of solvent under reduced pressure, the residue was purified by column chromatography (SiO_2, 5% ethyl acetate/hexane) to give pale yellow solid.

***p*-Monoformyl-tetra-*O*-propoxy-calix[4]arene (4a)** was obtained as pale yellow solid in a 49% yield; **^{1}H NMR** (300MHz , $CDCl_3$) δ = 9.57 (s, 1 H, -CO-$\underline{H}$), 7.00 (s, 2 H, Ar-$\underline{H}$), 6.78 - 6.72 (m, 4 H, Ar-$\underline{H}$), 6.72 - 6.65 (m, 2 H, Ar-$\underline{H}$), 6.46 - 6.37 (m, 3 H, Ar-$\underline{H}$), 4.47 (t, *J* = 14.3 Hz, 4 H, Ar-$\underline{CH_2}$-Ar), 3.97 - 3.77 (m, 8 H, -O-$\underline{CH_2}$-), 3.23 (d, *J* = 13.6 Hz, 2 H, Ar-$\underline{CH_2}$-Ar), 3.16 (d, *J* = 13.2 Hz, 2 H, Ar-$\underline{CH_2}$-Ar), 1.99 - 1.85 (m, 8 H, -$\underline{CH_2}$-CH_3), 1.13 - 0.94 (m, 12 H, -$\underline{CH_3}$).

***p*-Monoformyl-tetra-*O*-butoxy-calix[4]arene (4b)** was obtained as pale yellow solid in a 57% yield; **^{1}H NMR** (300MHz , $CDCl_3$) δ = 9.57 (s, 1 H, -CO-$\underline{H}$), 7.01 (s, 2 H, Ar-$\underline{H}$), 6.78 - 6.72 (m, 4 H, Ar-$\underline{H}$), 6.71 - 6.64 (m, 2 H, Ar-$\underline{H}$), 6.48 - 6.36 (m, 3 H, Ar-$\underline{H}$), 4.46 (t, *J* = 14.3 Hz, 4 H, Ar-C$\underline{H_2}$-Ar), 4.02 - 3.80 (m, 8 H, -O-$\underline{CH_2}$-), 3.23 (d, *J* = 13.6 Hz, 2 H, Ar-C$\underline{H_2}$-Ar), 3.16 (d, *J* = 13.2 Hz, 2 H, Ar-C$\underline{H_2}$-Ar), 1.89 (quin, *J* = 7.7 Hz, 8 H, -CH_2-$\underline{CH_2}$- CH_2), 1.54 - 1.34 (m, 8 H-$\underline{CH_2}$-CH_3), 1.05 - 0.96 (m, 12 H, -$\underline{CH_3}$).

***p*-Monoformyl-tetra-*O*-pentoxy-calix[4]arene (4c)** was obtained as a yellow oil in a 49% yield; **^{1}H NMR** (300 MHz, $CDCl_3$) δ = 9.57 (s, 1 H, -CO-$\underline{H}$), 7.00 (s, 2 H, Ar-$\underline{H}$), 6.72 - 6.79 (m, 4 H, Ar-$\underline{H}$), 6.65 - 6.72 (m, 2 H, Ar-$\underline{H}$), 6.36 - 6.48 (m, 3 H, Ar-$\underline{H}$), 4.46 (t, *J*=14.12 Hz, 4 H, Ar-$\underline{CH_2}$-Ar), 3.78 - 4.03 (m, 8 H, -O-$\underline{CH_2}$-), 3.23 (d, *J* = 13.57 Hz,

2 H, Ar-$\underline{CH_2}$-Ar), 3.16 (d, *J* = 13.57 Hz, 2 H, Ar-$\underline{CH_2}$-Ar), 1.90 (quin, *J* = 7.34 Hz, 8 H, -O-CH_2-$\underline{CH_2}$-), 1.22 - 1.50 (m, 16 H, -$\underline{CH_2}$-$\underline{CH_2}$-CH_3), 0.85 - 1.00 (m, 12 H, -$\underline{CH_3}$).

***p*-Monocarboxylato-tetra-*O*-alkoxy-calix[4]arene (5a - c)** was synthesised according to an amended literature procedure.[79] Sulfamic acid (0.60 g, 6.2 mmol) dissolved in water (5 mL) and sodium chlorite (0.64 g, 5.8 mmol) dissolved in water (5 mL) were added to a solution of the appropriate aldehyde **4a - c** (0.58 mmol) in dichloromethane (10 mL) and acetone (30mL). The resulting solution was stirred at room temperature for 24 hours before organics were removed under reduced pressure. The resulting aqueous solution was then extracted with dichloromethane (3x15 mL). The organic layer was washed with deionised water (3x30 mL) and dried over anhydrous magnesium sulfate. Organics were evaporated under reduced pressure and the product was recrystallised from cold methanol to give **5a - c** as a white powder.

***p*-Monocarboxylato-tetra-*O*-propoxy-calix[4]arene (5a)** was obtained as a white powder in a 78% yield; **^{1}H NMR** (300MHz , $CDCl_3$) δ = 7.31 (s, 2 H, Ar-$\underline{H}$), 6.69 - 6.58 (m, 6 H, Ar-$\underline{H}$), 6.58 - 6.46 (m, 3 H, Ar-$\underline{H}$), 4.48 (d, *J* = 7.7 Hz, 2 H, Ar-$\underline{CH_2}$-Ar), 4.44 (d, *J* = 8.1 Hz, 2 H, Ar-$\underline{CH_2}$-Ar), 3.96 - 3.79 (m, 8 H, -O-$\underline{CH_2}$-), 3.21 (d, *J* = 13.9 Hz, 2 H, Ar-$\underline{CH_2}$-Ar), 3.16 (d, *J* = 13.6 Hz, 2 H, Ar-$\underline{CH_2}$-Ar), 2.00 - 1.82 (m, 8 H, -$\underline{CH_2}$-CH_3), 1.05 - 0.95 (m, 12 H, -$\underline{CH_3}$); **^{13}C{^{1}H} NMR** (75 MHz, $CDCl_3$) δ = 172.0, 161.6, 156.6, 156.5, 135.6, 135.4, 134.9, 134.4, 130.5, 128.6, 128.2, 128.1, 122.6, 122.2, 121.8, 30.9, 23.2, 10.3; **MS** *m/e* 579 (M - H^+).

***p*-Monocarboxylato-tetra-*O*-butoxy-calix[4]arene (5b)** was obtained as a white powder in a 71% yield; **^{1}H NMR** (300MHz , $CDCl_3$) δ = 7.32 (s, 2 H, Ar-$\underline{H}$), 6.69 - 6.59 (m, 6 H, Ar-$\underline{H}$), 6.58 - 6.47 (m, 3 H, Ar-$\underline{H}$), 4.48 (d, *J* = 7.7 Hz, 2 H, Ar-$\underline{CH_2}$-Ar), 4.43 (d, *J* = 7.7 Hz, 2 H, Ar-$\underline{CH_2}$-Ar), 4.01 - 3.83 (m, 8 H, -O-$\underline{CH_2}$-), 3.21 (d, *J* = 13.6 Hz, 2 H, Ar-$\underline{CH_2}$-Ar), 3.16 (d, *J* = 13.6 Hz, 2 H, Ar-$\underline{CH_2}$-Ar), 1.96 - 1.82 (m, 8 H,-CH_2-$\underline{CH_2}$-CH_2-), 1.54 - 1.37 (m, 8 H, -$\underline{CH_2}$-CH_3), 1.04 - 0.96 (m, 12 H, -$\underline{CH_3}$); **^{13}C{^{1}H} NMR** (75 MHz, $CDCl_3$) δ = 172.1, 161.7, 156.5, 135.6, 135.3, 135.2, 135.0, 134.4, 130.5, 128.6, 128.2, 128.1, 128.1, 122.6, 122.2, 121.8, 74.8, 32.32, 30.9, 19.3, 14.1, 14.0; **MS** *m/e* 691 (M - H^+).

***p*-Monocarboxylato-tetra-*O*-pentoxy-calix[4]arene (5c)** was obtained as a white powder in a 62% yield; **^{1}H NMR** (300MHz , $CDCl_3$) δ = 7.31 (s, 2 H, Ar-H), 6.68 - 6.59 (m, 6 H, Ar-H), 6.59 - 6.46 (m, 3 H, Ar-H), 4.47 (d, *J* = 7.3 Hz, 2 H, Ar-CH_2-Ar), 4.43 (d, *J* = 7.3 Hz, 2 H, Ar-CH_2-Ar), 4.00 - 3.83 (m, 8 H, -O-CH_2-), 3.21 (d, *J* = 13.9 Hz, 2 H, Ar-CH_2-Ar), 3.15 (d, *J* = 13.6 Hz, 2 H, Ar-CH_2-Ar), 1.98 - 1.83 (m, *J* = 6.6 Hz, 8 H, -O-CH_2-CH_2-CH_2-), 1.48 - 1.32 (m, *J* = 3.7 Hz, 16 H, -CH_2-CH_2-CH_3), 0.98 - 0.92 (m, 12 H, -CH_3); **^{13}C{^{1}H} NMR** (75 MHz, $CDCl_3$) δ = 171.5, 161.6, 156.5, 156.4, 135.6, 135.4, 135.0, 134.5, 130.4, 128.5, 128.2, 128.1, 122.5, 122.1, 121.8, 77.4, 77.0, 76.6, 75.1, 75.0, 30.9, 29.9, 28.3, 22.8, 22.7, 14.1; **MS** *m/e* 747 (M - H^+).

Synthesis of **6** - **13** was carried out according to a general procedure in which a dmf solution of a specific TM(II) ion and calixarene **5a** was carefully layerd with a methanolic solution of specific co-ligand. Clear solutions of **6** - **13** were left to evaporate over several weeks.

Synthesis of $[Co_2(5a)_4(bpy)_2]$·6dmf (6): A mixture of **5a** (50.1 mg, 0.076 mmol) and $Co(NO_3)_2.6H_2O$ (12.3 mg, 0.042 mmol) was dissolved in 2 mL of DMF, followed by layering of 1 ml of a MeOH solution of 4,4'-bipyridine (12.0 mg, 0.077 mmol). Slow evaporation over several weeks resulted in the formation of pink crystals suitable for X-ray diffraction studies, which were filtered, washed and dried to afford 26.0 mg of solid (20% yield). **EA** calc for $C_{202}H_{250}N_{10}O_{30}Co_2$, C, 71.02; H 7.38; N, 4.10%. Found C, 75.23; H, 7.24, N, 2.13%. **IR** ν_{max} 3215 cm^{-1} (OH), 2925 cm^{-1} and 2874 cm^{-1} (C-H), 1649 cm^{-1} (C=O), 1601 cm^{-1} (C-O), 1549 cm^{-1} (C-C), 1383 cm^{-1} (C-H), 725 cm^{-1} (C-H). PXRD analysis revealed that the material becomes amorphous upon removal from the mother liquor / drying, which is consistent with the discrepancy between theoretical and experimental results of elemental analysis.

Synthesis of $[Mn_2(5a)_4(bpy)_2]$·6dmf (7): An analogous procedure to **6** was used to synthesise **7** but with $Mn(NO_3)_2.6H_2O$ (7.6 mg, 0.042 mmol) in place of $Co(NO_3)_2.6H_2O$. Slow evaporation over several weeks resulted in the formation of pale yellow crystals suitable for X-ray diffraction studies which were filtered, washed and dried to afford 23.3 mg of solid (18% yield). **EA** calc for $C_{202}H_{250}N_{10}O_{30}Mn_2$, C, 71.19; H, 7.39; N, 4.11%. Found C, 74.32; H, 7.26; N, 1.99%. **IR** ν_{max} 3225 cm^{-1} (OH), 2937 cm^{-1} and 2879 cm^{-1} (C-H), 1666 cm^{-1} (C=O), 1617 cm^{-1} (C-O), 1551 cm^{-1} (C-C), 1393

cm^{-1} (C-H), 731 cm^{-1} (C-H).). PXRD analysis revealed that the material becomes amorphous upon removal from the mother liquor / drying, which is consistent with the discrepancy between theoretical and experimental results of elemental analysis.

Synthesis of $[Cd_2(5a)_4(bpy)_2]\cdot 6dmf$ (8): An analogous procedure to **6** was used to synthesise **8** but with $Cd(NO_3)_2.6H_2O$ (13.0 mg, 0.042 mmol) in place of $Co(NO_3)_2.6H_2O$. Slow evaporation over several weeks resulted in the formation of colourless crystals suitable for X-ray diffraction studies which were filtered, washed and dried to afford 27.3 mg of solid (21% yield). **EA** calc for $C_{202}H_{250}N_{10}O_{30}Cd_2$, C, 68.87; H, 7.15; N, 3.98%. Found C, 71.59; H, 6.70; N, 1.72%. **IR** ν_{max} 3211 cm^{-1} (OH), 2945 cm^{-1} and 2855 cm^{-1} (C-H), 1651 cm^{-1} (C=O), 1623 cm^{-1} (C-O), 1567 cm^{-1} (C-C), 1391 cm^{-1} (C-H), 717 cm^{-1} (C-H). Single crystals of **8** were poorly diffracting and only partial structure solution was possible. The unit cell parameters of **8**: a = 11.356(4), b = 15.621(3), c = 27.461(5) Å, α = 89.173(3), β = 80.612(3), γ = 80.169(3)°, V = 4782.8(4) $Å^3$.). PXRD analysis revealed that the material becomes amorphous upon removal from the mother liquor / drying, which is consistent with the discrepancy between theoretical and experimental results of elemental analysis.

Synthesis of $[Co_2(5a)_4(bpa)_2]\cdot 8dmf$ (9): An analogous procedure to **6** was used to synthesise **9** but with 4,4'-bpyridylethane (12.0 mg, 0.077 mmol) in place of 4,4'-bipyridine. Slow evaporation over several weeks resulted in the formation of pink crystals suitable for X-ray diffraction studies which were filtered, washed and dried to afford 19.3 mg of solid (15% yield). **EA** calc for $C_{212}H_{272}N_{12}O_{32}Co_2$, C, 70.37; H, 7.58; N, 4.65%. Found C, 74.41; H, 7.12; N, 1.83%. **IR** ν_{max} 3251 cm^{-1} (OH), 2951 cm^{-1} and 2884 cm^{-1} (C-H), 1659 cm^{-1} (C=O), 1632 cm^{-1} (C-O), 1564 cm^{-1} (C-C), 1387 cm^{-1} (C-H), 722 cm^{-1} (C-H).). PXRD analysis revealed that the material becomes amorphous upon removal from the mother liquor / drying, which is consistent with the discrepancy between theoretical and experimental results of elemental analysis.

Synthesis of $[Cd_2(5a)_4(bpa)_2]\cdot 8dmf$ (10): An analogous procedure to **8** was used but with 4,4'-bipyridylethane (12.0 mg, 0.077 mmol) in place of 4,4'-bipyridine. Slow evaporation over several weeks resulted in the formation of colourless crystals suitable for X-ray diffraction studies, which were filtered, washed and dried to afford 22.1 mg of solid (17% yield). **EA** calc for $C_{212}H_{272}N_{12}O_{32}Cd_2$, C, 68.35; H, 7.36; N, 4.51%. Found

C, 71.81; H, 6.99; N, 1.84%. **IR** ν_{max} 3241 cm^{-1} (OH), 2947 cm^{-1} (C-H), 1642 cm^{-1} (C=O), 1611 cm^{-1} (C-O), 1528 cm^{-1} (C-C), 1377 cm^{-1} (C-H), 729 cm^{-1} (C-H). Single crystals of **10** were poorly diffracting and only partial structure solution was possible. Unit cell parameters for **10**: a = 12.949(4), b = 13.786(4), c = 27.997(9) Å, α = 92.116(4), β = 96.737(5), γ = 100.031(5)°, V = 4879.1(1) $Å^3$.). PXRD analysis revealed that the material becomes amorphous upon removal from the mother liquor / drying, which is consistent with the discrepancy between theoretical and experimental results of elemental analysis.

Synthesis of $[Co_2(5a)_4(bpe)_2]$·8dmf (11): An analogous procedure to **6** was used but with 4,4'-bpyridylethene (13.7 mg, 0.075 mmol) in place of 4,4'-bpyridine. Slow evaporation over several weeks resulted in the formation of pink crystals suitable for X-ray diffraction studies, which were filtered, washed and dried to afford 32.5 mg of solid (25% yield). **EA** calc for $C_{212}H_{268}N_{12}O_{32}Co_2$, C, 70.45; H, 7.47; N, 4.65%. Found C, 71.81; H, 6.99; N, 1.84%. **IR** ν_{max} 3226 cm^{-1} (OH), 2902 cm^{-1} (C-H), 1639 cm^{-1} (C=O), 1611 cm^{-1} (C-O), 1548 cm^{-1} (C-C), 1382 cm^{-1} (C-H), 1074 cm^{-1} (C-O), 724 cm^{-1} (C-H). PXRD analysis revealed that the material becomes amorphous upon removal from the mother liquor / drying, which is consistent with the discrepancy between theoretical and experimental results of elemental analysis.

Synthesis of $[Mn(5a)_2(phen)(H_2O)]$ (12): A mixture of **5a** (49.9 mg, 0.076 mmol) and $Mn(NO_3)_2.H_2O$ (14.8 mg, 0.083 mmol) was dissolved in 2 mL of DMF, followed by layering of 1 ml of a MeOH solution of 1,10-phenanthroline (14.2 mg, 0.079 mmol). Slow evaporation of the solvents over several weeks resulted in the formation of pale yellow crystals suitable for X-ray diffraction studies which were filtered, washed and dried to afford 40.6 mg of solid (35% yield). **EA** calc for $C_{94}H_{106}N_2O_{13}Mn_1$, C, 73.95; H, 7.00; N, 1.83%. Found C, 74.87 : 6.91 : 1.82 %. **IR** ν_{max} 3267 cm^{-1} (OH), 2979 cm^{-1} and 2953 cm^{-1} (C-H), 1655 cm^{-1} (C=O), 1602 cm^{-1} (C-O), 1543 cm^{-1} (C-C), 1362 cm^{-1} and 1338 cm^{-1} (C-H), 1117 cm^{-1} and 1100 cm^{-1} (C-O), 709 cm^{-1} (C-H).). PXRD analysis revealed that the material becomes amorphous upon removal from the mother liquor / drying, which is consistent with the discrepancy between theoretical and experimental results of elemental analysis.

Synthesis of [Cd(5a)$_2$(phen)(dmf)]·(H$_2$O) (13): An analogous procedure to **12** was used but with Cd(NO$_3$)$_2$.4H$_2$O (23.0 mg, 0.075 mmol) in place of Mn(NO$_3$)$_2$.H$_2$O. Slow evaporation of the solvents over several weeks resulted in the formation of colourless crystals suitable for X-ray diffraction studies, which were filtered, washed and dried to afford 36.1 mg of solid (29% yield). **EA** calc for $C_{94}H_{106}N_2O_{13}Cd_1$, C, 71.07; H, 6.82; N, 2.56%. Found C, 71.93; H, 6.79; N, 1.84%. **IR** ν_{max} 3200 cm^{-1} (OH), 2968 cm^{-1} and 2947 cm^{-1} (C-H), 1650 cm^{-1} (C=O), 1599 cm^{-1} (C-O), 1515 cm^{-1} (C-C), 1375 cm^{-1} and 1349 cm^{-1} (C-H), 1200 cm^{-1} and 1158 cm^{-1} (C-O), 726 cm^{-1} (C-H).). PXRD analysis revealed that the material becomes amorphous upon removal from the mother liquor / drying, which is consistent with the discrepancy between theoretical and experimental results of elemental analysis.

2.4.2. Crystallographic tables for compounds 6 - 13

Complex number	**6**	**7**	**9**
Formula	$C_{101}H_{125}N_5O_{15}Co_1$	$C_{101}H_{125}N_5O_{15}Mn_1$	$C_{106}H_{134}N_6O_{16}Co_1$
*M*r	1708.08	1704.07	1807.12
Crystal system	*P*-1	*P*-1	*P*-1
Space group	Triclinic	Triclinic	Triclinic
T/K	100(2)	100(2)	100(2)
a /Å	11.298(2)	11.4976(13)	13.0333(8)
b /Å	15.849(3)	15.6590(17)	13.5524(7)
c /Å	27.416(5)	27.5020(3)	27.8507(18)
α / ^{o}	89.235(3)	89.205(2)	92.526(4)
β / ^{o}	80.416(3)	80.631(2)	95.448(4)
γ /^{o}	80.184(3)	80.179(2)	99.997(4)
U /Å^3	4769.2(15)	4813.4(9)	4813.6(5)
Z	2	2	2
F(000)	1662	1909	1934
D_c / g cm^{-3}	1.086	1.236	1.247
μ / mm^{-1}	0.237	0.205	0.247
$2\Theta_{max}$ / ^{o}	51.0	52.9	46.5
Data collected	40803	44795	56245
Unique reflections	13695	15282	13735
R_{int}	0.0874	0.0602	0.1234
Obs data ($I > 2\sigma > (I)$)	9588	11063	7559
Parameters	1071	1209	1209
Restraints	193	0	0
R_1 (observed data)	0.0848	0.0972	0.0633
ωR_2 (all data)	0.2226	0.2712	0.1571
GooF	1.226	1.027	0.949
Max/min residuals [eÅ^3]	0.714 / -0.425	0.767 / -0.539	0.763 / -0.419

Complex number	**11**	**12**	**13**
Formula	$C_{106}H_{132}N_6O_{16}Co_1$	$C_{94}H_{104}N_2O_{13}Mn_1$	$C_{97}H_{111}N_3O_{13}Cd_1$
*M*r	1805.11	1524.73	1653.27
Crystal system	*P*-1	*P*-1	*Pbcn*
Space group	Triclinic	Triclinic	Orthorhombic
T/K	100(2)	100(2)	100(2)
a /Å	12.9816(18)	9.6926(8)	9.5285(10)
b /Å	13.5780(2)	18.8194(17)	18.7569(14)
c /Å	27.7690(4)	24.9780(2)	47.5290(4)
α / ^{o}	93.021(4)	77.167(4)	90.00
β / ^{o}	95.356(4)	85.174(5)	90.00
γ /^{o}	99.997(4)	89.000(5)	90.00
U /Å^3	4787.7(13)	4426.7(6)	8494.7(13)
Z	2	2	4
F(000)	1930	1622	3488
D_c / g cm^{-3}	1.252	1.144	1.293
μ / mm^{-1}	0.249	0.209	0.324
$2\Theta_{max}$ / ^{o}	41.9	54.3	54.5
Data collected	36329	41840	39312
Unique reflections	10021	12763	9402
R_{int}	0.1409	0.0716	0.1346
Obs data ($I > 2\sigma > (I)$	5160	6937	4221
Parameters	1141	1078	505
Restraints	22	342	31
R_1 (observed data)	0.0730	0.0595	0.0549
ωR_2 (all data)	0.1599	0.1362	0.1132
GooF	0.984	0.905	0.840
Max/min residuals [eÅ^3]	0.566 / -0.367	0.656 / -0.395	1.148 / -1.051

2.5. References

[1] F. H. Allen, in *Acta Crystallogr.*, **2002**, *B58*, 380.

[2] M. Eddaoudi, J. Kim, N. Rosi, D. Vodak, J. Wachter, M. O'Keeffe and O. M. Yaghi, *Science*, **2002**, *295*, 469.

[3] J. L. C. Rowsell and O. M. Yaghi, *Angew. Chem. Int. Ed.*, **2005**, *44*, 4670.

[4] T. R. Cook, Y.-R. Zheng and P. J. Stang, *Chem. Rev.*, **2012**, *113*, 734.

[5] S. Kennedy, G. Karotsis, C. M. Beavers, S. J. Teat, E. K. Brechin and S. J. Dalgarno, *Angew. Chem., Int. Ed.*, **2010**, *49*, 4205.

[6] E. Y. Choi and Y.-U. Kwon, *Inorg. Chem. Commun.*, **2004**, *7*, 942.

[7] L. Liu, Z. Li, B. Wang, G. Li, L. Wang, X. Meng and Z. He, *Cryst. Growth & Des.*, **2009**, *9*, 5244.

[8] L.-F. Ma, L.-Y. Wang, Y.-Y. Wang, S. R. Batten and J.-G. Wang, *Inorg. Chem.*, **2008**, *48*, 915.

[9] S. Fletcher and A. D. Hamilton, *Curr. Opin. Chem. Biol.*, **2005**, *9*, 632.

[10] P. P. Cholewa, C. M. Beavers, S. J. Teat and S. J. Dalgarno, *Cryst. Growth & Des.*, **2013**, *13*, 2703.

[11] S. Kennedy, C. M. Beavers, S. J. Teat and S. J. Dalgarno, *Cryst. Growth & Des.*, **2011**, *12*, 679.

[12] P. J. Nichols, C. L. Raston and J. W. Steed, *Chem. Commun.*, **2001**, 1062.

[13] J. L. Atwood, L. J. Barbour and A. Jerga, *Angew. Chem. Int. Ed.*, **2004**, *43*, 2948.

[14] J. L. Atwood, L. J. Barbour, P. K. Thallapally and T. B. Wirsig, *Chem. Commun.*, **2005**, 51.

[15] G. M. J. Schmidt, *Pure Appl. Chem.*, **1971**, *27*, 647.

[16] A. Bencini and V. Lippolis, *Coord. Chem. Rev.*, **2010**, *254*, 2096.

[17] K.-L. Zhang, H.-Y. Gao, Z.-C. Pan, W. Liang and G.W. Diao, *Polyhedron*, **2007**, *26*, 5177.

[18] H. Wang, K. Wang, D. Sun, Z.-H. Ni and J. Jiang, *Cryst. Eng. Comm.*, **2011**, *13*, 279.

[19] A. Spek, *Acta Crystallogr. Sect. D*, **2009**, *65*, 148.

[20] C. A. Hunter and J. K. M. Sanders, *J. Am. Chem. Soc.*, **1990**, *112*, 5525.

[21] A. Ninagawa and H. Matsuda, *Makromol. Chem., Rapid Commun.*, **1982**, *3*, 65.

[22] D. R. Stewart and C. D. Gutsche, *J. Am. Chem. Soc.*, **1999**, *121*, 4136.

[23] C. D. Gutsche, J. S. Rogers, D. Stewart and K. A. See, *Pure Appl. Chem.*, **1990**, *62*, 485.

[24] L. Qing and A. D. Hamilton, *C. R. Chimie*, **2002**, *5*, 441.

Chapter 3. Di-*p*-carboxylatocalix[4]arene as a di-topic linker in the formation of coordination polymers

In Chapter 2 it was shown how with the use of mono-*p*-CO_2[4], a mono-topic ligand, it is possible to synthesise a molecular panel based on a binuclear metal cluster and construct 1-D CPs with di-topic bipyridyls acting as linkers. It was also shown how the "directional bonding approach" could be used to construct a discrete complex using a) phen to restrict the number of available binding sites around the metal centre and b) mono-*p*-CO_2[4] as a co-ligand. Successful syntheses of two target motifs have encouraged further investigation of *p*-carboxylatocalix[4]arene as potential candidates for the design and construction of various multi-dimensional supramolecular assemblies.

When using a "directional bonding approach", depending on the desired dimensionality of the structure one wants to obtain, it is very important to carefully choose / pre-organise a metal complex which will act as a node in the target network. The second key component is the ligand which acts as a linker between the metal centres / nodes; there is therefore a necessary requirement of the ligand to be at least di-topic. Furthermore, when designing 3D CPs or PMs the choice of the ligand / linker has to be made carefully, as its shape will strongly influence the structural features of the material synthesised. Given the cavity-containing shape calix[4]arene possess and the relative ease with which one can functionalise its framework, di-*p*-carboxylatocalix[4]arene was chosen as a suitable candidate to be utilised as a di-topic linker for design and construction of 1-3D CPs. In this chapter results from the investigation into the use of di-*p*-carboxylatocalix[4]arene as a di-topic linker for the construction of metal-based 1-D multi-component assemblies will be discussed.

3.1. Design strategies for linear coordination polymers

Analysis of the extended structure of [Mn(**5a**)$_2$(phen)(H$_2$O)] (**12**) (Chapter 2.2.1) revealed an interesting feature in the solid state packing of discrete complexes in the -1 1 0 plane, that being a near linear alignment of neighbouring complexes. In each mono-*p*-CO$_2$[4] the unsubstituted arene distal to the carboxylate containing arene faces an symmetry equivalent (s.e.) unsubstituted arene from neighbouring complex, as shown in Figure 3.1. The arrangement of discrete complexes in **12** suggest that, by introducing a carboxylic group to the arene distal to the carboxylic group containing arene, and maintaining the relative orientation of neighbouring complexes, one could potentially construct a linear CP assembled from di-*p*-carboxylatocalixarene (di-*p*-CO$_2$[4]), with the TM acting as node and the di-*p*-CO$_2$[4] acting as a di-topic linker. Analysis of **12** also reveals that coordinated phen, apart from restricting the number of binding cites around the metal centre, is also involved in non-covalent interactions which contribute to self-assembly. As a result, the scope of this investigation was expanded to study whether these non-covalent interactions were essential for these complexes to self-assemble in such a manner, and what effect their disruption would have on the overall assembly. In summary, due to all of the structural features exhibited by **12**, it was decided that it would be an excellent starting point to further fine-tune the design strategy of coordination polymers by substituting di-*p*-CO$_2$[4]s for mono-*p*-CO$_2$[4] building blocks.

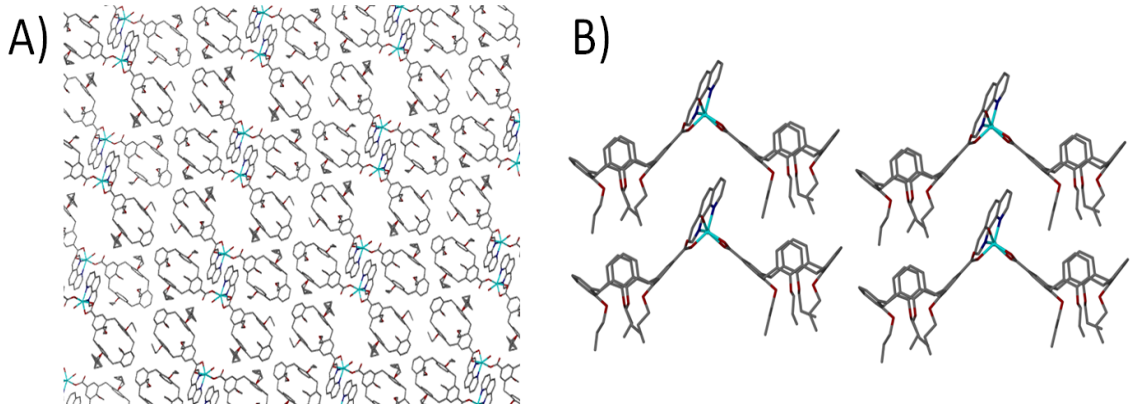

Figure 3.1 (A) Extended structure showing the linear alignment of discrete complexes of **12**. (B) Side view of aligned complexes in the extended structure of **12**. Hydrogen atoms and solvent molecules omitted for clarity.

3.1.1. Synthesis of di-p-carboxylatocalix[4]arene

The investigation began by synthesising a series of di-*p*-CO_2[4]s. The primary aim was to synthesise di-*p*-CO_2[4]s containing four alkoxy chains at the lower-rim, however despite reported literature procedures, it was not possible to isolate an isomerically pure material.[80, 81] Lately it was reported that during the di-formylation step of a tetra-*O*-alkoxy-calix[4]arene, formation of both diametrical (1,3) and proximal (1,2) isomers occurs and that their separation using chromatographic methods is very difficult.[82] Instead, a series of di-*p*-carboxylato-di-*O*-alkoxy-calix[4]arenes (**16a - c**) were synthesised according to literature procedure as shown in Figure 3.2.[80] The reason our attention focused on di-*p*-CO_2[4]s containing two alkyl chains and two hydroxyl groups at the lower-rim was that the di-formylation of a di-alkoxy-calix[4]arene yields an isomerically pure product. The selectivity of the di-formylation step can be attributed to the stoichiometric control and varying reactivity of *para* positions throughout the calixarene framework. The difference in such reactivity is caused by the alkoxy chains present at the lower-rim, which deactivate the *para* positions of the alkylated arenes towards electrophilic aromatic substitution. In contrast the lower-rim hydroxyl groups are strongly activating. As a result mainly arenes containing hydroxyl substituents undergo formylation and the desired isomer (diametrical) can be readily isolated using trituration methods. The resulting di-*p*-CO_2[4]s maintain a cone conformation due to the hydrogen bonding interactions present at the lower-rim, but as a result of the lower-rim di-alkylation the macrocycles adopt a C_2 rather than C_4 symmetry. Nevertheless the cavity remains open, with all four arenes splayed away from the calixarene annulus. Di-*p*-CO_2[4]s with methyl and ethyl chains were not considered due to their poor solubility.

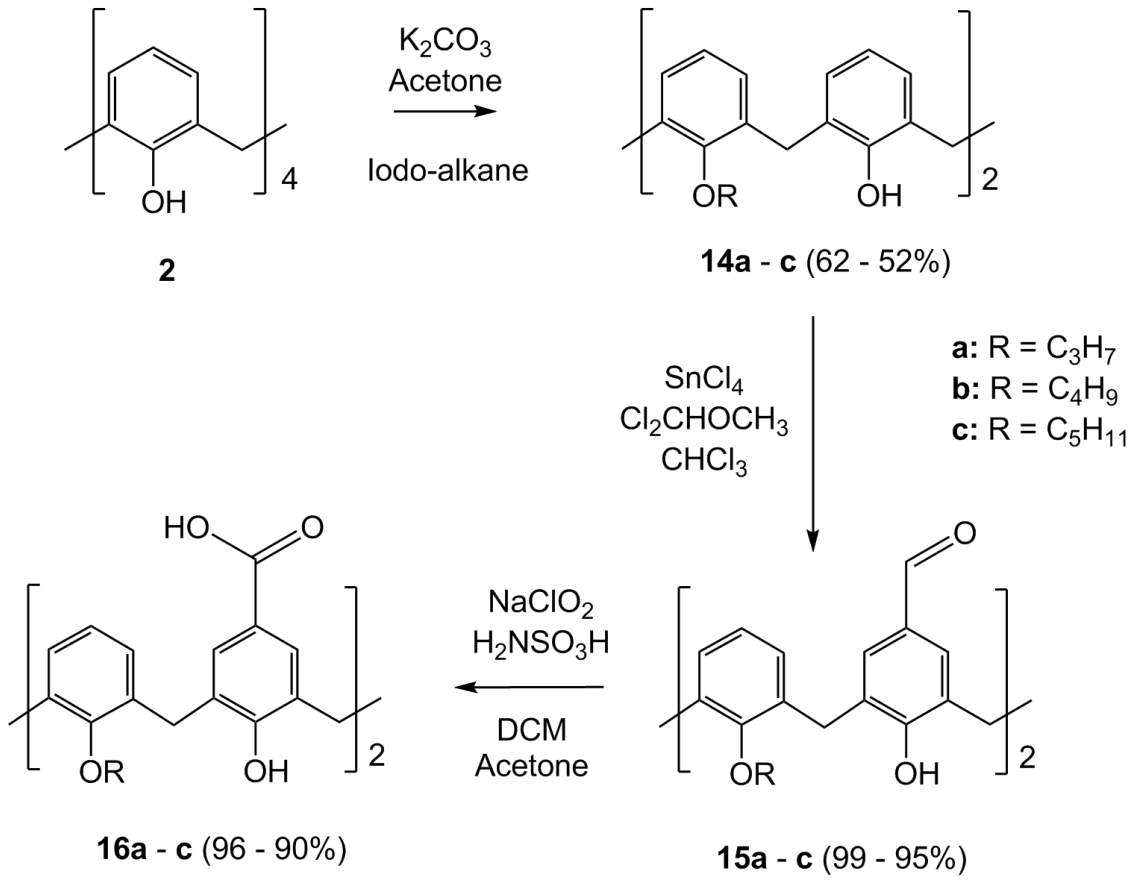

Figure 3.2 Schematic of the synthesis of di-*p*-carboxylatocalix[4]arenes **16a - c.**

3.2. Assembly of linear CPs

One of the main challenges in this part of the investigation was to reproduce structural features exhibited by **12**, but using a calixarene containing two carboxylic acid groups and that adopts a partially pinched-cone conformation. As a result of synthetic issues discussed in section 3.1.1, di-*p*-CO_2[4]s utilised contained only two alkyl chains introduced to the lower-rim, that in turn decreased the macrocycle solubility even further. However, solubility tests revealed that calixarenes **16a - c** remain soluble in dmf, which was the solvent used to synthesise **12**.

After synthesising a series of di-*p*-CO_2[4]s (**16a - c**) ambient reactions were carrying out in which dmf solutions containing a TM(II) ion (Co, Mn, Cu, Ni, Cd, Zn or Ni) and di-*p*-CO_2[4] were layered with a methanolic solution of phen. Clear solutions were left to slowly evaporate over a period of time which varied from several weeks to several months to yield crystalline materials suitable for SCXRD analysis. None of the reactions involving **16c** afforded single crystals suitable for structural analysis. The

series of results obtained when using di-*p*-CO_2[4]s **16a - b** reveal that some of the synthesised materials exhibit markedly different solid-state structural features. In order to maintain a logical flow in results presented, this chapter will be focused on materials comprising 1-D structures. The rest of results obtained using di-*p*-CO_2[4]s as a di-topic linker will be discussed in Chapter 6.

The first crystalline product isolated was pale pink single crystals of [Co(**16a**)phen(H_2O)]·dmf (**17**). Structural analysis revealed formation of the desired target motif (Fig. 2.8, similar to the motif adopted by **12**) with both carboxylate groups coordinated to the metal centres, leading to the formation of a linear 1-D CP as shown in Figure 3.3. The crystals of **17** are in a triclinic cell and structure was solved in the space group *P*-1. The unit cell parameters are a = 10.4507(3) Å, b = 14.6043(5) Å and c = 15.6549(5) Å, and α = 100.820(2)º, β = 106.867(3)º and γ = 96.430(2)º. The asymmetric unit contains one Co(II) ion, one di-*p*-CO_2[4] **16a**, one phen, one aquo ligand and one uncoordinated dmf of crystallisation. The coordination complex formed comprises two di-*p*-CO_2[4]s**,** each coordinated to Co(1) *via* one of the carboxylate groups: the O(6)-C(29)-O(5) group is coordinated in a monodentate fashion *via* O(6) and s.e. O(7)'-C(30)'-O(8)' carboxylate group is bonded in a bidentate fashion with bond lengths of 2.0092(6) Å, 2.1683(7) Å and 2.1776(7) Å respectively. The aquo ligand is coordinated to the metal centre *via* the Co(1)-O(9) bond (2.0800(6) Å).

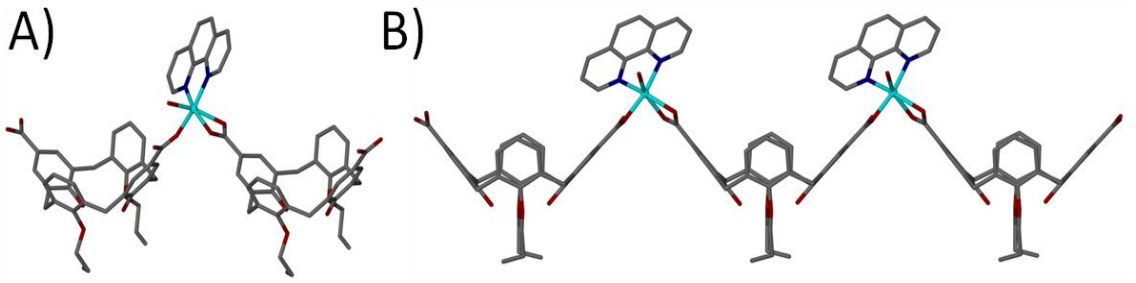

Figure 3.3 (A) Ball and stick representation of the coordination complex formed in **17** showing two different binding modes exhibited by carboxylate groups. (B) Extended structure in **17** showing linear CP chain. Hydrogen atoms and dmf of crystallisation omitted for clarity.

As expected phen is coordinated as a chelate, restricting space around the metal centre with Co(1)-N(1) and Co(1)-N(2) distances of 2.1051(7) Å and 2.1235(7) Å respectively. Symmetry expansion reveals that the phen is involved in π-stacking with s.e. phen molecules from a neighbouring CP, however the closest contact distance of 3.42 Å suggests that the interactions are relatively weak (Fig 3.4A).[75] Further analysis shows that the dmf of crystallisation is residing in the calixarene cavity. Inspection of the distances between hydrogen atoms H(62A) and H(62B) of dmf of crystallisation and the aryl rings of the calixarene, which are 2.57 Å and 2.78 Å, indicate host-guest CH···π interactions (Fig. 3.4B).[68] The di-*p*-CO_2[4] adopts the expected partially pinched-cone conformation with narrow (ε) and wide (δ) cone angles of ~89° and ~109° respectively (measured between *para* carbon atoms of distal calixarene aryl rings and a centroid generated from phenolic oxygen atoms). Analysis of the extended crystal structure shows linear CPs interweave to form bi-layer arrays. The solid state packing observed in **17** results in a structure lacking solvent channels as shown in Figure 3.5.

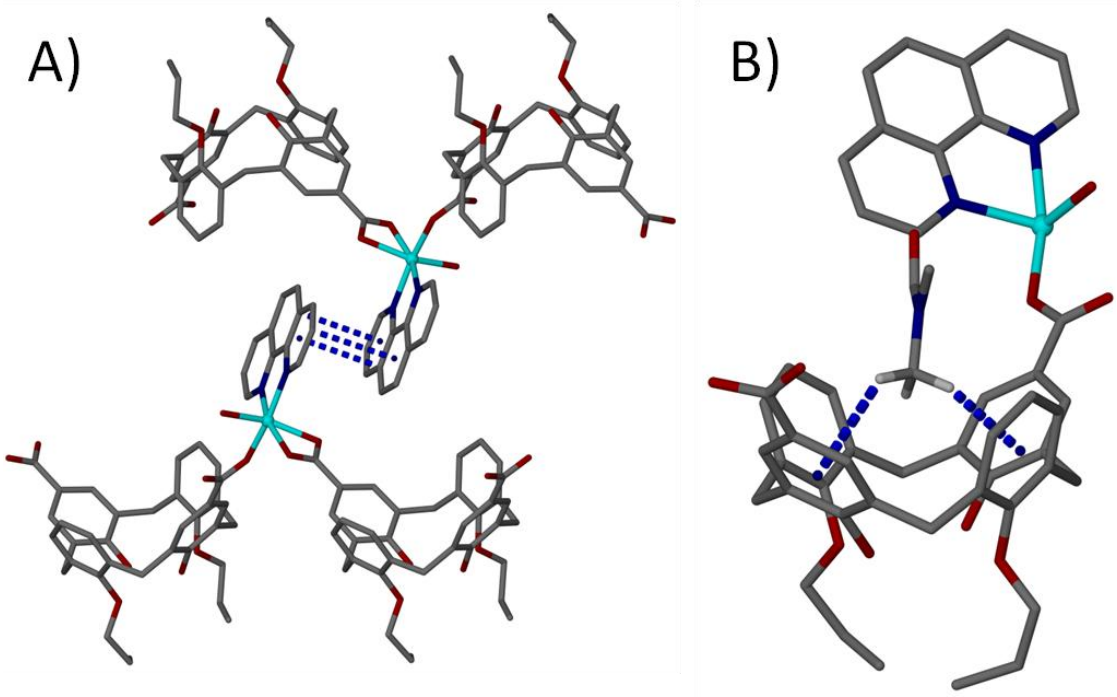

Figure 3.4 Ball and stick representation of non-covalent interactions observed in **17**: (A) π-stacking between phens from neighbouring CPs and (B) CH···π interactions between dmf hydrogen atoms and two aryl rings of di-*p*-CO_2[4] **16a**. Hydrogen atoms, except those involved in CH···π interactions, and dmf of crystallisation omitted for clarity.

However, due to the inherent cavity of the di-*p*-CO_2[4] the structure contains solvent pockets. Being interested in de-solvation of these solvent pockets, as well as the associated sorption properties of the material, the crystalline solid was filtered and dried in air. Subsequent PXRD experiments show that the material becomes amorphous upon removal from mother liquor / drying. As a result of this further analysis of the sorption properties of the synthesised material was not carried out.

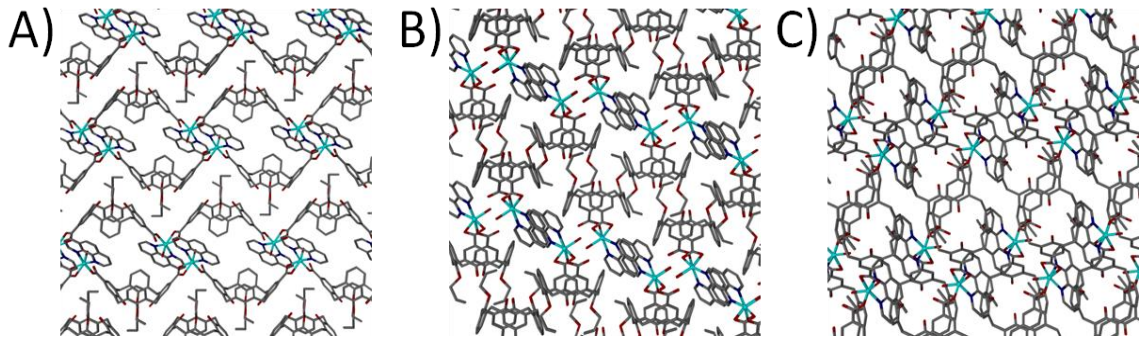

Figure 3.5 Ball and stick representation of solid state packing in **17** showing view along three unit cell axes: (A) *a* axis, (B) *b* axis and (C) *c* axis. Hydrogen atoms and dmf of crystallisation omitted for clarity.

The same reaction procedure, using Cd(II) in place of Co(II), resulted in colourless blocks of [Cd(**16a**)(phen)(dmf)]·(dmf)$(H_2O)_2$ (**18**) that were suitable for diffraction studies. The crystals of **18** are in a triclinic cell and structure was solved in space group *P*-1. The unit cell parameters in **18** (a = 10.918(3) Å, b = 14.334(4) Å and c = 18.082(5) Å, and α = 102.665(4)º, β = 106.769(3)º and γ = 104.641(3)º) are marginally different to the ones observed in **17**, however formation of a 1-D linear CP chain is also observed (Fig. 3.6). The asymmetric unit contains a coordination complex comprising one Cd(II), one di-*p*-CO_2[4] **16a**, one phen and one dmf. The asymmetric unit also contains uncoordinated one disordered dmf of crystallisation and two disordered water molecules. A notable difference observed in **18** compared to **17** is that both carboxylate moieties are coordinated to the metal centre in a bidentate fashion, with Cd(1)-O(5), Cd(1)-O(6), Cd(1)-O(7)' and Cd(1)-O(8)' bond lengths of 2.365(4) Å, 2.398(3) Å, 2.434(5) Å and 2.376(5) Å respectively. Phen is coordinated in an anticipated fashion with Cd(1)-N(1) and Cd(1)-N(2) distances of 2.386(4) Å and 2.393(4) Å respectively.

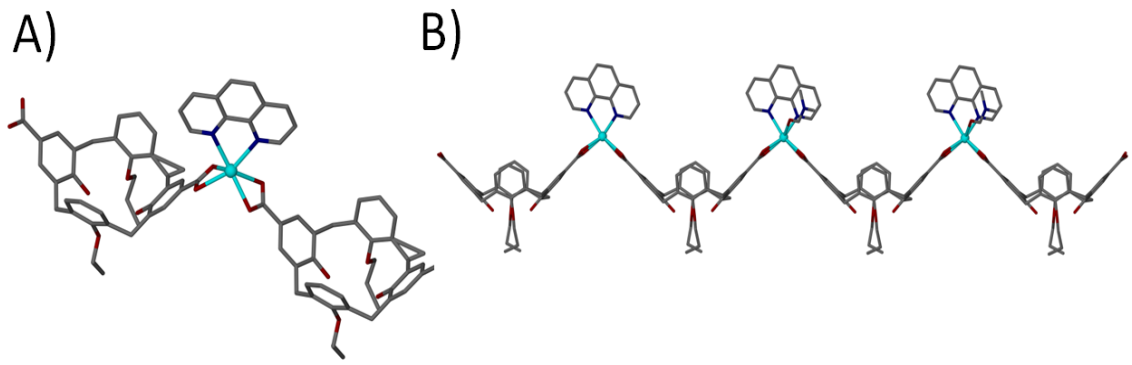

Figure 3.6 (A) Ball and stick representation of the coordination complex formed in **18**. (B) Assembled 1-D linear CP chain in **18**. Dmf of crystallisation, hydrogen atoms and ligated solvent molecules omitted for clarity.

The dmf is coordinated to the Cd(1) *via* oxygen atom with bond length of 2.341(4) Å. The di-*p*-CO_2[4] adopts the expected partially pinched-cone conformation with narrow and wide cone angles of ~88° and ~113° respectively. Extension of the asymmetric unit in **18** reveals further differences in the solid state packing compared to **17**. The calixarene cavity is no longer occupied by dmf but rather by a s.e. phen ligand from a neighbouring CP, with the two CPs knitted together through two crystallographically unique host-guest CH···π interactions (Fig. 3.7).

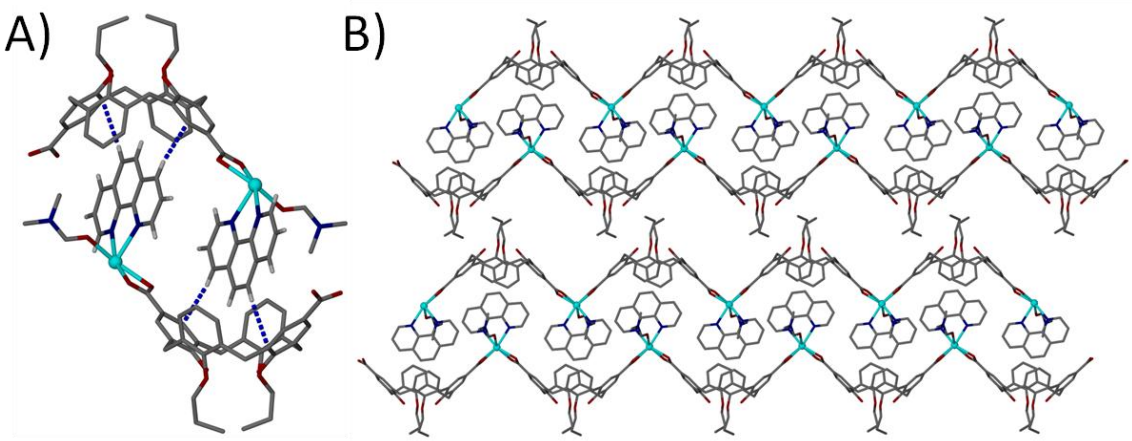

Figure 3.7 (A) Section of the extended structure in **18** showing complementary host-guest CH···π interactions (blue dashed lines) between neighbouring cavities of and ligated phen. (B) Extended structure in **18** showing the interdigitation of 1-D chains and the bi-layer assembly. Dmf of crystallisation and hydrogen atoms except those involved in CH···π interactions omitted for clarity.

Further analysis of the extended structure reveals interwoven pairs of 1-D chains which assemble to form bi-layer arrays as shown in Figure 3.8B, similar to those found in **17** (Fig 3.5A). However, as a result of these differences in solid state packing in **17** and **18,** the assembly in **18** contains 1-D solvent channels (running along the *a* axis of unit cell) filled with the disordered dmf of crystallisation and water molecules (Fig 3.8). The solvent channel conforms to a parallelogram of approximate dimensions ~7 nm x 10 nm. As a result of this structural feature exhibited by **18** in the solid state we decided to investigate gas sorption properties. Attained crystals of **18** were filtered, dried in air, and analysed with PXRD. Analysis of the powder pattern of **18** reveals the dried material loses crystallinity and turns amorphous upon removal from mother liquor / drying, thus analysis of gas sorption properties was abandoned.

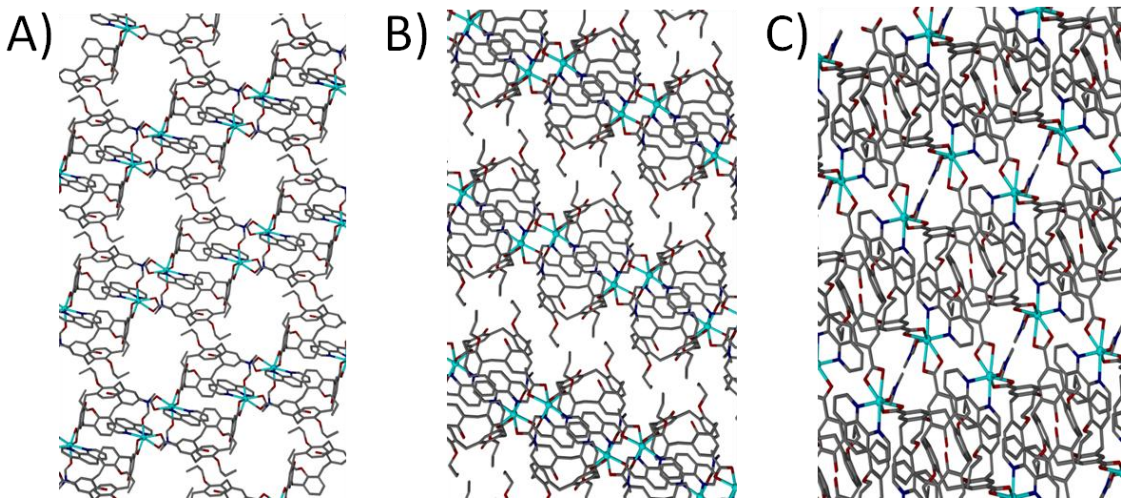

Figure 3.8 Ball and stick representation of solid state packing in **18** showing view along three unit cell axes: (A) *a* axis, (B) *b* axis and (C) *c* axis. Hydrogen atoms and dmf of crystallisation omitted for clarity.

One of the aims of the investigation was to study the robustness of the design strategy by looking at various di-*p*-CO_2[4]s. As already mentioned, di-*p*-CO_2[4]s containing pentoxy chains at the lower-rim did not yield crystalline material. However, reactions in which di-*p*-CO_2[4] containing butoxy chains was used, did yield crystalline material. Reaction of Cd(II) with di-*p*-CO_2[4] **16b** and phen resulted in clear yellowish solution which, after a few months of slow evaporation, produced colourless blocks suitable for SCXRD analysis. The crystals are in a triclinic cell and the structure was

solved in space group *P*-1. The unit cell parameters are a = 10.9671(5) Å, b = 14.2215(6) Å and c = 18.5034(8) Å, and α = 110.695(2)º, β = 90.387(2)º and γ = 106.035(2)º and the formed crystals are of formula [Cd(**16b**)(phen)$(H_2O)_{0.5}(dmf)_{0.5}$]·$(H_2O)_{0.5}(dmf)_{0.5}$ (**19**), as shown in Figure 3.9. The asymmetric unit in **19** comprises one Cd(II) ion, one di-*p*-CO_2[4] **16b**, one phen and one aquo ligand. The asymmetric unit also contains two molecules of dmf and two water molecules, which due to disorder were all modelled at half occupancy. The coordination complex formed consists of two di-*p*-CO_2[4] **16b** coordinated to Cd(1) *via* one of the carboxylate groups, both in a bidentate fashion with Cd(1)-O(5), Cd(1)-O(6), Cd(1)-O(7)' and Cd(1)-O(8)' bond lengths of 2.365(2) Å, 2.384(2) Å, 2.410(4) Å and 2.363(3) Å respectively. Phen is coordinated to Cd(1) as a chelate with Cd(1)-N(1) and Cd(1)-N(2) distances of 2.366(2) Å and 2.383(3) Å respectively. One half occupancy water molecule and dmf are coordinated to the metal *via* their oxygen atoms with respective bond lengths of 2.377(8) Å and 2.301(7) Å. The di-*p*-CO_2[4] adopts the expected partially pinched-cone conformation with narrow and wide cone angles of ~88° and ~111° respectively (measured between diametrical *para* carbon atoms and centroid generated from phenolic oxygen atoms). Symmetry expansion of the asymmetric unit reveals that as in **18**, calixarene cavity is occupied by a s.e. ligated phen from a neighbouring CP, with the two CPs knitted together through two crystallographically unique host-guest CH···π interactions (Fig. 3.10A). As a result of this, **19** assembles to form a bi-layer type array, similar to the one observed in **18** (Fig. 3.10B).

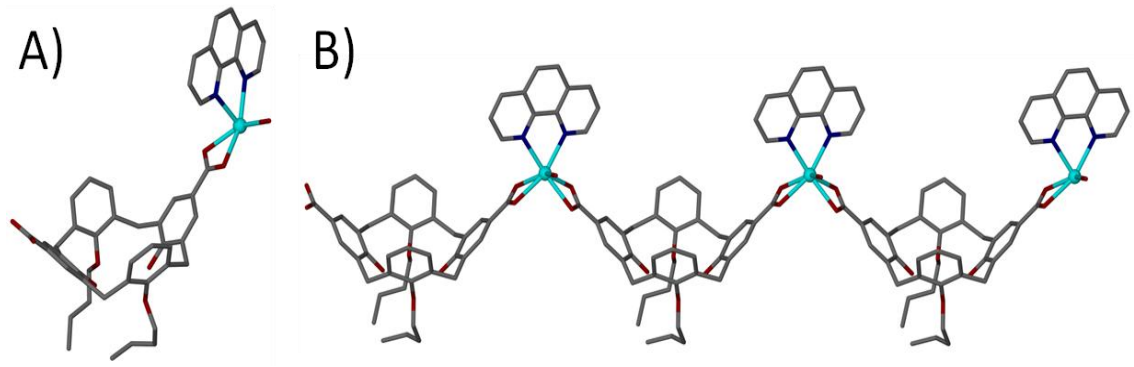

Figure 3.9 (A) Ball and stick representation of asymmetric unit in **19**. (B) Side view of the linear CP chain formed in **19**. Hydrogen atoms and dmf of crystallisation omitted for clarity. Ligated solvent molecules shown only as water.

Analysis of extended crystal structure in **19** reveals 1-D solvent channels, which conform to a parallelogram of approximate dimensions of ~7 nm x ~10 nm running along axis *a* of the unit cell, as shown in Figure 3.11A. Comparison of structural features exhibited by **18** and **19** indicates that both structures are almost identical: a) a ligated solvent molecule (in case of **19** all figures show only the aquo ligand) b) the same binding mode of carboxylate moieties to the metal centre c) the relative orientation of co-ligands in the coordination sphere and d) the alignment and the solid packing of CP chains.

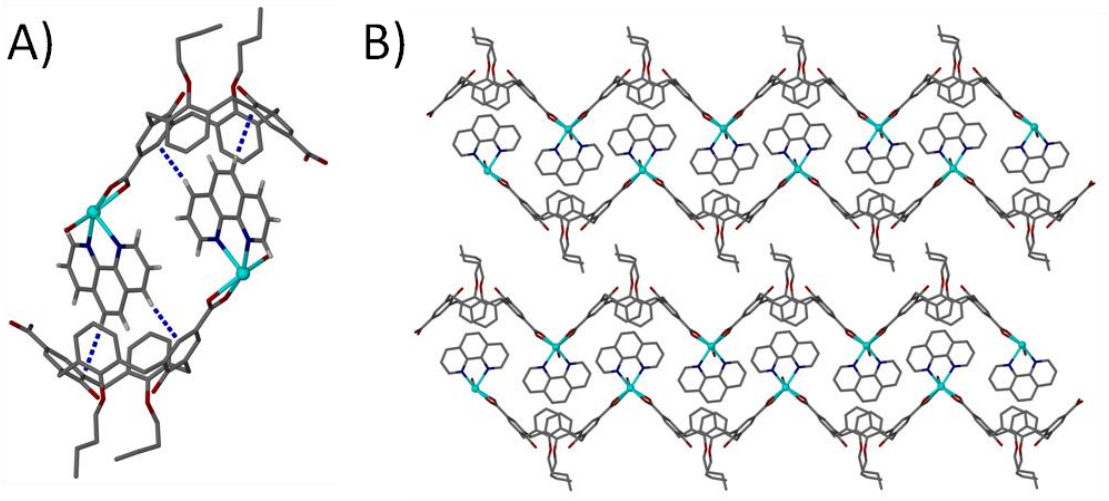

Figure 3.10 (A) Section of the extended structure in **19** showing complementary host-guest CH···π interactions (blue dashed lines) between neighbouring cavities of and ligated phen. (B) Extended structure in **19** showing the interdigitation of 1-D chains and the bi-layer assembly. Dmf of crystallisation and hydrogen atoms except those involved in CH···π interactions omitted for clarity.

However, comparison of their lattice parameters reveals that they are not isostructural. The subtle difference can be associated with the length of alkyl chains at the lower-rim, which possibly due to steric reasons, dictate the distance between layers of CP chains. This becomes evident after inspecting Figures 3.7B and Figure 3.10B whereby the displacement between aligned CPs in **18** and **19** is marginally different (distances between Cd(II) centres from two neighbouring CPs being ~2.0 nm and ~2.1 nm long). Similarly as in case of **18**, PXRD analysis of filtered crystals of **19**, reveals loss of crystallinity upon removal from mother liquor / drying and subsequent analysis of gas sorption properties was abandoned.

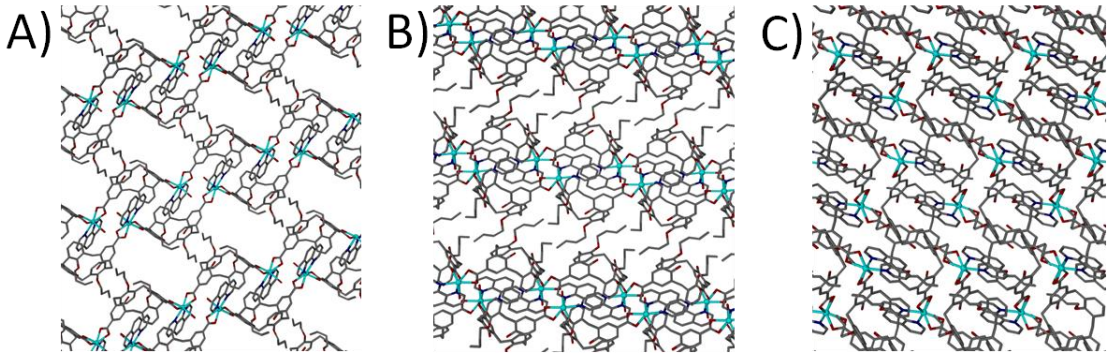

Figure 3.11 Ball and stick representation of solid state packing in **19** showing view along three unit cell axes: (A) *a* axis, (B) *b* axis and (C) *c* axis. Hydrogen atoms and dmf of crystallisation omitted for clarity.

Syntheses using Ni(II) ions with di-*p*-CO_2[4]s **16a** and **16c** did not yield crystalline product, however slow evaporation of the reaction solution containing di-*p*-CO_2[4] **16b** resulted in formation of pale green crystalline needles. The crystals are in a triclinic cell and the structure was solved in space group *P*-1. The unit cell parameters are a = 10.5006(5) Å, b = 14.5683(7) Å and c = 16.5574(8) Å, and α = 99.437(3)º, β = 108.082(3)º and γ = 99.174(3)º. Structural analysis shows that the components also form a 1-D CP chain of formula [Ni(**16b**)(phen)(H_2O)]·dmf (**20**), as shown in Figure 3.12. The asymmetric unit contains one Ni(II), one phen, di-*p*-CO_2[4] **16b**, one aquo ligand and one dmf of crystallisation.

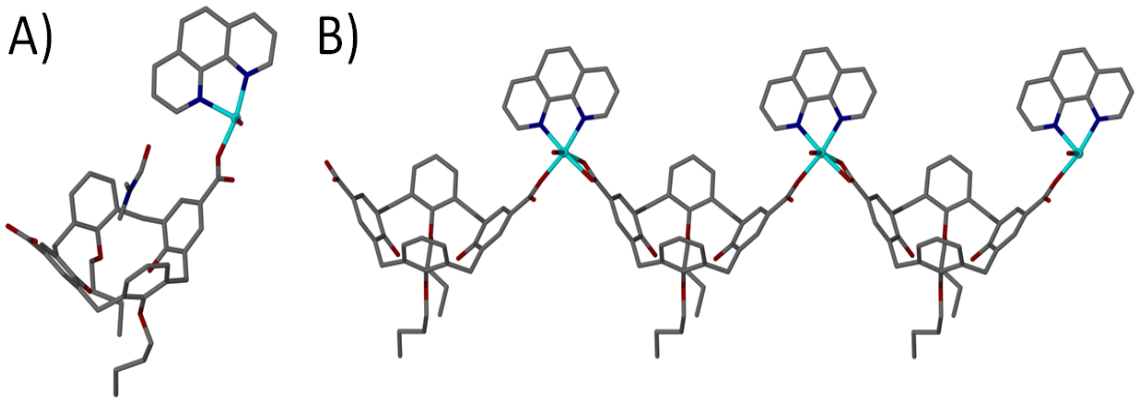

Figure 3.12 (A) Ball and stick representation of the asymmetric unit in **20**. (B) Extended structure in **20** showing linear CP chain. Hydrogen atoms and dmf of crystallisation omitted for clarity.

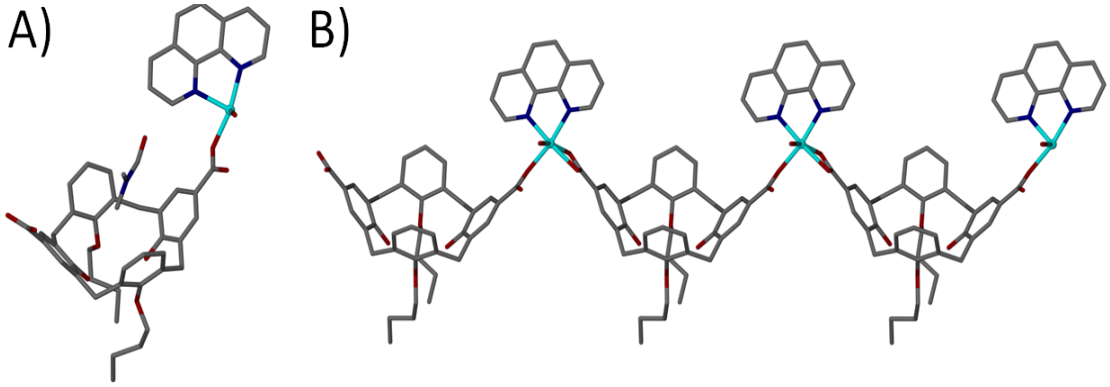

Figure 3.12 (A) Ball and stick representation of the asymmetric unit in **20**. (B) Extended structure in **20** showing linear CP chain. Hydrogen atoms and dmf of crystallisation omitted for clarity.

As in **17**, the coordination complex formed comprises two di-*p*-CO_2[4]s **16b**, bonded to metal centres *via* carboxylate groups: the O(5)-C(29)-O(6) groups in bonded to Ni(1) in a monodentate fashion *via* O(5) with the bond length of 2.013(4) Å, whilst the second di-*p*-CO_2[4] **16b** is coordinated to Ni(1) in a bidentate fashion *via* s.e. O(7)'-C(30)'-O(8)', with respective Ni(1)-O(7)' and Ni(1)-O(8)' bond lengths of 2.139(4) Å and 2.103(4) Å. Phen, as expected, is coordinated to Ni(1) in a chelating fashion, with Ni(1)-N(1) and Ni(1)-N(2) distances of 2.053(5) Å and 2.064(5) Å respectively. The last component making up the coordination sphere is an aquo ligand, with Ni(1)-O(9) bond length of 2.046(5) Å. Expansion of the asymmetric unit around the cavity of di-*p*-CO_2[4] **16b** reveals a dmf of crystallisation residing in the calixarene cavity, a feature already observed in **17**. The di-*p*-CO_2[4] adopts the expected partially pinched-cone conformation with narrow and wide cone angles of ~89° and ~108° respectively. The distances between hydrogen atoms H(60A) and H(60B) of the dmf and the calixarene aryl rings are 2.66 Å and 2.89 Å, indicating a presence of host-guest CH···π interactions (Fig. 3.13A). Further analysis of the extended structure in **20** shows that neighbouring CPs align together in a fashion similar to that observed in **17**, with neighbouring ligated phens undergoing π-stacking, as shown in Figure 3.13B. The solid state packing in **20** shows alignment of linear CPs chains as a result of which solvent channels are absent in the crystal structure (Fig. 3.14), as also observed in **17**. In order to improve poor the reaction yield we further elongated the evaporation period, however this resulted in an inhomogeneous product which was unsuitable for PXRD analysis.

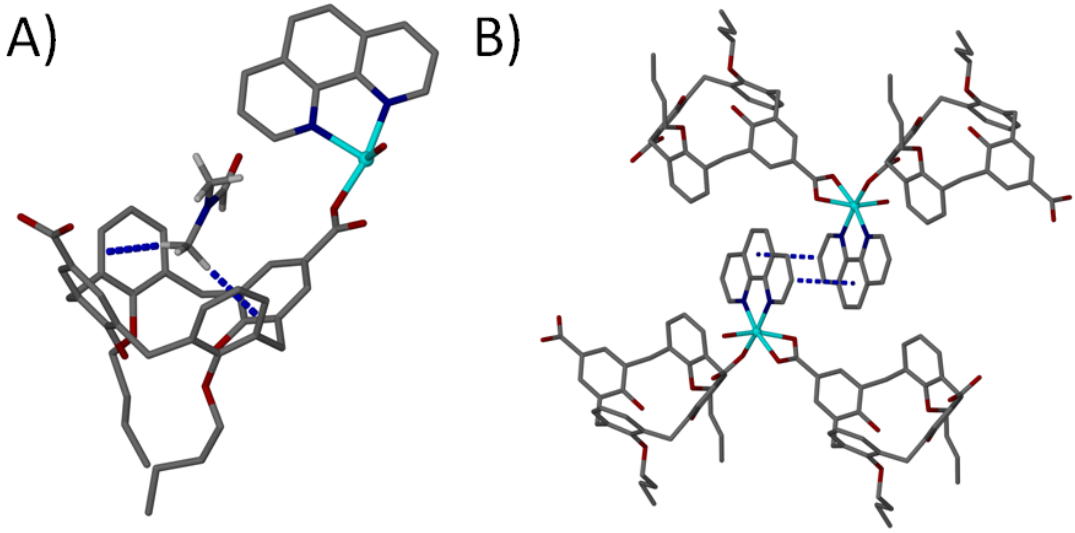

Figure 3.13 (A) The asymmetric unit in **20** showing complementary host-guest CH···π interactions between dmf hydrogen atoms and two calixarene aromatic rings. (B) Section of the extended structure in **20** showing π-stacking between ligated phens from a neighbouring CP. Hydrogen atoms and solvent molecules omitted for clarity.

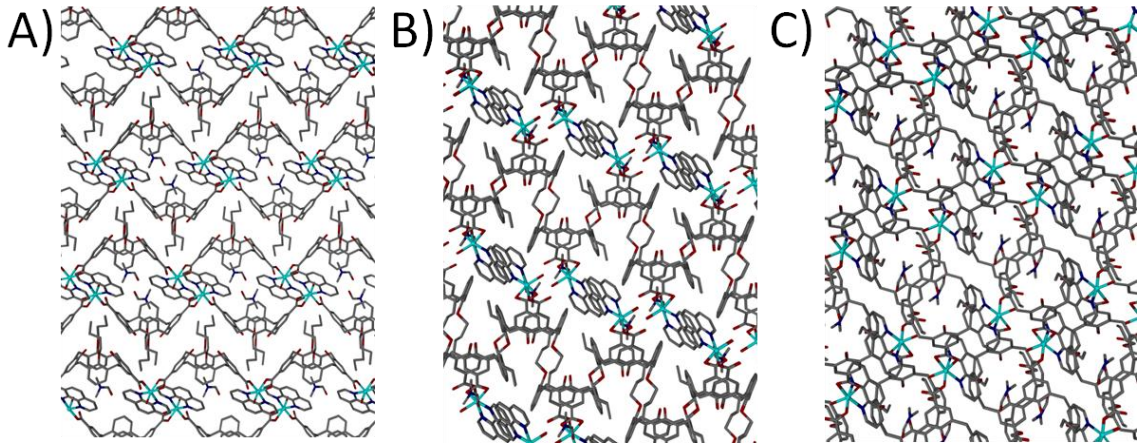

Figure 3.14 Ball and stick representation of solid state packing in **20** showing view along three unit cell axes: (A) *a* axis, (B) *b* axis and (C) *c* axis. Hydrogen atoms and dmf of crystallisation omitted for clarity.

Reaction of Co(II) ions with di-*p*-CO_2[4] **16b** and phen, followed by slow evaporation, yielded pink crystalline blocks of formula [Co(**16b**)(phen)(H_2O)]·$(dmf)_2(H_2O)_{0.5}$ (**21**) (Figure 3.15A). The crystals of **21** are in a monoclinic cell and the structure was solved in space group *C*2/*c*. The unit cell parameters are a = 40.974(8) Å, b = 16.686(3) Å and c = 15.874(8) Å, and β =

108.588(11)º. The asymmetric unit consists of one Co(II) ion, one di-*p*-CO_2[4] **16b**, one phen and an aquo ligand. The asymmetric unit also contains uncoordinated solvent molecules (half a water and two dmf). Structural analysis reveals formation of linear CP chains, as shown in Figure 3.15B. The coordination complex formed comprises two di-*p*-CO_2[4]s **16b** which are coordinated to Co(1) *via* carboxylate groups: the O(5)-C(29)-O(6) group is bonded in a bidentate fashion, with respective bond lengths of 2.166(6) Å and 2.158(6) Å, and the s.e. O(7)'-C(30)'-O(8)' group in a monodentate fashion *via* the O(8)' atom with a bond length of 2.073(6) Å. The coordination sphere also consists of phen, bonded to Co(1) in a chelating fashion *via* N(1) and N(2) with respective bond lengths of 2.103(7) Å and 2.140(7) Å, and one aquo ligand bonded to Co(1) *via* O(9) with bond distance of 2.050(6) Å. The di-*p*-CO_2[4] adopts the expected partially pinched-cone conformation with narrow and wide cone angles of ~87° and ~118° respectively. Symmetry expansion around the calixarene cavity reveals that the interior of the macrocycle is occupied by a s.e. ligated phen from a neighbouring CP chain. The distance between three hydrogen atoms of phen and s.e. calixarene aryl rings range from 2.81-2.90 Å, indicating complementary host-guest CH···π interactions (Fig. 3.16A).

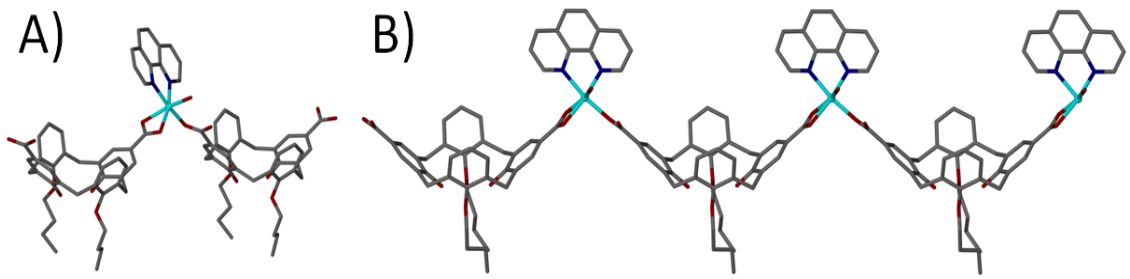

Figure 3.15 (A) Ball and stick representation of coordination complex formed in **21**. (B) Extended structure in **21** showing linear CP chain. Hydrogen atoms and dmf of crystallisation omitted for clarity.

Furthermore in this host-guest pair, phen and one of the aromatic rings of the di-*p*-CO_2[4] align together in a parallel fashion, and with the distance between them of ~3.4 Å, suggesting the presence of a π-stacking interaction. Examination of the extended structure in **21** shows that the alignment of linear CP chains is different to that observed in **17** - **20**. This interwoven nature of CP packing results from complementary non-covalent interactions and invokes a degree of tilt between neighbouring CP chains. This

angle is sufficient to prevent bi-layer formation, thus allowing for back-to-back packing of the di-*p*-CO_2[4]s from neighbouring CP chains (Fig. 3.16B), resulting in the generation of infinite 1-D channels along the *c* axis of the unit cell, as shown in Figure 3.17. The side walls of the resulting di-*p*-CO_2[4] solvent channels are composed of di-*p*-CO_2[4] lower-rim alkyl chains and aryl rings. These solvent channels are occupied by dmf of crystallisation and thus presented the possibility to explore de-solvation, solvent exchange and alternative guest storage. However, PXRD analysis revealed that single crystals lose their crystallinity upon removal from mother liquor / drying, rendering further analysis impossible.

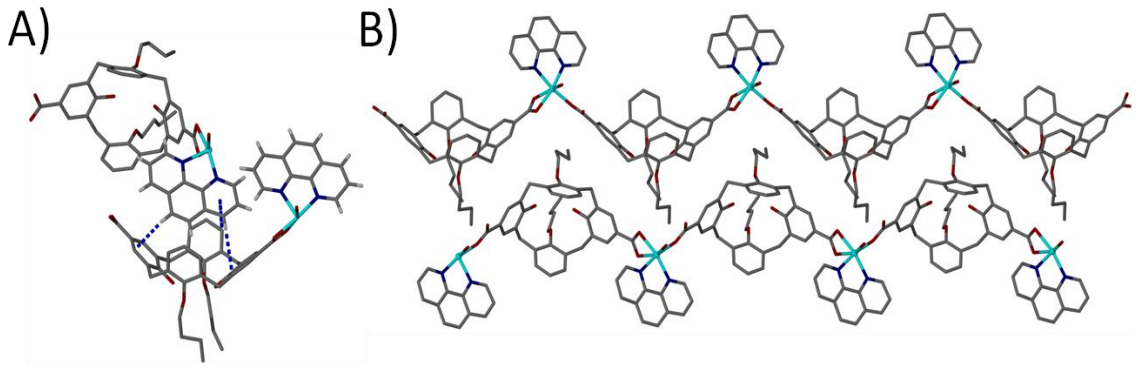

Figure 3.16 (A) Section of the extended structure in **21** showing (A) CH···π and π-stacking and (B) the back-to-back packing of linear CP. Hydrogen atoms and dmf of crystallisation omitted for clarity.

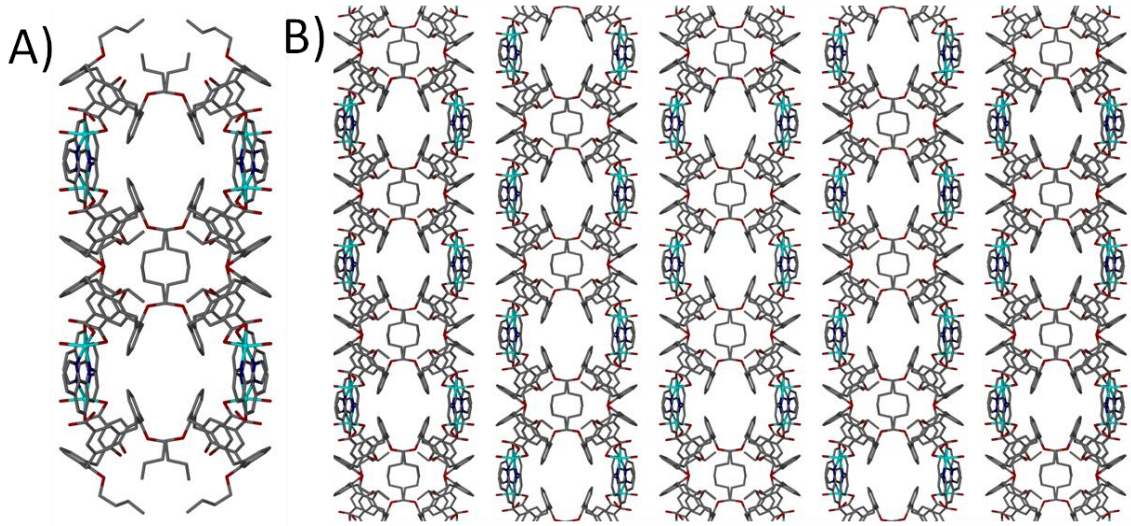

Figure 3.17 (A) Ball and stick representation of the back-to-back packing of linear CP in **21**. (B) Extended structure in **21** along *c* axis of the unit cell showing 1-D solvent channels. Hydrogen atoms and solvent molecules omitted for clarity.

Synthesis in which Cu(II) ions were used with di-*p*-CO_2[4] **16b** and phen, followed by subsequent slow evaporation of the reaction mixture yielded green crystalline blocks of formula [Cu_2(**16b**)$(phen)_2(H_2O)_2$]·$(dmf)_4(H_2O)_2$ (**22**) (Fig. 3.18A). The crystals of **22** are in a monoclinic cell and the structure was solved in space group *C*2/*c*. The unit cell parameters are *a* = 26.4551(10) Å, *b* = 14.5002(5) Å and *c* = 40.5787(19) Å, and β = 105.655(2)º. The asymmetric unit consists of a binuclear Cu(II) complex comprising one ligated molecule of di-*p*-CO_2[4] **16b**, two ligated molecules of phen and two aquo ligands. The asymmetric unit also contains uncoordinated dmf of crystallisation and two water molecules. Structural analysis reveals formation of linear 1-D CP chains comprising binuclear Cu(II) complexes (Fig. 3.18B). Each Cu(II) centre possesses one aquo ligand with Cu(1)-O(9) and Cu(2)-O(10) bond lengths of 2.160(4) Å and 2.191(3) Å respectively. To each of the Cu(II) ions there is one phen ligated as a chelate with Cu(1)-(N1), Cu(1)-N(2), Cu(2)-N(3) and Cu(2)-N(4) bond lengths of 2.054(4) Å, 2.004(4) Å, 2.017(4) Å and 2.018(4) Å respectively.

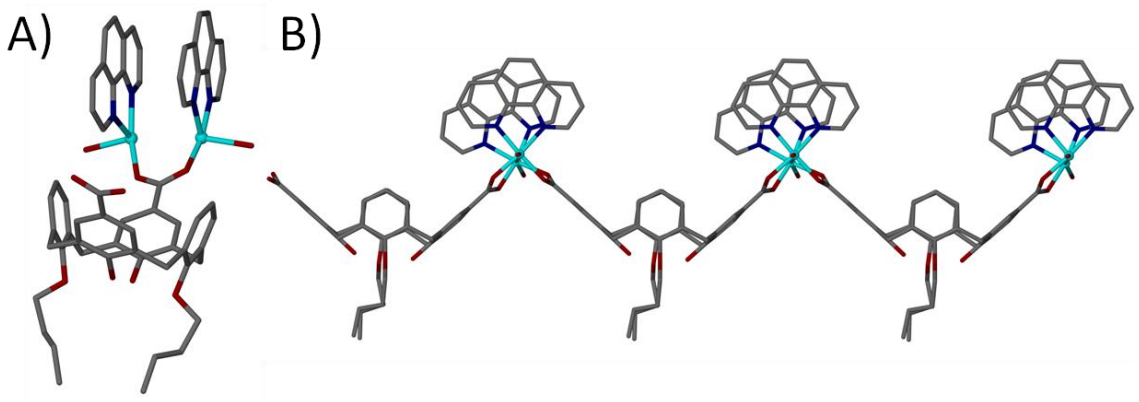

Figure 3.18 Ball and stick representation of: (A) binuclear coordination complex formed in **22** and (B) side view of the linear CP chain. Hydrogen atoms and dmf of crystallisation omitted for clarity.

Both of the carboxylate groups of the di-*p*-CO_2[4] **16b** are coordinated in a bridging fashion. The carboxylate comprising atoms O(5)-C(29)-O(6) forms Cu(1)-O(5) and Cu(2)-O(6) bonds of respective lengths of 1.923(3) Å and 1.955(3) Å. The second carboxylate moiety comprising atoms (7)-C(30)-O(8) is coordinated to a s.e. Cu(II) binuclear cluster *via* Cu(1)'-O(7) and Cu(2)'-O(8) bonds of respective lengths of 1.963(3) Å and 1.939(3) Å. The di-*p*-CO_2[4] adopts the expected partially pinched-

cone conformation with narrow and wide cone angles of ~84° and ~115° respectively. Symmetry expansion around the calixarene cavity reveals that the interior of the macrocycle is occupied by dmf of crystallisation. Closer inspection shows that the distance between dmf hydrogen atom and one of the calixarene aryl rings is 2.76 Å which suggests a presence of a complementary host-guest CH···π interaction (Fig 3.19A). Structural analysis reveals that both ligated phens are within a distance of ~3.4 Å from each other which suggests a presence of π-stacking (Fig 3.19B). Furthermore symmetry expansion of the asymmetric unit shows that the alignment of neighbouring CPs results in an overlap of phens comprising N(1) and N(2) atoms and its s.e., and being ~3.4 Å apart it is indicative of π-stacking interaction (Fig. 3.19C). Analysis of the extended crystal structure reveals two interconnected solvent channels, one running along the *c* axis of the unit cell and the second running in -1 1 0 direction (Fig. 3.20).

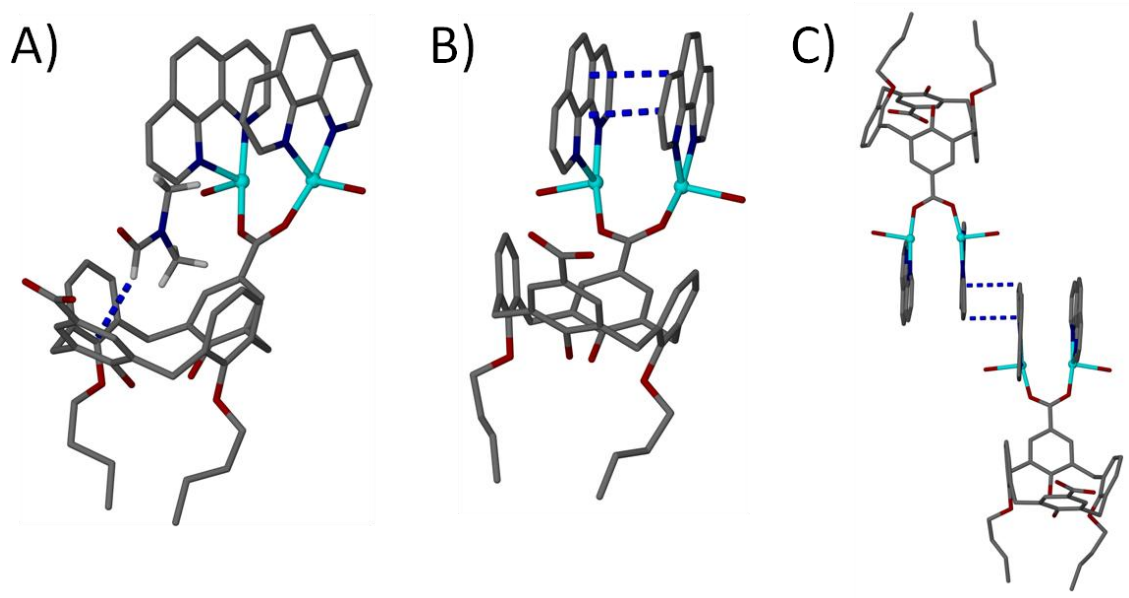

Figure 3.19 (A) The complementary host-guest CH···π interactions in **22** between a dmf hydrogen atom and one of the calixarene aryl rings. (B) Section of extended structure in **22** showing π-stacking between ligated phens within the binculear cluster. (C) Section of extended structure in **22** showing π-stacking between phens from neighbouring CPs. Hydrogen atoms and solvent molecules omitted for clarity.

Due to high disorder of the dmf of crystallisation and water molecules occupying the solvent channels they were removed with the routine SQUEEZE.[74] Presence of

solvent channels occupied by co-crystallised dmf and water molecules presented the possibility to explore de-solvation, solvent exchange and alternative guest storage. However, an attempt to improve poor reaction yields and isolate a homogeneous product turned out unsuccessful, making **22** unsuitable for PXRD and subsequent sorption analysis.

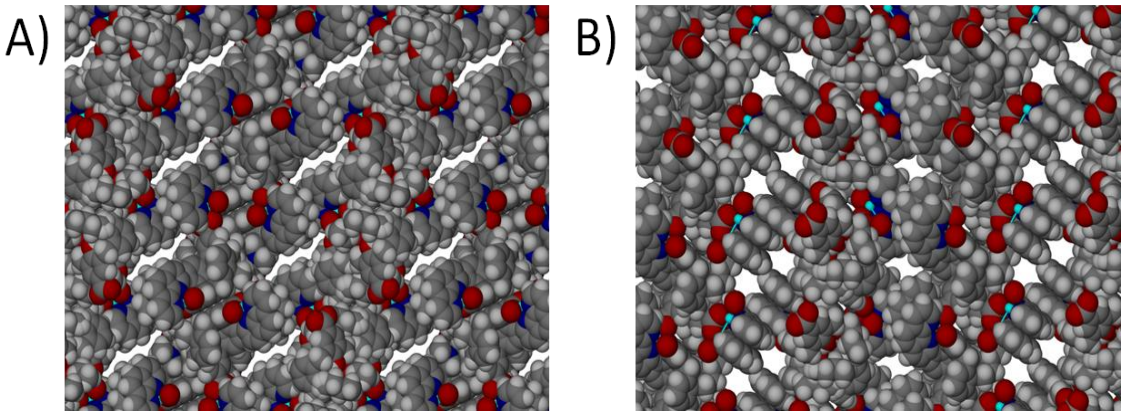

Figure 3.20 Space filling representation of the crystal packing in **22** (A) along *c* axis of the unit cell and (B) cross-section of the -1 1 0 plane. Dmf of crystallisation and water molecules are removed for clarity.

An attempt to synthesise a Cu(II) based linear CP with di-*p*-CO_2[4] **16a**, resulted in crystalline material of formula $[Cu_2(\mathbf{16a})(phen)_2(H_2O)_2]\cdot(dmf)_6$ (**23**). The crystals are in a monoclinic cell and the structural analysis was carried out in space group *C*2/*c*. The asymmetric unit also consists of a binuclear Cu(II) complex comprising one ligated molecule of di-*p*-CO_2[4] **16a**, two ligated phens and two aquo ligands, which is in good agreement with **22**. Due to crystals being weakly diffracting it has not been possible to carry out full structural refinement, however the cell parameters and partially solved crystal structure of **23** indicate that **22** and **23** are isostructural. Unfortunately, attempts to improve the poor reaction yields and inhomogeneity of the product were unsuccessful.

All synthesised materials which yielded crystalline product discussed so far in this chapter, as anticipated, form linear CP regardless of the TM(II) ion or di-*p*-CO_2[4] used, proving the design strategy robust. However, subtle differences in the coordination sphere and complementary host-guest interactions can altogether have a

profound effect on the final outcome of the assembly. In **17** and **21** the solid state packing is noticeably different, what is in contrast with **18** and **19**, whereby the use of the same TM but di-*p*-CO_2[4] with a different length alkyl chain results in almost identical solid state packing. Similarly, the solid state packing in **22** and **23** is the same regardless of the length of the di-*p*-CO_2[4] lower-rim alkyl chain. Analysis of di-*p*-CO_2[4] cone angles in **17 - 23** suggests that the obtuseness of these angles is dictated by the type of guest molecule inside the calixarene cavity, and that the length of alkyl chains has no noticeable impact. However, it is ambiguous why the di-*p*-CO_2[4] cavity in **17** is occupied by dmf, whereas in **21** this is by phen, and what governs the preference of the di-*p*-CO_2[4] cavity over specific guest molecule. It is also observed that depending on the TM, employed differences in binding modes of carboxylate moieties to the metal centre can be observed: monodentate and bidentate (**17**, **20** and **21**) vs. bidentate and bidentate (**19** and **20**) vs. monodentate bridging (**22** and **23**).

3.3. Fine-tuning of the assembly - phen derivatives

Structural analysis of **17 - 23** reveals the validity of the design strategy to successfully synthesise linear CPs. One of the key aspects of this strategy is the use of phen as a co-ligand to restrict binding sites available in the coordination sphere. Furthermore, ligated phens participate in non-covalent interactions (CH···π and π-stacking) contributing towards stabilisation of self-assembly and influencing the solid state packing. In order to better understand the role of ligated phen in the stabilisation and solid state packing of linear CPs further investigation was needed to provide more scientific evidence. It was anticipated that by using various phen derivatives in the synthesis of CPs, through steric hindrance, one can promote / demote non-covalent interactions, gaining better understanding, and ultimately better control, over the self-assembly of CPs. Additionally, part of the research was to study the role of substituted phen as a co-ligand and its impact on the formation of bi-layer arrays, as observed in **17**-**20**, and whether this type of array could be disrupted.

Similarly as in the syntheses of **17 - 23**, di-*p*-CO_2[4]s (**16a - c**) were used to carry out a series of ambient reactions in which dmf solutions containing a TM(II) ion (Co, Mn, Cu, Ni, Cd, Zn or Ni) and di-*p*-CO_2[4] were layered with methanolic solution of different phen derivative. The phen derivatives investigated were 2-methyl-1,10-

phenanthroline (2-me-phen), 3-methyl-1,10-phenanthroline (3-me-phen), 4-methyl-1,10-phenanthroline (4-me-phen) and 3,4,7,8-tetra-methyl-1,10-phenanthroline (t-me-phen). After carrying out reactions clear solutions were left to slowly evaporate over a period of time, which varied from several weeks to several months, to yield crystalline product suitable for structural analysis. As previously, none of the reactions in which di-*p*-CO_2[4] **16c** was used afforded single crystals suitable for structural analysis.

Reaction of Co(II) ions with di-*p*-CO_2[4] **16b** and 2-me-phen and subsequent slow evaporation of the reaction mixture yielded crystalline material. Pink blocks of [Co(**16b**)(2-me-phen)(H_2O)]·$(dmf)_2(H_2O)_{0.5}$ (**24**) are in a monoclinic cell and crystal structure was solved in space group *C*2/*c* (Fig 3.21A). The asymmetric unit comprises one Co(II) ion, one di-*p*-CO_2[4] **16b**, one 2-me-phen, an aquo ligand, two dmf of crystallisation and water molecule. Structural analysis shows that all bond lengths in both coordination complexes are consistent and form linear CP chains which pack in a back-to-back fashion to give 1-D solvent channels. Given this and that the comparison of cell parameters of **21** (a = 40.974(8) Å, b = 16.686(3) Å and c = 15.874(8) Å, and β = 108.588(11)º) and **24** (a = 40.9540(2) Å, b = 16.7019(8) Å and c = 15.8395(7) Å and β = 107.997(2)º) reveals that structures are isostructural. The difference in the overall formula of the asymmetric unit in both structures arises from different occupancy of infinite 1-D channels by solvent molecules (Fig. 3.21B).

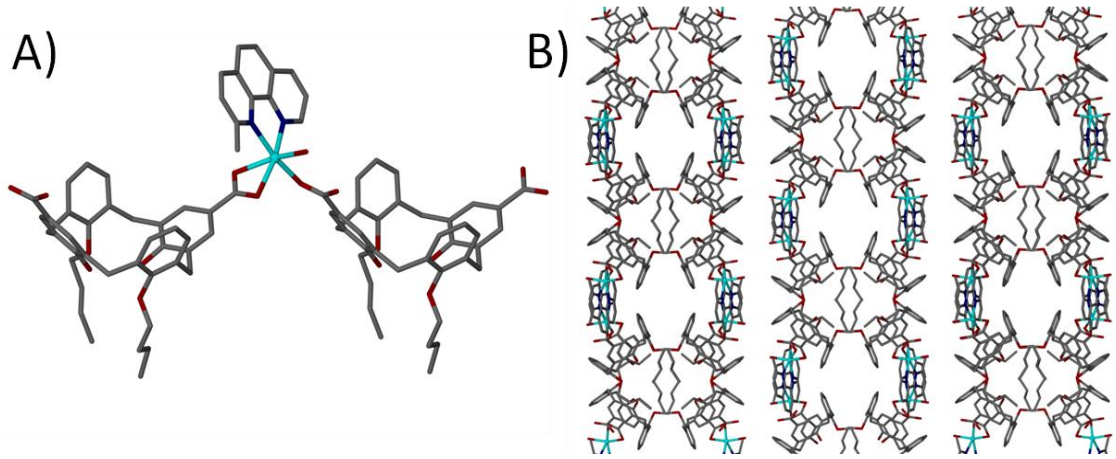

Figure 3.21 (A) Ball and stick representation of the coordination complex formed in **24**. (B) Extended structure in **24** along *c* axis of the unit cell showing the back-to-back packing and resulting 1-D solvent channels formed by linear CPs in **24**. Hydrogen atoms and solvent molecules omitted for clarity.

Structural analysis in **21** reveals empty space around the 2-position in the ligated phen, thus allowing the methyl substituent from 2-me-phen in **24** to occupy that void without affecting the assembly. Slow evaporation of reaction mixtures containing Co(II), di-*p*-CO_2[4] **16b** and 3-me-phen, 4-me-phen or t-me-phen did not yield material suitable for SCXRD analysis which indicates that positioning of the methyl substituent may be significantly disrupting the self-assembly. Similarly, as in the case of **21**, PXRD analysis reveals that crystals of **24** lose their crystallinity upon removal from mother liquor / de-solvation.

Structural analysis of **17**, in which di-*p*-CO_2[4] containing lower-rim propoxy chains was used, shows no free space around ligated phen to accommodate methyl substituents, and suggests that the use of any of the phen derivatives can disrupt the efficient bi-layer packing and yield a different supramolecular architecture. Unfortunately, all reactions in which Co(II), di-*p*-CO_2[4] **16a** and 2-me-phen, 3-me-phen or 4-me-phen were used did not yield single crystals, suggesting that using substituted phen may not only disrupt the bi-layer packing but also interfere with self-assembly, obstructing formation of supramolecular assemblies.

Reaction of Ni(II) ions with di-*p*-CO_2[4] **16b** and 2-me-phen afforded crystalline material suitable for structural analysis. Green blocks of [Ni(**16b**)(2-me-phen)(H_2O)]·$(dmf)_2(H_2O)_{0.5}$ (**25**) are in a monoclinic cell and the crystal structure was solved in space group *I*2/*a*. The inspection of cell parameters reveals that **25** (*a* = 15.7924(10) Å, *b* = 16.6359(11) Å and *c* = 39.2230(3) Å, and β = 94.752(2)º) is isostructural with **21** and **24** and that the overall formula of asymmetric unit in **24** and **25** is the same. Structural analysis reveals that coordination complexes in **25**, as in **21** and **24,** form linear CP chains which are interwoven together and assemble in back-to-back fashion to give 1-D solvent channels running along *a* axis of the unit cell (Fig. 3.22). Interestingly, such back-to-back packing does not occur in **20,** which is synthesised using also Ni(II) ion but phen rather than 2-me-phen as a co-ligand, and in which formation of bi-layer arrays is observed instead. Structural analysis reveals that the bonding fashion of the carboxylate moieties to the Ni(II) centre in **20** and **25** is the same, with one carboxylate group bonded in a monodentate fashion and the second one as a chelate. The key difference is in the occupancy of the di-*p*-CO_2[4] cavity - in **20** it is occupied by a dmf molecule, whereas in **25** it is occupied by 2-me-phen from neighbouring CP chain, a similar feature observed in **24**. Similarly, as in **21** and **24**, in

25 the 2-me-phen resides in the di-*p*-CO_2[4] cavity at an angle, resulting in 2-me-phen and calixarene aryl rings being involved in both CH···π and π-stacking, and concomitant alignment of neighbouring CP in a back-to-back fashion. Unfortunately, crystals of **25** also lose crystallinity upon removal from mother liquor / drying, making them unsuitable for gas sorption and storage analysis.

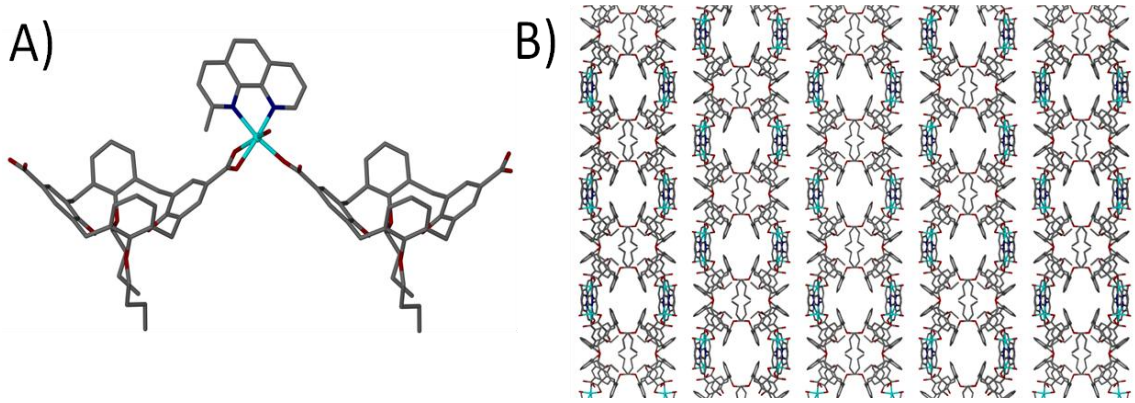

Figure 3.22 (A) Ball and stick representation of the coordination complex **24**. (B) Extended structure in **24** along *a* axis of the unit cell showing the back-to-back packing and resulting 1-D solvent channels formed by linear CPs in **24**. Hydrogen atoms and solvent molecules omitted for clarity.

A series of reactions using phen derivatives and subsequent slow evaporation yields crystalline material suitable for SCXRD analysis in only two reaction mixtures. In both of these reactions the co-ligand used is a 2-me-phen and resulting structures **24** and **25** are isostructural. Inspection of cell parameters of **24** and **25** reveals that they are isostructural with **21**, in which phen was used instead 2-me-phen. One feature exhibited by all three structures in the solid state is the phen (**21**) and 2-me-phen (**24** and **25**) residing in the cavity of di-*p*-CO_2[4] from a neighbouring CP. This occurs regardless of the presence / absence of a methyl group at the 2-position. Interestingly **25**, as opposed to **21** and **24** in which Co(II) and di-*p*-CO_2[4] **16b** are employed, is not isostructural with **20** (both are synthesised using Ni(II) and di-*p*-CO_2[4] **16b**). Unfortunately, given that the rest of reactions with derivatives of phen did not yield crystalline material, we were unable to gain a better insight, and thus better understanding of the role steric factors can play in the assembly of linear CPs. However, reactions in which 3-me-phen and 4-me-phen are used do not yield crystalline products. This could be an indication

that the methyl groups impede participation of phen derivatives in non-covalent interactions (CH···π and π-stacking), thus suggesting that these interactions play an important role in stabilisation of self-assembly and can have profound effect on the packing in the solid state.

3.4. Summary

In this chapter we have demonstrated that di-*p*-CO_2[4]s can be utilised as building blocks for construction of infinite 1-D coordination polymers. As anticipated, functionalisation of the calix[4]arene upper-rim with two carboxylic moieties gives a di-topic building block that can act as a linker between TMs. The series of 1-D CPs which we synthesised display a number of similarities in the solid state regardless of the transition metal ion used during the synthesis, proving the robustness of the design strategy. We utilised a chelating ligand, phen, to restrict the number of available binding sites around the metal centre; this decreases the number of ways the linker (di-*p*-CO_2[4]) and the node (metal centres) can connect together, ultimately providing us with relative control over the directionality during the formation of CPs. Structural analysis of synthesised materials shows some degree of variation in the solid state packing. In some cases formation of bi-layer arrays is observed, whereas in others this efficient packing is disrupted and leads to back-to-back packing of calixarenes thus formation of solvent channels in the solid state. It is ambiguous what impact the length of alkyl chains has on the alignment of neighbouring CPs and to what degree it affects the solid state packing. In **17** and **21** (Co(II), phen and di-*p*-CO_2[4] **16a** and **16b** respectively) the solid state packing is noticeably different. This is in contrast to the solid state packing observed in **18** and **19** (Cd(II), phen and di-*p*-CO_2[4] **16a** and **16b** respectively), and **22** and **23** (Cu(II), phen and di-*p*-CO_2[4] **16a** and **16b** respectively), whereby the use of the same TM(II) ion but di-*p*-CO_2[4] with a different length alkyl chain results in structures exhibiting almost identical solid state packing. However, considering that reactions in which di-*p*-CO_2[4] **16c** was used did not yield crystalline material, the length of calixarene lower-rim alkyl chain must have a substantial impact on the self-assembly. Analysis of di-*p*-CO_2[4] cone angles in **17** - **23** suggests that the obtuseness of these angles is dictated by the type of guest molecule residing in the

calixarene cavity. However, it is ambiguous what governs the preference of the di-*p*-CO_2[4] cavity for specific guest molecule during the self-assembly.

The investigation of the influence of phen on the self-assembly *via* non-covalent interactions (CH···π and π-stacking) has not provided enough evidence to draw a definite conclusion. The number of obtained results when using 2-me-phen is too small to help better understand the role of these interactions on the packing of 1-D CPs. However, the lack of results when using 3-me-phen and 4-me-phen suggest that steric factors perhaps weaken / disrupt these non-covalent interactions, and that their presence is key during the self-assembly of neighbouring 1-D CPs.

3.5. Experimental

General experimental procedures and specifications of analytical instruments used are provided in Chapter 8.

3.5.1. Synthesis of compounds 14a - c, 15a - c, 16a - c and 17 - 23

Di-*O*-alkoxy-calix[4]arene (14a - c) was synthesised according to literature procedure.[83] Compound **2** (2.00 g, 4.7 mmol) was dissolved in acetone (80 mL) and potassium carbonate (3.26 g, 23.6 mmol) was added followed by the desired iodoalkane (23.6 mmol). The mixture was heated at reflux at 80ºC under nitrogen for 24 hours. The reaction was quenched with 1M HCl (150 mL) and stirred for 1 hour. The organic layer was separated, washed with water and dried over anhydrous magnesium sulfate. The solvent was removed under reduced pressure and the residue was recrystallised in acetone to give a white powder in each case.

Di-*O*-propoxy-calix[4]arene (14a) was obtained in 56% yield; **^{1}H NMR** (300MHz, $CDCl_3$) δ = 8.31 (s, 2 H, -OH), 7.06 (d, *J* = 7.3 Hz, 4 H, Ar-H), 6.93 (d, *J* = 7.3 Hz, 4 H, Ar-H), 6.82 - 6.71 (m, 2 H, Ar-H), 6.70 - 6.60 (m, 2 H, Ar-H), 4.34 (d, *J* = 12.8 Hz, 4 H, Ar-CH_2-Ar), 3.99 (t, *J* = 6.2 Hz, 4 H, -O-CH_2-), 3.39 (d, *J* = 13.2 Hz, 4 H, Ar-CH_2-Ar), 2.09 (sxt, *J* = 7.0 Hz, 4 H, -CH_2-CH_3), 1.33 (t, *J* = 7.3 Hz, 6 H, -CH_3).

Di-*O*-butoxy-calix[4]arene (14b) was obtained in 52% yield; **^{1}H NMR** (300MHz, $CDCl_3$) δ = 8.27 (s, 2 H, -OH), 7.06 (d, *J* = 7.3 Hz, 4 H, Ar-H), 6.93 (d, *J* = 7.7 Hz, 4 H,

Ar-H), 6.80 - 6.72 (m, 2 H, Ar-H), 6.70 - 6.61 (m, 2 H, Ar-H), 4.33 (d, *J* = 12.8 Hz, 4 H, Ar-CH_2-Ar), 4.02 (t, *J* = 6.2 Hz, 4 H, -O-CH_2-), 3.39 (d, *J* = 13.2 Hz, 4 H, Ar-CH_2-Ar), 2.12 - 1.99 (m, 4 H, -CH_2-CH_2-CH_2-), 1.88 - 1.72 (m, 4 H, -CH_2-CH_3), 1.11 (t, *J* = 7.3 Hz, 6 H, -CH_3).

Di-*O*-pentoxy-calix[4]arene (14c) was obtained in 62% yield; **^{1}H NMR** (300MHz, $CDCl_3$) δ = 8.30 (s, 2 H, -OH), 7.05 (d, *J* = 7.3 Hz, 4 H, Ar-H), 6.95 (d, *J* = 7.4 Hz, 4 H, Ar-H), 6.81 - 6.70 (m, 2 H, Ar-H), 6.75 - 6.63 (m, 2 H, Ar-H), 4.32 (d, *J* = 12.6 Hz, 4 H, Ar-CH_2-Ar), 4.00 (t, *J* = 6.3 Hz, 4 H, -O-CH_2-), 3.40 (d, *J* = 13.0 Hz, 4 H, Ar-CH_2-Ar), 2.12 - 1.99 (m, 4 H, -O-CH_2-CH_2-CH_2-), 1.52-1.38 (m, 8 H, -CH_2-CH_2-CH_3), 0.90 (t, *J* = 7.2 Hz, 6 H, -CH_3).

***p*-Di-formyl-di-*O*-alkoxy-calix[4]arene (15a - c)** was synthesised according to amended literature procedure.[84] The appropriate di-*O*-alkoxy-calix[4]arene (1.5 mmol) was dissolved in chloroform (25 mL) and the solution was cooled to -15ºC, and then tin tetrachloride (4.0 g, 15.4 mmol) and 1,1-dichloromethylmethyl ether (0.44 g, 3.9 mmol) were rapidly added. The solution was stirred under nitrogen at room temperature for 30 min. and quenched with de-ionised water. The organic layer was separated, washed with de-ionised water and dried over anhydrous sodium sulfate. Solvent was evaporated under reduced pressure to give pale yellow solid.

***p*-Di-formyl-di-*O*-propoxy-calix[4]arene (15a)** was obtained in a 98% yield; **^{1}H NMR** (300MHz, $CDCl_3$) δ = 9.80 (s, 2 H, -CO-H), 9.27 (s, 2 H, -OH), 7.65 (s, 4 H, Ar-H), 6.99 (d, *J* = 7.3 Hz, 4 H, Ar-H), 6.88 - 6.75 (m, 2 H, Ar-H), 4.32 (d, *J* = 13.2 Hz, 4 H, Ar-CH_2-Ar), 4.03 (t, *J* = 6.2 Hz, 4 H, -O-CH_2-), 3.52 (d, *J* = 13.2 Hz, 4 H, Ar-CH_2-Ar), 2.15 - 2.03 (m, 4 H, -CH_2-CH_3), 1.34 (t, *J* = 7.3 Hz, 6 H, -CH_3).

***p*-Di-formyl-di-*O*-butoxy-calix[4]arene (15b)** was obtained in a 99% yield. **^{1}H NMR** (300MHz, $CDCl_3$) δ = 9.80 (s, 2 H, -CO-H), 9.23 (s, 2 H, -OH), 7.65 (s, 4 H, Ar-H), 6.98 (d, *J* = 7.7 Hz, 4 H, Ar-H), 6.88 - 6.76 (m, 2 H, Ar-H), 4.31 (d, *J* = 13.2 Hz, 4 H, Ar-CH_2-Ar), 4.06 (t, *J* = 6.4 Hz, 4 H, -O-CH_2-), 3.52 (d, *J* = 12.8 Hz, 4 H, Ar-CH_2-Ar), 2.13 - 2.00 (m, 4 H, -CH_2-CH_2-CH_2-), 1.80 (sxt, *J* = 14.9 Hz, 4 H, -CH_2-CH_3), 1.13 (t, *J* = 7.3 Hz, 6 H, -CH_3).

***p*-Di-formyl-di-*O*-pentoxy-calix[4]arene (15c)** was obtained in a 95% yield. **^{1}H NMR** (300MHz, $CDCl_3$) δ = 9.81 (s, 2 H, -CO-H), 9.24 (s, 2 H, -OH), 7.68 (s, 4 H, Ar-H), 6.98 (d, *J* = 7.7 Hz, 4 H, Ar-H), 6.90 - 6.78 (m, 2 H, Ar-H), 4.32 (d, *J* = 12.6 Hz, 4 H, Ar-CH_2-Ar), 4.01 (t, *J* = 6.4 Hz, 4 H, -O-CH_2-), 3.40 (d, *J* = 12.8 Hz, 4 H, Ar-CH_2-Ar), 2.12 - 1.96 (m, 4 H, -O-CH_2-CH_2-CH_2-), 1.55-1.40 (m, 8 H, -CH_2-CH_2-CH_3), 0.88 (t, *J* = 7.2 Hz, 6 H, -CH_3).

***p*-Di-carboxylato-di-*O*-alkoxy-calix[4]arene (16a - c)** was synthesised according to literature procedure.[84] Appropriate di-*O*-alkoxy-*p*-di-formyl-calix[4]arene (**15a - c**) (0.71 mmol) was dissolved in a mixture of acetone (50 mL) and chloroform (50 mL), and then sulfamic acid (0.27 g, 2.8 mmol) dissolved in water (3 mL) and sodium chlorite (0.22 g, 2.4 mmol) dissolved in water (3 mL) were added. The reaction was stirred for 3 hours at room temperature. The organic solvents were removed under reduced pressure. The white solid was taken up with HCl(10%) and filtered to give pale yellow solid.

***p*-Di-carboxylato-di-*O*-propoxy-calix[4]arene (16a)** was obtained in a 96% yield; **^{1}H NMR** (300MHz, DMSO-d_6) δ = 9.12 (s, 2 H, -OH), 7.74 (s, 4 H, Ar-H), 7.00 (d, *J* = 7.7 Hz, 4 H, Ar-H), 6.80 - 6.72 (m, 2 H, Ar-H), 4.10 (d, *J* = 12.8 Hz, 4 H, Ar-CH_2-Ar), 3.90 (t, *J* = 5.7 Hz, 4 H, -O-CH_2-), 3.53 (d, *J* = 12.8 Hz, 4 H, Ar-CH_2-Ar), 2.01 - 1.86 (m, 4 H, -CH_2-CH_3), 1.24 (t, *J* = 7.3 Hz, 6 H, -CH_3); **^{13}C{^{1}H} NMR** (75 MHz, DMSO-d_6) δ = 167.1, 157.0, 151.5, 133.1, 130.2, 129.1, 127.6, 125.5, 121.3, 78.2, 30.2, 22.9, 10.7; **MS** *m/e* 595 ($M - H^+$).

***p*-Di-carboxylato-di-*O*-butoxy-calix[4]arene (16b)** was obtained in a 95% yield; **^{1}H NMR** (300MHz, DMSO-d_6) δ = 9.20 (s, 2 H, -OH), 7.86 (s, 4 H, Ar-H), 7.12 (d, *J* = 7.7 Hz, 4 H, Ar-H), 6.92 - 6.84 (m, 2 H, Ar-H), 4.22 (d, *J* = 12.8 Hz, 4 H, Ar-CH_2-Ar), 4.06 (t, *J* = 5.9 Hz, 4 H, -O-CH_2-), 3.66 (d, *J* = 12.8 Hz, 4 H, Ar-CH_2-Ar), 2.11 - 1.99 (m, 4 H, -CH_2-CH_2-CH_2-), 1.84 (sxt, *J* = 7.3 Hz, 4 H, -CH_2-CH_3), 1.14 (t, *J* = 7.3 Hz, 6 H, -CH_3); **^{13}C{^{1}H} NMR** (75 MHz, DMSO-d_6) δ = 167.1, 157.0, 151.6, 137.2, 130.2, 129.1, 127.6, 125.5, 121.3, 78.3, 31.7, 30.2, 18.8, 13.9; **MS** *m/e* 623 ($M - H^+$).

***p*-Di-carboxylato-di-*O*-pentoxy-calix[4]arene (16c)** was obtained in a 90% yield; **^{1}H NMR** (300MHz, DMSO-d_6) δ = 9.18 (s, 2 H, -OH), 7.90 (s, 4 H, Ar-H), 7.20 (d, *J* = 7.4

Hz, 4 H, Ar-H), 6.99 - 6.87 (m, 2 H, Ar-H), 4.32 (d, *J* = 12.8 Hz, 4 H, Ar-CH_2-Ar), 4.13 (t, *J* = 6.2 Hz, 4 H, -O-CH_2-), 3.74 (d, *J* = 12.8 Hz, 4 H, Ar-CH_2-Ar), 2.19 - 2.08 (m, 4 H, -O-CH_2-CH_2-CH_2-), 1.67-1.52 (m, 8 H, -CH_2-CH_2-CH_3), 0.98 (t, *J* = 7.2 Hz, 6 H, -CH_3); **$^{13}C\{^1H\}$ NMR** (75 MHz, DMSO-d_6) δ = 167.2, 157.1, 151.9, 136.5, 130.8, 129.2, 127.6, 125.7, 121.1, 78.6, 32.2, 31.3, 19.5, 14.1, 10.1; **MS** *m/e* 651 (M - H^+).

Synthesis of 17: A mixture of **16a** (30.0 mg, 0.05 mmol) and $Co(NO_3)_2.6H_2O$ (36.5 mg, 0.125 mmol) was dissolved in 2 mL of dmf, followed by layering of 1 ml of a MeOH solution of 1,10-phenanthroline (9.0 mg, 0.05 mmol). Slow evaporation over several weeks resulted in the formation of pink crystals suitable for X-ray diffraction studies, which were filtered washed and dried to afford 19.4 mg of solid (42 % yield). **EA** calc for $C_{51}H_{49}N_3O_{10}Co_1$, C, 66.37; H 5.35; N, 4.55%. Found C, 69.12; H, 4.75, N, 3.27%. **IR** ν_{max} 3255 cm^{-1} (OH), 2935 cm^{-1} and 2894 cm^{-1} (C-H), 1644 cm^{-1} (C=O), 1609 cm^{-1} (C-O), 1559 cm^{-1} (C-C), 1387 cm^{-1} (C-H), 726 cm^{-1} (C-H). PXRD analysis revealed that the material becomes amorphous upon removal from the mother liquor / drying, which is consistent with the discrepancy between theoretical and experimental results of elemental analysis.

Synthesis of 18: A mixture of **16a** (30.0 mg, 0.05 mmol) and $Cd(NO_3)_2.6H_2O$ (29.6 mg, 0.125 mmol) was dissolved in 2 mL of dmf, followed by layering of 1 ml of a MeOH solution of 1,10-phenanthroline (9.0 mg, 0.05 mmol). Slow evaporation over several weeks resulted in the formation of colourless crystals suitable for X-ray diffraction studies, which were filtered, washed with dmf and dried to afford 18.2 mg of solid (38% yield). **EA** calc for $C_{108}H_{112}N_8O_{24}Cd_2$, C, 64.09; H 5.58; N, 5.54%. Found C, 69.06; H, 4.97, N, 3.26%. **IR** ν_{max} 3173 cm^{-1} (OH), 2929 cm^{-1} and 2881 cm^{-1} (C-H), 1650 cm^{-1} (C=O), 1611 cm^{-1} (C-O), 1547 cm^{-1} (C-C), 1397 cm^{-1} (C-H), 721 cm^{-1} (C-H). PXRD analysis revealed that the material becomes amorphous upon removal from the mother liquor / drying, which is consistent with the discrepancy between theoretical and experimental results of elemental analysis.

Synthesis of 19: A mixture of **16b** (31.3 mg, 0.05 mmol) and $Cd(NO_3)_2.6H_2O$ (29.6 mg, 0.125 mmol) was dissolved in 2 mL of dmf, followed by layering of 1 ml of a MeOH solution of 1,10-phenanthroline (9.0 mg, 0.05 mmol). Slow evaporation over

several weeks resulted in the formation of colourless crystals suitable for X-ray diffraction studies, which were filtered, washed with dmf and dried to afford 12.1 mg of solid (26% yield). **EA** calc for $C_{56}H_{62}N_{11}O_4Cd_1$, C, 62.31; H 5.79; N, 5.19%. Found C, 65.69; H, 5.03, N, 3.02%. **IR** ν_{max} 3204 cm^{-1} (OH), 2960 cm^{-1} and 2892 cm^{-1} (C-H), 1645 cm^{-1} (C=O), 1608 cm^{-1} (C-O), 1551 cm^{-1} (C-C), 1402 cm^{-1} (C-H), 718 cm^{-1} (C-H). PXRD analysis revealed that the material becomes amorphous upon removal from the mother liquor / drying, which is consistent with the discrepancy between theoretical and experimental results of elemental analysis.

Synthesis of 20: A mixture of **16b** (31.3 mg, 0.05 mmol) and $Ni(NO_3)_2.6H_2O$ (36.5 mg, 0.125 mmol) was dissolved in 2 mL of dmf, followed by layering of 1 ml of a MeOH solution of 1,10-phenanthroline (9.0 mg, 0.05 mmol). Slow evaporation over several weeks resulted in the formation of green crystals suitable for X-ray diffraction studies, which were filtered, washed with dmf and dried to afford 5.7 mg of solid (11% yield). **EA** calc for $C_{53}H_{55}N_3O_{10}Ni_1$, C, 66.82; H 5.82; N, 4.41%. Found C, 69.69; H, 5.36, N, 3.21%. **IR** ν_{max} 3230 cm^{-1} (OH), 2971 cm^{-1} and 2888 cm^{-1} (C-H), 1649 cm^{-1} (C=O), 1610 cm^{-1} (C-O), 1545 cm^{-1} (C-C), 1397 cm^{-1} (C-H), 723 cm^{-1} (C-H). Due to inhomogeneity of the product PXRD experiments were not carried out. Discrepancy between theoretical and experimental results of elemental analysis suggests the material becomes amorphous upon removal from mother liquor / drying.

Synthesis of 21: A mixture of **16b** (31.3 mg, 0.05 mmol) and $Co(NO_3)_2.6H_2O$ (36.5 mg, 0.125 mmol) was dissolved in 2 mL of dmf, followed by layering of 1 ml of a MeOH solution of 1,10-phenanthroline (9.0 mg, 0.05 mmol). Slow evaporation over several weeks resulted in the formation of pink crystals suitable for X-ray diffraction studies which were filtered, washed with dmf and dried to give 18.8 mg of solid (36% yield). **EA** calc for $C_{56}H_{63}N_4O_{11.50}Co_1$, C, 64.48; H 6.09; N, 5.37%. Found C, 70.12; H, 5.16, N, 3.17%. **IR** ν_{max} 3215 cm^{-1} (OH), 2982 cm^{-1} and 2875 cm^{-1} (C-H), 1655 cm^{-1} (C=O), 1614 cm^{-1} (C-O), 1551 cm^{-1} (C-C), 1380 cm^{-1} (C-H), 720 cm^{-1} (C-H). PXRD analysis revealed that the material becomes amorphous upon removal from the mother liquor / drying, which is consistent with the discrepancy between theoretical and experimental results of elemental analysis.

Synthesis of 22: A mixture of **16b** (31.3 mg, 0.05 mmol) and $Cu(NO_3)_2.3H_2O$ (30.2 mg, 0.125 mmol) was dissolved in 2 mL of dmf, followed by layering of 1 ml of a MeOH solution of 1,10-phenanthroline (9.0 mg, 0.05 mmol). Slow evaporation over several weeks resulted in the formation of green crystals suitable for X-ray diffraction studies which were filtered, washed with dmf and dried to give 8.1 mg of solid (11% yield). **EA** calc for $C_{74}H_{90}N_8O_{16}Cu_2$, C, 60.27; H 6.15; N, 7.06%. Found C, 69.53; H, 5.42, N, 5.87%. **IR** ν_{max} 3227 cm^{-1} (OH), 2976 cm^{-1} and 2889 cm^{-1} (C-H), 1652 cm^{-1} (C=O), 1602 cm^{-1} (C-O), 1578 cm^{-1} (C-C), 1397 cm^{-1} (C-H), 717 cm^{-1} (C-H). Due to inhomogeneity of the product PXRD experiments were not carried out. Discrepancy between theoretical and experimental results of elemental analysis suggests the material becomes amorphous upon removal from mother liquor / drying.

Synthesis of 23: A mixture of **16a** (30.1 mg, 0.05 mmol) and $Cu(NO_3)_2.3H_2O$ (30.2 mg, 0.125 mmol) was dissolved in 2 mL of dmf, followed by layering of 1 ml of a MeOH solution of 1,10-phenanthroline (9.0 mg, 0.05 mmol). Slow evaporation over several weeks resulted in the formation of green crystals suitable for X-ray diffraction studies which were filtered, washed with dmf and dried to give 5.1 mg of solid (7% yield). **EA** calc for $C_{72}H_{86}N_8O_{16}Cu_2$, C, 59.78; H 5.99; N, 7.75%. Found C, 66.03; H, 6.10, N, 7.18%. **IR** ν_{max} 3248 cm^{-1} (OH), 2976 cm^{-1} and 2851 cm^{-1} (C-H), 1649 cm^{-1} (C=O), 1610 cm^{-1} (C-O), 1563 cm^{-1} (C-C), 1377 cm^{-1} (C-H), 718 cm^{-1} (C-H). Due to inhomogeneity of the product PXRD experiments were not carried out. Discrepancy between theoretical and experimental results of elemental analysis suggests the material becomes amorphous upon removal from mother liquor / drying.

Synthesis of 24: A mixture of **16b** (31.3 mg, 0.05 mmol) and $Co(NO_3)_2.6H_2O$ (36.5 mg, 0.125 mmol) was dissolved in 2 mL of dmf, followed by layering of 1 ml of a MeOH solution of 2-methyl-1,10-phenanthroline (9.7 mg, 0.05 mmol). Slow evaporation over several weeks resulted in the formation of pink crystals suitable for X-ray diffraction studies which were filtered, washed with dmf and dried to afford 15.2 mg of solid (29% yield). **EA** calc for $C_{114}H_{124}N_8O_{23}Co_2$, C, 65.45; H 5.97; N, 5.36%. Found C, 69.48; H, 5.22, N, 3.14%. **IR** ν_{max} 3247 cm^{-1} (OH), 2983 cm^{-1} and 2871 cm^{-1} (C-H), 1643 cm^{-1} (C=O), 1606 cm^{-1} (C-O), 1550 cm^{-1} (C-C), 1373 cm^{-1} (C-H), 728 cm^{-1} (C-H). PXRD analysis revealed that the material becomes amorphous upon removal

from the mother liquor / drying, which is consistent with the discrepancy between theoretical and experimental results of elemental analysis.

Synthesis of 25: A mixture of **16b** (31.3 mg, 0.05 mmol) and $Ni(NO_3)_2.6H_2O$ (36.5 mg, 0.125 mmol) was dissolved in 2 mL of dmf, followed by layering of 1 ml of a MeOH solution of 2-methyl-1,10-phenanthroline (9.7 mg, 0.05 mmol). Slow evaporation over several weeks resulted in the formation of colourless crystals suitable for X-ray diffraction studies which were filtered, washed with dmf and dried to afford 16.7 mg (32% yield). **EA** calc for $C_{114}H_{124}N_8O_{23}Ni_2$, C, 65.46; H 5.98; N, 5.36%. Found C, 69.43; H, 5.19, N, 3.11%. **IR** ν_{max} 3252 cm^{-1} (OH), 2978 cm^{-1} and 2881 cm^{-1} (C-H), 1649 cm^{-1} (C=O), 1608 cm^{-1} (C-O), 1548 cm^{-1} (C-C), 1373 cm^{-1} (C-H), 724 cm^{-1} (C-H). PXRD analysis revealed that the material becomes amorphous upon removal from the mother liquor / drying, which is consistent with the discrepancy between theoretical and experimental results of elemental analysis.

3.5.2. Crystallographic tables for compounds 17 - 25

Complex number	**17**	**18**	**19**
Formula	$C_{51}H_{51}N_3O_{10}Co_1$	$C_{54}H_{56}N_4O_{12}Cd_1$	$C_{56}H_{62}N_{11}O_4Cd_1$
*M*r	922.86	1012.00	1079.54
Crystal system	*P*-1	*P*-1	*P*-1
Space group	Triclinic	Triclinic	Triclinic
T/K	100(2)	173(2)	100(2)
a /Å	10.4507(3)	10.918(3)	10.9671(5)
b /Å	14.6043(5)	14.334(4)	14.2215(6)
c /Å	15.6549(5)	18.082(5)	18.5034(8)
α / ^{o}	100.820(2)	102.665(4)	110.695(2)
β / ^{o}	106.867(3)	106.769(3)	90.387(2)
γ /^{o}	96.430(2)	104.641(3)	106.035(2)
U /Å^3	2210.40(12)	2487.9(11)	2577.2(2)
Z	2	2	2
F(000)	966	992	1124
D_c / g cm^{-3}	1.387	1.282	1.391
μ / mm^{-1}	0.453	0.494	0.489
$2\Theta_{max}$ / ^{o}	76.0	55.8	72.1
Data collected	124185	30640	44494
Unique reflections	18343	11780	18545
R_{int}	0.0317	0.0638	0.0376
Obs data ($I > 2\sigma > (I)$	17068	8022	13353
Parameters	609	581	594
Restraints	0	8	8
R_1 (observed data)	0.0330	0.0558	0.0655
ωR_2 (all data)	0.0988	0.1406	0.1850
GooF	1.037	0.974	1.275
Max/min residuals [eÅ^3]	0.781 / -0.557	1.515 / -1.020	2.075 / -3.529

Complex number	**20**	**21**	**22**
Formula	$C_{53}H_{55}N_3O_{10}Ni_1$	$C_{112}H_{126}N_8O_{23}Co_2$	$C_{74}H_{90}N_8O_{16}Cu_2$
*M*r	952.73	2070.14	1474.68
Crystal system	*P*-1	*C*2/*c*	*C*2/*c*
Space group	Triclinic	Monoclinic	Monoclinic
T/K	100(2)	100(2)	100(2)
a /Å	10.5006(5)	40.974(8)	26.4551(10)
b /Å	14.5683(7)	16.686(3)	14.5002(5)
c /Å	16.5574(8)	15.874(8)	40.5787(19)
α / ^{o}	99.437(3)	90.00	90.00
β / ^{o}	108.082(3)	108.588(11)	105.655(2)
γ /^{o}	99.174(3)	90.00	90.00
U /Å^3	2314.7(2)	10287(3)	14989(10)
Z	2	8	8
F(000)	1004	4368	5056
D_c / g cm^{-3}	1.367	1.337	1.077
μ / mm^{-1}	0.484	0.400	0.619
$2\Theta_{max}$ / ^{o}	54.3	41.8	58.1
Data collected	18335	35178	78141
Unique reflections	7889	5376	15400
R_{int}	0.0388	0.1676	0.0568
Obs data ($I > 2\sigma > (I)$	5358	3777	11796
Parameters	571	699	702
Restraints	9	104	19
R_1 (observed data)	0.0895	0.0887	0.0866
ωR_2 (all data)	0.2373	0.2198	0.2433
GooF	1.050	1.124	1.054
Max/min residuals [eÅ^3]	2.296 / -2.428	0.834 / -0.552	1.391 / -1.663

Complex number	**24**	**25**
Formula	$C_{114}H_{124}N_8O_{23}Co_2$	$C_{114}H_{124}N_8O_{23}Ni_2$
*M*r	2092.06	2091.62
Crystal system	*C2/c*	*I2/a*
Space group	Monoclinic	Monoclinic
T/K	100(2)	100(2)
a /Å	40.9540(2)	15.7924(10)
b /Å	16.7019(8)	16.6359(11)
c /Å	15.8395(7)	39.2230(3)
α / ^{o}	90.00	90.00
β / ^{o}	107.997(2)	94.752(2)
γ /^{o}	90.00	90.00
U /Å^3	10304.3(8)	10269.2(13)
Z	4	4
F(000)	4408	4416
D_c / g cm^{-3}	1.349	1.353
μ / mm^{-1}	0.400	0.445
$2\Theta_{max}$ / ^{o}	51.4	44.1
Data collected	38498	23949
Unique reflections	9792	6236
R_{int}	0.0506	0.0536
Obs data ($I > 2\sigma > (I)$	6749	4512
Parameters	642	635
Restraints	13	19
R_1 (observed data)	0.0618	0.0725
ωR_2 (all data)	0.1691	0.1847
GooF	1.051	1.044
Max/min residuals [eÅ^3]	0.859 / -0.788	1.010 / -0.690

3.6. References

[1] A. Arduini, S. Fanni, G. Manfredi, A. Pochini, R. Ungaro, A. R. Sicuri and F. Ugozzoli, *J. Org. Chem.*, **1995**, *60*, 1448.

[2] V. Arora, H. M. Chawla and A. Santra, *Tetrahedron*, **2002**, *58*, 5591.

[3] M. Galli, J. A. Berrocal, S. Di Stefano, R. Cacciapaglia, L. Mandolini, L. Baldini, A. Casnati and F. Ugozzoli, *Org. Biomol. Chem.*, **2012**, *10*, 5109.

[4] C. A. Hunter and J. K. M. Sanders, *J. Am. Chem. Soc.*, **1990**, *112*, 5525.

[5] P. J. Nichols, C. L. Raston and J. W. Steed, *Chem. Commun.*, **2001**, 1062.

[6] A. Spek, *Acta Crystallogr. Sect. D*, **2009**, *65*, 148

[7] P. J. Dykstra, J. A. J. Brunink, K.E. Bugge, D. N. Reinhoudt, S. Harkema, R. Ungaro, F. Ugozzoli and E. Ghidini, *J. Am. Chem. Soc.*, **1989**, *111*, 7567.

[8] A. Arduini, M. Fabbi, M. Mantovani, L. Mirone, A. Pochini, A. Secchi and R. Ungaro, *J. Org. Chem.*, **1995**, *60*, 1454.

Chapter 4. Alternative di-*p*-carboxylatocalixarenes as di-topic linkers in the construction of coordination polymers

In Chapter 3 it was demonstrated that, with the use of synthetic chemistry, it is possible to selectively introduce specific functional groups to the upper- and lower-rim of the calixarene framework and attain a desired target molecular building block, which can then be utilised as a di-topic linker to construct 1-D CPs. Considering the tetra-*p*-carboxylatocalixarene-based structures highlighted in Chapter 1, it is apparent that the calixarene conformation (e.g. cone vs. pinched-cone) can have a profound effect on the outcome of assembly (MOPs vs. binuclear aqua-bridged metal clusters). This also relates to the conformation displayed by di-*p*-CO_2[4] structures **17** - **25** in this thesis; in all cases the di-*p*-CO_2[4]s adopt a partially-pinched cone conformation and are of C_2 symmetry. These conformational characteristics led to the synthesis of di-*p*-CO_2[4]s that would possess a different conformation relative to calixarenes **14a** - **c** and or exploit the C_2 symmetry of a di-alkoxy-calix[4]arene through selective functionalisation at the *para* carbon atoms of alkylated arenes (rather than non-alkylated arenes such as those in di-*p*-CO_2[4]s **14a** - **c**). By synthesising these new di-*p*-CO_2[4] building units it was anticipated that they could be utilised in the construction of supramolecular assemblies in similar way in which **14a** - **c** were used to assemble compounds **17** - **25**. However, considering that the relative orientation of the carboxylic acids in 'alternative' di-*p*-CO_2[4]s is different, the resulting assemblies are expected to exhibit different structural features in the solid state.

4.1. Alternative di-*p*-carboxylatocalixarenes as new building blocks for the construction of CPs

The inherent shape of a di-*O*-alkoxy-calix[4]arene and the subsequent positioning of carboxyl groups at the calixarene upper-rim enables its use as a di-topic linker to connect metal centres and form CPs. Analysis of crystal structures of the CPs in Chapter 3 (**17** – **25)** reveals that di-*p*-CO_2[4]s adopt a partially pinched-cone conformation with a resultant C_2 symmetry. In **17** - **25** the distance between the *para* carbon atoms of distal arenes containing hydroxyl groups is approximately 2 Å longer than that found between the *para* carbon of the other distal alkylated arenes (Fig. 4.1).

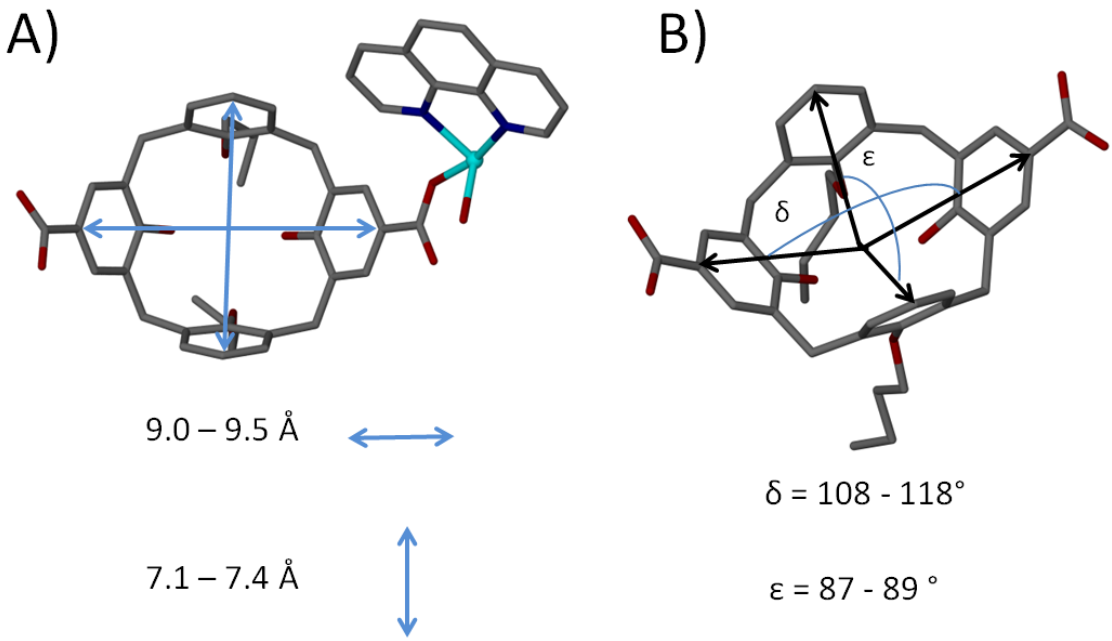

Figure 4.1 (A) Range of distances found between distal arene *para* carbon atoms in di-*p*-CO_2[4]s in **17** - **25**. (B) Angles δ and ε between distal arene *para* carbon atoms and a centroid generated between phenolic oxygen atoms of di-*p*-CO_2[4]s in **17** - **25**.

Further analysis also reveals that the angle between *para* carbon atoms from distal arenes containing hydroxyl groups and the centroid generated from phenolic oxygen atoms, δ, is significantly larger than the corresponding angle, ε, between *para* carbon atoms from distal alkylated arenes containing alkoxy chains. The narrow angle ε is observed to be just less than 90º (87 - 89º) whereas the wide-angle δ varies from 108 -

118º in **17 - 25**. The magnitude of the wide angle is observed to be at the low and high ends of this range when the cavity is occupied by dmf and phen respectively. This difference in the relative orientation of the two pairs of distal *para* carbon atoms prompted the synthesis of an 'alternative' di-*p*-carboxylatocalix[4]arene (*alt*-di-*p*-CO_2[4]). In this alternative form the carboxyl groups are introduced to *para* carbons of arenes containing alkoxy chains, also allowing it to be utilised as a di-topic building block. Given that the bite angle between carboxyl moieties in *alt*-di-*p*-CO_2[4]s differs markedly from that observed in di-*p*-CO_2[4]s, we anticipated that by using *the former* as building blocks, the outcome of metal-directed assembly would be concomitantly different supramolecular architectures.

4.1.1. Synthesis of alternative di-p-carboxylatocalix[4]arenes

A series of *alt*-di-*p*-CO_2[4]s, **29a - c**, were synthesised according to a modified literature procedure.[85, 86] Compared to di-*p*-CO_2[4]s **14a - c**, the synthesis of **29a - c** involves two additional steps as shown in Figure 4.2. In order to selectively functionalise the *para* carbon atoms of the alkylated arenes one must first alter the reactivity of those carbons *para* to the hydroxyl groups in **14a - c**; this can be achieved by introducing protecting nosyl group to afford **26a - c** respectively. Due to this deactivation, subsequent formylation occurs at the *para* carbon atoms of alkylated arenes to afford **27a - c**. Literature reported the de-protection of **27a - c** to be unsuccessful.[85] However, oxidation of formylated derivatives affords *p*-carboxylatocalixarenes **28a - c** and subsequently allows for de-protection of the arene in each case to give *alt*-di-*p*-CO_2[4]s **29a - c**.[86]

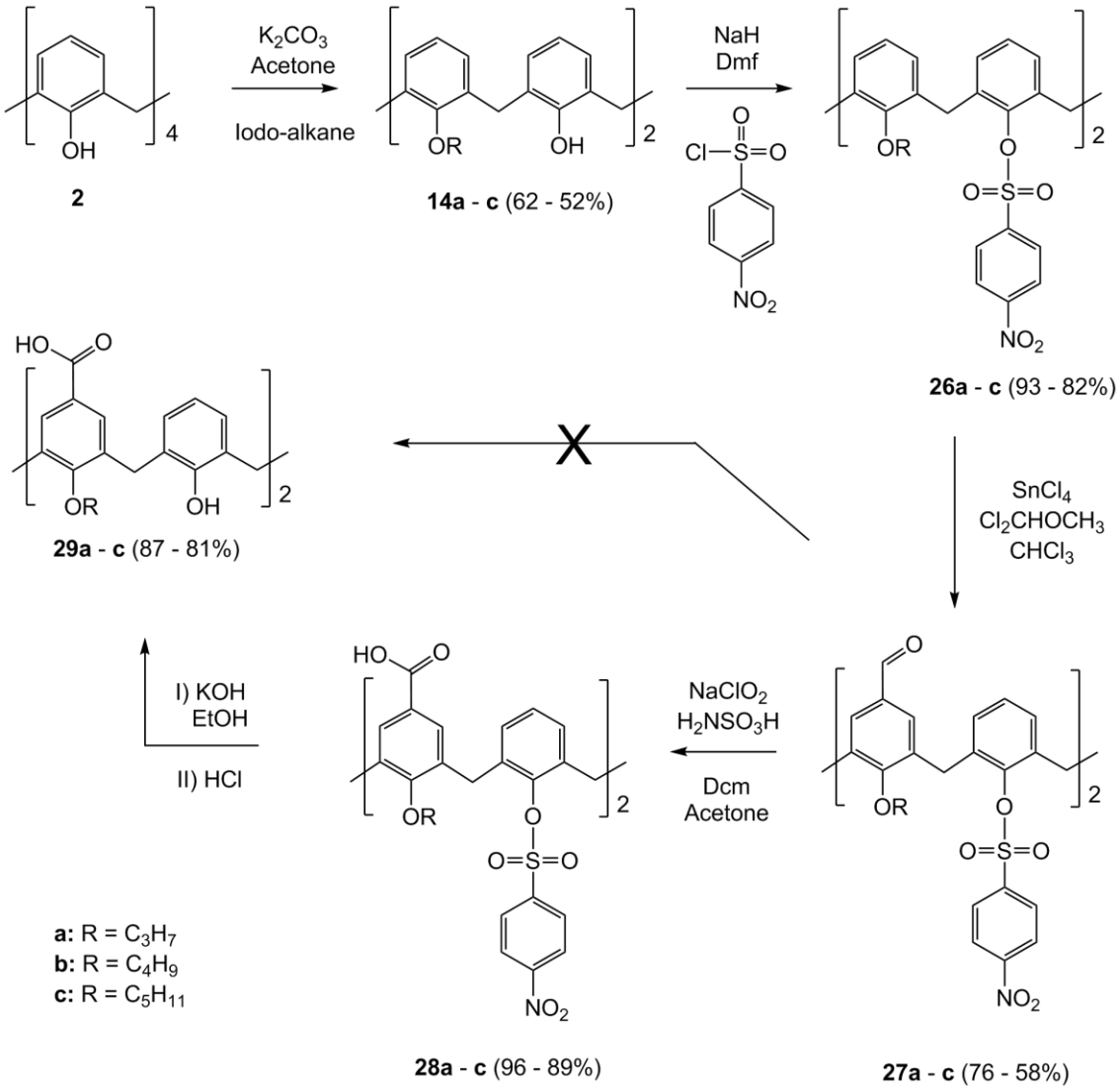

Figure 4.2 Schematic of the synthesis of *alt*-di-*p*-CO_2[4]s **29a - c**.[85, 86]

4.2. Self-assembly of *alt*-di-*p*-CO_2[4] with TM(II) and phen

Following the synthesis of a library of *alt*-di-*p*-CO_2[4]s the focus of the investigation turned to a) their utility as di-topic linkers for the construction of supramolecular assemblies and b) comparison with structures obtained using di-*p*-CO_2[4]. A good starting point was thus to carry out reactions analogous to those used to synthesise **17 - 25**. A series of reactions were carried out in which dmf solutions containing a TM(II) nitrate salt (Co, Mn, Cu, Cd, Zn or Ni) and appropriate *alt*-di-*p*-CO_2[4] were layered with methanolic solution of phen, 2-me-phen, 3-me-phen, 4-me-phen or t-me-phen. Clear solutions were left to slowly evaporate over a period of time, which varied from weeks to months to yield crystals suitable for SCXRD analysis.

None of the reactions in which *alt*-di-*p*-CO_2[4] **29c** was used yielded crystals suitable for structural analysis. Given that some of the new materials synthesised exhibit markedly different solid-state structural features their discussion will be divided into two chapters. This chapter will focus on 1-D CP- structures, whereas Chapter 5 details the remaining results of this area of investigation.

Reaction of Co(II) ions with *alt*-di-*p*-CO_2[4] **29a** and phen, followed by slow evaporation, yielded crystalline material of formula [Co(**29a**)phen(H_2O)]·dmf (**30**). The pale pink single crystals of **30** were in a monoclinic cell and the structure was solved in space group $P2_1/n$. The unit cell parameters are a = 11.2141(4) Å, b = 12.9667(5) Å and c = 30.9925(10) Å, and β = 91.012(2)º. The asymmetric unit comprises one Co(II) ion, one *alt*-di-*p*-CO_2[4] **29a**, one phen, one aquo ligand and one uncoordinated dmf of crystallisation. The coordination complex formed in **30** consists of one Co(II), two *alt*-di-*p*-CO_2[4] **29a**, one phen and one aquo ligand (Fig. 4.3A). As in the case of **17**, **21** and **22**, each calixarene in **30** is coordinated to two Co(II) centres *via* carboxylate moieties: the O(5)-C(29)-O(6) group is coordinated in a monodentate fashion to Co(1) *via* O(5) with the bond length of 1.986(5) Å, while the O(7)-C(30)-O(8) group is coordinated to s.e. Co(1)' in a bidentate fashion with respective bond lengths of 2.159(7) Å and 2.123(5) Å. The aquo ligand is coordinated to the metal centre *via* the Co(1)-O(9) bond (2.091(6) Å). As expected phen is coordinated as a chelate, thereby restricting space around the metal centre with respective Co(1)-N(1) and Co(1)-N(2) distances of 2.126(9) Å and 2.056(8) Å. Symmetry expansion of reveals formation of 1-D CPs which adopt a spiral shape, rather than linear as observed when di-*p*-CO_2[4] **16a** and **16b** are used as building blocks (Fig 4.3B). The spiral shape of the formed CP in **30** is illustrated by the green line in Figure 4.3C. This result indicates that the use of a calixarene with an alternative positioning of the two carboxyl groups at the upper-rim, as anticipated, can yield a markedly different supramolecular assembly in the solid state. The *alt*-di-*p*-CO_2[4] adopts a partially pinched-cone conformation with distances between distal arene *para* carbon atoms of 7.45 Å and 8.82 Å. The angles measured between diametrical *para* carbon atoms and centroid generated from phenolic oxygen atoms, ε and δ, are 90.7° and 106.9° respectively, which are consistent with those observed in di-*p*-CO_2[4]s in **17** - **25**.

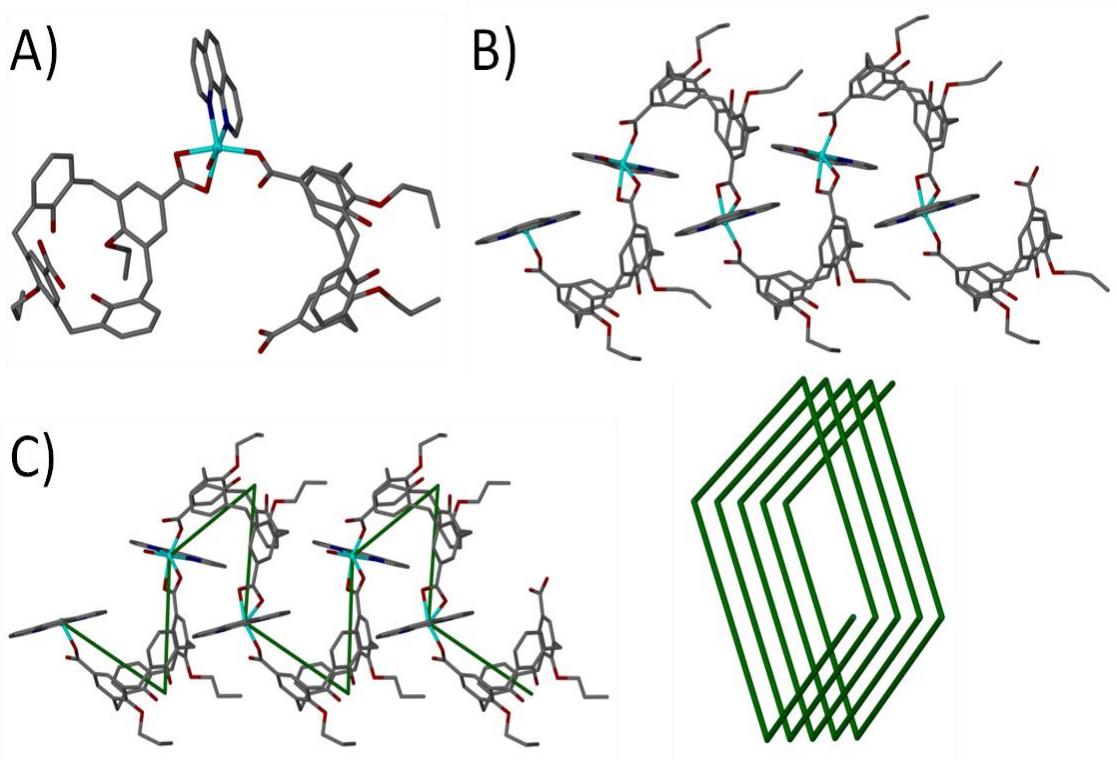

Figure 4.3 (A) Ball and stick representation of the coordination complex formed in **30**. (B) Extended structure in **30** showing the spiral CP. (C) Green line connecting metal centres and centroids generated from phenolic oxygen atoms illustrating the spiral shape of the CP formed in **30**. Hydrogen atoms and dmf of crystallisation omitted for clarity.

The dmf of crystallisation resides in the *alt*-di-*p*-CO_2[4] cavity and forms host-guest CH···π interactions, with distances between four hydrogen atoms of dmf and calixarene aromatic rings ranging from 2.56 - 3.00 Å (Fig 4.4A).[68] Further analysis reveals that phen is not involved in π-stacking, but phen hydrogen atoms do participate in CH···π interactions with 1) phen from a neighbouring twisted CP (3.04 Å contact distance) and 2) an aromatic ring from a s.e. calixarene in the same CP (2.85 Å contact distance), as shown in Figure 4.4B. Inspection of the solid-state packing reveals that the twisted CPs are packed together in an efficient manner, excluding the formation of solvent channels. However, examination of the *alt*-di-*p*-CO_2[4]s forming the spiral CPs results in formation of solvent pockets filled with co-crystallised dmf molecules. Given our interest in the generation of porous materials compound **30** was further analysed. Crystalline material was filtered and dried, however PXRD experiments show that the material had become amorphous upon removal from the mother liquor / drying.

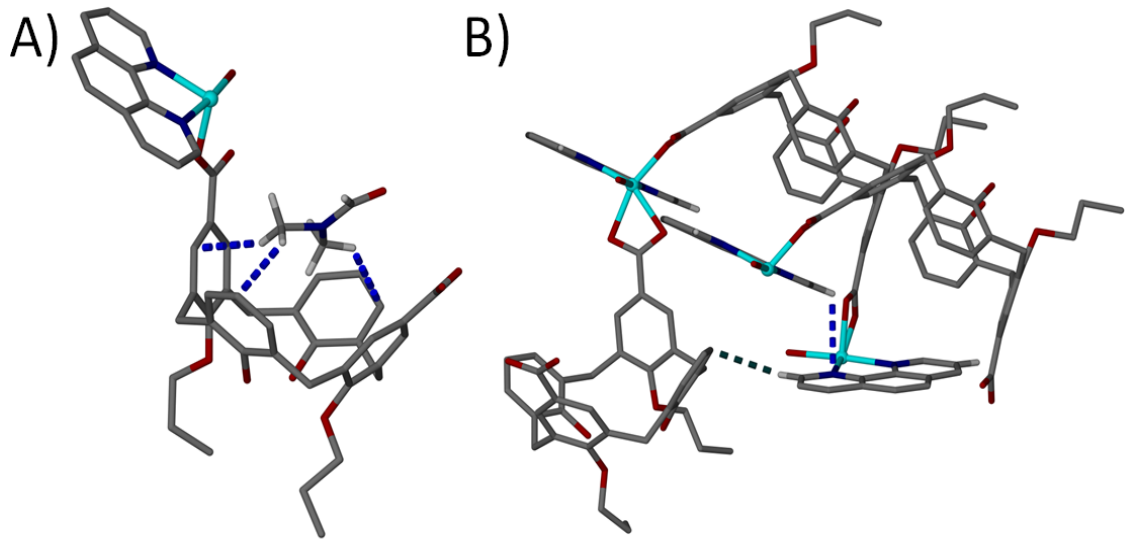

Figure 4.4 (A) Asymmetric unit in **30** showing complementary host-guest CH···π interactions between dmf hydrogen atoms and calixarene aromatic rings. (B) Section of the extended structure in **30** showing CH···π interaction between phen hydrogen atom and calixarene aromatic ring from the same spiral CP (green dashed line) and CH···π interaction between neighbouring twisted CPs (blue dashed line). Hydrogen atoms, except those involved in CH···π interactions, omitted for clarity.

The reaction of Co(II) with *alt*-di-*p*-CO_2[4] **29b** and phen resulted in pink solution which after several weeks of slow evaporation produced pale pink blocks suitable for SCXRD analysis. Attained crystals are in a monoclinic cell and the structure was solved in space group $P2_1/n$. The asymmetric unit is comprising one Co(II) ion, one *alt*-di-*p*-CO_2[4] **29b**, one phen, one aquo ligand and one dmf of crystallisation. Structure analysis reveals formation of coordination complex of formula [Co(**29b**)(phen)(H_2O)]·dmf (**31**), which assembles in the solid-state to form twisted 1-D CPs as shown in Figure 4.5. The unit cell parameters of **31** (a = 11.8055(9) Å, b = 12.5516(9) Å and c = 32.702(2) Å, and β = 91.264(5)º) are marginally different to those of **30** (a = 11.2141(4) Å, b = 12.9667(5) Å and c = 30.9925(10) Å, and β = 91.012(2)º), and comparison of TM-ligand bond lengths in **30** and **31** reveals that the metal coordination spheres in both compounds are near-identical.

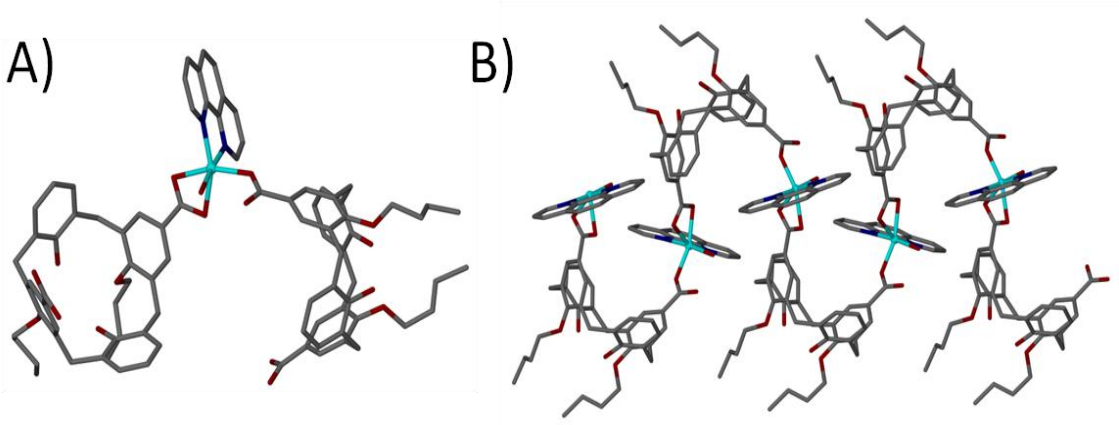

Figure 4.5 (A) Ball and stick representation of coordination complex **31**. (B) Extended structure showing spiral CP formed in **31**. Hydrogen atoms and dmf of crystallisation omitted for clarity.

As in the case of **30,** each *alt*-di-*p*-CO_2[4] is coordinated to two Co(II) centres *via* its carboxylate groups: the O(7)-C(30)-O(8) group is coordinated to Co(1) in a monodentate fashion *via* O(7) with a bond length of 2.000(5) Å, while the O(5)-C(29)-O(6) group is coordinated to s.e. Co(1)' in a bidentate fashion with the bond lengths of 2.125(5) Å and 2.190(5) Å respectively. The aquo ligand is coordinated to the metal centre *via* the Co(1)-O(9) bond, which is 2.091(5) Å long. Furthermore, symmetry expansion of the asymmetric unit in **31** reveals very similar solid-state packing of spiral 1-D CPs to that observed in **30**. Structural analysis of **31** shows that the a*lt*-di-*p*-CO_2[4] in **29b** also adopts a partially pinched-cone conformation, with distances between distal arene *para* carbon atoms of 7.43 Å and 8.99 Å. The angles ε and δ are 90.1° and 108.7° respectively, what is in good agreement with those found in **30**, and the calixarene cavity in **31** is also occupied by dmf of crystallisation, resulting in host-guest CH···π interactions (Fig 4.6A). Further analysis of the extended structure reveals that phen is also not involved in π-stacking, however phen hydrogen atoms are involved in CH···π interactions similarly as in **30** with 1) phen from a neighbouring twisted CP (3.08 Å contact distance) and 2) an aromatic system from a s.e. calixarene in the same CP (2.90 Å contact distance), as shown in Figure 4.6B. Crystals of **31** were filtered and dried, however PXRD experiments show that the dried material had become amorphous, suggesting that **31** loses crystallinity upon removal from the mother liquor / drying.

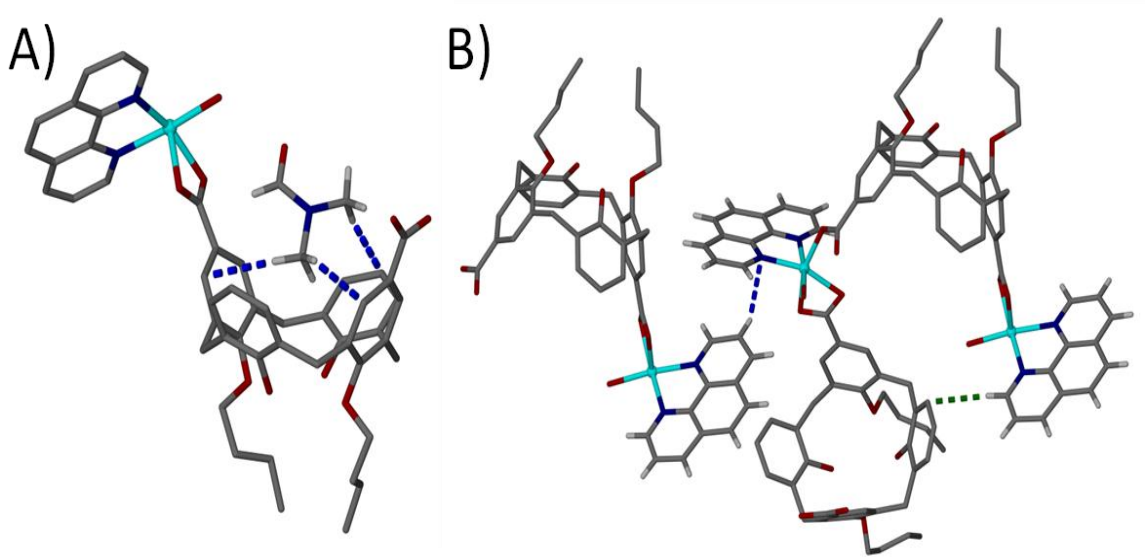

Figure 4.6 (A) Asymmetric unit in **31** showing complementary host-guest CH···π interactions between dmf hydrogen atoms and calixarene aromatic rings. (B) Section of the extended structure in **31** showing CH···π interactions between phen hydrogen atom and calixarene aromatic ring (green dashed line) and CH···π interactions between neighbouring twisted CPs (blue dashed line). Hydrogen atoms, except those involved in CH···π interactions, omitted for clarity.

The reaction of Ni(II) with *alt*-di-*p*-CO_2[4] **29b** and phen resulted in a green solution which, after few months of slow evaporation, yielded small green blocks suitable for SCXRD analysis. Structure analysis reveals formation of the coordination complex of formula [Ni(**29b**)(phen)(H_2O)]·dmf (**32**) (Fig. 4.7A). The crystals are in a monoclinic cell and the structure was solved in space group $P2_1/n$. Comparison of unit cell parameters of **32** with those of **31** reveals that they are almost identical: a = 11.6753(5) Å, b = 12.4874(4) Å and c = 32.6697(11) Å, and β = 91.466(2)º (cell parameters of **31** are: a = 11.8055(9) Å, b = 12.5516(9) Å and c = 32.702(2) Å, and β = 91.264(5)º). The asymmetric unit contains one Ni(II) ion, one *alt*-di-*p*-CO_2[4] **29b**, one phen, one aquo ligand and one uncoordinated dmf of crystallisation. The coordination complexes in **32** form spiral CPs (Fig 4.7B), identical to those formed in **31**, thus given almost identical cell parameters and solid state structural features in **31** and **32**, they can be considered isostructural. Given that attempts to attain a homogeneous crystalline product of **32** did not succeed it was not possible to carry out any further analysis.

Attempts to synthesise a twisted CP with a Ni(II) metal centre using calixarene **29a** in place of **29b** did not yield a crystalline material.

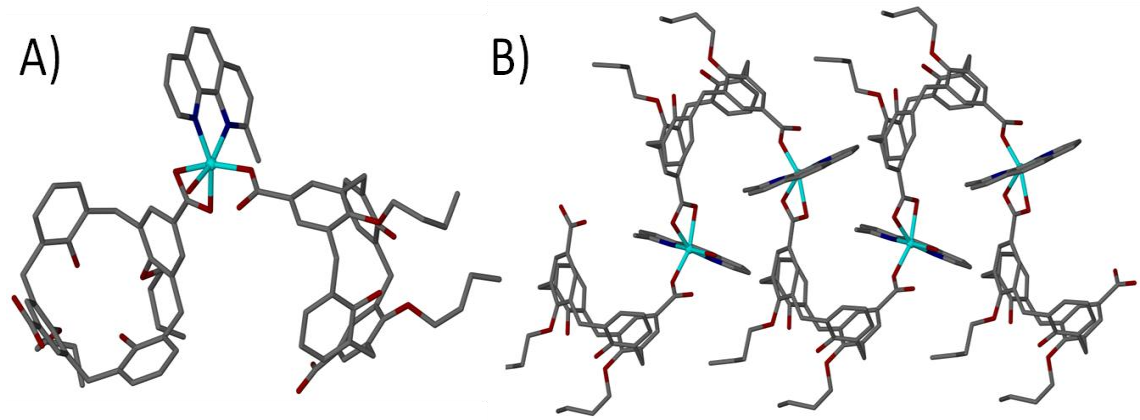

Figure 4.7 (A) Ball and stick representation of coordination complex formed in **32**. (B) Spiral CP found in the extended structure of **32**. Hydrogen atoms and dmf of crystallisation omitted for clarity.

In this chapter it has been shown that exploitation of the C_2 symmetry of the di-*O*-alkylated-calix[4]arene enables the synthesis of new building blocks (*alt*-di-*p*-CO_2[4]s **29 a-c**). As a consequence of the C_2 symmetry the positioning of carboxyl groups has a significant effect on the outcome of metal-directed assembly. A reaction of Co(II) or Ni(II) ions with *alt*-di-*p*-CO_2[4] and phen results in the formation of spiral 1-D CPs (**30** - **32**) that are markedly different to the linear 1-D CPs (**17** - **21**) synthesised using the same TM(II) ions, phen and di-*p*-CO_2[4]s. As a result of the spiral shape of the CPs formed here, compounds **30** - **32** exhibit very different solid-state packing relative to the aforementioned 1-D CPs (**17** - **21**).

4.3. Self-assembly of *alt*-di-*p*-CO_2[4] with TM(II) and phen derivatives

Part of the investigation was to further study the role of phen derivatives as a co-ligand in the assembly and evaluate its impact on solid-state packing. Having proven that synthetic pre-organisation of calixarene functionality can be successfully utilised to synthesise materials displaying different structural features with phen (linear vs. spiral

CPs), avenues of investigation turned to the influence of various methyl-substituted phens on assembly and solid-state packing. A reaction of Co(II) ions, *alt*-di-*p*-CO_2[4] **29a** and 2-me-phen resulted in a pink solution which, after several weeks of slow evaporation, yielded pale pink crystals suitable for SCXRD analysis. The crystals are in a monoclinic cell and the structure was solved in space group $P2_1/n$. The asymmetric unit comprises one Co(II) ion, one *alt*-di-*p*-CO_2[4] **29a**, one 2-me-phen, one ligated water and one uncoordinated dmf of crystallisation. Solution of the crystal structure reveals formation of a coordination complex of formula [Co(**29a**)(2-me-phen)(H_2O)]·dmf (**33**) (Fig. 4.8A). Inspection of unit cell parameters of **33** reveals that, despite the use of 2-me-phen in the synthesis, the cell parameters of **33** (a = 11.1299(9) Å, b = 13.1246(11) Å and c = 31.509(2) Å and β = 92.918(3)º) remain very similar to those of **30** (a = 11.2141(4) Å, b = 12.9667(5) Å and c = 30.9925(10) Å, and β = 91.012(2)º). Extension of the asymmetric unit in the crystal structure of **33** reveals the formation of spiral CPs (Fig 4.8B) which pack in solid state in the same manner as the spiral 1-D CPs pack in **30** - **32**. Despite the methyl substituent being present, the same hydrogen atoms of 2-me-phen are involved in the CH···π interactions as those in the phen containing structures (Fig 4.9A). Furthermore, as in **30** - **32**, the *alt*-di-*p*-CO_2[4] cavity is occupied by a dmf of crystallisation what results in complementary host-guest CH···π interactions (Fig. 4.9B). Crystals of **33** were filtered and dried, however PXRD experiments show that the dried material had become amorphous, suggesting that **33** loses crystallinity upon removal from the mother liquor / drying.

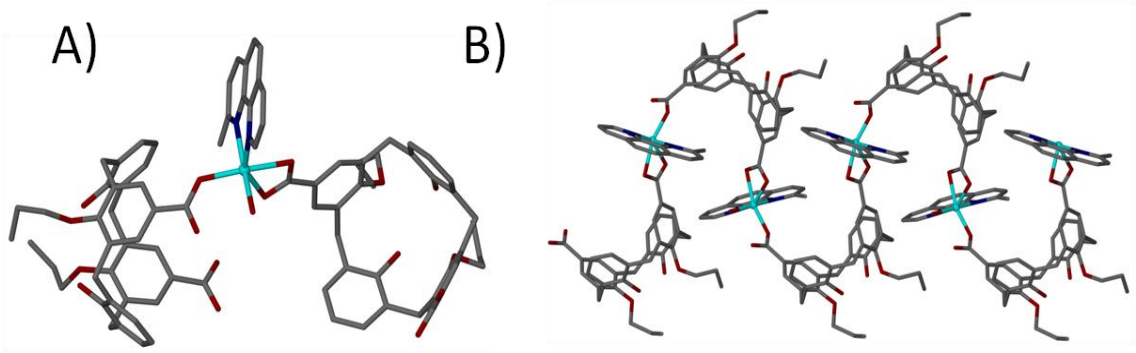

Figure 4.8 (A) Ball and stick representation of coordination complex formed in **33**. (B) Extended structure showing spiral CP formed in **33**. Hydrogen atoms and dmf of crystallisation omitted for clarity.

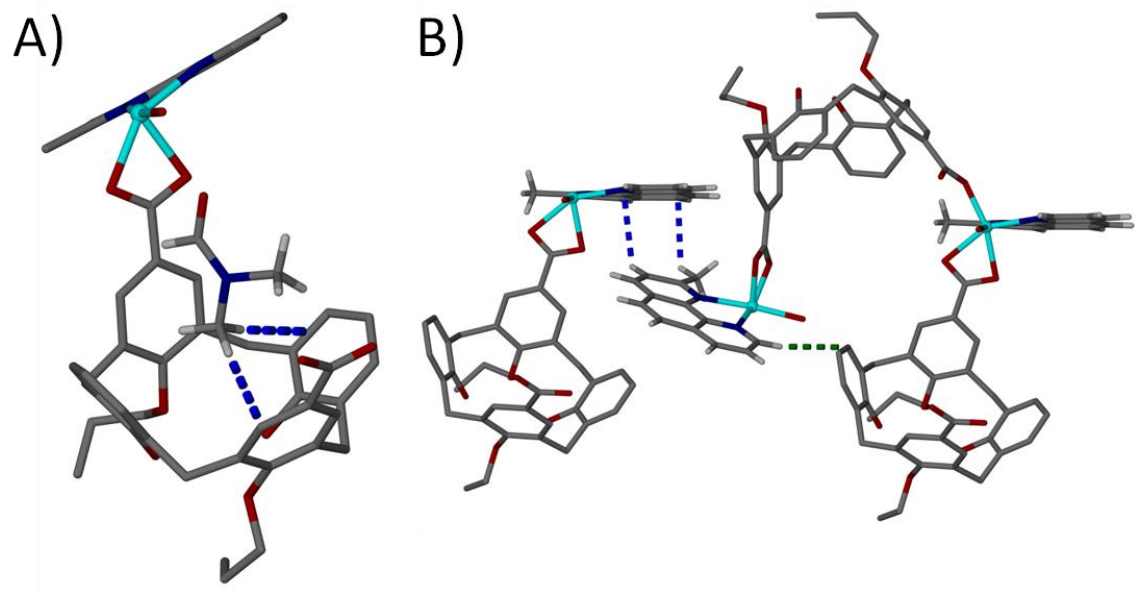

Figure 4.9 (A) Asymmetric unit in **33** showing complementary host-guest CH···π interaction between dmf hydrogen atoms and calixarene aromatic rings. (B) Section of the extended structure in **33** showing CH···π interactions between phen hydrogen atom and calixarene aromatic ring (green dashed line) and CH···π interactions between neighbouring twisted CPs (blue dashed line). Hydrogen atoms, except those involved in CH···π interactions, omitted for clarity.

Slow evaporation of a green solution containing Ni(II), *alt*-di-*p*-CO_2[4] **29a** and 2-me-phen resulted in crystalline green small blocks which were analysed using SCXRD. Analysis of collected data reveals formation of a complex of formula [Ni(**29a**)(2-me-phen)(H_2O)]·dmf (**34**) which assemble together to form spiral CPs (Fig 4.10). The crystals are in a monoclinic cell and the structure was solved in space group $P2_1/n$. The asymmetric unit contains one Ni(II) ion, one *alt*-di-*p*-CO_2[4] **29a**, one 2-me-phen, an aquo ligand and one uncoordinated dmf of crystallisation. Inspection of cell parameters of **34** (a = 11.0936(16) Å, b = 12.9117(19) Å and c = 31.661(5) Å, and β = 92.649(2)º), together with analysis of extended structure, reveals that **34** is isostructural with **33**, and both exhibit identical structural features in the solid state as **30 - 32**. Given that attempts to attain a homogeneous crystalline product of **34** did not succeed and further analysis was not carried out.

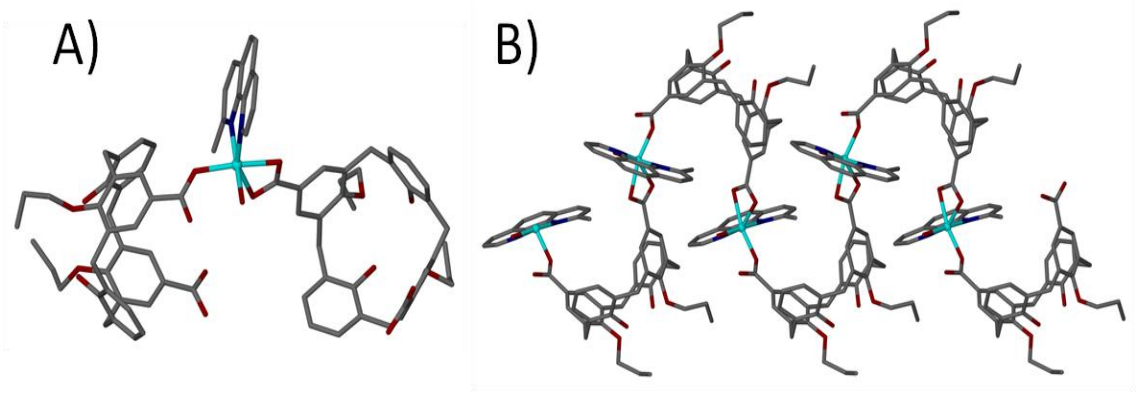

Figure 4.10 (A) Ball and stick representation of coordination complex formed in **34**. (B) Extended structure showing spiral CP formed in **34**. Hydrogen atoms and dmf of crystallisation omitted for clarity.

Slow evaporation of reaction solutions containing Co(II) or Ni(II), *alt*-di-*p*-CO_2[4] **29b** and 2-me-phen also resulted in the formation of crystalline materials. Analyses of collected data reveals formation of complexes of formula [Co(**29b**)(2-me-phen)(H_2O)]·(dmf) (**35**) and [Ni(**29b**)(2-me-phen)(H_2O)]·(dmf) (**36**) respectively, which assemble to form twisted 1-D CPs identical to those discussed above (Fig. 4.11). Crystals of both materials are in a monoclinic cell and structures were solved in space group $P2_1/n$. The unit cell parameters of **35** (a = 11.2423(4) Å, b = 13.1599(6) Å and c = 32.5801(12) Å and β = 90.668(2)º) and **36** (a = 11.2656(6) Å, b = 12.9401(7) Å and c = 32.6181(15) Å and β = 90.369(3)º) are in good agreement with unit cell parameters of **31** and **32**, thus given same cell parameters and the almost identical solid state packing they can be considered isostructural with **31** and **32**. Structural analysis of **35** and **36** shows that similarly as in previously discussed structures, in which *alt*-di-*p*-CO_2[4] **29a** was used (**33** and **34**), the methyl substituent at 2-position also does not affect the solid-state packing, and components in resulting structures undergo same type of non-covalent interactions. Crystals of **35** were filtered and dried, however PXRD experiments show that the dried material had become amorphous, suggesting that **35** loses crystallinity upon removal from the mother liquor / drying. Attempts to attain a homogeneous crystalline product of **36** did not succeed and further analysis was not carried out.

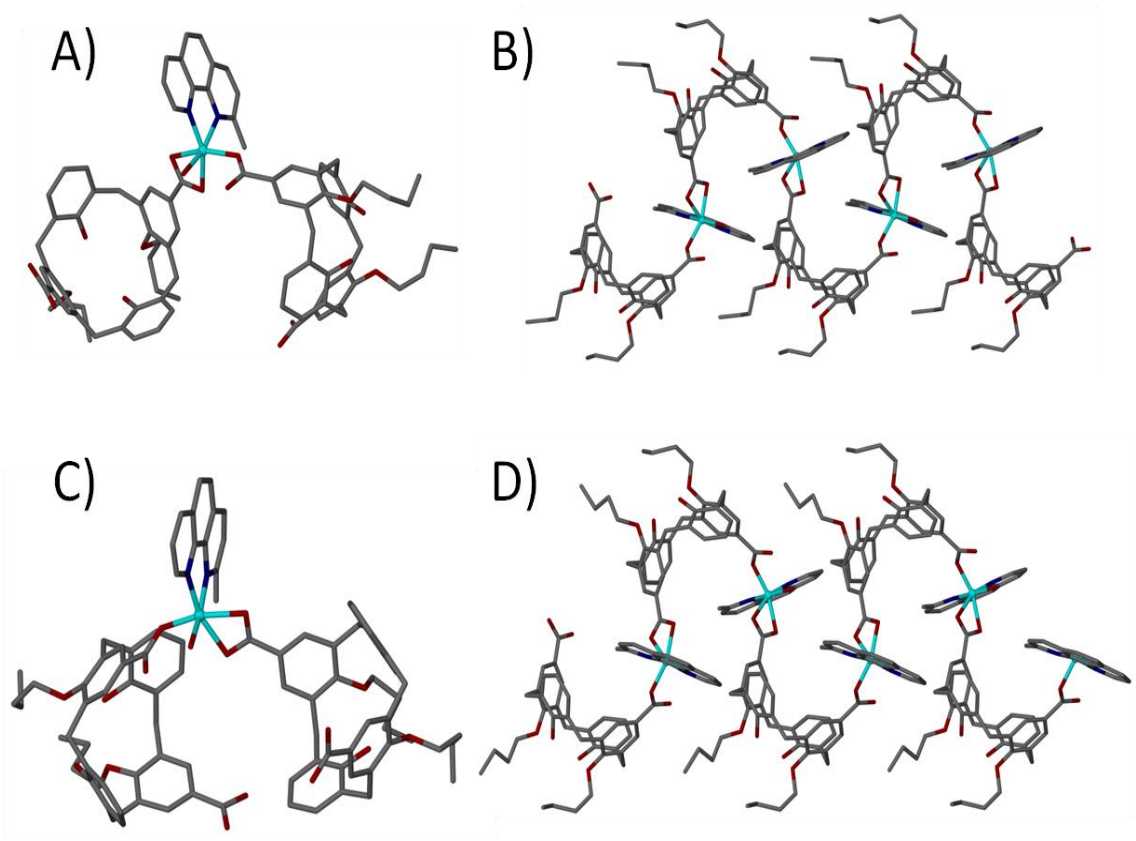

Figure 4.11 Ball and stick representation of coordination complex formed in (A) **35** and (B) **36**. Extended structure showing spiral CP formed in (C) **35** and (D) **36**. Hydrogen atoms and dmf of crystallisation omitted for clarity.

Reaction of Zn(II) ions with di-*p*-CO_2[4] **16a** - **c** and phen or phen derivatives in majority of cases yielded fine white powder, which with the use of PXRD analyses were confirmed to be amorphous. However, reactions of Zn(II) with *alt*-di-*p*-CO_2[4] **29a** or **29b** and 2-me-phen yielded crystalline colourless plates. A SCXRD analysis reveals that reaction of Zn(II) ions with *alt*-di-*p*-CO_2[4] **29a** and 2-me-phen results in crystals of formula [Zn(**29a**)(2-me-phen)(H_2O)]·(dmf) (**37**). The crystals of **37** are in a monoclinic cell and the structure was solved in space group $P2_1/n$. The unit cell parameters of **37** (a = 11.1266(5) Å, b = 13.3137(6) Å and c = 31.4424(12) Å and β = 93.048(3)º) are marginally different to those of **33** and **34**. The asymmetric unit contains one Zn(II) ion, one *alt*-di-*p*-CO_2[4] **29a**, one 2-me-phen, one aquo ligand and one uncoordinated dmf of crystallisation. Structural analysis of **37** reveals formation of a coordination complex comprising one Zn(II), two *alt*-di-*p*-CO_2[4] **29a**, one 2-me-phen

and one aquo ligand (Fig. 4.12A). Symmetry expansion of the asymmetric unit reveals formation of spiral 1-D CPs (Fig 4.12B). The *alt*-di-*p*-CO_2[4] **29a** is coordinated to two Zn(II) centres *via* its carboxylate groups, however unlike in previously discussed structures, in **37** both of the carboxylate moieties are coordinated to the metal centre in a monodentate fashion: the O(5)-C(29)-O(6) group is coordinated to Zn(1) *via* O(5) with the bond length of 1.996(9) Å and the O(7)-C(30)-O(8) groups is coordinated to s.e. Zn(1)' *via* O(7) with the bond length of 2.007(10) Å. The aquo ligand is coordinated to Zn(1) *via* O(9) atom to form a 2.149(9) Å long bond. As expected 2-me-phen is coordinated as a chelate restricting space around the metal centre with Zn(1)-N(1) and Zn(1)-N(2) distances of 2.244(12) Å and 2.059(12) Å respectively. Structural analysis of **37** shows that a*lt*-di-*p*-CO_2[4] **29a** also adopts a partially pinched-cone conformation, with distances between distal arene *para* carbon atoms of 7.41 Å and 8.79 Å. The angles ε and δ are 89.9° and 105.8° respectively, what is in good agreement with those found in *alt*-di-*p*-CO_2[4] containing structures discussed so far. The *alt*-di-*p*-CO_2[4] **29a** cavity is occupied by dmf of crystallisation what results in complementary host-guest CH···π interactions between dmf hydrogen atoms and calixarene aryl rings. Each of the ligated 2-me-phen in **37** is involved in two different CH···π interactions, what is concomitant with those found in **33** - **36** (Fig. 4.13). Attempts to attain a homogeneous crystalline product of **37** did not succeed and further analysis was not carried out.

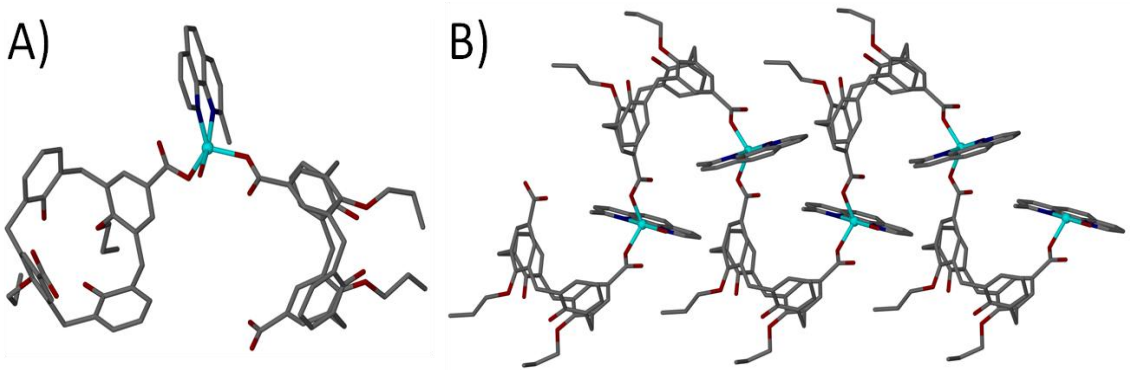

Figure 4.12 (A) Ball and stick representation of coordination complex formed in **37**. (B) Extended structure showing spiral CP formed in **37**. Hydrogen atoms and dmf of crystallisation omitted for clarity.

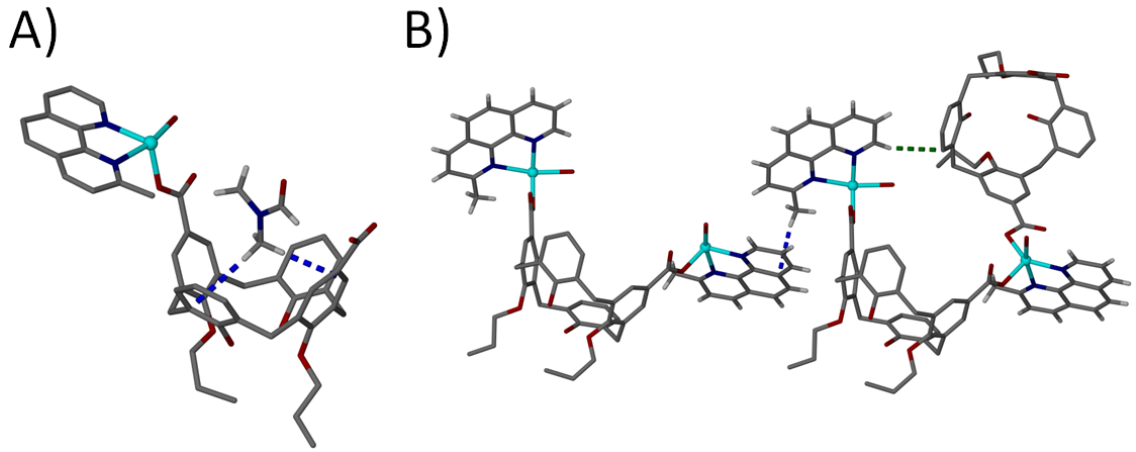

Figure 4.13 (A) Asymmetric unit in **37** showing complementary host-guest CH···π interaction between dmf hydrogen atoms and calixarene two aromatic rings. (B) Section of the extended structure in **37** showing CH···π interactions between phen hydrogen atom and calixarene aromatic ring (green dashed line) and CH···π interactions between neighbouring twisted CPs (blue dashed line). Hydrogen atoms, except those involved in CH···π interactions, omitted for clarity.

Reaction of Zn(II) ions with di-*p*-CO_2[4] **16b** and 2-me-phen, followed by slow evaporation, results in formation of colourless plates. Structural analysis reveals that the crystals are of formula [Zn(**29b**)(2-me-phen)(H_2O)]·(dmf) (**38**) (Fig. 4.14A). The crystals are in a triclinic cell and the structure was solved in space group *P*-1. The asymmetric unit contains one Zn(II), one di-*p*-CO_2[4] **16b**, one 2-me-phen, an aquo ligand and one uncoordinated dmf of crystallisation. Symmetry expansion of the asymmetric unit reveals formation of a coordination complexes comprising one Zn(II), two *alt*-di-*p*-CO_2[4] **29b**, one 2-me-phen and one aquo ligand which assemble together and form spiral CPs, identical to those observed in **37** (Fig 4.14B). Inspection of unit cell parameters of **38** (a = 11.1352(5) Å, b = 13.2505(5) Å and c = 32.5430(!2) Å, α = 89.629(3)º, β = 89.734(3)º and γ = 86.432(5)º) reveals that they slightly differ from those of **37**. Structural analysis shows that the asymmetric unit contains two *alt*-di-*p*-CO_2[4] **29b** both of which are coordinated to the Zn(II) ions *via* carboxylate groups in a monodentate fashion. The first *alt*-di-*p*-CO_2[4], CAL1, comprising groups O(5)-C(29)-O(6) and O(7)-C(30)-O(8) is coordinated to Zn(1) *via* O(5) with the bond length of 1.964(3) Å and coordinated to s.e. Zn(2)' *via* O(7) with the bond length of 1.985(4) Å.

The second *alt*-di-*p*-CO_2[4], CAL2, comprising carboxylate groups O(15)-C(69)-O(16) and O(17)-C(70)-O(18), is coordinated to Zn(1) *via* O(16) with the bond length of 1.974(4) Å and to Zn(2) *via* O(17) with the bond length of 1.969(4) Å. To each of the metal centres there is one bonded aquo ligand with respective Zn(1)-O(20) and Zn(2)-O(21) bonds being 2.120(3) Å and 2.122(4) Å long. Both 2-me-phen of the asymmetric unit are coordinated as a chelate restricting space around the metal centre with Zn(1)-N(1), Zn(1)-N(2), Zn(2)-N(3) and Zn(2)-N(4) distances of 2.243(4) Å, 2.096(4) Å, 2.055(6) Å and 2.175(7) Å respectively. Analysis of the extended crystal structure of **38** reveals that formed twisted CPs assemble together in a same fashion as those in **37** (Fig 4.15). Structural analysis of **38** shows that both a*lt*-di-*p*-CO_2[4]s **29b** also adopt a partially pinched-cone conformation, with distances between distal arene *para* carbon atoms in CAL1 of 7.57 Å and 8.77 Å, and in CAL2 of 7.09 Å and 9.06 Å. The angles ε and δ in CAL1 are 91.2° and 105.3°, and in CAL2 ε and δ are 89.6° and 109.6° respectively, what is in good agreement with those found in **37** and in *alt*-di-*p*-CO_2[4] containing structures already discussed. Further analysis shows that cavities of both *alt*-di-*p*-CO_2[4] **29b** are occupied by dmf of crystallisation what results in complementary host-guest CH···π interactions between dmf hydrogen atoms and calixarene aryl rings.

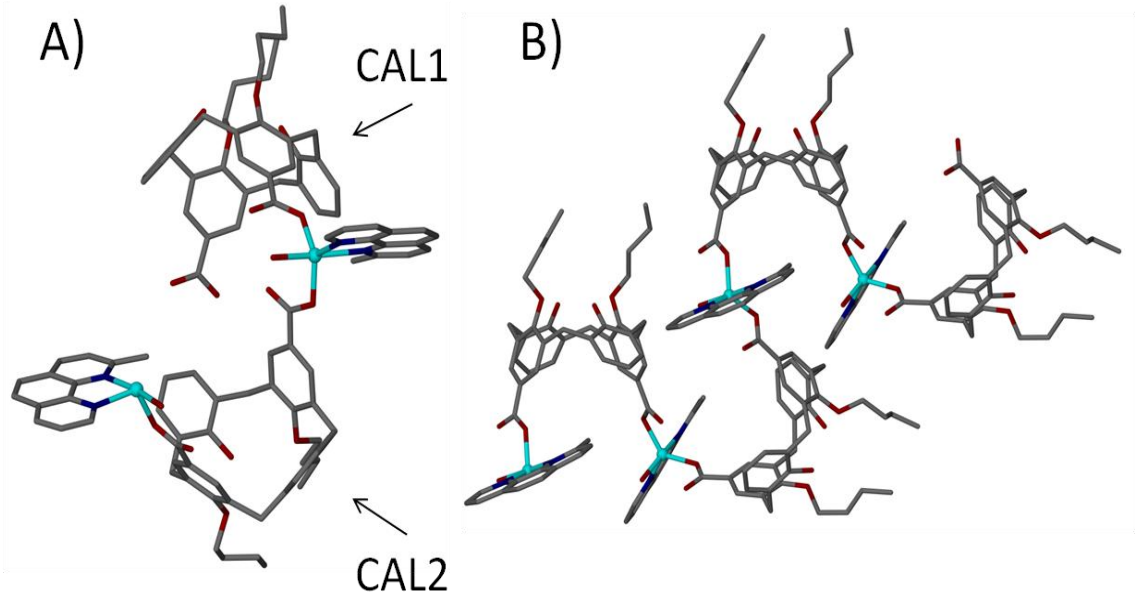

Figure 4.14 (A) Ball and stick representation of the asymmetric unit in **38**. (B) Extended structure showing spiral CP formed in **38**. Hydrogen atoms and dmf of crystallisation omitted for clarity.

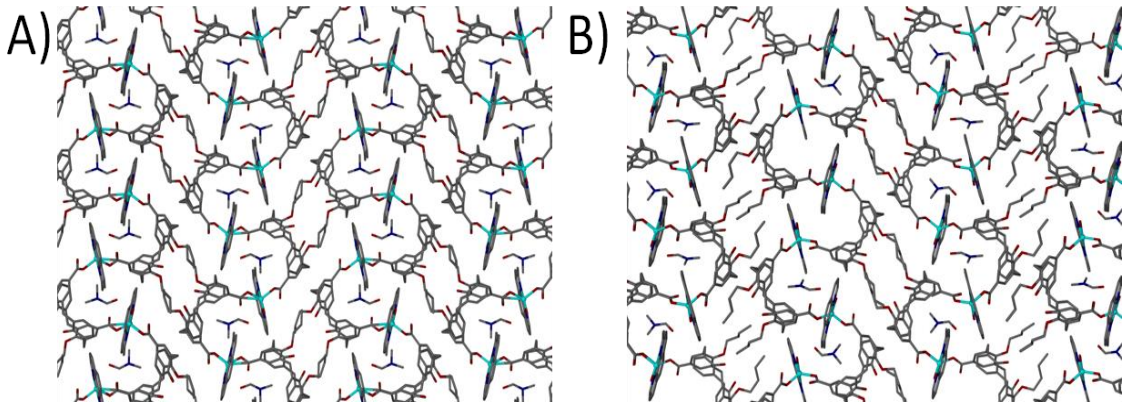

Figure 4.15 Ball and stick representation of packing along *a* axis in (A) **38** and (B) **37**. Hydrogen atoms omitted for clarity.

Each of the ligated 2-me-phen is involved in two different CH···π interactions, what is concomitant with those found in **33** - **37** (Fig. 4.16). As in the case of **37** attempts to attain a homogeneous crystalline product of **38** were unsuccessful and further analysis of the synthesised material was not carried out.

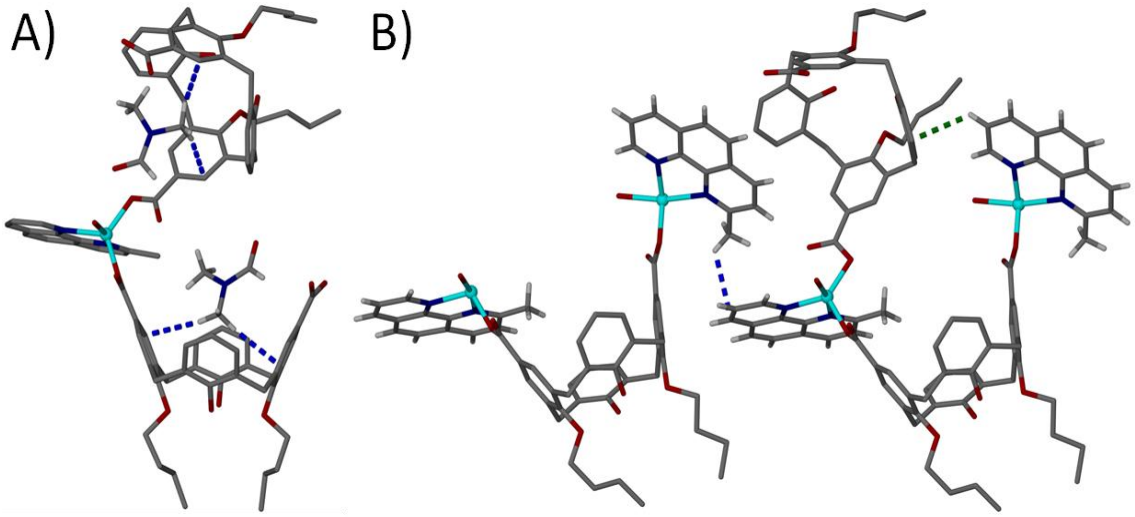

Figure 4.16 (A) Asymmetric unit in **38** showing complementary host-guest CH···π interaction between dmf hydrogen atoms and calixarene two aromatic rings. (B) Section of the extended structure in **38** showing CH···π interactions between 2-me-phen hydrogen atom and calixarene aromatic ring (green dashed line) and CH···π interactions between neighbouring twisted CPs (blue dashed line). Hydrogen atoms, except those involved in CH···π interactions, omitted for clarity.

In the course of studying reactions of TM(II), *alt*-di-*p*-CO_2[4] **29a-c** and 3-me-phen only one reaction yielded material suitable for SCXRD analysis. The reaction of Ni(II), *alt*-di-*p*-CO_2[4] **29a** and 3-me-phen resulted in formation of green crystals of formula [Ni(**29a**)(3-me-phen)(H_2O)]·5dmf (**39**) (Fig. 4.17A). The green single crystals of **39** are in a monoclinic cell and the structure was solved in space group *C*2/*c*. Inspection of unit cell parameters of **39** (a = 38.586(3) Å, b = 11.9927(8) Å and c = 32.252(2) Å and β = 120.640(2)º) reveals that they differ from those of spiral CPs already discussed. The asymmetric unit comprises one Ni(II), one di-*p*-CO_2[4] **29a**, one 3-me-phen, an aquo ligand and five dmf of crystallisation. Symmetry expansion of the asymmetric unit reveals formation of coordination complexes comprising one Ni(II), two *alt*-di-*p*-CO_2[4] **29a**, one 3-me-phen and one aquo ligand which assemble together and form spiral CPs (Fig 4.17B).

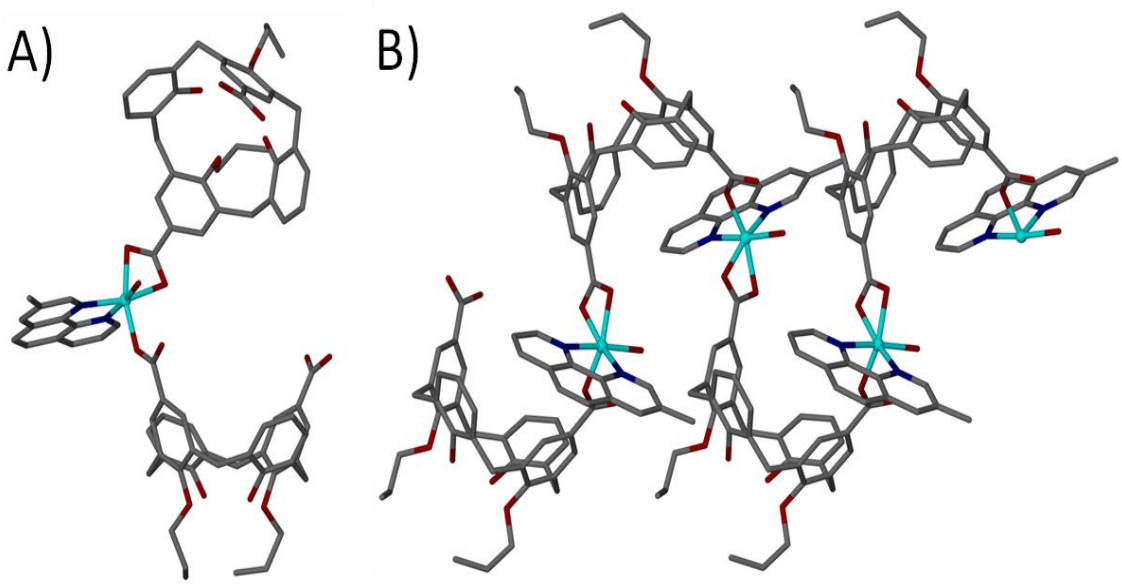

Figure 4.17 (A) Ball and stick representation of the coordination complex formed in **39**. (B) Extended structure showing spiral CPs formed in **39**. Hydrogen atoms and dmf of crystallisation omitted for clarity.

Structural analysis shows that *alt*-di-*p*-CO_2[4] **29a** is coordinated to two Ni(II) centres *via* carboxylate groups: the O(5)-C(29)-O(6) group is coordinated in a monodentate fashion to Ni(1) *via* O(5) with the bond length of 2.008(3) Å, while the O(7)-C(30)-O(8) group is coordinated to s.e. Ni(1)' in a bidentate fashion with respective bond

lengths of 2.095(2) Å and 2.134(3) Å. The aquo ligand is coordinated to the metal centre *via* the Ni(1)-O(9) bond, (2.040(2) Å). As expected 3-me-phen is coordinated as a chelate restricting space around the metal centre with Ni(1)-N(1) and Ni(1)-N(2) distances of 2.053(3) Å and 2.078(3) Å respectively. Structural analysis of **39** that a*lt*-di-*p*-CO_2[4] also adopts a partially pinched-cone conformation with distance between distal arene *para* carbon atoms of 7.40 Å and 8.93 Å. The angles ε and δ are 89.5° and 108.1° respectively. These parameters are consistent with those found in *alt*-di-*p*-CO_2[4] containing structures already discussed. One of the co-crystallised dmf molecules resides in the *alt*-di-*p*-CO_2[4] cavity and results in complementary host-guest CH···π interactions, with the distance between four hydrogen atoms of dmf and calixarene aromatic rings ranging from 2.66 - 2.93 Å (Fig 4.18A).[75] Structural analysis reveals that two hydrogen atoms of the methyl group of 3-me-phen are involved in CH···π interactions with 3-me-phen from neighbouring twisted CPs, with the distance between methyl group hydrogen atoms and s.e. 3-me-phen of 3.00 Å and 3.09 Å respectively.

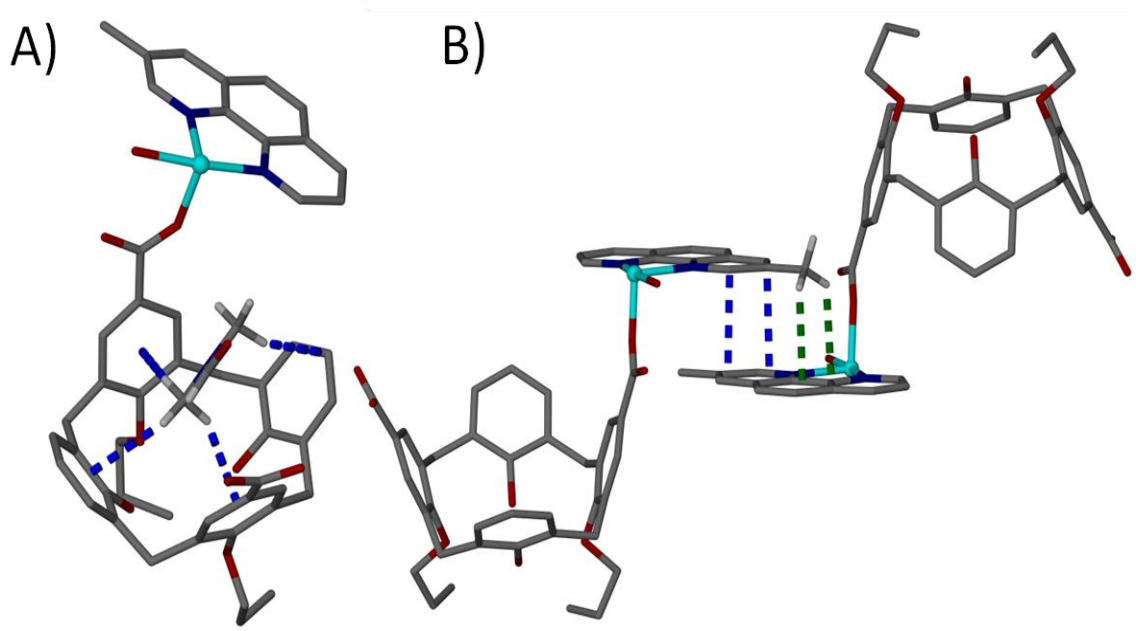

Figure 4.18 (A) Asymmetric unit in **39** showing complementary host-guest CH···π interaction between dmf four hydrogen atoms and calixarene four aromatic rings. (B) Section of the extended structure in **39** showing CH···π interactions between 3-me-phen methyl hydrogen atoms and 3-me-phen from a neighbouring twisted CPs (green dashed line) and a π-stacking between neighbouring twisted CPs (blue dashed line). Hydrogen atoms, except those involved in CH···π interactions, omitted for clarity.

Further analysis shows that 3-me-phens from neighbouring twisted CPs are ~3.4 Å apart suggesting that there is also a π-stacking between them (Fig 4.18B). Inspection of the solid-state packing reveals that the twisted CPs are packed together differently to those in **30** - **38**, resulting in formation of solvent channels filled with dmf of crystallisation (Fig. 4.19). Given our interest in porous materials and their potential application for gas storage / absorption we decided to further analyse the synthesised material. Crystals of **39** were filtered and dried, however PXRD experiments show that the dried material had become amorphous, suggesting that **39** loses crystallinity upon removal from the mother liquor / drying.

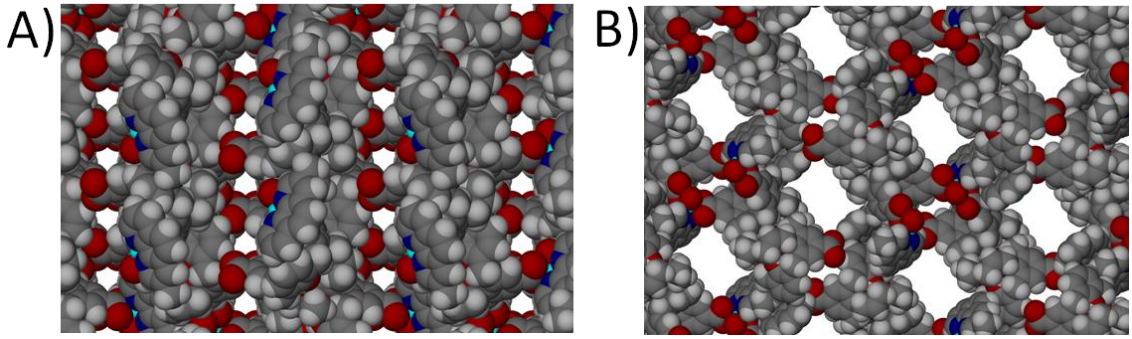

Figure 4.19 A space filling representation of solvent channels in **39** running along (A) *a* axis and (B) *b* axis of the unit cell. Dmf of crystallisation occupying solvent channels omitted for clarity.

None of the attempts to synthesise CPs using 4-me-phen yielded crystals suitable for SCXRD studies. However, use of a more bulky phen, containing four methyl substituents (t-me-phen) provided a useful series of results. Reaction of Co(II), *alt*-di-*p*-CO_2[4] **29a** and t-me-phen, followed by slow evaporation, resulted in formation of red crystals of formula [Co(**29a**)(t-me-phen)(H_2O)]·4dmf (**40**), shown in Figure 4.20A. The crystals are in a monoclinic cell and the structure was solved in space group *C*2/*c*. The asymmetric unit contains one Co(II), one *alt*-di-*p*-CO_2[4] **29a**, one t-me-phen, one aquo ligand and four dmf of crystallisation. Symmetry expansion of the asymmetric unit reveals formation of coordination complexes comprising one Co(II), two *alt*-di-*p*-CO_2[4] **29a**, one t-me-phen and one aquo ligand which assemble together and form spiral CPs (Fig 4.20B). The unit cell parameters of **40** (a = 33.589(2) Å, b = 11.8935(8) Å and c = 31.6039(19) Å and β = 117.376(2)º) differ from those of spiral

CPs discussed above. Structural analysis shows that *alt*-di-*p*-CO_2[4] **29a** is coordinated to two Co(II) centres *via* carboxylate groups: the O(5)-C(29)-O(6) group is coordinated to Co(1) in a monodentate fashion *via* O(5) with the bond length of 2.031(3) Å, while the O(7)-C(30)-O(8) group is coordinated to s.e. Co(1)' in a bidentate fashion with respective bond lengths of 2.197(3) Å and 2.129(2) Å. The aquo ligand is coordinated to the metal centre *via* the Co(1)-O(9) bond, which is 2.084(3) Å long.

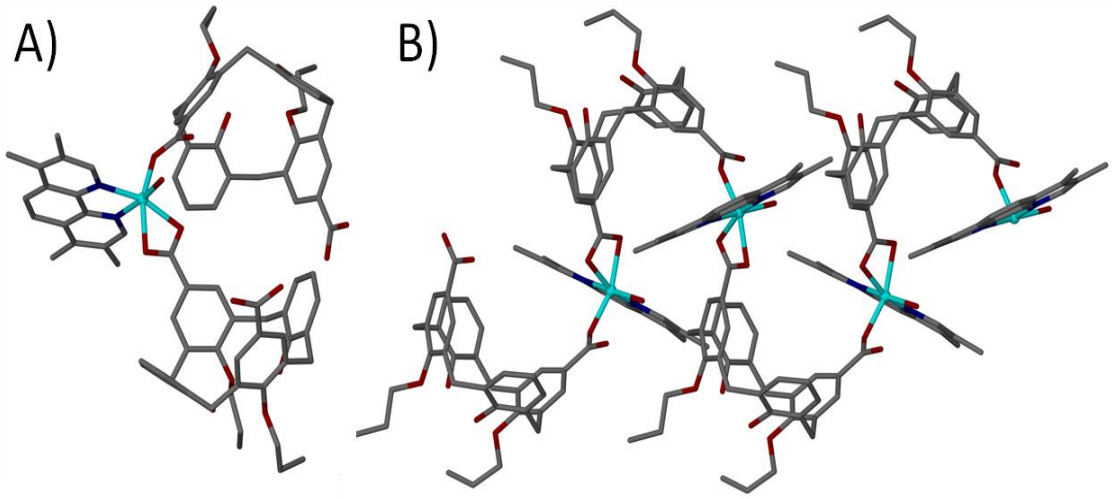

Figure 4.20 (A) Ball and stick representation of the coordination complex formed in **40.** (B) Extended structure showing spiral CPs formed in **40**. Hydrogen atoms and dmf of crystallisation omitted for clarity.

The t-me-phen is coordinated as a chelate with Co(1)-N(1) and Co(1)-N(2) distances of 2.099(3) Å and 2.107(3) Å respectively. The *alt*-di-*p*-CO_2[4] adopts a partially pinched-cone conformation with distance between distal arene *para* carbon atoms of 7.53 Å and 8.68 Å and the angles ε and δ measured to be 90.7° and 104.7° respectively; these parameters are consistent with those in the *alt*-di-*p*-CO_2[4] containing structures already discussed. One of the dmf of crystallisation resides in the *alt*-di-*p*-CO_2[4] cavity what results in a complementary host-guest CH···π interactions, with the distance between four hydrogen atoms of dmf and calixarene aromatic rings ranging from 2.73 - 3.00 Å (Fig 4.21A). Structural analysis reveals that one of hydrogen atoms of methyl groups (at position 3-) of the t-me-phen is involved in a CH···π interaction with s.e. calixarene aryl ring from the same twisted CPs (green dashed line in Fig 4.21B). Further analysis also shows that hydrogen atoms of methyl groups (at positions 7- and

8-) of t-me-phen undergo CH···π interactions with s.e. t-me-phen from a neighbouring twisted CP (blue dashed lines in Fig. 4.22B). The distance between stacked s.e. t-me-phens from neighbouring twisted CPs is too large (~3.6 Å) for the co-ligands to undergo π-stacking. Inspection of the solid state packing reveals that twisted CPs are packed together differently to what is observed in **30** - **39**, however there are no solvent channels present (Fig. 4.22). Despite that, given our interest in porous materials and their potential application for gas storage / absorption we decided to further analyse the synthesised material. Crystals of **40** were filtered and dried, however PXRD experiments show that the dried material had become amorphous, suggesting that **40** loses crystallinity upon removal from the mother liquor / drying.

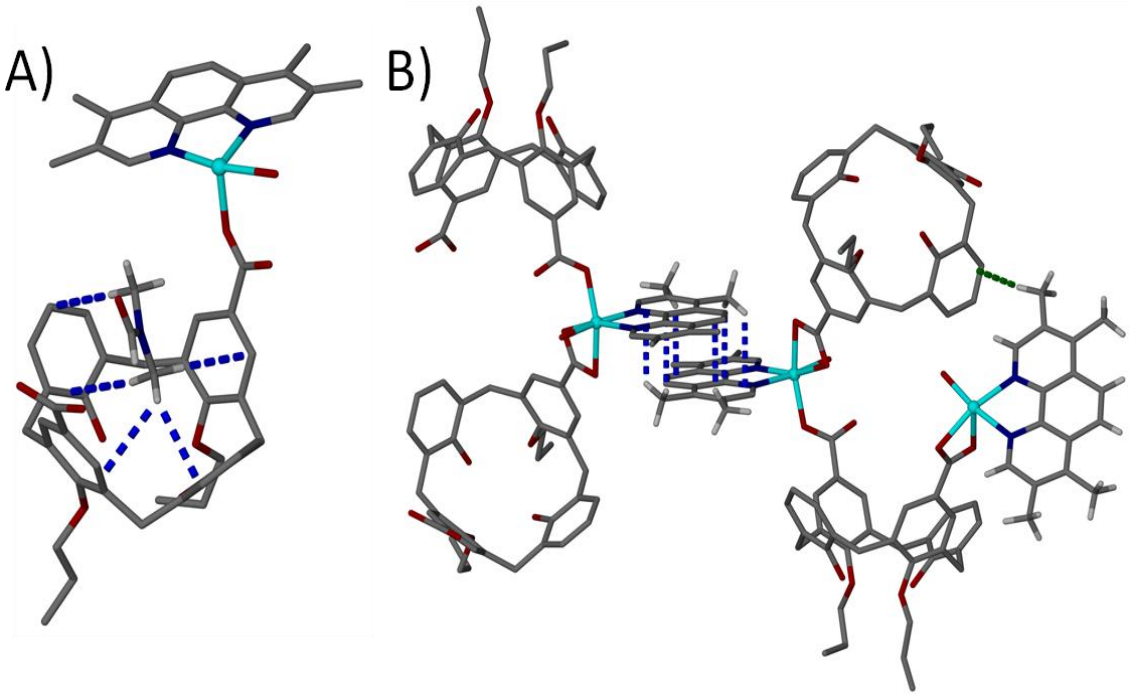

Figure 4.21 A) Asymmetric unit in **40** showing complementary host-guest CH···π interaction between dmf four hydrogen atoms and calixarene four aromatic rings. (B) Section of the extended structure in **40** showing CH···π interactions between 3-me-phen methyl hydrogen atom and 3-me-phen from neighbouring twisted CPs (blue dashed line). Hydrogen atoms, except those involved in CH···π interactions, omitted for clarity.

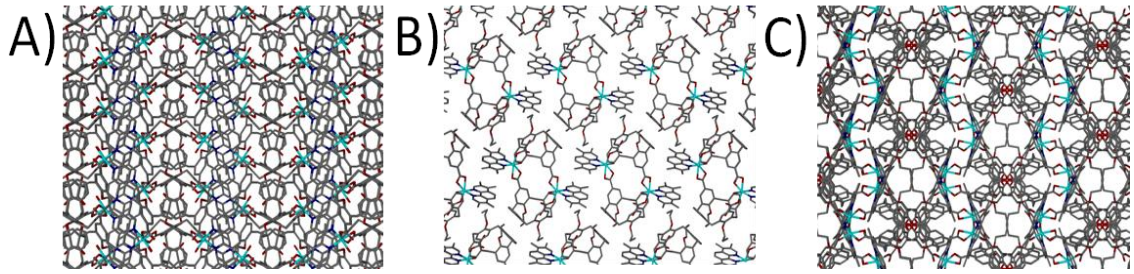

Figure 4.22 Ball and stick representation the packing in **40** along (A) *a* axis, (B) *b* axis and (C) *c* axis of the unit cell. Hydrogen atoms and dmf of crystallisation omitted for clarity.

Reaction of Co(II), *alt*-di-*p*-CO_2[4] **29b** and t-me-phen, followed by slow evaporation, resulted in formation of red crystals of formula [Co(**29b**)(t-me-phen)(H_2O)]·4dmf (**41**) (Fig. 4.23A). The crystals are in a monoclinic cell and the structure was solved in space group *C*2/*c*. The asymmetric unit contains one Co(II), one *alt*-di-*p*-CO_2[4] **29b**, one t-me-phen, one aquo ligand and four uncoordinated dmf of crystallisation. Symmetry expansion of the asymmetric unit reveals formation of coordination complexes comprising one Co(II), two *alt*-di-*p*-CO_2[4] **29a**, one t-me-phen and one aquo ligand which assemble together and form spiral CPs (Fig 4.23B). The unit cell parameters of **41** (a = 33.761(2) Å, b = 12.9725(10) Å and c = 31.8346(19) Å and β = 116.371(3)º) differ marginally from those of **40**. Structural analysis shows that the contents of the coordination sphere in **41** are consistent with those in **40**. The *alt*-di-*p*-CO_2[4] **29b** is coordinated to two Co(II) centres *via* carboxylate groups: the O(5)-C(29)-O(6) group is coordinated in a monodentate fashion to Co(1) *via* O(5) with the bond length of 2.015(4) Å, while the O(7)-C(30)-O(8) group is coordinated to s.e. Co(1)' in a bidentate fashion with respective bond lengths of 2.193(4) Å and 2.142(4) Å. The coordination sphere also comprises an aquo ligand bonded to the metal centre *via* the Co(1)-O(9) bond (2.100(4) Å). The t-me-phen is coordinated as a chelate with Co(1)-N(1) and Co(1)-N(2) distances of 2.089(4) Å and 2.116(5) Å respectively. The *alt*-di-*p*-CO_2[4] adopts a partially pinched-cone conformation with distance between distal arene *para* carbon atoms of 7.60 Å and 8.62 Å and the angles ε and δ measured to be 91.5° and 103.5° respectively. This is in good agreement with the corresponding parameters in **40** (7.53 Å, 8.68 Å, 90.7° and 104.7° respectively).

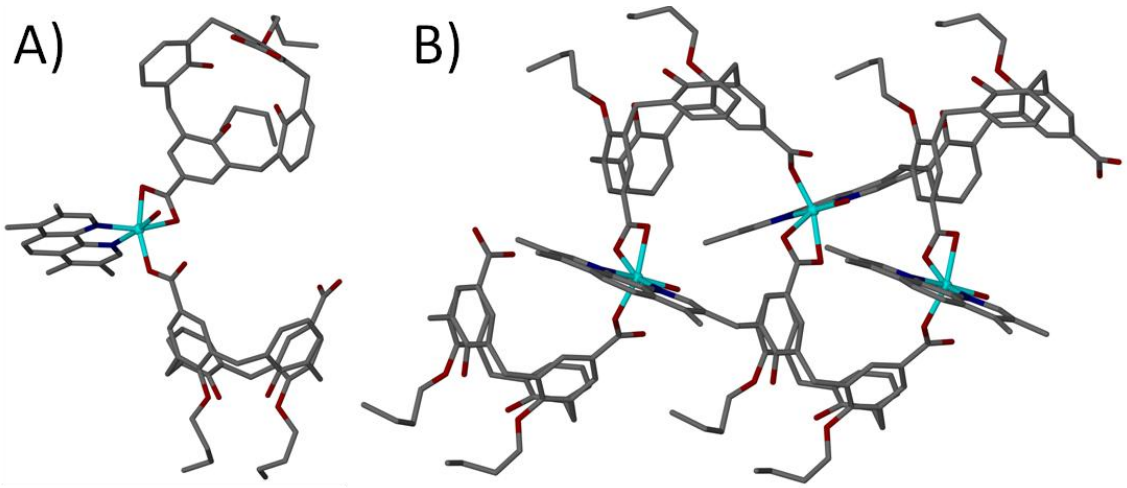

Figure 4.23 (A) Ball and stick representation of the coordination complex formed in **41**. (B) Extended structure showing spiral CPs formed in **41**. Hydrogen atoms and dmf of crystallisation omitted for clarity.

One of the four dmf of crystallisation resides in the *alt*-di-*p*-CO_2[4] cavity and results in host-guest CH···π interactions. The distance between methyl three hydrogen atoms of dmf and calixarene aromatic rings ranges from 2.79 - 2.93 Å (Fig 4.24A).

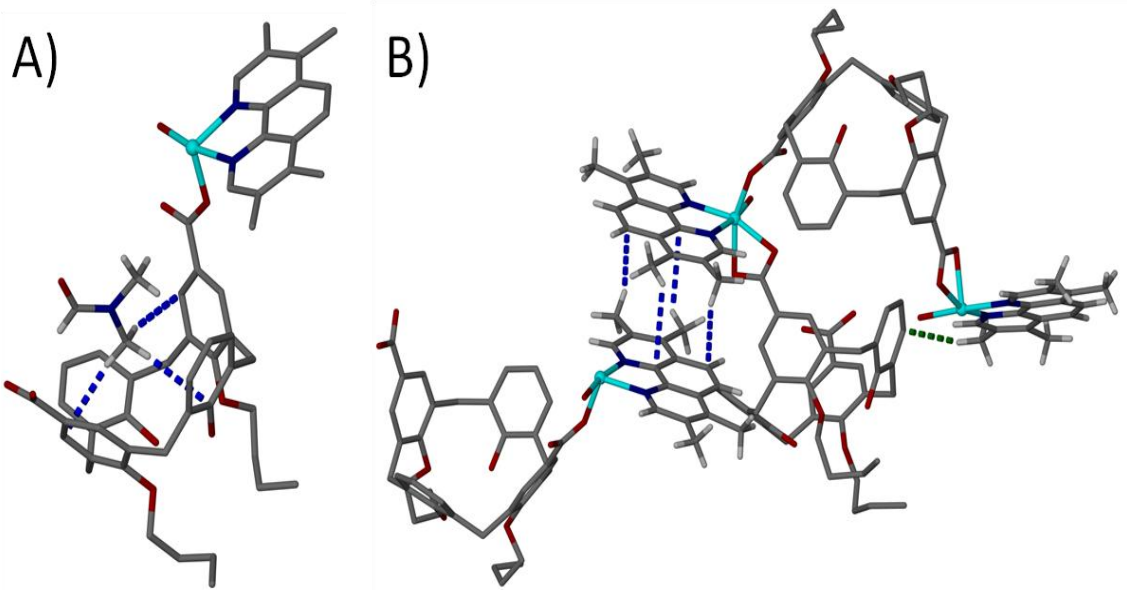

Figure 4.24 A) Asymmetric unit in **41** showing complementary host-guest CH···π interaction between dmf four hydrogen atoms and calixarene four aromatic rings. (B) Section of the extended structure in **41** showing CH···π interactions between 3-me-phen methyl hydrogen atom and calixarene aromatic ring from the same CP (green dashed line) and a π-stacking between neighbouring spiral CPs (blue dashed line). Hydrogen atoms, except those involved in CH···π interactions, omitted for clarity.

Structural analysis reveals that t-me-phen undergoes non-covalent interactions in a similar manner as that in **40**, with one of hydrogen atoms of the methyl groups (at 3-position) participating in a CH···π interaction with s.e. calixarene aryl ring from the same twisted CPs (green dashed line in Fig 4.24B), and hydrogen atoms of methyl groups (at 7- and 8-positions) undergoing CH···π interactions with s.e. t-me-phen from a neighbouring twisted CP (blue dashed lines in Fig. 4.24B). As in the case of **40,** the distance between stacked s.e. t-me-phens from neighbouring twisted CPs is too large (~3.6 Å) for the co-ligands to undergo π-stacking. Inspection of the solid-state packing reveals that the twisted CPs are packed in the same manner as in **40**, and results in exclusion of any solvent channels (Fig. 4.25). Crystals of **31** were filtered and dried, however PXRD experiments show that the dried material had become amorphous, suggesting that **41** loses crystallinity upon removal from the mother liquor / drying.

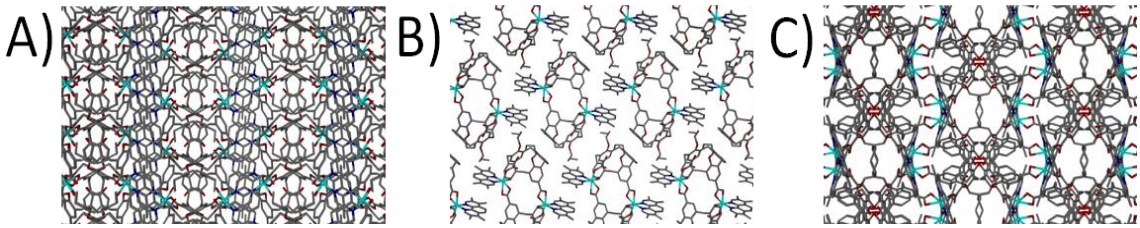

Figure 4.25 Ball and stick representation the packing in **41** along (A) *a* axis, (B) *b* axis and (C) *c* axis. Hydrogen atoms and dmf of crystallisation omitted for clarity.

The second TM(II) which when reacted with *alt*-di-*p*-CO_2[4] **29a** or **29b** and t-me-phen results in formation of crystalline green product is Ni(II). The green crystals of formula [Ni(**29a**)(t-me-phen)(H_2O)]·4dmf (**42**) are in a monoclinic cell and the crystal structure was solved in space group *C*2/*c*. The asymmetric unit contains one Ni(II), one *alt*-di-*p*-CO_2[4] **29a**, one t-me-phen, one aquo ligand and four uncoordinated dmf of crystallisation. Symmetry expansion of the asymmetric unit reveals formation of coordination complexes comprising one Ni(II), two *alt*-di-*p*-CO_2[4] **29a**, one t-me-phen and one aquo ligand which assemble together and form spiral CP identical to those in **40** (Fig 4.26). The unit cell parameters of **42** (a = 33.5750(11) Å, b = 12.8713(5) Å and c = 31.2863(11) Å and β = 117.237(2)º) are near-identical to those of **40**. Given same cell parameters and the almost identical solid state packing, **42** can be considered isostructural with **40**.

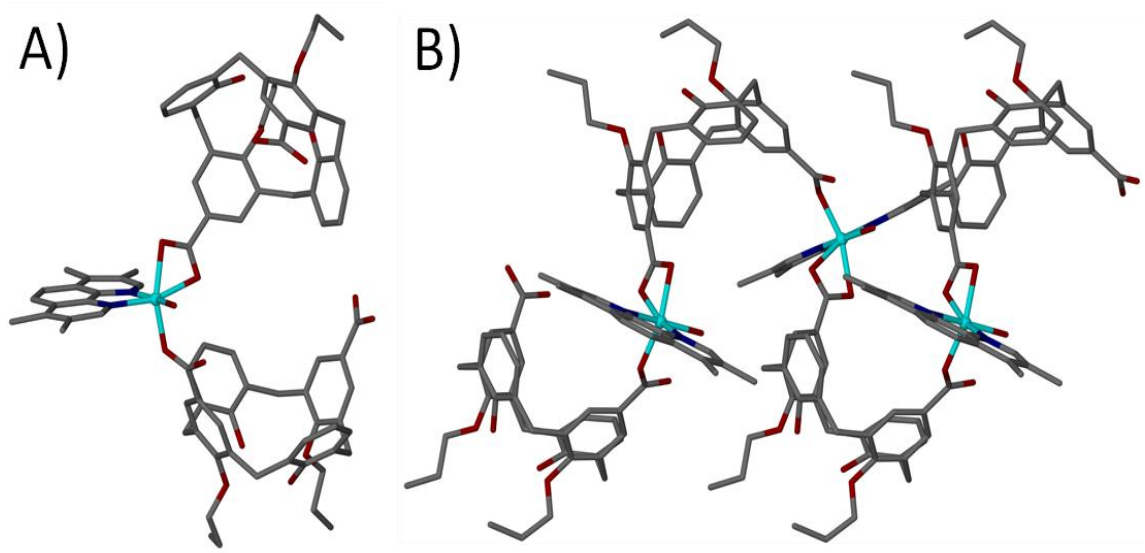

Figure 4.26 (A) Ball and stick representation of the coordination complex formed in **42**. (B) Extended structure showing spiral CPs formed in **42**. Hydrogen atoms and dmf of crystallisation omitted for clarity.

Reaction of Ni(II), *alt*-di-*p*-CO_2[4] **29b** and t-me-phen results in green crystals of formula [Ni(**29b**)(t-me-phen)(H_2O)]·4dmf (**43**) which are in a monoclinic cell and the crystal structure was also solved in space group *C*2/*c*. The asymmetric unit contains one Ni(II), *alt*-di-*p*-CO_2[4] **29b**, one t-me-phen, one aquo ligand and four uncoordinated dmf of crystallisation. Symmetry expansion of the asymmetric unit reveals formation of coordination complexes comprising one Ni(II), two *alt*-di-*p*-CO_2[4] **29b**, one t-me-phen and one aquo ligand. Formed complexes assemble together to form spiral CPs identical to the ones in **41** (Fig 4.27). The unit cell parameters of **43** (a = 33.901(11) Å, b = 12.9612(18) Å and c = 31.384(5) Å and β = 115.68(3)º) are near-identical to those of **41**. As in the case of **40** and **42**, both **41** and **43** have similar cell parameters and almost identical solid-state packing, and can thus be considered isostructural. Crystals of **42** and **43** were filtered and dried, however PXRD experiments show that the dried materials had become amorphous, suggesting that both materials lose crystallinity upon removal from the mother liquor / drying.

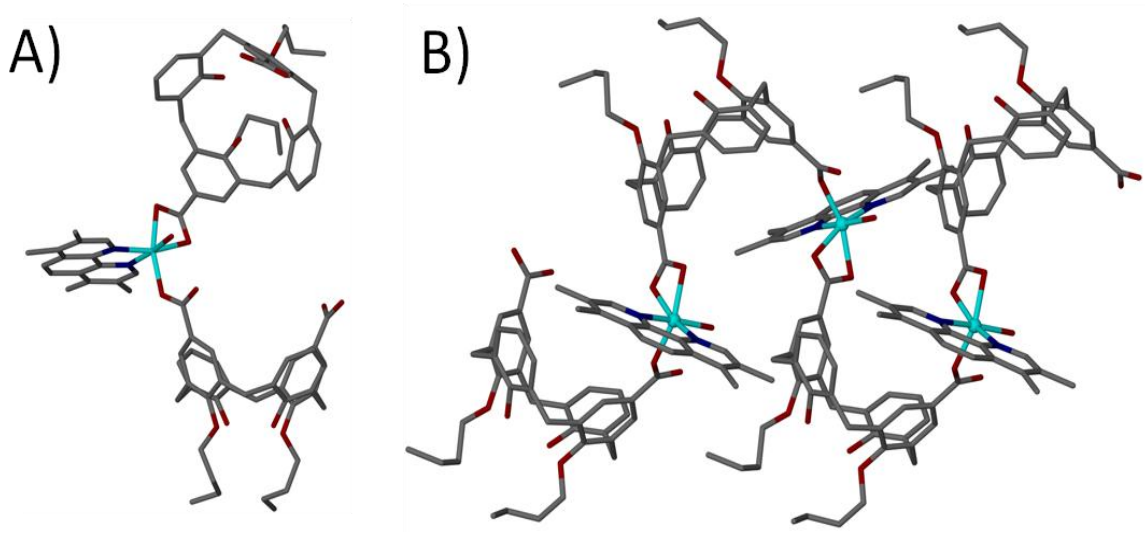

Figure 4.27 Ball and stick representation of the (A) coordination complex formed in **43** and (B) twisted CP found in the extended structure of **43**. Hydrogen atoms and dmf of crystallisation omitted for clarity.

The reaction of Co(II) and Ni(II) with *alt*-di-*p*-CO_2[4] **29a** or **29b** and 2-me-phen results in formation of spiral 1-D CPs **33** - **36** which are isostructural with **30** - **32**. This suggests that the use of a co-ligand with a methyl substituent introduced to the 2-position does not affect the shape of the spiral 1-D CP and the overall solid state packing. The use of 3-me-phen as a co-ligand yielded crystals of **39** containing similar looking spiral 1-D CPs, which pack differently than spiral CPs pack when using phen or 2-me-phen. Unfortunately it has not been possible to isolate crystalline product from other reactions in which 3-me-phen was used, and there is therefore not enough evidence to fully understand the impact of 3-me-phen on the solid-state packing of spiral CPs. Reactions in which most bulky phen derivative was used, t-me-phen, yielded crystalline product (**40** - **43**). Structural analysis reveals formation of spiral 1-D CPs which, in the solid state, pack differently to CPs containing mono-methyl substituted phens.

4.4. Summary

In the previous chapter it was shown that linear 1-D CPs can be constructed by using di-*p*-CO_2[4] **16a - b** as a di-topic building block. In this chapter it has been demonstrated that by synthetic pre-organisation of calixarene framework, whereby two carboxyl groups are introduced to the other two *para* positions of the calixarene upper-rim, the C_2 symmetry can be utilised to construct supramolecular architectures different to those when di-*p*-CO_2[4]s are employed. The use of *alt*-di-*p*-CO_2[4]s **29a - b** as di-topic building blocks results in formation of spiral 1-D CPs **30 - 43** which exhibit different solid state packing to the materials synthesised using di-*p*-CO_2[4]s **17 - 25**. Structural analysis of **30 - 43** reveals that the use of calixarenes with propyl or butyl substituents at the lower-rim yield the same general supramolecular architectures. However, when calixarenes with pentyl substituents at the lower-rim are used in the reaction it is not possible to isolate crystalline product. It has also been found that reactions in which Co(II) or Ni(II) and *alt*-di-*p*-CO_2[4]s are used yield isostructural materials what is in contrast with reaction in which these TM(II) are used with di-*p*-CO_2[4]s.

The study of the influence of phen and its derivatives on the self-assembly has provided new structural insight. It has been found that when using *alt*-di-*p*-CO_2[4] as a building block and phen or 2-me-phen as a chelate restricting available binding sites around the metal centre (Co(II) or Ni(II)), the synthesised materials are isostructural. Regardless of whether phen (**30 - 32**) or 2-me-phen (**33 - 36**) was used, the solid-state packing of the spiral CPs formed is the same. Reactions in which 3-me-phen or 4-me-phen are used as a co-ligand yield amorphous solids which, apart from **39**, lose crystallinity upon removal from mother liquor / de-solvation. This suggests the importance of participation of phen or its derivatives in non-covalent interactions / stabilisation of assembly. The use in the reaction of a more bulky co-ligand, t-me-phen, results in formation of spiral 1-D CPs (**40 - 43**) that are near identical to those found for **30 - 39**. However, as a result of four methyl groups present in the t-me-phen, the non-covalent interactions observed between phens from neighbouring CPs in **30 - 39** are disturbed. This results in different solid-state packing of CPs in **40 - 43** compared to **30 - 39**. Some of the synthesised materials possess solvent channels, but unfortunately they do not exhibit stability to de-solvation, which is essential for the use of materials for gas storage / absorption.

4.5. Experimental

General experimental procedures and specifications of analytical instruments used are provided in Chapter 8.

4.5.1. Synthesis of compounds 26a - c, 27a - c, 28a - c, 29a - c and 30a - c

Di-*O*-alkoxy-di-*O*-bis(*p*-nitrobenezenesulfonyloxy)-calix[4]arenes (**26a - c**) were synthesised according to literature procedure.[85] The appropriate di-*O*-alkoxy-calix[4]arene **14a-c** (9.32 mmol) was dissolved in anhydrous dmf (200 mL). Sodium hydride (1.60 g, 40.0 mmol, 60% suspension in mineral oil) was added to the mixture and stirred at 0^{o}C for 30 minutes. To the cooled solution *p*-nitrobenzene sulfonyl chloride (8.71 g, 39.2 mmol) was added and the mixture was stirred at room temperature for 7 days. Then, the mixture was acidified with 1M HCl and extracted with dichloromethane (4x100 mL), washed with deionised water, brine, and dried over anhydrous magnesium sulfate. The solvent was removed under reduced pressure and the oily residue was re-dissolved in dichloromethane (20 mL). Addition of methanol (150 mL) resulted in a precipitate which was filtered and washed with methanol to give pale yellow solid in each case.

Di-*O*-propoxy-di-*O*-bis(*p*-nitrobenezenesulfonyloxy)-calix[4]arene (**26a**) was obtained in 93% yield; mp: 255-258 ^{o}C; **^{1}H NMR** (300MHz, $CDCl_3$) δ = 8.35 – 8.32 (m, 4H, Ar-H (Nos)), 7.94 – 7.91 (m, 4H, Ar-H(Nos)), 7.00 – 6.95 (m, 4H, Ar-H), 6.83 – 6.79 (m, 2H, Ar-H), 6.38 – 6.32 (m, 2H, Ar-H), 6.13 – 6.06 (m, 4H, Ar-H), 3.90 (d, *J* = 13.2 Hz, 4H, Ar-CH_2-Ar), 3.85 – 3.79 (m, 4H, -O-CH_2-), 2.71 (d, *J* = 13.2 Hz, 4 H, Ar-CH_2-Ar), 1.71 – 1.59 (m, 4 H, -O-CH_2-CH_2-), 1.03 (t, *J* = 7.4 Hz, 6H, -CH_3); **MS** *m/e* 902 ($M + Na^+$).

Di-*O*-butoxy-di-*O*-bis(*p*-nitrobenezenesulfonyloxy)-calix[4]arene (**26b**) was obtained in 90% yield; mp: 255-258 ^{o}C; **^{1}H NMR** (300MHz, $CDCl_3$) δ = 8.36 – 8.33 (m, 4H, Ar-H (Nos)), 7.96 – 7.93 (m, 4H, Ar-H(Nos)), 7.00 – 6.95 (m, 4H, Ar-H), 6.87 – 6.82 (m, 2H, Ar-H), 6.40 – 6.34 (m, 2H, Ar-H), 6.16 – 6.09 (m, 4H, Ar-H), 3.92 (d, *J* = 13.2 Hz, 4H, Ar-CH_2-Ar), 3.87 – 3.79 (m, 4H, -O-CH_2-), 2.74 (d, *J* = 13.2 Hz, 4 H, Ar-CH_2-Ar),

1.91 – 1.79 (m, 4 H, -O-CH_2-CH_2-), 1.32 – 1.18 (m, 4H, -CH_2-CH_3), 0.96 (t, *J* = 7.4 Hz, 6H, -CH_3); **MS** *m/e* 930 ($M + Na^+$).

Di-*O*-pentoxy-di-*O*-bis(*p*-nitrobenezenesulfonyloxy)-calix[4]arene (**26c**) was obtained in 82% yield; mp: 250-258 ^oC; **^{1}H NMR** (300MHz, $CDCl_3$) δ = 8.35 – 8.31 (m, 4H, Ar-H (Nos)), 7.98 – 7.96 (m, 4H, Ar-H(Nos)), 7.03 – 6.99 (m, 4H, Ar-H), 6.90 – 6.86 (m, 2H, Ar-H), 6.44 – 6.39 (m, 2H, Ar-H), 6.14 – 6.08 (m, 4H, Ar-H), 3.95 (d, *J* = 13.2 Hz, 4H, Ar-CH_2-Ar), 3.77 – 3.72 (m, 4H, -O-CH_2-), 2.71 (d, *J* = 13.2 Hz, 4 H, Ar-CH_2-Ar), 1.88 – 1.79 (m, 4 H, -O-CH_2-CH_2-), 1.42 – 1.34 (m, 4H, -CH_2- CH_2-CH_3), 1.22 – 1.15 (m, 4H, -CH_2-CH_3) 0.85 (t, *J* = 7.4 Hz, 6H, -CH_3); **MS** *m/e* 958 ($M + Na^+$).

***p*-Di-formyl-di-*O*-alkoxy-di-*O*-bis(*p*-nitrobenezenesulfonyloxy)-calix[4]arene** (**27a - c**) was synthesised according to literature procedure.[85] The appropriate di-*O*-alkoxy-di-*O*-bis(*p*-nitrobenzenesulfonyloxy)-calix[4]arene **26a - c** (2.76 mmol), hexamethylenetetramine (12.0 g, 85.6 mmol) and trifluoroacetic acid (50 mL) were stirred together at 90^{o}C for 24 hours. The reaction mixture was cooled to room temperature, poured onto 400 mL of cold water and extracted with dichloromethane (3x100 mL). The combined organic layers were washed with water, brine and dried over anhydrous magnesium sulfate. The solvent was removed under reduced pressure and the oily residue was dissolved in dichloromethane (20 mL). The addition of methanol (150 mL) resulted in a precipitate, which was filtered and washed with methanol to give pale yellow solid in each case.

***p*-Di-formyl-di-*O*-propoxy-di-*O*-bis(*p*-nitrobenezenesulfonyloxy)-calix[4]arene** (**27a**) was obtained in 74% yield; mp > 300 ^oC. **^{1}H NMR** (300MHz, DMSO-d_6) δ = 9.86 (s, 2H, -COH), 8.56 – 8.50 (m, 4H, Ar-H (Nos)), 8.15 – 8.10 (m, 4H, Ar-H(Nos)), 7.67 (s, 4H, Ar-H), 6.58 – 6.53 (m, 2H, Ar-H), 6.38 – 6.33 (m, 2H, Ar-H), 6.17 – 6.10 (m, 4H, Ar-H), 3.94 (d, *J* = 13.2 Hz, 4H, Ar-CH_2-Ar), 3.89 – 3.82 (m, 4H, -O-CH_2-), 3.15 (d, *J* = 13.2 Hz, 4 H, Ar-CH_2-Ar), 1.40 – 1.28 (m, 4H, -CH_2-CH_3), 0.96 (t, *J* = 7.4 Hz, 6H, -CH_3); **MS** *m/e* 958 ($M + Na^+$).

***p*-Di-formyl-di-*O*-butoxy-di-*O*-bis(*p*-nitrobenezenesulfonyloxy)-calix[4]arene** (**27b**) was obtained in 76% yield, mp > 300 ^oC. **^{1}H NMR** (300MHz, DMSO-d_6) δ = 9.88 (s, 2H, -COH), 8.54 – 8.49 (m, 4H, Ar-H (Nos)), 8.13 – 8.08 (m, 4H, Ar-H(Nos)), 7.68 (s,

4H, Ar-H), 6.57 – 6.52 (m, 2H, Ar-H), 6.37 – 6.32 (m, 2H, Ar-H), 6.16 – 6.09 (m, 4H, Ar-H), 3.92 (d, *J* = 13.2 Hz, 4H, Ar-CH_2-Ar), 3.88 – 3.80 (m, 4H, -O-CH_2-), 3.13 (d, *J* = 13.2 Hz, 4 H, Ar-CH_2-Ar), 1.83 – 1.76 (m, 4 H, -O-CH_2-CH_2-), 1.28 – 1.16 (m, 4H, -CH_2-CH_3), 0.92 (t, *J* = 7.4 Hz, 6H, -CH_3); **MS** *m/e* 986 ($M + Na^+$).

***p*-Di-formyl-di-*O*-pentoxy-di-*O*-bis(*p*-nitrobenezenesulfonyloxy)-calix[4]arene** (**27c**) was obtained in 58% yield; mp > 300 ^oC. **^{1}H NMR** (300MHz, DMSO-d_6) δ = 9.85 (s, 2H, -COH), 8.52 – 8.47 (m, 4H, Ar-H (Nos)), 8.11 – 8.07 (m, 4H, Ar-H(Nos)), 7.66 (s, 4H, Ar-H), 6.55 – 6.50 (m, 2H, Ar-H), 6.35 – 6.29 (m, 2H, Ar-H), 6.13 – 6.07 (m, 4H, Ar-H), 3.91 (d, *J* = 13.2 Hz, 4H, Ar-CH_2-Ar), 3.84 – 3.78 (m, 4H, -O-CH_2-), 3.10 (d, *J* = 13.2 Hz, 4 H, Ar-CH_2-Ar), 1.81 – 1.75 (m, 4 H, -O-CH_2-CH_2-), 1.41 – 1.34 (m, 4H, -CH_2- CH_2-CH_3), 1.18 – 1.06 (m, 4H, -CH_2-CH_3) 0.71 (t, *J* = 7.4 Hz, 6H, -CH_3); **MS** *m/e* 1014 ($M + Na^+$).

***p*-Di-carboxylato-di-*O*-alkoxy-di-*O*-bis(*p*-nitrobenezenesulfonyloxy)-calix[4]arene** (**28a - c**) was synthesised according to modified literature procedure**.**[86] An appropriate *p*-di-formyl-di-*O*-alkoxy-di-*O*-bis(*p*-nitrobenzenesulfonyloxy)-calix[4]arene (**28a - c**) (0.52 mmol) was dissolved in a mixture of acetone (25 mL) and dichloromethane (75 mL) and was cooled to 0^oC. To the cooled solution sulfamic acid (0.20 g, 2.06 mmol) dissolved in water (3 mL) and sodium chlorite (0.16 g, 1.77 mmol) dissolved in water (3 mL) were added. The mixture was stirred at room temperature for 24 h. The solvents were removed under reduced pressure. The solid was taken up with 1M HCl, filtered, washed with deionised water and dried to give pale yellow solid in each case.

***p*-Di-carboxylato-di-*O*-propoxy-di-*O*-bis(*p*-nitrobenezenesulfonyloxy)-calix[4]arene** (**28a**) was obtained in 96% yield; mp (decomp.): > 270^oC; **^{1}H NMR** (300MHz, DMSO-d_6) δ = 12.88 (s, 2H, -COOH), 8.63 – 8.59 (m, 4H, Ar-H (Nos)), 8.28 – 8.18 (m, 4H, Ar-H(Nos)), 7.89 (s, 4H, Ar-H), 6.69 – 6.62 (m, 2H, Ar-H), 6.47 – 6.39 (m, 4H, Ar-H), 4.05 – 3.98 (m, 4H, Ar-CH_2-Ar), 3.90 – 3.86 (m , 4H, -O-CH_2-), 3.27 – 3.18 (m, 4H, Ar-CH_2-Ar), 1.42 – 1.35 (m, 4H, -CH_2-CH_3) 1.10 (t, *J* = 7.3 Hz, 6H, -CH_3); **^{13}C{^{1}H} NMR** (100 MHz, DMSO-d_6) δ = 166.7, 155.7, 152.9, 135.5, 135.0, 132.7, 130.2, 129.5, 128.3, 128.6, 127.2, 124.3, 120.0, 77.1, 32.3, 30.3, 15.8; **MS** *m/e* 990 ($M + Na^+$); **EA** calc for $C_{48}H_{42}N_2O_{16}S_2$, C, 59.62; H, 4.38; N, 2.90%. Found C, 59.43; H, 4.46, N,

2.93%; **IR** ν_{max} 2965 cm^{-1} and 2949 cm^{-1} (C-H), 3000 – 2780 cm^{-1} (broad COOH), 1675 cm^{-1} (C=O), 1610 cm^{-1} (C-O), 1527 cm^{-1} and 1345 cm^{-1} (N-O).

***p*-Di-carboxylato-di-*O*-butoxy-di-*O*-bis(*p*-nitrobenezenesulfonyloxy)-calix[4]arene** (**28b**) was obtained in 95% yield; mp (decomp.): > 270°C; **^{1}H NMR** (300MHz, DMSO-d_6) δ = 12.84 (s, 2H, -COO<u>H</u>), 8.59 – 8.55 (m, 4H, Ar-<u>H</u> (Nos)), 8.18 – 8.14 (m, 4H, Ar-<u>H</u>(Nos)), 7.82 (s, 4H, Ar-<u>H</u>), 6.63 – 6.57 (m, 2H, Ar-<u>H</u>), 6.41 – 6.35 (m, 4H, Ar-<u>H</u>), 3.99 – 3.93 (m, 4H, Ar-<u>CH_2</u>-Ar), 3.89 – 3.86 (m , 4H, -O-<u>CH_2</u>-), 3.19 – 3.14 (m, 4H, Ar-<u>CH_2</u>-Ar), 1.85 – 1.73 (m, 4H, -O-CH_2-<u>CH_2</u>-), 1.22 – 1.12 (m, 4H, -<u>CH_2</u>-CH_3), 0.92 (t, *J* = 7.3 Hz, 6H, -<u>CH_3</u>). **^{13}C{^{1}H} NMR** (100 MHz, DMSO-d_6) δ = 166.3, 155.4, 152.6, 134.9, 134.0, 130.3, 128.9, 128.7, 127.6, 127.4, 126.9, 123.3, 119.4, 76.4, 31.4, 30.3, 18.8, 13.9; **MS** *m/e* 1018 (M + Na^+). **EA** calc for $C_{50}H_{46}N_2O_{16}S_2$, C, 60.35; H, 4.66; N, 2.82%; Found C, 60.47; H, 4.91, N, 2.90%. **IR** ν_{max} 2961 cm^{-1} and 2943 cm^{-1} (C-H), 3000 – 2760 cm^{-1} (broad COOH), 1680 cm^{-1} (C=O), 1602 cm^{-1} (C-O), 1531 cm^{-1} and 1367 cm^{-1} (N-O).

***p*-Di-carboxylato-di-*O*-pentoxy-di-*O*-bis(*p*-nitrobenezenesulfonyloxy)-calix[4]arene** (**28c**) was obtained in 89% yield; mp (decomp.): > 265°C; **^{1}H NMR** (300MHz, DMSO-d_6) δ = 12.80 (s, 2H, -COO<u>H</u>), 8.55 – 8.51 (m, 4H, Ar-<u>H</u> (Nos)), 8.13 – 8.10 (m, 4H, Ar-<u>H</u>(Nos)), 7.80 (s, 4H, Ar-<u>H</u>), 6.65 – 6.56 (m, 2H, Ar-<u>H</u>), 6.40 – 6.34 (m, 4H, Ar-<u>H</u>), 3.97 – 3.92 (m, 4H, Ar-<u>CH_2</u>-Ar), 3.87 – 3.84 (m , 4H, -O-<u>CH_2</u>-), 3.18 – 3.13 (m, 4H, Ar-<u>CH_2</u>-Ar), 1.84 – 1.75 (m, 4H, -O-CH_2-<u>CH_2</u>-), 1.36 – 1.27 (m, 4H, -<u>CH_2</u>-CH_2-CH_3), 1.18 – 1.10 (m, 4H, -<u>CH_2</u>-CH_3), 0.78 (t, *J* = 7.3 Hz, 6H, -<u>CH_3</u>); **^{13}C{^{1}H} NMR** (100 MHz, DMSO-d_6) δ = 166.3, 155.4, 152.6, 134.9, 134.0, 130.3, 128.9, 128.7, 127.6, 127.4, 126.9, 123.3, 119.4, 76.4, 31.4, 30.3, 18.8, 15.4, 13.9; **MS** *m/e* 1046 (M + Na^+); **EA** calc for $C_{52}H_{50}N_2O_{16}S_2$, C, 61.05; H, 4.93; N, 2.74%; Found C, 60.97; H, 5.01, N, 2.87%; **IR** ν_{max} 2988 cm^{-1} and 2951 cm^{-1} (C-H), 3000 – 2745 cm^{-1} (broad COOH), 1678 cm^{-1} (C=O), 1608 cm^{-1} (C-O), 1533 cm^{-1} and 1377 cm^{-1} (N-O).

***Alt*-*p*-di-carboxylato-di-*O*-alkoxy-calix[4]arenes** (**29a - c**) were synthesised according to modified literature procedure**.**[85] An appropriate *p*-di-carboxylato-di-*O*-alkoxy-di-*O*-bis(*p*-nitrobenezenesulfonyloxy)-calix[4]arene (**29a - c**) (0.50 mmol) was dissolved in a mixture of ethanol (80 mL) and dichloromethane (80 mL) containing 50 molar equivalent of potassium hydroxide (1.47 g, 26.0 mmol). The mixture was stirred at

room temperature for 24 h, then acidified with 1M HCl and extracted with dichloromethane (3x100 mL). The combined organic layers were washed with deionised water, brine and dried over anhydrous magnesium sulfate. The solvents were removed under reduced pressure and the solid residue was taken up with hexane and filtered to give pale yellow solid in each case.

***Alt-p*-di-carboxylato-di-*O*-propoxy-calix[4]arene** (**29a**) was obtained in 87% yield; mp: > 300^{o}C; **^{1}H NMR** (300MHz, DMSO-d_6) δ = 12.77 (s, 2H, -COOH), 8.28 (s, 2H, -OH), 7.65 (s, 4H, Ar-H), 7.25 – 7.19 (m, 4H, Ar-H), 6.69 – 6.62 (m, 2H, Ar-H), 4.19 (d, *J* = 13.0 Hz, 4H, Ar-CH_2-Ar), 4.00 (t, *J* = 6.0 , 4H, -O-CH_2-), 3.59 (d, *J* = 13.0 Hz, 4H, Ar-CH_2-Ar), 1.96 – 1.86 (m, 4H, -CH_2-CH_3), 1.27 (t, *J* = 7.4 Hz, 6 H, -CH_3); **^{13}C{^{1}H} NMR** (100 MHz, DMSO-d_6) δ = 168.7, 157.6, 154.6, 136.1, 130.9, 129.3, 128.5, 127.2, 120.1, 75.3, 30.4, 29.0, 16.2. **MS** *m/e* 620 (M + Na^+); **EA** calc for $C_{36}H_{36}O_8$, C, 72.47; H, 6.08%; Found C, 72.40; H, 6.48%; **IR** ν_{max} 3344 cm^{-1} (OH), 2953 cm^{-1} and 2934 cm^{-1} (C-H), 3000 – 2750 cm^{-1} (COOH), 1672 cm^{-1} (C=O), 1601 cm^{-1} (C-O).

***Alt-p*-di-carboxylato-di-*O*-butoxy-calix[4]arene** (**29b**) was obtained in 82% yield; mp: > 300^{o}C; **^{1}H NMR** (300MHz, DMSO-d_6) δ = 12.75 (s, 2H, -COOH), 8.26 (s, 2H, -OH), 7.62 (s, 4H, Ar-H), 7.24 – 7.18 (m, 4H, Ar-H), 6.69 – 6.62 (m, 2H, Ar-H), 4.18 (d, *J* = 13.0 Hz, 4H, Ar-CH_2-Ar), 3.98 (t, *J* = 6.0 , 4H, -O-CH_2-), 3.59 (d, *J* = 13.0 Hz, 4H, Ar-CH_2-Ar), 2.08 – 1.94 (m, 4H, -O-CH_2-CH_2-), 1.82 – 1.74 (m, 4 H, -CH_2-CH_3), 1.10 (t, *J* = 7.4 Hz, 6 H, -CH_3). **^{13}C{^{1}H} NMR** (100 MHz, DMSO-d_6) δ = 166.3, 155.4, 152.6, 134.0, 130.3, 128.9, 127.6, 127.3, 119.4, 76.4, 31.8, 30.3, 18.8, 13.9; **MS** *m/e* 648 (M + Na^+); **EA** calc for $C_{38}H_{40}O_8$, C, 73.06; H, 6.45%; Found C, 72.58; H, 6.48%. **IR** ν_{max} 3330 cm^{-1} (OH), 2957 cm^{-1} and 2929 cm^{-1} (C-H), 3000 – 2760 cm^{-1} (COOH), 1686 cm^{-1} (C=O), 1600 cm^{-1} (C-O).

***Alt-p*-di-carboxylato-di-*O*-pentoxy-calix[4]arene** (**29c**) was obtained in 81% yield; mp: > 300^{o}C; **^{1}H NMR** (300MHz, DMSO-d_6) δ = 12.73 (s, 2H, -COOH), 8.23 (s, 2H, -OH), 7.60 (s, 4H, Ar-H), 7.21 – 7.16 (m, 4H, Ar-H), 6.67 – 6.60 (m, 2H, Ar-H), 4.17 (m, 4H, Ar-CH_2-Ar), 3.96 (m, 4H, -O-CH_2-), 3.55 (m, 4H, Ar-CH_2-Ar), 1.88 – 1.74 (m, 4H, -O-CH_2-CH_2-), 1.42 – 1.31(m, 4H, -CH_2-CH_2-CH_3), 1.21 – 1.07 (m, 4H, -CH_2-CH_3), 0.81 (t, *J* = 7.3 Hz, 6H, -CH_3); **^{13}C{^{1}H} NMR** (100 MHz, DMSO-d_6) δ = 167.7, 155.9, 152.8, 134.6, 130.7, 129.4, 128.5, 127.8, 119.0, 76.8, 31.6, 31.5, 18.8, 14.1, 10.0;

MS *m/e* 676 ($M + Na^+$); **EA** calc for $C_{40}H_{44}O_8$, C, 73.60; H, 6.79%; Found C, 73.48; H, 6.98%; **IR** ν_{max} 3320 cm^{-1} (OH), 2951 cm^{-1} and 2920 cm^{-1} (C-H), 3000 – 2742 cm^{-1} (COOH), 1661 cm^{-1} (C=O), 1596 cm^{-1} (C-O).

Synthesis of 30: A mixture of **29a** (30.0 mg, 0.05 mmol) and $Co(NO_3)_2.6H_2O$ (36.5 mg, 0.125 mmol) was dissolved in 2 mL of dmf, followed by layering of 1 ml of a MeOH solution of 1,10-phenanthroline (9.0 mg, 0.05 mmol). Slow evaporation over several weeks resulted in the formation of pink crystals suitable for X-ray diffraction studies, which were filtered washed and dried to afford 12.6 mg of solid (27% yield). **EA** calc for $C_{51}H_{51}N_3O_{10}Co_1$, C, 66.37; H 5.56; N, 4.54%. Found C, 69.02; H, 4.63, N, 3.38%. **IR** ν_{max} 3245 cm^{-1} (OH), 2945 cm^{-1} and 2887 cm^{-1} (C-H), 1651 cm^{-1} (C=O), 1612 cm^{-1} (C-O), 1567 cm^{-1} (C-C), 1380 cm^{-1} (C-H), 722 cm^{-1} (C-H). PXRD analysis revealed that the material becomes amorphous upon removal from the mother liquor / drying, which is consistent with the discrepancy between theoretical and experimental results of elemental analysis.

Synthesis of 31: A mixture of **29b** (31.3 mg, 0.05 mmol) and $Co(NO_3)_2.6H_2O$ (36.5 mg, 0.125 mmol) was dissolved in 2 mL of dmf, followed by layering of 1 ml of a MeOH solution of 1,10-phenanthroline (9.0 mg, 0.05 mmol). Slow evaporation over several weeks resulted in the formation of pink crystals suitable for X-ray diffraction studies, which were filtered washed and dried to afford 14.1 mg of solid (30% yield). **EA** calc for $C_{106}H_{110}N_6O_{20}Co_2$, C, 66.80; H 5.82; N, 4.41%. Found C, 68.44; H, 4.51, N, 3.27%. **IR** ν_{max} 3267 cm^{-1} (OH), 2952 cm^{-1} and 2879 cm^{-1} (C-H), 1655 cm^{-1} (C=O), 1622 cm^{-1} (C-O), 1569 cm^{-1} (C-C), 1382 cm^{-1} (C-H), 725 cm^{-1} (C-H). PXRD analysis revealed that the material becomes amorphous upon removal from the mother liquor / drying, which is consistent with the discrepancy between theoretical and experimental results of elemental analysis.

Synthesis of 32: A mixture of **29b** (31.3 mg, 0.05 mmol) and $Ni(NO_3)_2.6H_2O$ (36.5 mg, 0.125 mmol) was dissolved in 2 mL of dmf, followed by layering of 1 ml of a MeOH solution of 1,10-phenanthroline (9.0 mg, 0.05 mmol). Slow evaporation over several weeks resulted in the formation of green crystals suitable for X-ray diffraction studies, which were filtered washed and dried to afford 2.3 mg of solid (5% yield). **EA** calc for $C_{53}H_{55}N_3O_{10}Ni_1$, C, 66.82; H 5.82; N, 4.41%. Found C, 68.57; H, 4.69, N, 3.48%. **IR**

ν_{max} 3271 cm^{-1} (OH), 2953 cm^{-1} and 2872 cm^{-1} (C-H), 1650 cm^{-1} (C=O), 1625 cm^{-1} (C-O), 1540 cm^{-1} (C-C), 1388 cm^{-1} (C-H), 717 cm^{-1} (C-H). Due to inhomogeneity of the product PXRD experiments were not carried out. Discrepancy between theoretical and experimental results of elemental analysis suggests the material becomes amorphous upon removal from mother liquor / drying.

Synthesis of 33: A mixture of **29a** (30.0 mg, 0.05 mmol) and $Co(NO_3)_2.6H_2O$ (36.5 mg, 0.125 mmol) was dissolved in 2 mL of dmf, followed by layering of 1 ml of a MeOH solution of 2-methyl-1,10-phenanthroline (9.7 mg, 0.05 mmol). Slow evaporation over several weeks resulted in the formation of pink crystals suitable for X-ray diffraction studies, which were filtered washed and dried to afford 5.5 mg of solid (12% yield). **EA** calc for $C_{104}H_{106}N_6O_{20}Co_2$, C, 66.54; H 5.69; N, 4.48%. Found C, 68.61; H, 4.57, N, 3.32%. **IR** ν_{max} 3270 cm^{-1} (OH), 2954 cm^{-1} and 2862 cm^{-1} (C-H), 1649 cm^{-1} (C=O), 1617 cm^{-1} (C-O), 1533 cm^{-1} (C-C), 1376 cm^{-1} (C-H), 720 cm^{-1} (C-H). PXRD analysis revealed that the material becomes amorphous upon removal from the mother liquor / drying, which is consistent with the discrepancy between theoretical and experimental results of elemental analysis.

Synthesis of 34: A mixture of **29a** (30.0 mg, 0.05 mmol) and $Ni(NO_3)_2.6H_2O$ (36.5 mg, 0.125 mmol) was dissolved in 2 mL of dmf, followed by layering of 1 ml of a MeOH solution of 2-methyl-1,10-phenanthroline (9.7 mg, 0.05 mmol). Slow evaporation over several weeks resulted in the formation of green crystals suitable for X-ray diffraction studies, which were filtered washed and dried to afford 6.5 mg of solid (14% yield). **EA** calc for $C_{52}H_{53}N_3O_{10}Ni_1$, C, 66.54; H 5.69; N, 4.48%. Found C, 68.37; H, 4.48, N, 3.29%. **IR** ν_{max} 3270 cm^{-1} (OH), 2963 cm^{-1} and 2874 cm^{-1} (C-H), 1655 cm^{-1} (C=O), 1629 cm^{-1} (C-O), 1530 cm^{-1} (C-C), 1371 cm^{-1} (C-H), 722 cm^{-1} (C-H). Due to inhomogeneity of the product PXRD experiments were not carried out. Discrepancy between theoretical and experimental results of elemental analysis suggests solvent loss upon removal from mother liquor / drying.

Synthesis of 35: A mixture of **29b** (31.3 mg, 0.05 mmol) and $Co(NO_3)_2.6H_2O$ (36.5 mg, 0.125 mmol) was dissolved in 2 mL of dmf, followed by layering of 1 ml of a MeOH solution of 2-methyl-1,10-phenanthroline (9.7 mg, 0.05 mmol). Slow

evaporation over several weeks resulted in the formation of pink crystals suitable for X-ray diffraction studies, which were filtered washed and dried to afford 5.1 mg of solid (11% yield). **EA** calc for $C_{54}H_{57}N_3O_{10}Co_1$, C, 67.07; H 5.94; N, 4.35%. Found C, 68.63; H, 4.77, N, 3.49%. **IR** ν_{max} 3270 cm^{-1} (OH), 2967 cm^{-1} and 2870 cm^{-1} (C-H), 1662 cm^{-1} (C=O), 1615 cm^{-1} (C-O), 1532 cm^{-1} (C-C), 1379 cm^{-1} (C-H), 720 cm^{-1} (C-H). PXRD analysis revealed that the material becomes amorphous upon removal from the mother liquor / drying, which is consistent with the discrepancy between theoretical and experimental results of elemental analysis.

Synthesis of 36: A mixture of **29b** (31.3 mg, 0.05 mmol) and $Ni(NO_3)_2.6H_2O$ (36.5 mg, 0.125 mmol) was dissolved in 2 mL of dmf, followed by layering of 1 ml of a MeOH solution of 2-methyl-1,10-phenanthroline (9.7 mg, 0.05 mmol). Slow evaporation over several weeks resulted in the formation of green crystals suitable for X-ray diffraction studies, which were filtered washed and dried to afford 2.8 mg of solid (6% yield). **EA** calc for $C_{108}H_{114}N_6O_{20}Ni_2$, C, 67.09; H 5.94; N, 4.35%. Found C, 68.50; H, 4.61, N, 3.58%. **IR** ν_{max} 3280 cm^{-1} (OH), 2978 cm^{-1} and 2859 cm^{-1} (C-H), 1648 cm^{-1} (C=O), 1622 cm^{-1} (C-O), 1564 cm^{-1} (C-C), 1385 cm^{-1} (C-H), 726 cm^{-1} (C-H). Due to inhomogeneity of the product PXRD experiments were not carried out. Discrepancy between theoretical and experimental results of elemental analysis suggests solvent loss upon removal from mother liquor / drying.

Synthesis of 37: A mixture of **29a** (30.0 mg, 0.05 mmol) and $Zn(NO_3)_2.6H_2O$ (37.2 mg, 0.125 mmol) was dissolved in 2 mL of dmf, followed by layering of 1 ml of a MeOH solution of 2-methyl-1,10-phenanthroline (9.7 mg, 0.05 mmol). Slow evaporation over several weeks resulted in the formation of colourles crystals suitable for X-ray diffraction studies, which were filtered washed and dried to afford 10.4 mg of solid (22% yield). **EA** calc for $C_{52}H_{53}N_3O_{10}Zn_1$, C, 66.07; H 5.65; N, 4.44%. Found C, 67.38; H, 5.27, N, 4.11%. **IR** ν_{max} 3295 cm^{-1} (OH), 2989 cm^{-1} and 2863 cm^{-1} (C-H), 1658 cm^{-1} (C=O), 1612 cm^{-1} (C-O), 1569 cm^{-1} (C-C), 1386 cm^{-1} (C-H), 724 cm^{-1} (C-H). Due to inhomogeneity of the product PXRD experiments were not carried out. Discrepancy between theoretical and experimental results of elemental analysis suggests solvent loss upon removal from mother liquor / drying.

Synthesis of 38: A mixture of **29b** (31.3 mg, 0.05 mmol) and $Zn(NO_3)_2.6H_2O$ (37.2 mg, 0.125 mmol) was dissolved in 2 mL of dmf, followed by layering of 1 ml of a MeOH solution of 2-methyl-1,10-phenanthroline (9.7 mg, 0.05 mmol). Slow evaporation over several weeks resulted in the formation of colourless crystals suitable for X-ray diffraction studies, which were filtered washed and dried to afford 10.1 mg of solid (20% yield). **EA** calc for $C_{54}H_{57}N_3O_{10}Zn_1$, C, 66.63; H 5.90; N, 4.32%. Found C, 67.70; H, 5.49, N, 4.08%. **IR** ν_{max} 3293 cm^{-1} (OH), 2984 cm^{-1} and 2866 cm^{-1} (C-H), 1657 cm^{-1} (C=O), 1616 cm^{-1} (C-O), 1570 cm^{-1} (C-C), 1382 cm^{-1} (C-H), 723 cm^{-1} (C-H). Due to inhomogeneity of the product PXRD experiments were not carried out. Discrepancy between theoretical and experimental results of elemental analysis suggests solvent loss upon removal from mother liquor / drying.

Synthesis of 39: A mixture of **29a** (30.0 mg, 0.05 mmol) and $Ni(NO_3)_2.6H_2O$ (36.5 mg, 0.125 mmol) was dissolved in 2 mL of dmf, followed by layering of 1 ml of a MeOH solution of 3-methyl-1,10-phenanthroline (9.7 mg, 0.05 mmol). Slow evaporation over several weeks resulted in the formation of green crystals suitable for X-ray diffraction studies, which were filtered washed and dried to afford 11.7 mg of solid (19% yield). **EA** calc for $C_{64}H_{80}N_7O_{14}Ni_1$, C, 62.49; H 6.56; N, 7.97%. Found C, 66.61; H, 5.59, N, 4.48%. **IR** ν_{max} 3280 cm^{-1} (OH), 2976 cm^{-1} and 2853 cm^{-1} (C-H), 1639 cm^{-1} (C=O), 1610 cm^{-1} (C-O), 1568 cm^{-1} (C-C), 1372 cm^{-1} (C-H), 720 cm^{-1} (C-H). PXRD analysis revealed that the material becomes amorphous upon removal from the mother liquor / drying, which is consistent with the discrepancy between theoretical and experimental results of elemental analysis.

Synthesis of 40: A mixture of **29a** (30.0 mg, 0.05 mmol) and $Co(NO_3)_2.6H_2O$ (36.5 mg, 0.125 mmol) was dissolved in 2 mL of dmf, followed by layering of 1 ml of a MeOH solution of 3,4,7,8-tetra-methyl-1,10-phenanthroline (11.8 mg, 0.05 mmol). Slow evaporation over several weeks resulted in the formation of red crystals suitable for X-ray diffraction studies, which were filtered washed and dried to afford 16.8 mg of solid (28% yield). **EA** calc for $C_{128}H_{160}N_{12}O_{26}Co_2$, C, 64.04; H 6.72; N, 7.00%. Found C, 67.48; H, 5.87, N, 4.29%. **IR** ν_{max} 3274 cm^{-1} (OH), 2960 cm^{-1} and 2861 cm^{-1} (C-H), 1645 cm^{-1} (C=O), 1619 cm^{-1} (C-O), 1564 cm^{-1} (C-C), 1371 cm^{-1} (C-H), 727 cm^{-1} (C-H). PXRD analysis revealed that the material becomes amorphous upon removal from the

mother liquor / drying, which is consistent with the discrepancy between theoretical and experimental results of elemental analysis.

Synthesis of 41: A mixture of **29b** (31.3 mg, 0.05 mmol) and $Co(NO_3)_2.6H_2O$ (36.5 mg, 0.125 mmol) was dissolved in 2 mL of dmf, followed by layering of 1 ml of a MeOH solution of 3,4,7,8-tetra-methyl-1,10-phenanthroline (11.8 mg, 0.05 mmol). Slow evaporation over several weeks resulted in the formation of red crystals suitable for X-ray diffraction studies, which were filtered washed and dried to afford 16.0 mg of solid (26% yield). **EA** calc for $C_{66}H_{84}N_6O_{13}Co_1$, C, 64.54; H 6.89; N, 6.84%. Found C, 67.85; H, 6.29, N, 4.16%. **IR** ν_{max} 3260 cm^{-1} (OH), 2953 cm^{-1} and 2850 cm^{-1} (C-H), 1648 cm^{-1} (C=O), 1627 cm^{-1} (C-O), 1561 cm^{-1} (C-C), 1379 cm^{-1} (C-H), 721 cm^{-1} (C-H). PXRD analysis revealed that the material becomes amorphous upon removal from the mother liquor / drying, which is consistent with the discrepancy between theoretical and experimental results of elemental analysis.

Synthesis of 42: A mixture of **29a** (30.0 mg, 0.05 mmol) and $Ni(NO_3)_2.6H_2O$ (36.5 mg, 0.125 mmol) was dissolved in 2 mL of dmf, followed by layering of 1 ml of a MeOH solution of 3,4,7,8-tetra-methyl-1,10-phenanthroline (11.8 mg, 0.05 mmol). Slow evaporation over several weeks resulted in the formation of green crystals suitable for X-ray diffraction studies, which were filtered washed and dried to afford 13.8 mg of solid (23% yield). **EA** calc for $C_{64}H_{80}N_6O_{13}Ni_1$, C, 64.06; H 6.72; N, 7.00%. Found C, 67.36; H, 5.87, N, 5.19%. **IR** ν_{max} 3268 cm^{-1} (OH), 2971 cm^{-1} and 2849 cm^{-1} (C-H), 1660 cm^{-1} (C=O), 1607 cm^{-1} (C-O), 1555 cm^{-1} (C-C), 1363 cm^{-1} (C-H), 720 cm^{-1} (C-H). PXRD analysis revealed that the material becomes amorphous upon removal from the mother liquor / drying, which is consistent with the discrepancy between theoretical and experimental results of elemental analysis.

Synthesis of 43: A mixture of **29b** (31.3 mg, 0.05 mmol) and $Ni(NO_3)_2.6H_2O$ (36.5 mg, 0.125 mmol) was dissolved in 2 mL of dmf, followed by layering of 1 ml of a MeOH solution of 3,4,7,8-tetra-methyl-1,10-phenanthroline (11.8 mg, 0.05 mmol). Slow evaporation over several weeks resulted in the formation of green crystals suitable for X-ray diffraction studies, which were filtered washed and dried to afford 15.3 mg of solid (25% yield). **EA** calc for $C_{132}H_{168}N_{12}O_{26}Ni_2$, C, 64.55; H 6.89; N, 6.84%. Found C, 66.73; H, 6.35, N, 5.21%. **IR** ν_{max} 3259 cm^{-1} (OH), 2961 cm^{-1} and 2877 cm^{-1} (C-H),

1649 cm^{-1} (C=O), 1613cm^{-1} (C-O), 1529 cm^{-1} (C-C), 1341 cm^{-1} (C-H), 718 cm^{-1} (C-H). PXRD analysis revealed that the material becomes amorphous upon removal from the mother liquor / drying, which is consistent with the discrepancy between theoretical and experimental results of elemental analysis.

4.5.2. Crystallographic tables for compounds 30 - 43

Complex number	**30**	**31**	**32**
Formula	$C_{51}H_{51}N_3O_{10}Co_1$	$C_{106}H_{112}N_6O_{20}Co_2$	$C_{53}H_{55}N_3O_{10}Ni_1$
*M*r	922.86	1907.96	952.73
Crystal system	$P2_1/n$	$P2_1/n$	$P2_1/n$
Space group	Monoclinic	Monoclinic	Monoclinic
T/K	100(2)	100(2)	100(2)
a /Å	11.2141(4)	11.8055(9)	11.6753(5)
b /Å	12.9667(5)	12.5516(9)	12.4874(4)
c /Å	30.9925(10)	32.702(2)	32.6697(11)
α / ^{o}	90.00	90.00	90.00
β / ^{o}	91.012(2)	91.264(5)	91.466(2)
γ /^{o}	90.00	90.00	90.00
U /Å^3	4505.9(3)	4844.5(6)	4761.5(3)
Z	4	2	4
F(000)	1932	1996	1732
D_c / g cm^{-3}	1.360	1.304	1.162
μ / mm^{-1}	0.445	0.416	0.458
$2\Theta_{max}$ / ^{o}	47.7	52.7	52.4
Data collected	26926	40319	39079
Unique reflections	5366	9908	7350
R_{int}	0.0449	0.0587	0.0424
Obs data ($I > 2\sigma > (I)$)	4061	4168	5675
Parameters	491	551	514
Restraints	16	17	8
R_1 (observed data)	0.0964	0.0984	0.1001
ωR_2 (all data)	0.2638	0.2796	0.3458
GooF	1.044	1.029	1.569
Max/min residuals [eÅ^3]	0.738 / -0.747	1.888 / -0.821	1.296 / -0.854

Complex number	**33**	**34**	**35**
Formula	$C_{104}H_{108}N_6O_{20}Co_2$	$C_{52}H_{55}N_3O_{10}Ni_1$	$C_{54}H_{57}N_3O_{10}Co_1$
*M*r	1879.91	940.72	966.76
Crystal system	$P2_1/n$	$P2_1/n$	$P2_1/n$
Space group	Monoclinic	Monoclinic	Monoclinic
T/K	100(2)	100(2)	100(2)
a /Å	11.1229(9)	11.0936(16)	11.2423(4)
b /Å	13.1246(11)	12.9117(19)	13.1599(6)
c /Å	31.509(2)	31.661(5)	32.5801(12)
α / ^{o}	90.00	90.00	90.00
β / ^{o}	92.918(3)	92.649(2)	90.668(2)
γ /^{o}	90.00	90.00	90.00
U /Å^3	4593.8(6)	4530.2(12)	4819.8(3)
Z	2	4	4
F(000)	1964	1976	1868
D_c / g cm^{-3}	1.355	1.376	1.229
μ / mm^{-1}	0.437	0.618	0.411
$2\Theta_{max}$ / ^{o}	43.5	62.3	51.8
Data collected	21404	57012	33681
Unique reflections	5426	11245	7210
R_{int}	0.0560	0.0810	0.0581
Obs data ($I > 2\sigma > (I)$	3703	8782	5584
Parameters	498	600	543
Restraints	4	102	20
R_1 (observed data)	0.0945	0.0808	0.1271
ωR_2 (all data)	0.2328	0.2293	0.4242
GooF	1.059	1.036	1.896
Max/min residuals [eÅ^3]	1.187 / -0.728	1.614/ -1.332	0.957 / -0.891

Complex number	**36**	**37**	**38**
Formula	$C_{108}H_{116}N_6O_{20}Ni_2$	$C_{52}H_{53}N_3O_{10}Zn_1$	$C_{54}H_{57}N_3O_{10}Zn_1$
*M*r	1935.53	945.39	973.45
Crystal system	$P2_1/n$	$P2_1/n$	*P*-1
Space group	Monoclinic	Monoclinic	Triclinic
T/K	100(2)	100(2)	100(2)
a /Å	11.2656(6)	11.1266(5)	11.1352(5)
b /Å	12.9401(7)	13.3137(6)	13.2505(5)
c /Å	32.6181(15)	31.4424(12)	32.5430(12)
α / ^{o}	90.00	90.00	89.629(3)
β / ^{o}	90.369(3)	93.048(3)	89.734(3)
γ /^{o}	90.00	90.00	86.432(3)
U /Å^3	4754.9(4)	4651.2(3)	4792.2(3)
Z	2	4	4
F(000)	2028	1976	2040
D_c / g cm^{-3}	1.346	1.347	1.346
μ / mm^{-1}	0.472	0.591	0.576
$2\Theta_{max}$ / ^{o}	54.4	47.9	60.6
Data collected	64842	20069	47410
Unique reflections	10564	5495	22037
R_{int}	0.0774	0.0394	0.0500
Obs data ($I > 2\sigma > (I)$	7353	4105	15954
Parameters	579	474	1073
Restraints	119	30	41
R_1 (observed data)	0.1554	0.1499	0.0994
ωR_2 (all data)	0.4901	0.4305	0.2715
GooF	2.209	1.879	1.033
Max/min residuals [eÅ^3]	1.271 / -1.034	1.263 / -1.362	2.144 / -1.495

Complex number	**39**	**40**	**41**
Formula	$C_{64}H_{80}N_7O_{14}Ni_1$	$C_{128}H_{160}N_{12}O_{26}Co_2$	$C_{66}H_{84}N_6O_{13}Co_1$
*M*r	1230.08	2400.63	1228.37
Crystal system	C_2/c	C_2/c	C_2/c
Space group	Monoclinic	Monoclinic	Monoclinic
T/K	100(2)	100(2)	100(2)
a /Å	38.586(3)	33.589(2)	33.761(2)
b /Å	11.9927(8)	12.8935(8)	12.9725(10)
c /Å	32.252(2)	31.6039(19)	31.8346(19)
α / ^{o}	90.00	90.00	90.00
β / ^{o}	120.640(2)	117.376(2)	116.371(3)
γ /^{o}	90.00	90.00	90.00
U /Å^3	12840.9(15)	12154.2(14)	12491.5(15)
Z	8	4	8
F(000)	3928	5080	4248
D_c / g cm^{-3}	0.968	1.310	1.071
μ / mm^{-1}	0.348	0.351	0.326
$2\Theta_{max}$ / ^{o}	44.9	47.6	46.0
Data collected	34615	34894	34886
Unique reflections	8332	9345	8650
R_{int}	0.0620	0.0613	0.0676
Obs data ($I > 2\sigma > (I)$	5021	6612	5035
Parameters	600	760	565
Restraints	8	6	9
R_1 (observed data)	0.0512	0.0591	0.0793
ωR_2 (all data)	0.1268	0.1324	0.2152
GooF	0.913	1.020	1.017
Max/min residuals [eÅ^3]	0.372/ -0.267	0.588 / -0.639	0.734 / -0.881

Complex number	**42**	**43**
Formula	$C_{64}H_{80}N_6O_{13}Ni_1$	$C_{132}H_{168}N_{12}O_{26}Ni_2$
*M*r	1200.76	2456.26
Crystal system	C_2/c	C_2/c
Space group	Monoclinic	Monoclinic
T/K	100(2)	100(2)
a /Å	33.5750(11)	33.901(11)
b /Å	12.8713(5)	12.9612(18)
c /Å	31.2863(11)	31.384(5)
α / ^{o}	90.00	90.00
β / ^{o}	117.237(2)	115.68(3)
γ /^{o}	90.00	90.00
U /Å^3	12021.4(8)	12428(5)
Z	8	4
F(000)	5088	4592
D_c / g cm^{-3}	1.324	1.161
μ / mm^{-1}	0.392	0.452
$2\Theta_{max}$ / ^{o}	80.6	50.7
Data collected	296297	14990
Unique reflections	28912	10240
R_{int}	0.0571	0.0913
Obs data ($I > 2\sigma > (I)$	23721	4170
Parameters	796	679
Restraints	4	15
R_1 (observed data)	0.0571	0.0855
ωR_2 (all data)	0.1684	0.2289
GooF	1.045	0.840
Max/min residuals [eÅ^3]	1.786/ -1.544	0.708 / -0.580

4.6. References

[1] O. Hudecek, P. Curinova, J. Budka and P. Lhoták, *Tetrahedron*, **2011**, *67*, 5213.

[2] S. Kennedy, P. Cholewa, R. D. McIntosh and S. J. Dalgarno, *Cryst. Eng. Commun.*, **2013**, *15*, 1520.

[3] P. J. Nichols, C. L. Raston and J. W. Steed, *Chem. Commun*, **2001**, 1062.

[4] C. A. Hunter and J. K. M. Sanders, *J. Am. Chem. Soc.*, **1990**, *112*, 5525.

Chapter 5. Dimeric metal-organic calixarene capsules

In previous chapters it was shown that with the use of a series of TM(II) ions, di-*p*-carboxylatocalix[4]arenes and phen (or its derivatives), it is possible to construct 1-D CPs. Through synthetic pre-organisation of the calixarene framework, and desired positioning of carboxylates at the upper-rim, one can design calixarene building blocks to selectively synthesise a linear and spiral 1-D CP. In Chapter 3 it was shown that reaction of a series of TM(II) ions (Co, Cd and Ni) with di-*p*-CO_2[4] **16a - b** and a co-ligand (phen and its derivatives), result in architectures adopting 1-D linear CP topology (**17 - 25**). It was found that the use of different TM ions results in the formation of materials that exhibit subtle differences within the metal coordination spheres. As a result of these differences, and the inclusion of different guest species by the calixarene cavity, it was found that these factors influence the self-assembly and the overall solid-state packing. Following on from this, in Chapter 4 it was shown that utilisation of di-*O*-alkoxy-calix[4]arene C_2 symmetry allows one to synthesise *alt*-di-*p*-CO_2[4]s **29a - b**. These can be used as alternative building blocks to react with a series of TM(II) ions (Co, Ni and Zn) and co-ligands (phen and its derivatives) to afford spiral 1-D CPs (**30 - 43**), structures that are markedly different to those containing linear CPs. Results which were attained using *alt*-di-*p*-CO_2[4]s **29a - b** show that, despite using various TM(II) ions (Co, Ni and Zn) in the reaction, the resulting coordination chemistry in the materials formed is near-identical. Furthermore, similar non-covalent interactions and solid-state packing was observed for all three assemblies.

In the course of the study into the use of *alt*-di-*p*-CO_2[4]s as potential building blocks for the construction of porous materials it was found that, under certain reaction conditions, the result of the self-assembly can be very different to the aforementioned spiral 1-D CPs. In Chapter 1 it was shown how *p*-carboxylatocalix[4]arenes can be utilised as building blocks to construct discrete structures, namely MOPs.[56] The strategy requires utilisation of the 'directional bonding' approach and fulfilment of

complementary symmetry criteria. De Mendoza and co-workers showed that, through synthetic pre-organisation of calixarene framework and careful selection of metal ion as a directing centre, complementary symmetry criteria are met and discrete structures can be synthesised.[57] During the investigation of the use of *alt*-di-*p*-CO_2[4] as a building block for construction of supramolecular assemblies, it was found that under certain conditions, reactions of Cd(II) and Zn(II) ions with *alt*-di-*p*-CO_2[4]s and phen or its derivatives, lead to the formation of discrete structures as a result of complementary symmetry. The result of this is the formation of metal-organic capsules rather than infinite spiral 1-D CPs. In this chapter discussion will be focused on results that yielded discrete supramolecular structures.

Apart from the study of the use of *p*-carboxylatocalix[4]arenes as potential building blocks for construction of supramolecular assemblies, a parallel study also investigated the impact of phen and its derivatives on the self-assembly. A series of reactions in which TM(II) ions, di-*p*-CO_2[4]s or *alt*-di-*p*-CO_2[4]s and phen-based co-ligands were used, showed that the presence of methyl substituents in phen, especially t-me-phen, can often disrupt / invoke non-covalent interactions present in the solid state in synthesised materials. This was found to have a significant effect on the solid-state packing of linear and spiral 1-D CPs. These observed changes result from using different phen derivatives, suggesting that this strategy could be potentially useful in allowing one to alter the solid state features displayed in synthesised materials. Given these observations, further research was undertaken to study the influence of phen and its derivatives on the self-assembly and solid-state packing of discrete supramolecular structures.

5.1. Tilted dimeric metal-organic calixarene capsules

In the course of the study of the applicability of *alt*-di-*p*-CO_2[4] as a building block for construction of supramolecular assemblies a series of different TM(II) ions were investigated. Discussion in Chapter 4 focused on results of reactions in which formation of spiral 1-D CPs was observed. The TM(II) ions that yield this type of assemblies are Co and Ni. Reaction of Zn(II) ions with *alt*-di-*p*-CO_2[4]s **29a - b** and 2-me-phen also results in the formation of spiral CPs (**37** and **38**), however in this chapter it will be shown that these are unlike the remaining structures containing the same

components. During the study it became evident that the use of certain TM(II) ions (Cd and Zn) in reactions with *alt*-di-*p*-CO_2[4]s and a phen-based co-ligands results in the formation of discrete rather than infinite structures, that exhibit markedly different solid-state packing.

Following the synthesis in which Cd(II) ions, *alt*-di-*p*-CO_2[4] **29a** and phen were employed, slow evaporation over a period of several weeks afforded crystalline material of formula [Cd_2(**29a**)$_2$(phen)$_2$(H_2O)(dmf)]·4dmf (**44**).[87] The colourless single crystals of **44** are in a monoclinic cell and the crystal structure was solved in space group $P2_1/n$. The unit cell parameters are a = 19.192(17) Å, b = 24.95(2) Å and c = 20.75(2) Å and β = 97.97(2)º. The asymmetric unit contains a discrete coordination complex formed which comprises two Cd(II) ions, two *alt*-di-*p*-CO_2[4]s **29a**, two phens, one aquo ligand, one dmf molecule and a dmf of crystallisation (Fig. 5.1A).

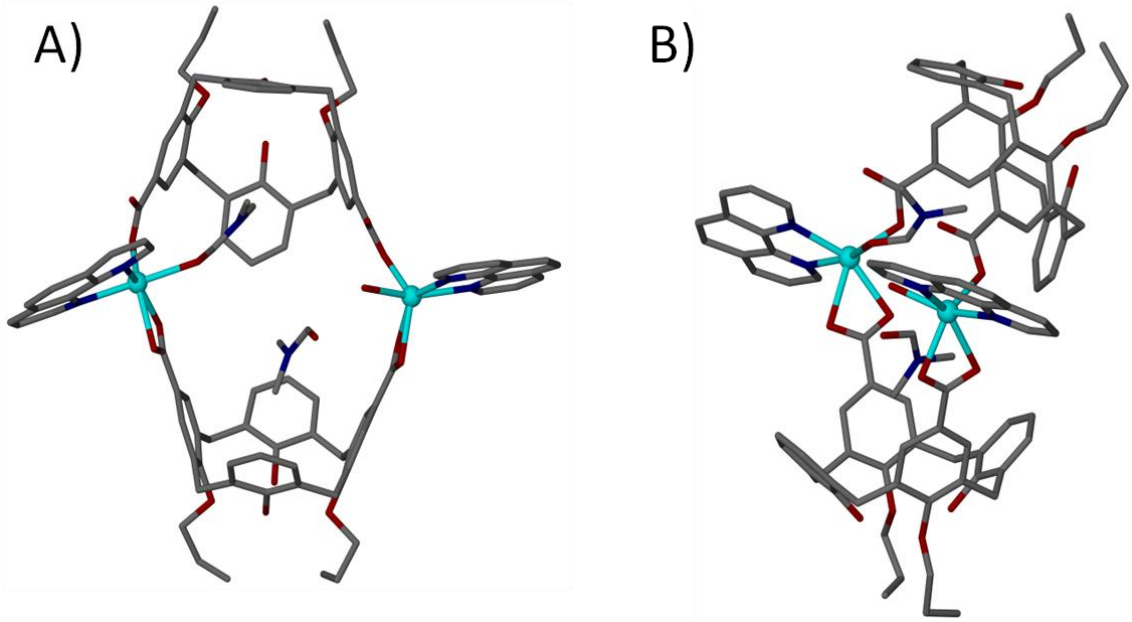

Figure 5.1 (A) Ball and stick representation of the asymmetric unit in **44**. (B) Side view of the tilted dimeric metal-organic capsule formed in **44**. Hydrogen atoms omitted for clarity.

The first of the *alt*-di-*p*-CO_2[4]s (CAL1) is coordinated to two Cd(II) centres *via* carboxylate groups, both of which are coordinated to the metal centre in a bidentate fashion: the O(5)-C(29)-O(6) group is coordinated to Cd(2) with respective bond

lengths of 2.385(7) Å and 2.342(8) Å, and the O(7)-C(30)-O(8) group to Cd(1) with respective bond lengths of 2.444(6) Å and 2.305(7) Å. The second *alt*-di-*p*-CO_2[4] (CAL2) is coordinated to the same two Cd(II) centres *via* carboxylate moieties, however both are bonded in a monodentate fashion: the O(15)-C(69)-O(16) group is coordinated to Cd(1) *via* O(15) and the O(17)-C(70)-O(18) group to Cd(2) *via* O(17) with respective bond lengths of 2.243(9) and 2.241(7) Å. The coordination sphere of Cd(1) is completed by an aquo ligand with the Cd(1)-O(9) bond distance of 2.324(8) Å. The second coordination sphere of Cd(2) is completed by a ligated dmf with the Cd(2)-O(105) bond length of 2.386(10) Å. As expected both phens are coordinated as a chelate, restricting space around the metal centres with Cd(1)-N(3), Cd(1)-N(4), Cd(2)-N(1) and Cd(2)-N(2) distances of 2.333(11), 2.354(9), 2.278(10) and 2.334(14) Å respectively. The orientation of both *alt*-di-*p*-CO_2[4]s results in the discrete complex of shape of a tilted dimeric metal-organic calixarene capsule (MOCC), as shown in Figure 5.1B. The tilt angle between centroids generated from both calixarene phenolic oxygen atoms and one generated between the two Cd(II) centres was found to be ~128˚. Analysis of **44** reveals that both phens are pointing away from the capsule. As expected both *alt*-di-*p*-CO_2[4]s adopt a partially pinched-cone conformation. In CAL1 the distances between diametrical arene *para* carbon atom pairs are 7.37 Å and 9.23 Å. In CAL2 the distance between the same pairs of carbon atoms is 7.49 Å and 8.90 Å. In CAL1 the angles ε and δ are measured to be 90.4° and 113.3° respectively, whereas in CAL2 these angles are 91.2° and 107.7°. For both CAL1 and CAL2 these parameters are consistent with those of the *alt*-di-*p*-CO_2[4]s in **30** - **43**. The interior of capsule is occupied by one dmf of crystallisation, one dmf bonded to Cd(2) and an aquo ligand coordinated to Cd(1) (Fig 5.2). The dmf of crystallisation which resides in the CAL1 cavity forms CH···π interactions; the distances between three hydrogen atoms of dmf and calixarene aryl rings ranges from 2.67 - 3.05 Å. The coordinated dmf molecule which resides in the CAL2 cavity also forms CH···π interactions; the distances between four hydrogen atoms of dmf and the calixarene aryl rings ranges from 2.72 - 3.06 Å. Further analysis reveals that both ligated phens are involved in π-stacking.[75] The phen coordinated to Cd(2) undergoes π-stacking with 1) a s.e. phen bonded to Cd(2)' (closest contact distance of 3.34 Å) and 2) a s.e. phen bonded to Cd(1)' from another s.e. MOCC (closest contact distance of 3.18 Å), as shown in Figure 5.3A.

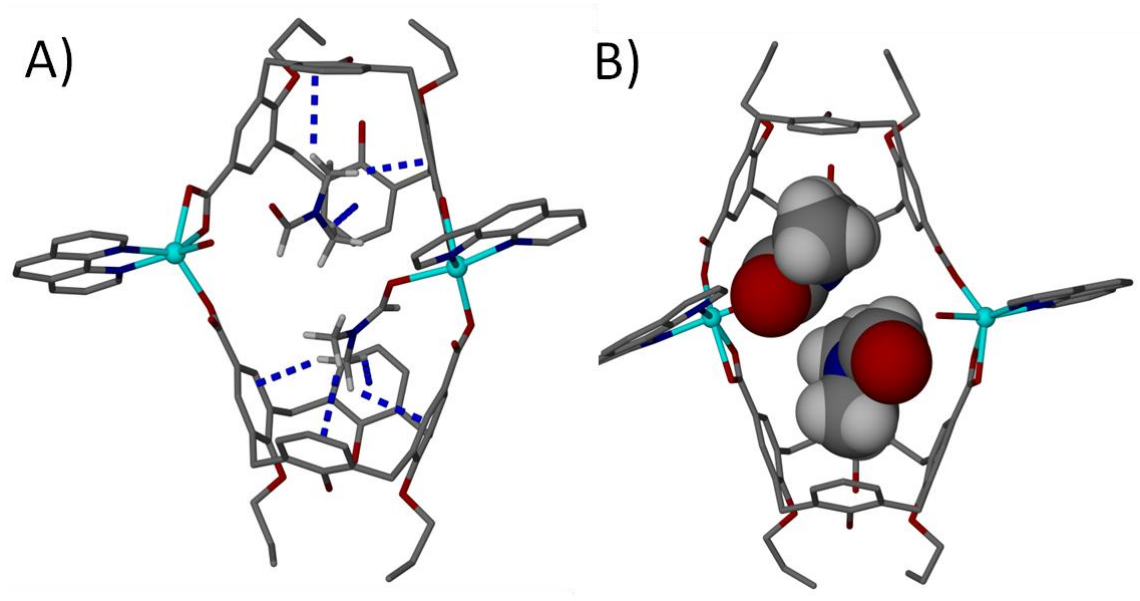

Figure 5.2 Views of the tilted dimeric metal-organic calixarene capsule found in **44**, containing two dmf molecules and an aquo ligand. (A) Complementary host-guest CH···π interactions (blue dashed lines) between the two dmf molecules (one ligated and one unbound) and the interior of calixarene cavity. (B) Space filling representation showing the MOCC cavity occupied by dmf molecules. Hydrogen atoms except those of dmf are omitted for clarity.

The second phen which is coordinated to Cd(1) undergoes π-stacking with 1) the aforementioned s.e. phen bonded to Cd(2)' and 2) an aromatic ring of CAL1 from another s.e. MOCC (closest contact distance of 3.31 Å), as shown in Figure 5.3B. Inspection of the solid-state packing in **44** shows that there are no solvent channels present. The dmf of crystallisation occupying voids between MOCCs, due to being highly disordered, was removed with the routine SQUEEZE.[74] Given our interest in design of materials with their potential application for gas storage / absorption we decided to further analyse the synthesised material. Crystalline material was filtered and dried, however PXRD experiments show that the dried material had become amorphous, indicating that **44** loses crystallinity upon removal from mother liquor / de-solvation.

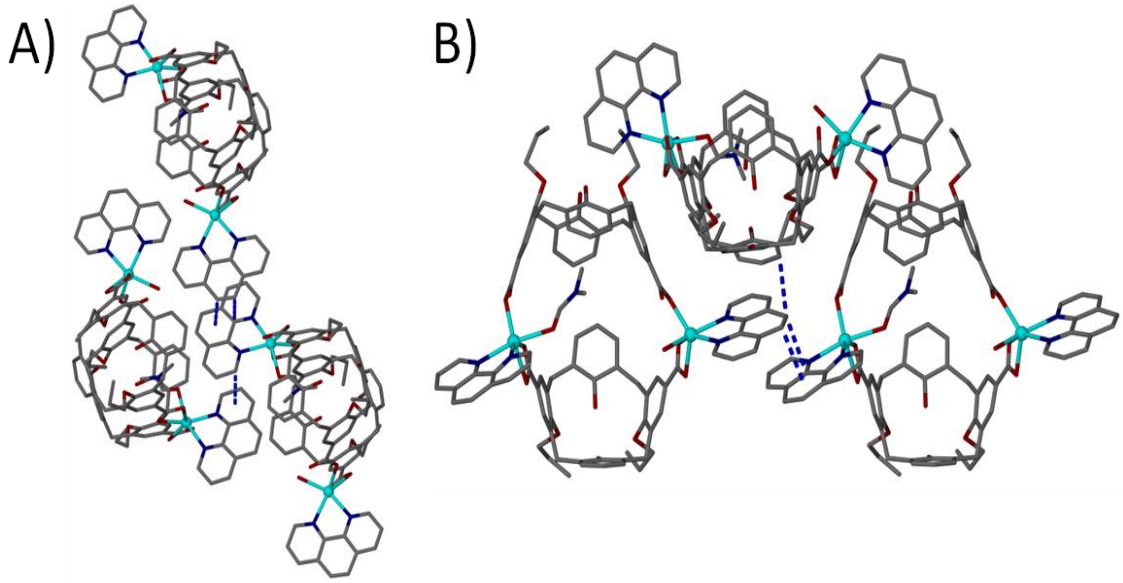

Figure 5.3 Section of the extended structure in **44** showing π-stacking (blue dashed lines) between (A) phen (bonded to Cd(2)) and phens from s.e. MOCCs and (B) phen (bonded to Cd(1)) and an aromatic ring of CAL1. Hydrogen atoms and dmf of crystallisation omitted for clarity.

Reaction of Cd(II) ions with *alt*-di-*p*-CO_2[4] **29b** and phen, following slow evaporation, yielded crystalline material of formula $[Cd_2(\mathbf{29b})_2(phen)_2(H_2O)(dmf)]\cdot 2(dmf)$ (**45**).[87] The colourless crystals of **45** are in a monoclinic cell and the crystal structure was solved in space group $P2_1/n$. The unit cell parameters of a = 19.2266(10) Å, b = 24.9668(14) Å and c = 20.7082(12) Å and β = 98.402(4)° which are marginally different to those of **44**. As in the case of **44**, attained crystals of **45** are composed of discrete tilted dimeric MOCCs (Fig. 5.4). The asymmetric unit contains two Cd(II) ions, two *alt*-di-*p*-CO_2[4] **29b**, two phen, one aquo ligand, one dmf molecule, and two dmf of crystallisation (Fig. 5.4A). The binding mode of all four carboxylate groups to Cd(II) ions in **45** is the same as in **44**. The first *alt*-di-*p*-CO_2[4]s (CAL1) is coordinated to two Cd(II) centres *via* carboxylate groups, both of which are bonded to the metal centre in a bidentate fashion: the O(5)-C(29)-O(6) group is coordinated to Cd(1) in a with respective bond lengths of 2.345(3) and 2.372(3) Å, and the O(7)-C(30)-O(8) group to Cd(2) with respective bond lengths of 2.450(3) and 2.326(4) Å. The second *alt*-di-*p*-CO_2[4] (CAL2) is coordinated to the same two Cd(II) centres *via* carboxylate groups, however both are bonded in a monodentate fashion: the O(13)-C(67)-O(14) group is coordinated to Cd(2) *via* O(14)

with the bond length of 2.203(4) Å, and the O(15)-C(68)-O(16) group to Cd(1) *via* O(15) with the bond distance of 2.218(3) Å. The coordination sphere of Cd(1) is completed by ligated dmf with the Cd(1)-O(17) bond length of 2.350(4) Å. The second coordination sphere of Cd(2) is completed by an aquo ligand with the Cd(2)-O(18) bond distance of 2.350(3) Å. Both phens are coordinated as a chelate restricting space around both of the metal centres, with Cd(1)-N(1), Cd(1)-N(2), Cd(2)-N(3) and Cd(2)-N(4) distances of 2.349(4), 2.288(3), 2.331(3) and 2.327(4) Å respectively. The tilt angle in **45** between centroids generated from both calixarene phenolic oxygen atoms and one generated between the two Cd(II) centres was found to be ~128˚, and is in good agreement with that found in **44**. Both of the *alt*-di-*p*-CO_2[4]s adopt a partially pinched-cone conformation. In CAL1 the distance between diametrical arene *para* carbon atom pairs is 7.26 Å and 9.24 Å, and in CAL2 the distance between the same pairs of carbon atoms is 7.48 Å and 8.83 Å. In CAL1 the ε and δ angles are 88.6° and 113.1° respectively, whereas in CAL2 these angles are 91.1° and 106.6°. For both of the *alt*-di-*p*-CO_2[4]s these parameters are consistent with those found in *alt*-di-*p*-CO_2[4]s in **44** and **30** - **43**. In **45** the interior of the dimeric capsule is occupied by two dmf molecules, one of which is bonded to Cd(1), and an aquo ligand of Cd(2).

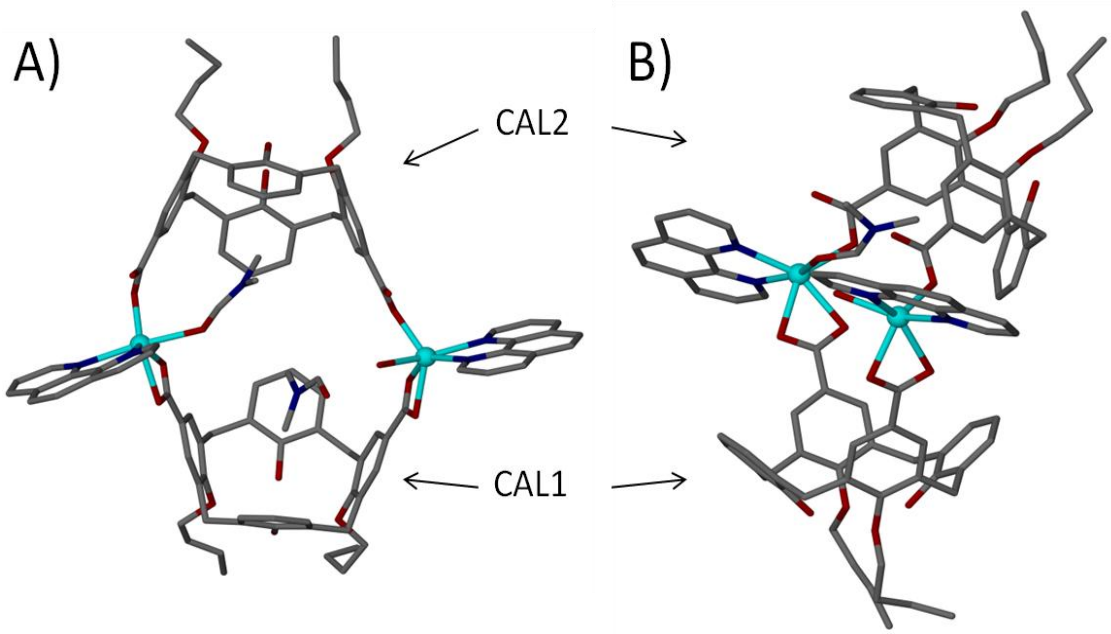

Figure 5.4 (A) Ball and stick representation of the asymmetric unit in **45**. (B) Side view of the tilted dimeric metal-organic capsule formed in **45**. Hydrogen atoms omitted for clarity.

The dmf of crystallisation residing in the CAL1 cavity forms CH···π interactions; the distances between three hydrogen atoms of dmf and calixarene aromatic rings ranges from 2.63 - 2.79 Å (Fig 5.5). The coordinated dmf which resides in the CAL2 cavity also forms CH···π interactions; the distances between four hydrogen atoms of dmf and the calixarene aromatic rings range from 2.73 - 2.96 Å. Analysis of the extended crystal structure of **45** reveals that solid-state packing is near-identical to that of **44**, and that both phens participate in π-stacking in a similar fashion. Phen coordinated to Cd(1) undergoes π-stacking with 1) a s.e. phen bonded to Cd(1)' (closest contact distance of 3.34 Å) and 2) a s.e. phen bonded to Cd(2)" from another s.e. MOCC (closest contact distance of 3.18 Å), as shown in Figure 5.6A. The second phen which is coordinated to Cd(2) undergoes π-stacking with 1) the aforementioned s.e. phen bonded to Cd(1)' and 2) an aromatic ring of CAL1 from another s.e. MOCC (closest contact distance of 3.31 Å), as shown in Figure 5.6B. Inspection of the solid-state packing in **45** shows that as in **44** there are no solvent channels present. The dmf of crystallisation occupying voids between MOCCs, due to being highly disordered, was removed with the routine SQUEEZE.[74]

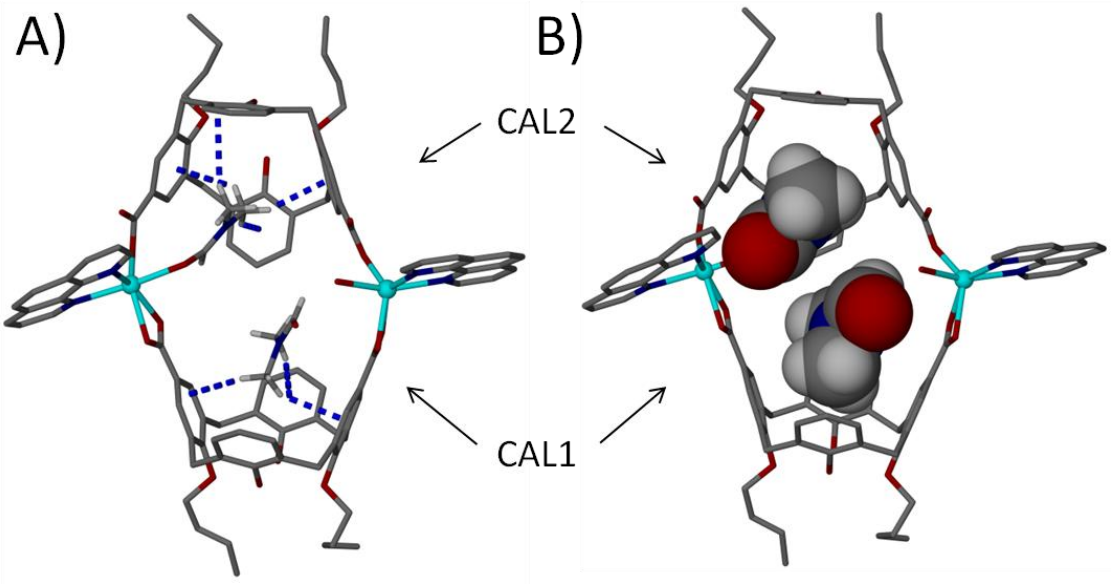

Figure 5.5 Views of the tilted dimeric MOCCs found in **45** containing two dmf molecules and an aquo ligand. (A) Complementary host-guest CH···π interactions (blue dashed lines) between the dmf molecules (one ligated and one unbound) and the interior of the calixarene cavity. (B) Space filling representation showing the MOCC cavity occupied by dmf molecules. Hydrogen atoms except those of dmf are omitted for clarity.

Given our interest in design of materials with their potential application for gas storage / absorption we decided to further analyse the synthesised material. Crystalline material was filtered and dried, however PXRD experiments show that the dried material turns amorphous, suggesting that **45** loses crystallinity upon removal from mother liquor / de-solvation.

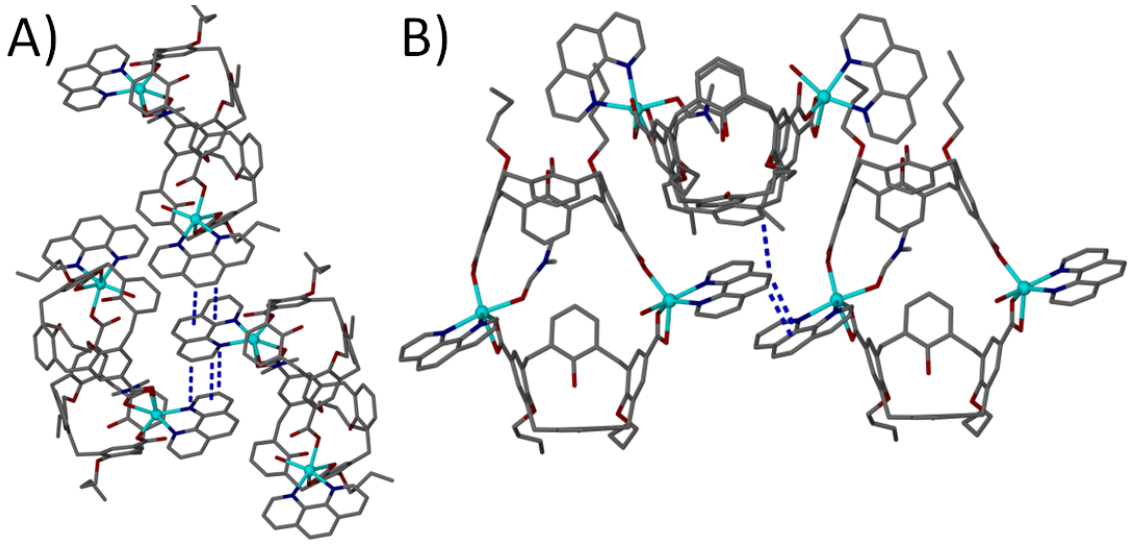

Figure 5.6 Section of the extended structure in **45** showing π-stacking (blue dashed lines) between (A) phen (bonded to Cd(1)) and phens from s.e. MOCC and (B) phen (bonded to Cd(1)) and an aromatic ring of CAL1. Hydrogen atoms and dmf of crystallisation omitted for clarity.

It has been demonstrated that with the use of TM(II) ions such as Co(II) and Ni(II), *alt*-di-*p*-CO_2[4] and phen-type co-ligand it is possible to construct 1-D spiral CPs. However, by choosing a different TM(II) ion, such as Cd(II), and reacting it with *alt*-di-*p*-CO_2[4]s and phen, one can construct a discrete structure adopting a shape of a tilted dimeric MOCC. Given the reaction conditions used to synthesise **44** and **45** are the same as the ones used to synthesise **30** - **43**, one can assume that a key factor that influences the final outcome of assembly must be the TM(II) ion employed.

5.2. Head-to-head dimeric metal-organic calixarene capsules

In Chapter 4 it was shown that reaction of Zn(II) ions, *alt*-di-*p*-CO_2[4] **29a** - **b** and 2-me-phen afforded spiral 1-D CPs **37** and **38**. Under the same reaction conditions,

but using phen instead of 2-me-phen, one can construct a markedly different supramolecular structure. Following the synthesis in which Zn(II) ions, *alt*-di-*p*-CO_2[4] **29a** and phen were employed, slow evaporation over a period of several weeks afforded crystalline material of formula $[Zn_2(\mathbf{29a})_2(phen)_2]\cdot 5dmf$ (**46**). The colourless single crystals of **46** are in a triclinic cell and the crystal structure was solved in space group *P*-1. The unit cell parameters are a = 16.2471(13) Å, b = 19.4535(11) Å and c = 20.9084(13) Å, α = 64.117(4)º, β = 80.915(4)º and γ = 69.740(4)º. Structure solution reveals the formation of a discrete coordination complex comprising two Zn(II) ions, two *alt*-di-*p*-CO_2[4]s **29a** and two phens. It is a head-to-head capsule with the analogous, non-tilted shape. The asymmetric unit contains two half-capsules, each being part of a symmetry unique capsule: first capsule (MOCC1) comprises two Zn(II) ions (Zn(1) and s.e. Zn(1)'), two *alt*-di-*p*-CO_2[4]s (CAL1 and s.e. CAL1') and two phens (one of which is s.e.), while the second capsule (MOCC2) comprises two Zn(II) ions (Zn(2) and s.e. Zn(2)'), two *alt*-di-*p*-CO_2[4]s (CAL2 and s.e. CAL2') and two phens (one of which is s.e.) (Fig 5.7). The first of the *alt*-di-*p*-CO_2[4]s (CAL1) is coordinated to two Zn(II) centres *via* carboxylate groups, both of which are bonded in a monodentate fashion: the O(5)-C(29)-O(6) group is coordinated to Zn(1) *via* O(5) with the bond length of 1.934(5) Å and the O(7)-C(30)-O(8) group to s.e. Zn(1)' *via* O(7) with the bond length of 1.939(6) Å. The second *alt*-di-*p*-CO_2[4] (CAL2) is coordinated to two Zn(II) ions *via* carboxylate groups, both also bonded in a monodentate fashion: the O(13)-C(69)-O(14) group is coordinated to Zn(2) *via* O(13) with the bond length of 1.907(6) Å and the O(15)-C(70)-O(16) group to s.e. Zn(2)' *via* O(15) with the bond length of 1.981(7) Å. As expected both phens are coordinated to Zn(II) ions as a chelate, thereby restricting space around both of the metal centres, with Zn(1)-N(2), Zn(1)-N(2), Zn(2)-N(3) and Zn(2)-N(4) bond lengths of 2.048(9), 2.053(10), 2.078(10) and 2.087(9) Å respectively. The relative orientation of both *alt*-di-*p*-CO_2[4]s forming each capsule results in the discrete complex adopting a shape of a straight / head-to-head dimeric MOCC, rather than tilted as in **45**, as shown in Figure 5.7. The angle found between centroids generated from both calixarene phenolic oxygen atoms and one generated between the two s.e. Zn(II) centres in both capsules was found to be exactly 180˚. Analysis of **46** reveals that both phens are pointing away from the capsule, as observed in **44** and **45**. Both of the *alt*-di-*p*-CO_2[4]s adopt a partially pinched-cone conformation. In CAL1 the distance between diametrical arene *para* carbon atom pairs are 7.80 Å and 8.16 Å respectively.

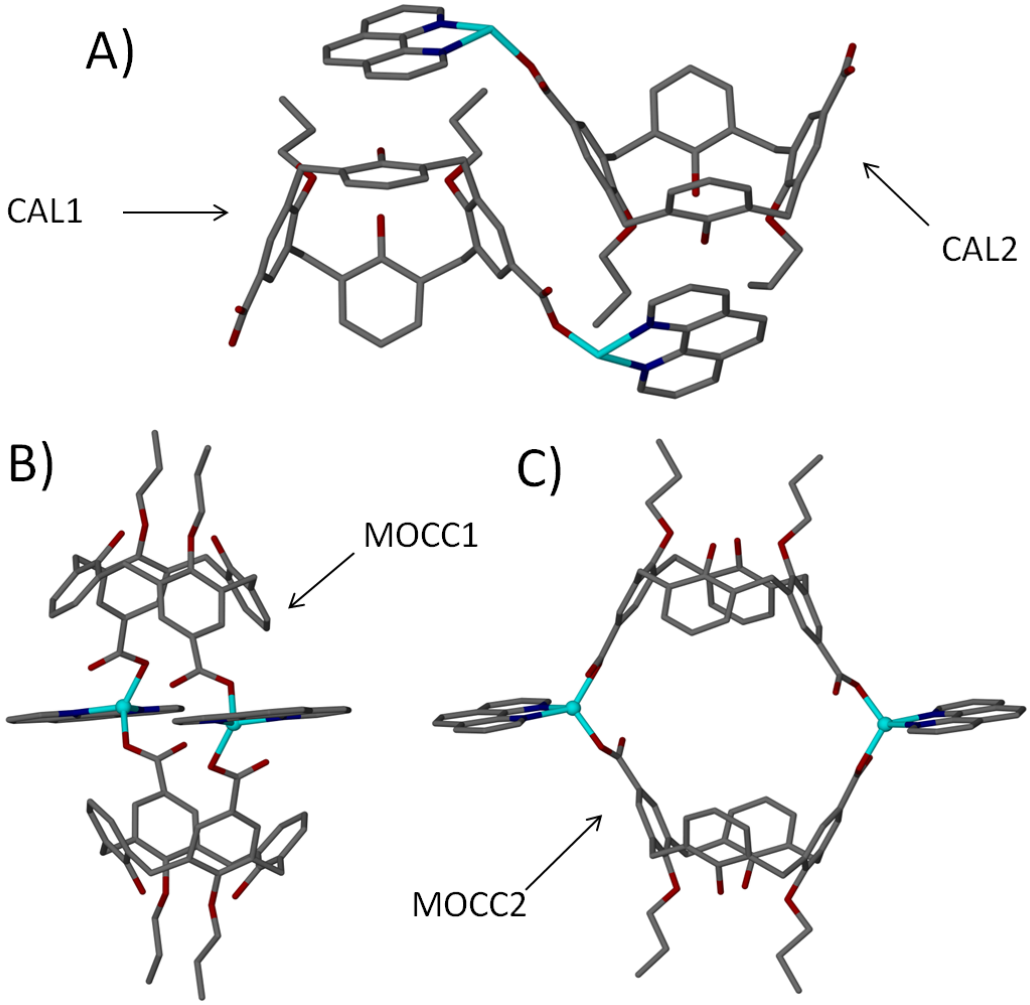

Figure 5.7 (A) Ball and stick representation of the asymmetric unit in **46** showing two symmetry unique half capsules. (B) and (C) Head-to-head dimeric metal-organic calixarene capsules formed in **46**. Hydrogen atoms and dmf of crystallisation omitted for clarity.

In CAL2 the distance between the same pair of carbon atoms is 7.79 Å and 8.46 Å. In CAL1 the angles ε and δ are measured to be 93.9° and 98.9° respectively, whereas in CAL2 these angles are 94.0° and 102.2°. For both CAL1 and CAL2 these parameters differ from those of *alt*-di-*p*-CO_2[4]s in **30** - **43**. The interior of each capsules is occupied by two dmf of crystallisation, however due to both of them being highly disordered, they were removed with the routine SQUEEZE.[74] Nevertheless, it is an interesting feature as in **44** and **45** the interior of the tilted MOCCs was occupied by coordinated dmf and an aquo ligand, whereas in **46** the interior of the MOCC is

occupied by unbound dmf of crystallisation. Further analysis reveals that both phens are involved in π-stacking. The phen coordinated to Zn(1) is involved in π-stacking with 1) a s.e. phen bonded to Zn(1)' from neighbouring MOCC1 (closest contact distance of 3.38 Å) and 2) an aromatic ring of CAL2 from a two neighbouring MOCCs2 (closest contact distance of 3.41 Å), as shown in Figure 5.8A. The second phen which is coordinated to Zn(2) undergoes π-stacking with 1) a s.e. phen bonded to Zn(2)' from a neighbouring MOCC2 (closest contact distance of 3.38 Å) and 2) an aromatic ring of CAL1 from a neighbouring MOCC1 (closest contact distance of 3.28 Å), as shown in Figure 5.8B. Inspection of the solid-state packing in **46** reveals solvent channels present in the crystal running along all three axes of the unit cell, as shown in Figure 5.9. As our interest lies in the design of materials with their potential application for gas storage / absorption we decided to further analyse the synthesised material. Crystalline material was filtered and dried, however PXRD experiments show that the dried material had become amorphous, suggesting that **46** loses crystallinity upon removal from mother liquor / de-solvation.

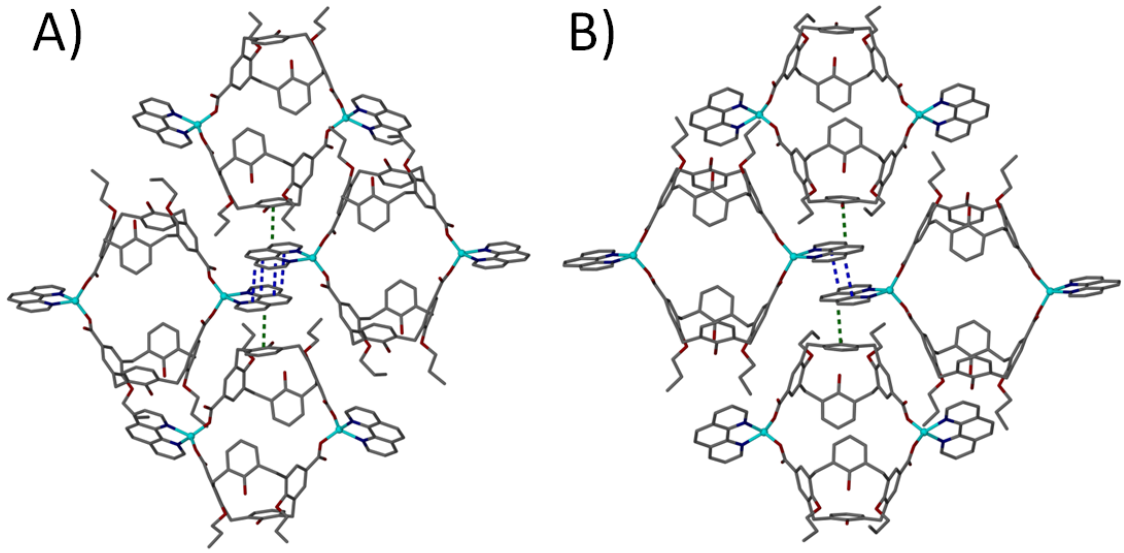

Figure 5.8 Section of the extended structure in **46** showing π-stacking. (A) π-stacking between phen from MOCC1 and 1) a s.e. phen from MOCC1 (blue dashed lines) and 2) calixarene aromatic ring from MOCC2 (green dashed line). (B) π-stacking between phen from MOCC2 and 1) a s.e. phen from MOCC2 (blue dashed lines) and 2) calixarene aromatic ring from MOCC1 (green dashed line). Hydrogen atoms and dmf of crystallisation omitted for clarity.

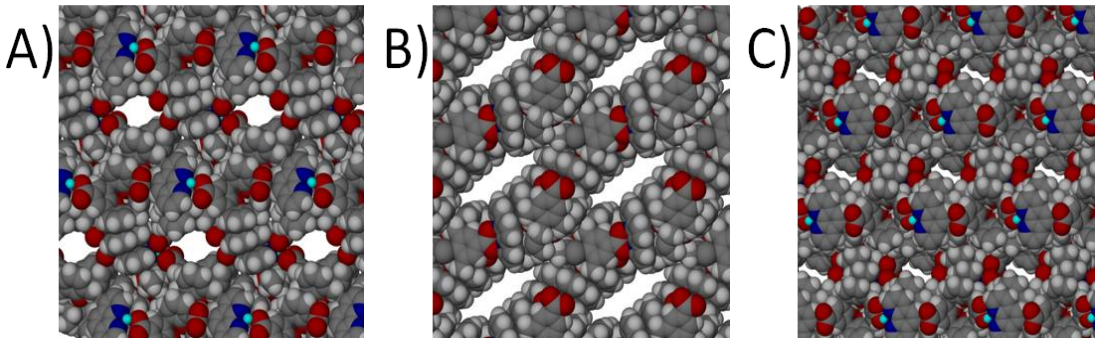

Figure 5.9 Space filling representation of the crystal packing in **46** along (A) *a* axis, (B) *b* axis and (C) *c* axis of the unit cell. Solvent molecules removed for clarity.

Reaction of Zn(II) ions with *alt*-di-*p*-CO_2[4] **29b** and phen, followed by slow evaporation over a period of several weeks afforded crystalline colourless plates of formula [Zn_2(**29b**)$_2$(phen)$_2$]·4dmf (**47**). Crystals of **47** are in a triclinic cell and the crystal structure was solved in space group *P*-1. The unit cell parameters of **47** are *a* = 16.819(2) Å, *b* = 18.499(2) Å and *c* = 20.614(3) Å, α = 93.067(2) º, β = 100.8540(10)º and γ = 112.9180(10)º, and are different to those of **46**. However, solution of the crystal structure reveals formation of head-to-head dimeric MOCCs near-identical to those formed in **46**. The asymmetric unit also contains two half-capsules, each being part of a symmetry unique capsule: first capsule (MOCC1) comprises two Zn(II) ions (Zn(1) and s.e. Zn(1)'), two *alt*-di-*p*-CO_2[4]s (CAL1 and s.e. CAL1') and two phens (one of which is s.e.), while the second capsule (MOCC2) comprises two Zn(II) ions (Zn(2) and s.e. Zn(2)'), two *alt*-di-*p*-CO_2[4]s (CAL2 and s.e. CAL2') and two phens (one of which is s.e.) (Fig 5.10). The *alt*-di-*p*-CO_2[4]s (CAL1) is coordinated to two Zn(II) centres *via* carboxylate groups: the O(5)-C(29)-O(6) group is coordinated to Zn(1) in a bidentate fashion, with respective bond lengths of 2.162(3) and 2.134(3) Å, whilst the O(7)-C(30)-O(8) group is bonded to s.e. Zn(1)' in a monodentate fashion *via* O(8) with the bond length of 1.916(3) Å. The second *alt*-di-*p*-CO_2[4] (CAL2) is also coordinated to two Zn(II) ions *via* carboxylate groups, however both are bonded to the metal centres in a monodentate fashion: the O(15)-C(69)-O(16) group is coordinated to Zn(2) *via* O(16) with the bond length of 1.966(3) Å, and the O(17)-C(70)-O(18) group to s.e. Zn(2)' *via* O(17) with the bond distance of 1.934(3) Å. As expected both phens are coordinated as a chelate, restricting space around both of the metal centres, with Zn(1)-N(2), Zn(1)-N(2), Zn(2)-N(3) and Zn(2)-N(4) bond lengths of 2.103(4), 2.069(3), 2.088(4) and

2.075(5) respectively. The angle between centroids generated from both calixarene phenolic oxygen atoms and one generated between two s.e. Zn(II) centres, in both capsules, was found to be exactly 180˚ (Fig. 5.10). Analysis of **47** reveals that similarly as in **46** both phens are pointing away from the capsule. Structural analysis reveals that both *alt*-di-*p*-CO_2[4]s adopt a partially pinched-cone conformation. In *alt*-di-*p*-CO_2[4] CAL1 the distances between diametrical arene *para* carbon atom pairs are 7.99 Å and 8.28 Å respectively. In *alt*-di-*p*-CO_2[4] CAL2 the distance between the same pairs of carbon atoms is 7.59 Å and 8.10 Å. In *alt*-di-*p*-CO_2[4] CAL1 the angles ε and δ are measured to be 95.9° and 99.6° respectively, whereas in *alt*-di-*p*-CO_2[4] CAL2 these angles are 95.3° and 96.8°. For both of *alt*-di-*p*-CO_2[4]s these parameters are marginally different to those of *alt*-di-*p*-CO_2[4]s in **46**.

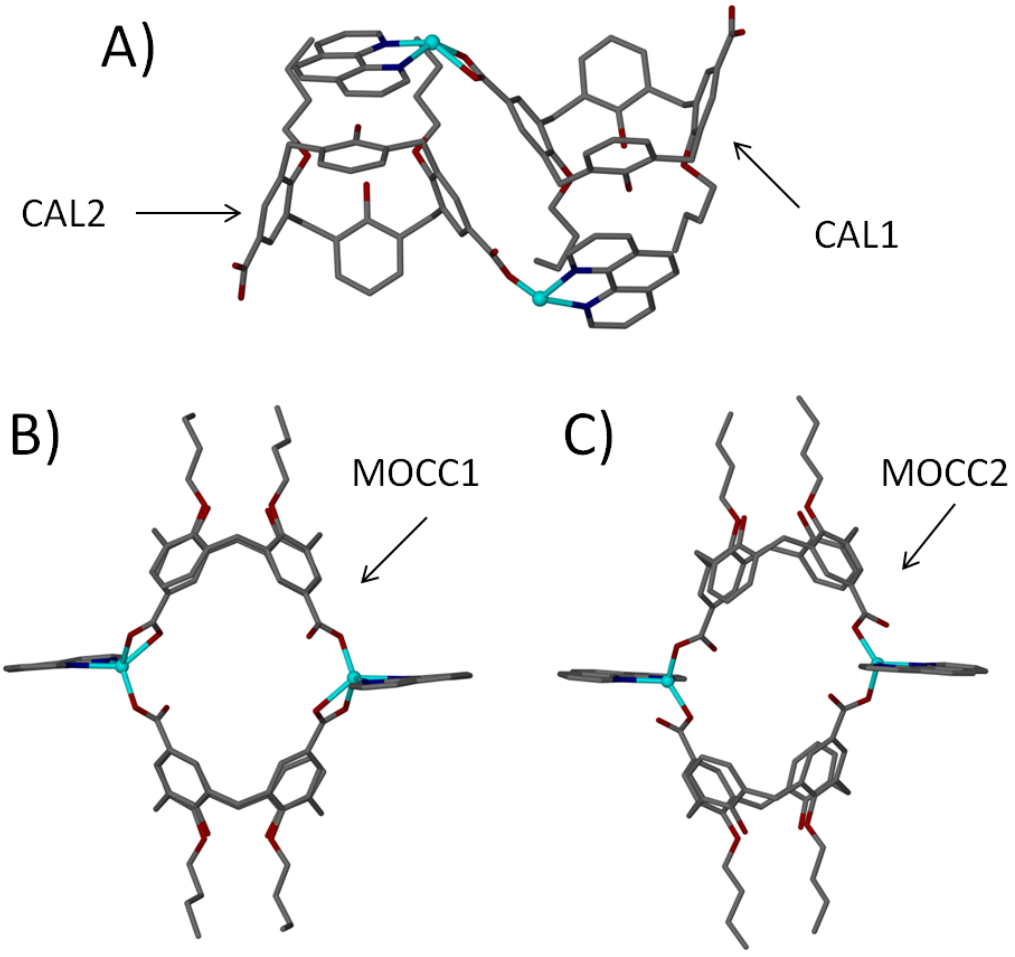

Figure 5.10 (A) Ball and stick representation of the asymmetric unit in **47** showing two symmetry unique half capsules. (B) and (C) Head-to-head dimeric MOCCs formed in **47**. Hydrogen atoms and dmf of crystallisation omitted for clarity.

Each of the *alt*-di-*p*-CO_2[4] cavity is occupied by one dmf of crystallisation. The dmf molecule which resides in the CAL1 cavity also forms CH···π interactions; the distance between three hydrogen atoms of dmf and calixarene aromatic rings range from 2.95 - 2.98 Å (Fig 5.11A). The dmf of crystallisation which resides in the CAL2 cavity also forms CH···π interactions; the distance between three hydrogen atoms of dmf and calixarene aryl rings ranges from 2.98 - 3.02 Å (Fig 5.11B). Further analysis of **47** reveals, that similarly as in **46**, both phens are involved in π-stacking. The phen coordinated to Zn(1) undergoes π-stacking with 1) a s.e. phen bonded to Zn(1)' from a s.e. MOCC1 (closest contact distance of 3.27 Å) and 2) an aromatic ring of CAL2 from neighbouring MOCCs2 (closest contact distance of 3.40 Å), as shown in Figure 5.12A. The second phen which is coordinated to Zn(2) undergoes π-stacking with 1) a s.e. phen bonded to Zn(2)' from MOCC2 (closest contact distance of 3.37 Å) and 2) an aromatic ring of CAL1 from neighbouring MOCCs1 (closest contact distance of 3.32 Å), as shown in Figure 5.12B. Inspection of the solid-state packing in **47** reveals solvent channels running all three axes of the unit cell, a feature that is observed in **46** (Fig. 5.13). The dmf of crystallisation occupying these channels due to being highly disordered, was removed with the routine SQUEEZE.[74]

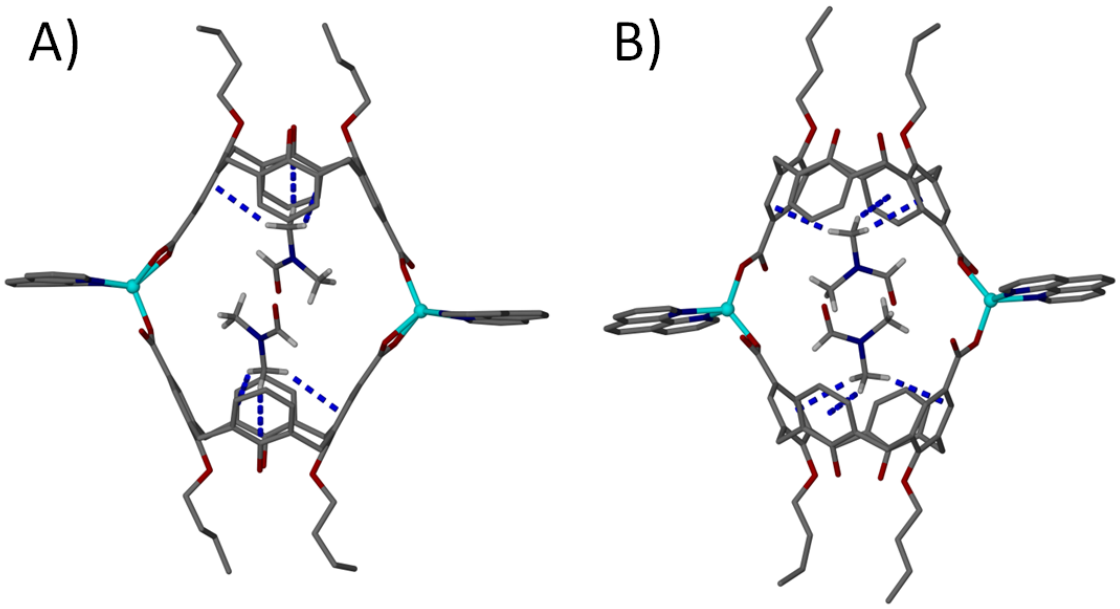

Figure 5.11 Head-to-head dimeric MOCCs formed in **47** encapsulating two dmf of crystallisation. Host-guest CH···π interactions (blue dashed lines) between the dmf of crystallisation and the interior of calixarene cavity in (A) MOCC1 and (B) MOCC2. Hydrogen atoms except those of dmf are omitted for clarity.

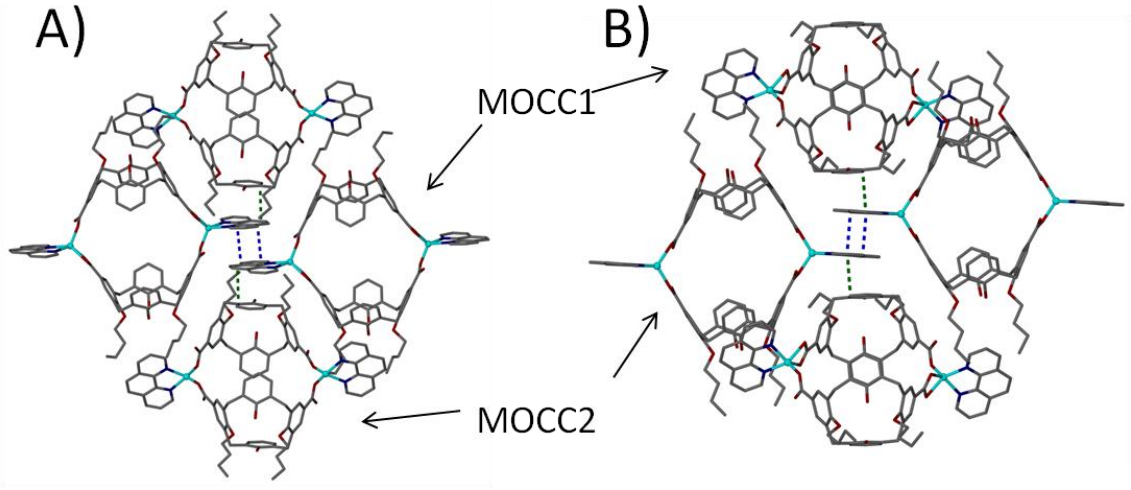

Figure 5.12 Section of the extended structure in **47** showing π-stacking. (A) π-stacking between phen from MOCC1 and 1) a s.e. phen from MOCC1 (blue dashed lines) and 2) calixarene aromatic rings from MOCC2 (green dashed line). (B) π-stacking between phen from MOCC2 and 1) a s.e. phen from MOCC2 (blue dashed lines) and 2) calixarene aromatic rings from MOCC1 (green dashed line). Hydrogen atoms and dmf of crystallisation omitted for clarity.

Given our interest in design of materials with their potential application for gas storage / absorption we decided to further analyse the synthesised material. Crystalline material was filtered and dried, however PXRD experiments show that the dried material had become amorphous, suggesting that **47** loses crystallinity upon removal from mother liquor / de-solvation.

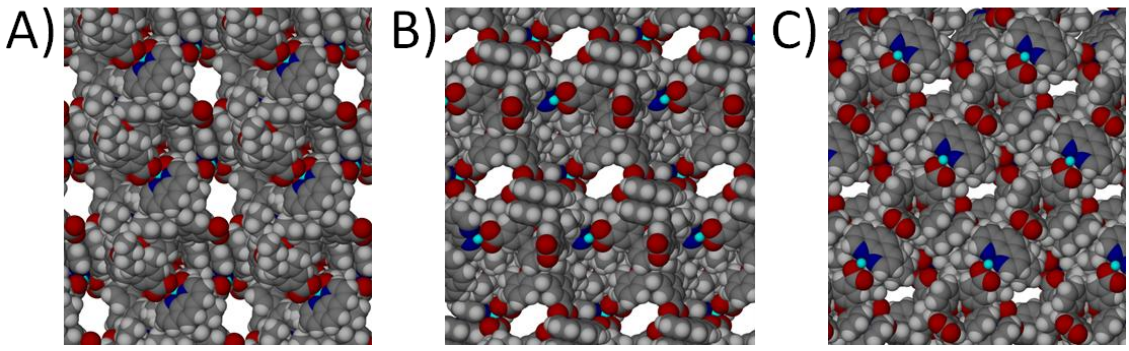

Figure 5.13 Space filling representation of the crystal packing in **47** along (A) *a* axis, (B) *b* axis and (C) *c* axis of the unit cell. Solvent molecules removed for clarity.

In the previous chapter it has been shown that *alt*-di-*p*-CO_2[4]s **29a - b** can be utilised to construct 1-D spiral CP. However, in section 5.1 it was demonstrated that by changing the TM(II) ions to Cd(II), the same reaction procedure that was used to synthesise spiral CPs can be utilised to construct tilted dimeric MOCCs instead. Furthermore, by changing in the synthesis the TM(II) ion from Cd(II) to Zn(II) it is possible to invoke changes to the coordination sphere which result in formation of a head-to-head dimeric MOCC. In Chapter 3 and 4 it was discussed how with the means of synthetic pre-organisation of the calixarene framework one can induce the shape of the assembled supramolecular structures and the solid-state packing. Now it has been demonstrated that by carefully selecting a TM(II) ion and reacting it with a specific *alt*-di-*p*-CO_2[4]s **29a - b** it is possible to synthesise materials exhibiting markedly different topological features.

5.3. Fine-tuning self-assembly using phen derivatives

In previous chapters it was shown that the use of phen derivatives instead of phen can affect the outcome of the assembly and the solid-state packing. In addition, the influence of phen and its derivatives on the assembly can be further emphasised by the markedly different structural features exhibited by **37** and **38** vs **46** and **47**, whereby the same reaction procedure but using 2-me-phen or phen results in formation of either spiral CPs or head-to-head dimeric MOCCs. Considering the differences in the structural features exhibited by some of the synthesised materials are dependent on the phen-based co-ligand used, it was decided to further study the influence of various methyl-substituted phens on assembly and the solid-state packing. Reaction of Cd(II) ions with *alt*-di-*p*-CO_2[4] **29b** and 2-me-phen, followed by slow evaporation, yielded crystalline material of formula $[Cd_2(\mathbf{29b})_2(\text{2-me-phen})_2]\cdot 5\text{dmf}$ (**48**).[88] Crystals of **48** are in a triclinic cell and the crystal structure was solved in space group *P*-1. The unit cell parameters of **48** are a = 17.4037(6) Å, b = 18.8062(7) Å and c = 21.2318(7) Å, α = 89.389(2) º, β = 73.509(2)º and γ = 65.333(2)º, and are different to those of **44 - 47**. However, structural analysis reveals formation of a head-to-head dimeric MOCC almost identical to those formed in **46** and **47**, rather than a tilted MOCC as observed in **44** and **45**, which were synthesised using Cd(II) ions. The asymmetric unit in **48**, same as in **46** and **47**, contains two half-capsules, each being part of a symmetry unique capsule: first

capsule (MOCC1) comprises two Cd(II) ions (Cd(1) and s.e. Cd(1)'), two *alt*-di-*p*-CO_2[4]s (CAL1 and s.e. CAL1') and two 2-me-phens (one of which is s.e.), while the second capsule (MOCC2) comprises two Cd(II) ions (Cd(2) and s.e. Cd(2)'), two *alt*-di-*p*-CO_2[4]s (CAL2 and s.e. CAL2') and two 2-me-phens (one of which is s.e.) (Fig 5.14). The asymmetric unit also contains five dmf of crystallisation. The *alt*-di-*p*-CO_2[4]s (CAL1) are coordinated to two Cd(II) ions *via* carboxylate groups, both of which are coordinated to the metal centre in a bidentate fashion: the O(5)-C(29)-O(6) group is coordinated to Cd(1), with respective bond lengths of 2.257(2) and 2.415(2) Å, and the O(7)-C(30)-O(8) group to s.e. Cd(1)', with respective bond lengths of 2.356(2) and 2.302(2) Å. The second *alt*-di-*p*-CO_2[4] (CAL2) is also coordinated to two Cd(II) ions *via* carboxylate groups, both of which are also bonded to the metal centres in a bidentate fashion: the O(15)-C(69)-O(16) group is coordinated to Cd(2), with respective bond lengths of 2.330(3) and 2.319(3) Å, and the O(17)-C(70)-O(18) group to s.e. Cd(2)', with respective bond lengths of 2.343(3) and 2.322(2) Å.

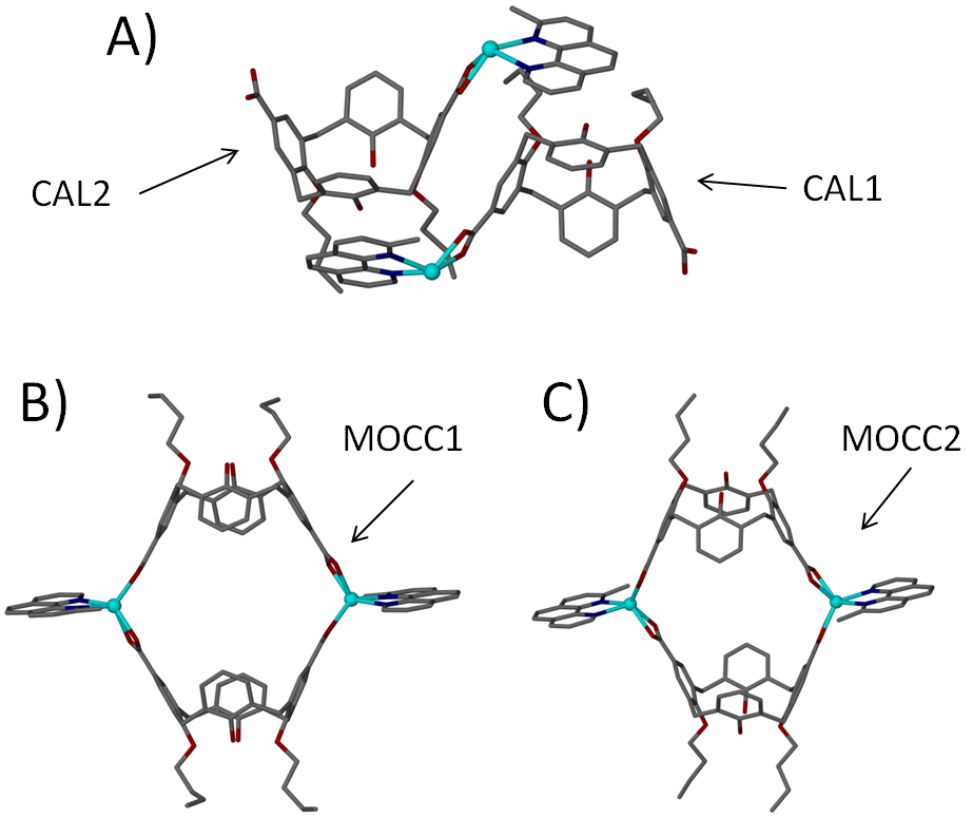

Figure 5.14 (A) Ball and stick representation of the asymmetric unit in **48** showing two symmetry unique half capsules. (B) and (C) Head-to-head dimeric MOCCs formed in **48**. Hydrogen atoms and dmf of crystallisation omitted for clarity.

This bonding mode of carboxylates to the metal centre is different to that observed in **44** and **45**, in which one of the *alt*-di-*p*-CO_2[4]s was coordinated to the metal centre *via* carboxylate groups in a monodentate fashion. Furthermore, in **48** none of the coordination spheres possess bonded solvent molecules, as opposed to **44** and **45,** in which an aquo ligand or a dmf molecule is coordinated to each of the metal centres. As expected both 2-me-phens are coordinated to Cd(II) ions as a chelate, thereby restricting space around both of the metal centres. Due to disorder in the structure, the 2-me-phen which is coordinated to Cd(1) was modelled over two positions at 75% and 25% occupancy, whilst in the second 2-me-phen which is coordinated to Cd(2), only the methyl group at 2-position required modelling over two positions at half occupancy. Resulting Cd(1)-N(1), Cd(1)-N(2), Cd(1)-N(3), Cd(1)-N(4), Cd(2)-N(5) and Cd(2)-N(6) bond distances are 2.266(3), 2.320(4), 2.330(8), 2.346(9), 2.328(4) and 2.299(4) Å respectively. The angle found between centroids generated from both calixarene phenolic oxygen atoms and one generated between two s.e. Cd(II) centres in both capsules was found to be exactly 180˚. Analysis of **48** reveals that both 2-me-phens are pointing away from the capsule, a feature observed in already discussed MOCCs. Structural analysis reveals that both *alt*-di-*p*-CO_2[4]s adopt a partially pinched-cone conformation. In *alt*-di-*p*-CO_2[4] CAL1 the distance between diametrical arene *para* carbon atom pairs is 7.93 Å and 8.27 Å respectively. In *alt*-di-*p*-CO_2[4] CAL2 the distance between the same pair of *para* carbon atoms is 7.66 Å and 8.75 Å. In *alt*-di-*p*-CO_2[4] CAL1 the angle ε and δ are measured to be 95.0° and 99.0° respectively, whereas in *alt*-di-*p*-CO_2[4] CAL2 these angles are 92.8° and 105.7°. For both of *alt*-di-*p*-CO_2[4]s these parameters are marginally different to those of *alt*-di-*p*-CO_2[4]s in **46** and **47**, however they are markedly different to those of **44** and **45**, in which tilted MOCCs are formed. Similarly, as in previously discussed head-to-head MOCCs the solvent molecules occupying the interior of the capsule are uncoordinated. Each of the *alt*-di-*p*-CO_2[4] cavity resides one dmf of crystallisation, however due to being highly disordered, they were removed with routine SQUEEZE.[74] Further analysis of **48** reveals that both 2-me-phens are involved in π-stacking, a feature observed in **46** and **47**. The 2-me-phen coordinated to Cd(1) undergoes π-stacking with 1) a s.e. 2-me-phen bonded to Cd(1)' from a neighbouring MOCC1 (closest contact distance of 3.29 Å) and 2) an aromatic ring of CAL2 from a neighbouring MOCC2 (closest contact distance of 3.37 Å), as shown in Figure 5.15A. The second 2-me-phen, which is coordinated to Cd(2), is also involved in π-stacking with 1) a s.e. 2-me-phen bonded to Cd(2)' from a

neighbouring MOCC2 (closest contact distance of 3.41 Å) and 2) an aromatic ring of CAL1 from a neighbouring MOCC1 (closest contact distance of 3.30 Å), as shown in Figure 5.15B. Analysis of the solid-state packing in **48** reveals solvent channels running along all three axes of the unit cell, a feature similar to that observed in **46** and **47**, as shown in Figure 5.16. As in the case of dmf molecules residing in calixarene cavity, the dmf of crystallisation occupying solvent channels, due to being highly disordered, was also removed with the routine SQUEEZE.[74] Structural analysis of **48** shows that the coordination spheres, shape of the formed capsules and the solid-state packing are almost identical to those of **46** and **47**, rather than **44** and **45**. The use of a more bulky 2-me-phen instead of phen has an effect on the rearrangements in the coordination sphere, and as a consequence on the overall shape of the formed capsule and solid-state packing. Considering our interest in design of materials with their potential application for gas storage / absorption we decided to further analyse the synthesised material. However, attempts to attain a homogeneous crystalline product of **48** did not succeed and further analysis was not carried out.

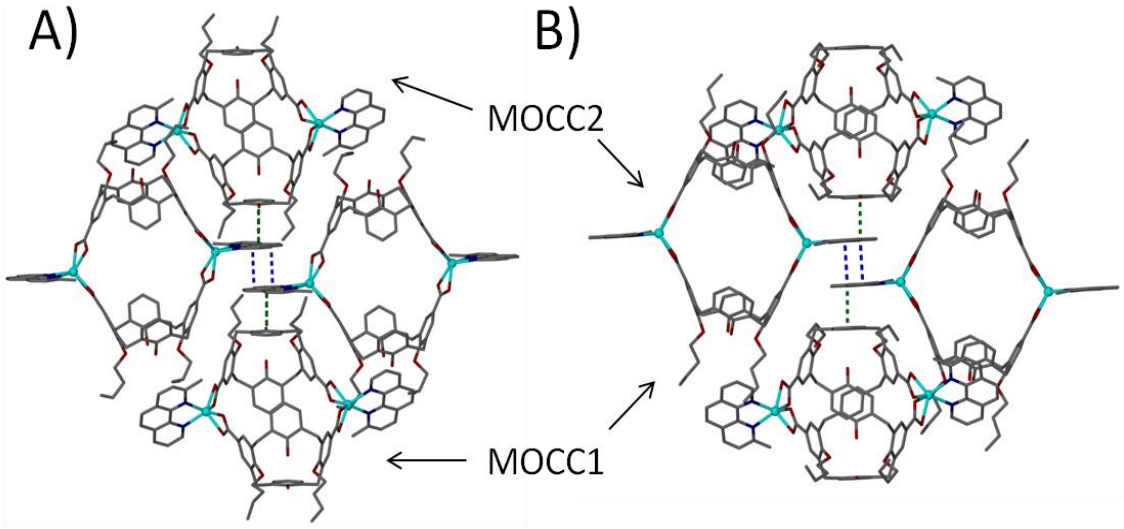

Figure 5.15 Section of the extended structure in **48** showing π-stacking. (A) π-stacking between 2-me-phens from MOCC1 and 1) a s.e. 2-me-phen from MOCC1 (blue dashed lines) and 2) calixarene aromatic rings from MOCC2 (green dashed line) and (B) π-stacking between 2-me-phens from MOCC2 and 1) a s.e. 2-me-phen from MOCC2 (blue dashed lines) and 2) calixarene aromatic rings from MOCC1 (green dashed line). Hydrogen atoms and dmf of crystallisation omitted for clarity.

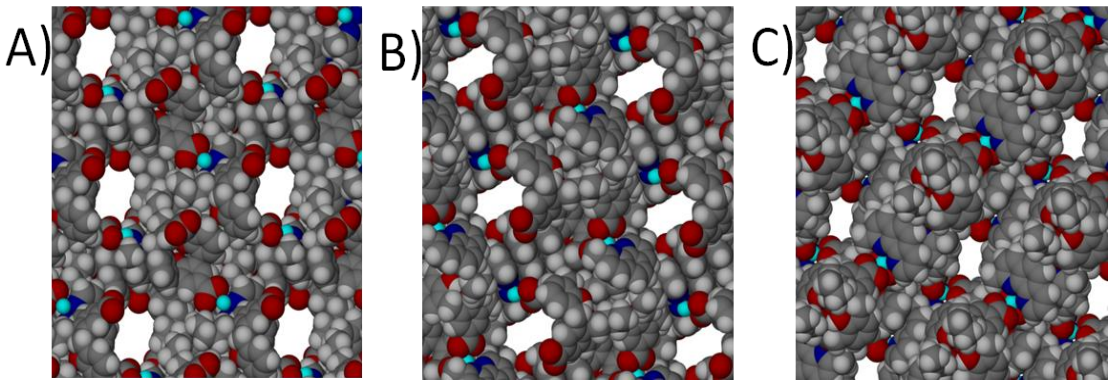

Figure 5.16 Space filling representation of the crystal packing in **48** along (A) *a* axis, (B) *b* axis and (C) *c* axis of the unit cell. Solvent molecules removed for clarity.

Reaction of Zn(II) ions with *alt*-di-*p*-CO_2[4] **29b** and t-me-phen, followed by slow evaporation over a period of several weeks afforded crystalline material of formula [Zn_2(**29b**)$_2$(t-me-phen)$_2$]·10dmf (**49**). Crystals of **49** are in a triclinic cell and the crystal structure was solved in space group *P*-1. The unit cell parameters of **48** are a = 17.75(2) Å, b = 19.60(2) Å and c = 21.227(19) Å, α = 78.88(4)º, β = 68.37(3)º and γ = 63.67(4)º, and are different to those of **46** and **47**. However, structural analysis reveals formation of a head-to-head dimeric MOCC almost identical to those formed in **46** and **47**. The asymmetric unit in **49**, same as in **46** - **48**, contains two half-capsules, each being part of a symmetry unique capsule: first capsule (MOCC1) comprises two Zn(II) ions (Zn(1) and s.e. Zn(1')), two *alt*-di-*p*-CO_2[4]s (CAL1 and s.e. CAL1') and two t-me-phens (one of which is s.e.), while the second capsule (MOCC2) comprises two Zn(II) ions (Zn(2) and s.e. Zn(2')), two *alt*-di-*p*-CO_2[4]s (CAL2 and s.e. CAL2') and two t-me-phens (one of which is s.e.) (Fig 5.17). The asymmetric unit also contains ten dmf of crystallisation, eight of which due to being highly disordered were removed with routine SQUEEZE.[74] The *alt*-di-*p*-CO_2[4]s (CAL1) is coordinated to two Zn(II) ions *via* carboxylate groups, both of which are coordinated to the metal centre in a monodentate fashion: the O(5)-C(29)-O(6) group is coordinated to Zn(1) *via* O(5) with the bond length of 1.934(5) Å, and the O(7)-C(30)-O(8) group to s.e. Zn(1)' *via* O(7) with the bond length 2.021(5) Å. The second *alt*-di-*p*-CO_2[4] (CAL2) which forms MOCC2 is also coordinated to two Zn(II) ions *via* carboxylate groups, both of which are also

bonded in a monodentate fashion: the O(13)-C(69)-O(14) group is coordinated to Zn(2) *via* O(13), with the bond length of 1.955(5) Å, and the O(15)-C(70)-O(16) group to s.e. Cd(2)' *via* O(15), with the bond length of 1.929(5) Å. This bonding mode of carboxylates to the metal centres is the same to that observed in **46** and **47**. As expected both t-me-phens are coordinated to Zn(II) ions as a chelate, thereby restricting space around both of the metal centres. Resulting Zn(1)-N(1), Zn(1)-N(2), Zn(2)-N(3) and Zn(2)-N(4) bond distances are 2.068(7), 2.110(7), 2.068(6) and 2.086(6) Å respectively. The angle found between centroids generated from both calixarene phenolic oxygen atoms and one generated between two s.e. Cd(II) centres in both capsules was found to be exactly 180˚. Analysis of **49** reveals that both t-me-phens are pointing away from the capsule, a feature observed in already discussed MOCCs. Structural analysis reveals that both *alt*-di-*p*-CO_2[4]s adopt a partially pinched-cone conformation. In *alt*-di-*p*-CO_2[4] CAL1 the distance between diametrical arene *para* carbon atom pairs is 7.87 Å and 8.22 Å respectively.

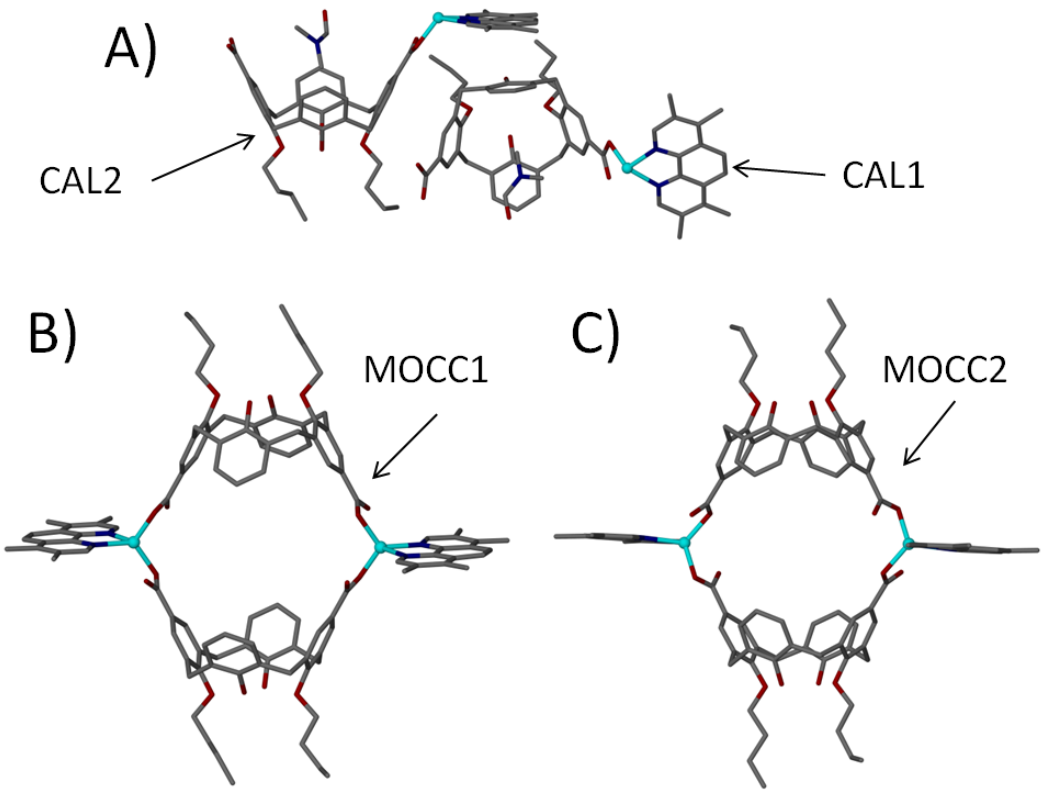

Figure 5.17 (A) Ball and stick representation of the asymmetric unit in **49** showing two symmetry unique half capsules. (B)and (C) Head-to-head dimeric MOCCs formed in **49**. Hydrogen atoms and dmf of crystallisation omitted for clarity.

In *alt*-di-*p*-CO_2[4] CAL2 the distances between the same pair of *para* carbon atoms are 7.97 Å and 8.15 Å. In *alt*-di-*p*-CO_2[4] CAL1 the angle ε and δ are measured to be 95.2° and 99.2° respectively, whereas in *alt*-di-*p*-CO_2[4] CAL2 these angles are 96.1° and 97.7°. For both CAL1 and CAL2 these parameters are consistent with those of *alt*-di-*p*-CO_2[4]s in **46** and **47**. Similarly, as in previously discussed head-to-head MOCCs the solvent molecules occupying the interior of the capsule are uncoordinated, with one dmf of crystallisation residing in each *alt*-di-*p*-CO_2[4] cavity. The dmf of crystallisation which resides in the CAL1 cavity forms CH···π interactions; the distance between three hydrogen atoms of dmf and the calixarene aromatic ring ranges from 2.80 - 2.92 Å (Fig 5.18A). Similarly, the dmf molecule residing in CAL2 cavity also forms CH···π interactions; the distance between three hydrogen dmf and calixarene aryl rings ranges from 2.69 - 2.87 Å (Fig 5.18B). Further analysis of **49** reveals that both t-me-phens are involved π-stacking interactions, a feature observed in **46** - **47**. The t-me-phen coordinated to Zn(1) undergoes π-stacking with 1) a s.e. t-me-phen bonded to Zn(1)' from a neighbouring MOCC1 (closest contact distance of 3.41 Å) and 2) an aromatic ring of CAL2 from a neighbouring MOCC2 (closest contact distance of 3.32 Å), as shown in Figure 5.19A.

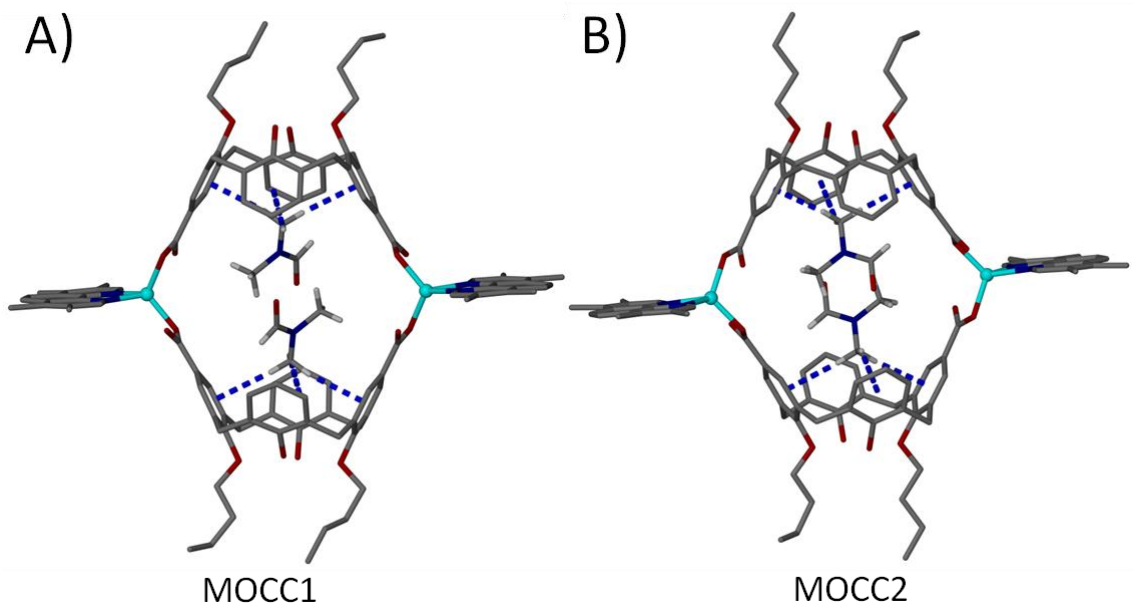

Figure 5.18 Views of the head-to-head dimeric MOCCs found in **49**, containing two dmf of crystallisation. Host-guest CH···π interactions (blue dashed lines) between the dmf of crystallisation and the interior of calixarene cavity in (A) MOCC1 and (B) MOCC2. Hydrogen atoms except those of dmf are omitted for clarity.

The second t-me-phen, which is coordinated to Zn(2), is also involved in π-stacking with 1) a s.e. t-me-phen bonded to Zn(2)' from a s.e. MOCC2 (closest contact distance of 3.40 Å) and 2) an aromatic ring of CAL1 from a neighbouring MOCC1 (closest contact distance of 3.38 Å), as shown in Figure 5.19B. Analysis of the solid-state packing in **49** shows that there are solvent channels running along all three axes of the unit cell, a feature similar to that observed in **46** - **48** , as shown in Figure 5.20. The dmf of crystallisation occupying solvent channels, due to being highly disordered, was removed with routine SQUEEZE.[74] Given our interest in design of materials with their potential application for gas storage / absorption we decided to further analyse the synthesised material. Crystalline material was filtered and dried, however PXRD experiments show that the dried material had become amorphous, suggesting that **49** loses crystallinity upon removal from mother liquor / de-solvation.

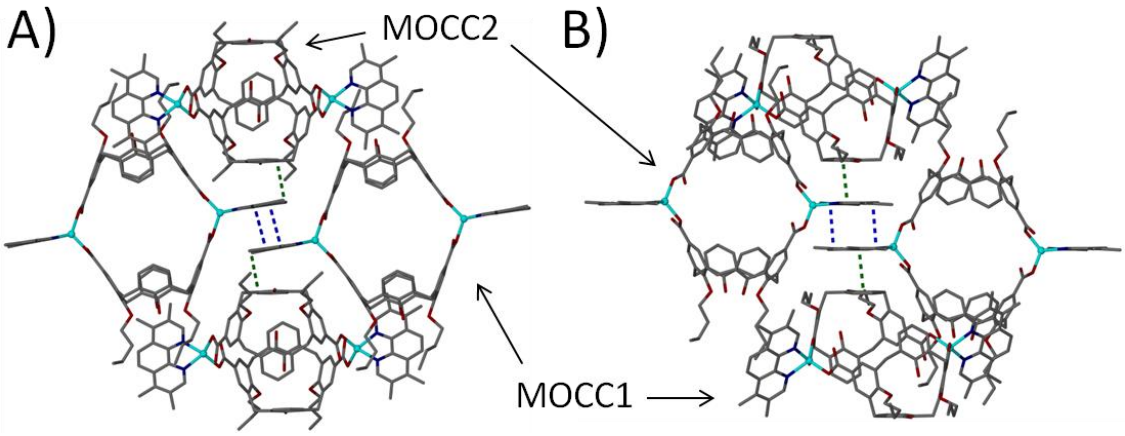

Figure 5.19 Section of the extended structure in **49** showing π-stacking. (A) π-stacking between t-me-phen from MOCC1 and 1) a s.e. t-me-phen from MOCC1 (blue dashed lines) and 2) calixarene aromatic rings from MOCC2 (green dashed line) and (B) π-stacking between t-me-phen from MOCC2 and 1) a s.e. t-me-phen from MOCC2 (blue dashed lines) and 2) calixarene aromatic rings from MOCC1 (green dashed line). Hydrogen atoms and dmf of crystallisation omitted for clarity.

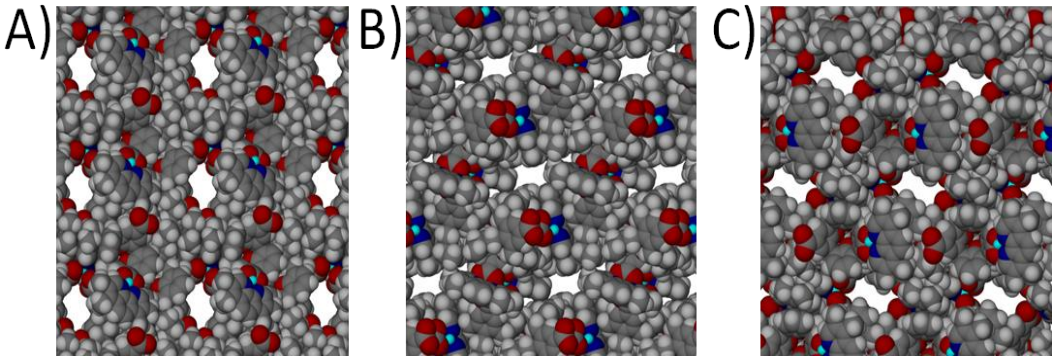

Figure 5.20 Space filling representation of the crystal packing in **49** along (A) *a* axis, (B) *b* axis and (C) *c* axis of the unit cell. Solvent molecules removed for clarity.

The reaction of Zn(II) ions with *alt*-di-*p*-CO_2[4] **29a** and t-me-phen yielded inhomogeneous mixture containing very small crystalline blocks, which were found to be weakly diffracting; this enabled only partial crystal structure solution. Although the unit cell parameters of differ from those of **44** - **49**, inspection of the crystal structure reveals formation on a head-to-head MOCC almost identical to that observed in **49**.

Reaction of Cd(II) ions with *alt*-di-*p*-CO_2[4] **29b** and t-me-phen, followed by slow evaporation a period of several weeks, afforded crystalline material of formula [Cd_2(**29b**)$_2$(t-me-phen)$_2$]·7dmf (**50**).[88] Crystals of **50** are in a triclinic cell and the crystal structure was solved in space group *P*-1. The unit cell parameters of **50** are a = 17.7359(10) Å, b = 19.8660(15) Å and c = 21.1162(12) Å, α = 79.620(5)º, β = 74.012(3)º and γ = 63.599(3)º, and are different to those of **44** - **49**. However, structural analysis reveals formation of a head-to-head dimeric MOCC almost identical to that formed in **49**. The asymmetric unit in **50**, same as in **46** - **49**, contains two half-capsules, each being part of a symmetry unique capsule: first capsule (MOCC1) comprises two Cd(II) ions (Cd(1) and s.e. Cd(1)'), two *alt*-di-*p*-CO_2[4]s (CAL1 and s.e. CAL1') and two t-me-phens (one of which is s.e.), while the second capsule (MOCC2) comprises two Cd(II) ions (Cd(2) and s.e. Cd(2)'), two *alt*-di-*p*-CO_2[4]s (CAL2 and s.e. CAL2') and two t-me-phens (one of which is s.e.) (Fig 5.21). The asymmetric unit also contains seven dmf of crystallisation, five of which due to being highly disordered were removed with routine SQUEEZE.[74] The *alt*-di-*p*-CO_2[4]s (CAL1) is coordinated to two Cd(II) ions *via* carboxylate groups, both of which are bonded to the metal centre in

a bidentate fashion: the O(5)-C(29)-O(6) group is coordinated to Cd(1), with respective bond lengths of 2.390(2) and 2.271(2) Å, and the O(7)-C(30)-O(8) group to s.e. Cd(1)' with respective bond lengths of 2.366(3) and 2.274(2) Å. The second *alt*-di-*p*-CO_2[4] (CAL2) is also coordinated to two Cd(II) ions *via* carboxylate groups, both of which are also bonded in a bidentate fashion: the O(13)-C(69)-O(14) group is coordinated to Cd(2) with respective bond lengths of 2.340(2) and 2.311(2) Å, and the O(15)-C(70)-O(16) group to s.e. Cd(2)', with respective bond lengths of 2.316(2) and 2.337(2) Å. This bonding mode of carboxylates to the metal centres is the same to that observed in **49**, but different to that observed in **44** and **45**. As expected both t-me-phens are coordinated to Cd(II) ions as a chelate, thereby restricting space around both of the metal centres. The resulting Cd(1)-N(100), Cd(1)-N(111), Cd(2)-N(120) and Cd(2)-N(131) bond distances are 2.323(3), 2.276(3), 2.297(3) and 2.311(3) Å respectively.

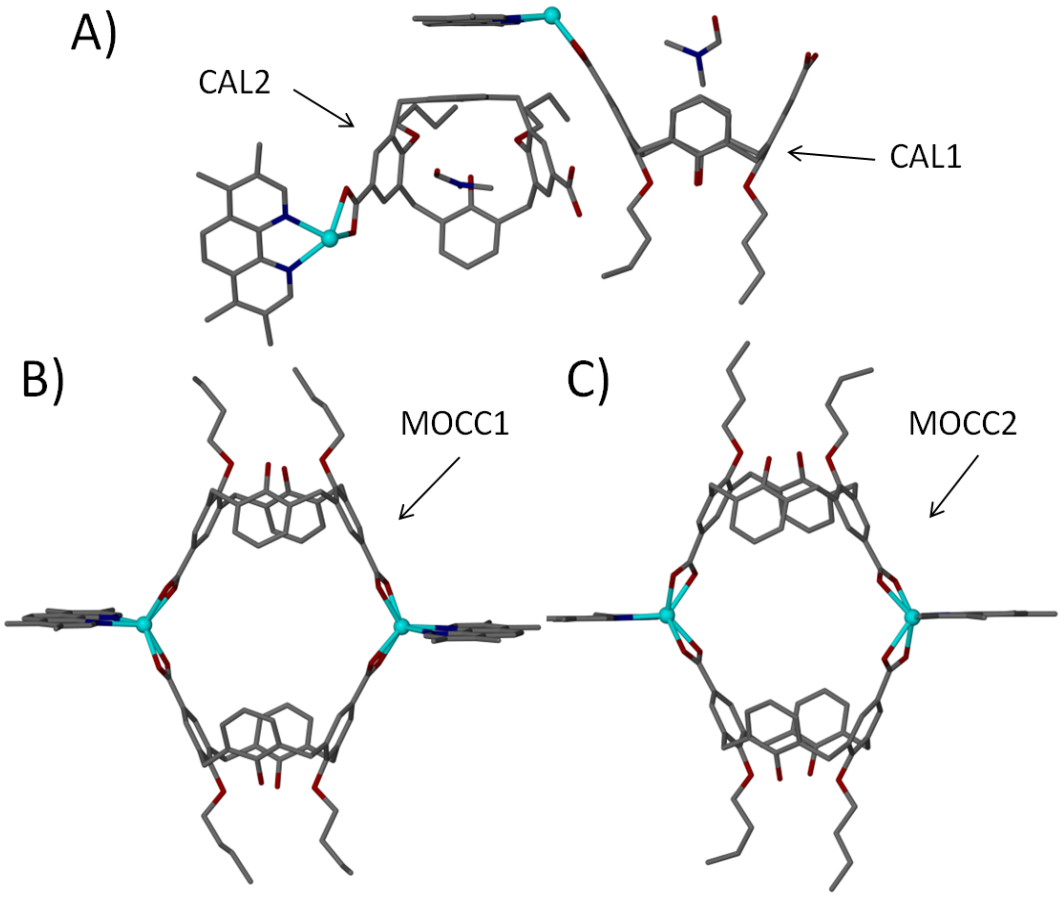

Figure 5.21 (A) Ball and stick representation of the asymmetric unit in **50** showing two symmetry unique half capsules. (B) and (C) Head-to-head dimeric MOCCs formed in **50**. Hydrogen atoms and dmf of crystallisation omitted for clarity.

The angle found between centroids generated from both calixarene phenolic oxygen atoms and one generated between two s.e. Cd(II) centres in both capsules was found to be exactly 180˚. Analysis of **50** reveals that both t-me-phens are pointing away from the capsule, a feature observed in all discussed MOCCs. Structural analysis reveals that both *alt*-di-*p*-CO_2[4]s adopt a partially pinched-cone conformation. In *alt*-di-*p*-CO_2[4] CAL1 the distance between diametrical arene *para* carbon atom pairs is 7.91 Å and 8.20 Å respectively. In *alt*-di-*p*-CO_2[4] CAL2 the distances between the same pair of *para* carbon atoms are 7.99 Å and 8.02 Å. In *alt*-di-*p*-CO_2[4] CAL1 the angles ε and δ are measured to be 95.0° and 98.1° respectively, whereas in *alt*-di-*p*-CO_2[4] CAL2 these angles are 95.5° and 95.7°. For both of *alt*-di-*p*-CO_2[4]s these parameters consistent with those of *alt*-di-*p*-CO_2[4]s in **49**. Similarly as in previously discussed head-to-head MOCCs, the solvent molecules occupying the interior of the capsule are uncoordinated, with one dmf of crystallisation residing in each *alt*-di-*p*-CO_2[4] cavity. In CAL1 the distances between three hydrogen atoms of dmf and calixarene aromatic rings range from 2.77 - 3.10 Å (Fig 5.22A). In CAL2 the distances between two hydrogen atoms of dmf and calixarene aromatic rings are 2.82 Å and 3.03 Å respectively (Fig 5.22B).

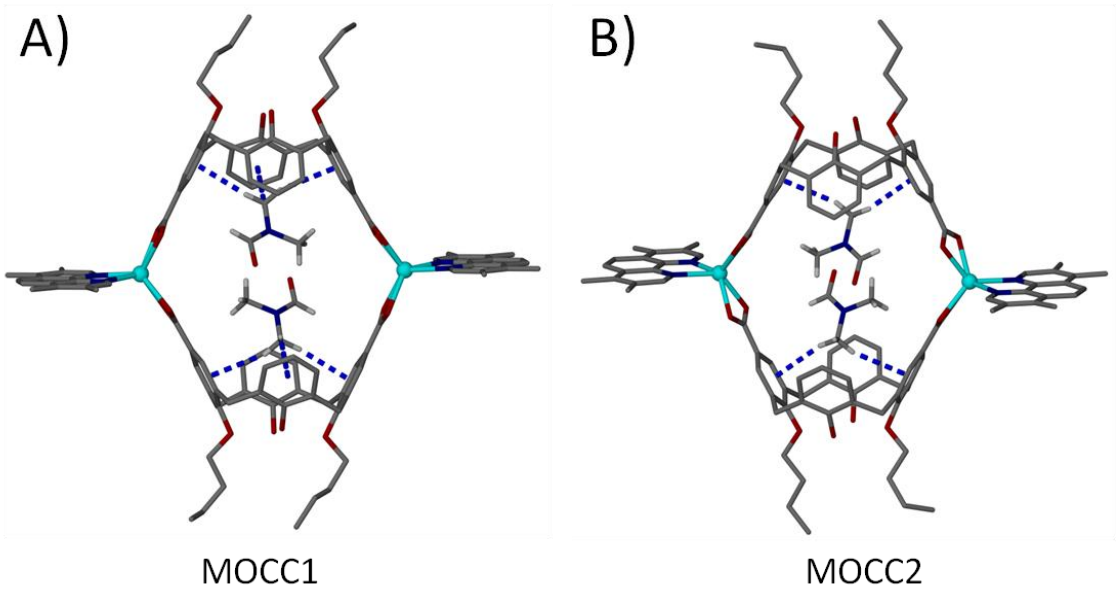

Figure 5.22 Head-to-head dimeric MOCCs found in **50**, containing two dmf of crystallisation. Host-guest CH···π interactions (blue dashed lines) between the dmf of crystallisation and the interior of calixarene cavity in (A) MOCC1 and (B) MOCC2. Hydrogen atoms except those of dmf are omitted for clarity.

Further analysis of **50** reveals that both t-me-phens are involved in π-stacking, a feature observed in **46** - **49**. The t-me-phen coordinated to Cd(1) undergoes π-stacking with 1) a s.e. t-me-phen bonded to Cd(1)' from a s.e. MOCC1 (closest contact distance of 3.39 Å) and 2) an aromatic ring of CAL2 from a neighbouring MOCC2 (closest contact distance of 3.36 Å), as shown in Figure 5.23A. However, the second t-me-phen which is coordinated to Cd(2), undergoes π-stacking with only one of the aromatic rings of CAL1 from a neighbouring MOCC1 (closest contact distance of 3.37 Å), as the distance between s.e. t-me-phen bonded to Cd(2)' is larger than 3.5 Å (Fig. 5.23B). Analysis of the solid-state packing in **50** shows solvent channels running along all three axes of the unit cell, a feature similar to that observed in **46** - **49**, as shown in Figure 5.24. The dmf of crystallisation occupying solvent channels, due to being highly disordered, was removed with routine SQUEEZE.[74] Given our interest in design of materials with their potential application for gas storage / absorption we decided to further analyse the synthesised material. Crystalline material was filtered and dried, however PXRD experiments show that the dried material had become amorphous, suggesting that **50** loses crystallinity upon removal from mother liquor / de-solvation.

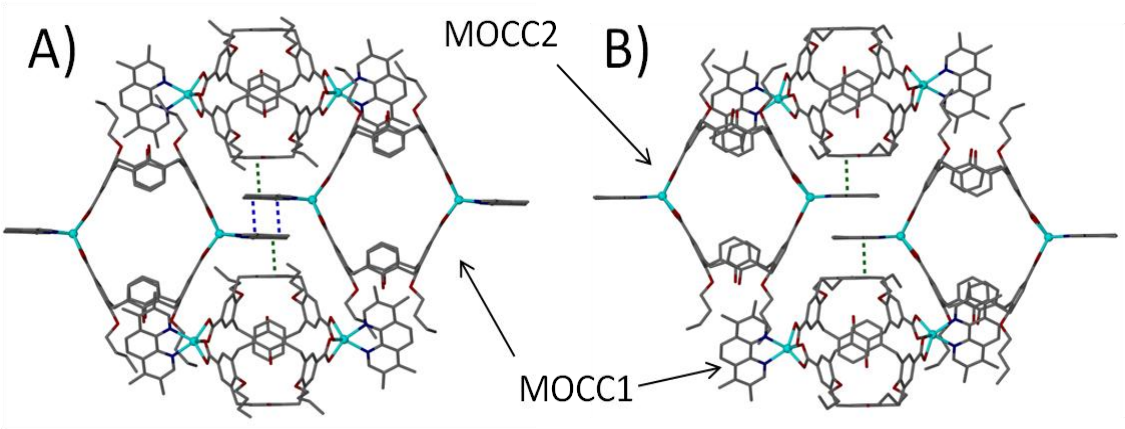

Figure 5.23 Section of the extended structure in **50** showing π-stacking. (A) π-stacking between t-me-phen from MOCC1 and 1) a s.e. t-me-phen from MOCC1 (blue dashed lines) and 2) calixarene aromatic rings from MOCC2 (green dashed line) and (B) π-stacking between t-me-phen from MOCC2 and calixarene aromatic rings from MOCC1 (green dashed line). Hydrogen atoms and dmf of crystallisation omitted for clarity.

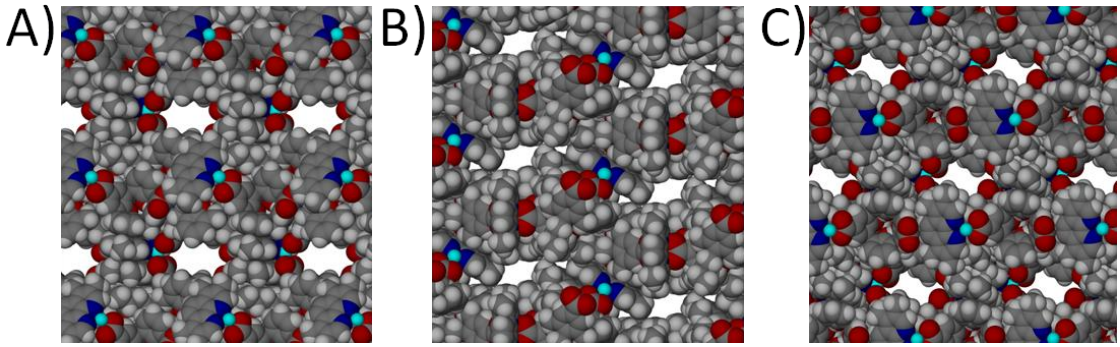

Figure 5.24 Space filling representation of the crystal packing in **50** along (A) *a* axis, (B) *b* axis and (C) *c* axis of the unit cell. Solvent molecules removed for clarity.

In section 5.1 it was shown that the reaction of Cd(II) with *alt*-di-*p*-CO_2[4]s **29a - b** and phen results in a formation of a tilted dimeric MOCC **44** and **45**. However, the use of 2-me-phen or t-me-phen as a co-ligand yielded crystals of **48** and **50** respectively, both containing straight / head-to-head MOCC. This suggests that the use of a co-ligand with a methyl substituent introduced to 2-position or a more bulky t-me-phen results in rearrangements in the coordination sphere, inducing changes to the overall shape of the formed capsule and their solid-state packing. In case of reactions of Zn(II) ions with *alt*-di-*p*-CO_2[4]s **29a - b** and phen, resulting crystals of **46** and **47** contain straight / head-to-head MOCCs. Interestingly, the use of 2-me-phen as a co-ligand also results in rearrangements in the coordination sphere, leading however to formation of spiral 1-D CPs **37** and **38**, as discussed in section 4.3. The use of more bulky t-me-phen yields crystals of **49** containing straight / head-to-head MOCCs, almost identical to those observed in **46 - 48** and **50**. Interestingly, the solid-state packing of straight / head-to-head capsules results in solvent channels running along all three unit cell axes, unfortunately PXRD experiments reveal that dried crystals turn amorphous upon removal from mother liquor / drying.

5.4. Summary

In Chapters 3 and 4 it was shown that, through synthetic pre-organisation of the calixarene framework, one can influence the shape of the assembled supramolecular structures as well as solid-state packing. Here it has been demonstrated that by

carefully selecting a TM(II) ion and reacting it with *alt*-di-*p*-CO_2[4] **29a - b** and phen one can synthesise a discrete capsule rather than a spiral 1-D CP. Differences in the shape of the assembly formed can be attributed to the complementary symmetry of the *alt*-di-*p*-CO_2[4] and certain TM(II) ions employed; it was been found that Ni(II) and Co(II) give spiral CPs **30 - 36** and **39 - 43**, whereas Cd(II) and Zn(II) give discrete MOCCs **44 - 50**.

The study of the influence of phen and its derivatives on the self-assembly has provided further evidence. It has been found that when using *alt*-di-*p*-CO_2[4] as a building block to react with Cd(II) ions and phen, formation of a tilted MOCC is observed (**44** and **45**). However, use of more bulky 2-me-phen or t-me-phen causes rearrangements in the coordination sphere and concomitantly changes the shape of the capsule formed from tilted to straight / head-to-head (**48** and **50**). In Chapter 4 it was shown that reaction of Zn(II) with *alt*-di-*p*-CO_2[4] 2**9a - b** and 2-me-phen results in formation of a spiral CPs (**37** and **38**). However, when using phen or t-me-phen as a co-ligand formation of straight / head-to-head capsule is observed (**46**, **47** and **49**). It has been also found that as a consequence of the difference in the shape of assembled MOCC (tilted vs straight / head-to-head), resulting structures show different solid-state packing. It has been observed that crystals containing straight MOCCs exhibit an increase in the amount of solvent channels running through them compared to those comprising both linear and spiral CPs, and tilted MOCCs. Unfortunately, there has been no observed improvement on the stability towards drying / de-solvation in MOCC-based materials.

5.5. Experimental

General experimental procedures and specifications of analytical instruments used are provided in Chapter 8. The synthesis of *alt*-di-*p*-CO_2[4]s **29a - b** is described in Chapter 4.

5.5.1. Synthesis of compounds 44 - 50

Synthesis of 44: A mixture of **29a** (30.0 mg, 0.05 mmol) and $Cd(NO_3)_2.6H_2O$ (29.6 mg, 0.125 mmol) was dissolved in 2 mL of dmf, followed by layering of 1 ml of a MeOH

solution of 1,10-phenanthroline (9.0 mg, 0.05 mmol). Slow evaporation over several weeks resulted in the formation of colorless crystals suitable for X-ray diffraction studies, which were filtered washed and dried to afford 11.6 mg of solid (24% yield). **EA** calc for $C_{111}H_{121}N_9O_{22}Cd_2$, C, 68.96; H 6.31; N, 6.52%. Found C, 71.51; H, 5.85, N, 4.72%. **IR** ν_{max} 3263 cm^{-1} (OH), 2957 cm^{-1} (C-H), 1659 cm^{-1} (C=O), 1604 cm^{-1} (C-O), 1537 cm^{-1} (C-C), 1376 cm^{-1} (C-H), 742 cm^{-1} (C-H). PXRD analysis revealed that the material becomes amorphous upon removal from the mother liquor / drying, which is consistent with the discrepancy between theoretical and experimental results of elemental analysis.

Synthesis of 45: A mixture of **29b** (31.3 mg, 0.05 mmol) and $Cd(NO_3)_2.6H_2O$ (29.6 mg, 0.125 mmol) was dissolved in 2 mL of dmf, followed by layering of 1 ml of a MeOH solution of 1,10-phenanthroline (9.0 mg, 0.05 mmol). Slow evaporation over several weeks resulted in the formation of pink crystals suitable for X-ray diffraction studies, which were filtered washed and dried to afford 8.5 mg of solid (17% yield). **EA** calc for $C_{109}H_{115}N_7O_{20}Cd_2$, C, 71.03; H 6.29; N, 5.32%. Found C, 72.62; H 6.01; N, 4.43%. **IR** ν_{max} 3255 cm^{-1} (OH), 2944 cm^{-1} and 2891 cm^{-1} (C-H), 1659 cm^{-1} (C=O), 1642 cm^{-1} (C-O), 1561 cm^{-1} (C-C), 1381 cm^{-1} (C-H), 713 cm^{-1} (C-H). PXRD analysis revealed that the material becomes amorphous upon removal from the mother liquor / drying, which is consistent with the discrepancy between theoretical and experimental results of elemental analysis.

Synthesis of 46: A mixture of **29a** (30.0 mg, 0.05 mmol) and $Zn(NO_3)_2.6H_2O$ (37.2 mg, 0.125 mmol) was dissolved in 2 mL of dmf, followed by layering of 1 ml of a MeOH solution of 1,10-phenanthroline (9.0 mg, 0.05 mmol). Slow evaporation over several weeks resulted in the formation of colorless crystals suitable for X-ray diffraction studies, which were filtered washed and dried to afford 7.2 mg of solid (14% yield). **EA** calc for $C_{111}H_{121}N_9O_{22}Zn_2$, C, 65.16; H 5.86; N, 6.16%. Found C, 67.11; H, 5.24, N, 4.25%. **IR** ν_{max} 3222 cm^{-1} (OH), 2960 cm^{-1} (C-H), 1668 cm^{-1} (C=O), 1616 cm^{-1} (C-O), 1528 cm^{-1} (C-C), 1388 cm^{-1} (C-H), 730 cm^{-1} (C-H). PXRD analysis revealed that the material becomes amorphous upon removal from the mother liquor / drying, which is consistent with the discrepancy between theoretical and experimental results of elemental analysis.

Synthesis of 47: A mixture of **29b** (31.3 mg, 0.05 mmol) and $Zn(NO_3)_2.6H_2O$ (37.2 mg, 0.125 mmol) was dissolved in 2 mL of dmf, followed by layering of 1 ml of a MeOH solution of 1,10-phenanthroline (9.0 mg, 0.05 mmol). Slow evaporation over several weeks resulted in the formation of colorless crystals suitable for X-ray diffraction studies, which were filtered washed and dried to afford 5.6 mg of solid (11% yield). **EA** calc for $C_{112}H_{120}N_8O_{20}Zn_2$, C, 66.30; H 5.96; N, 5.52%. Found C, 68.08; H, 5.47, N, 3.84%. **IR** ν_{max} 3185 cm^{-1} (OH), 2933 cm^{-1} (C-H), 1649 cm^{-1} (C=O), 1618 cm^{-1} (C-O), 1534 cm^{-1} (C-C), 1381 cm^{-1} (C-H), 720 cm^{-1} (C-H). PXRD analysis revealed that the material becomes amorphous upon removal from the mother liquor / drying, which is consistent with the discrepancy between theoretical and experimental results of elemental analysis.

Synthesis of 48: A mixture of **29b** (31.3 mg, 0.05 mmol) and $Cd(NO_3)_2.6H_2O$ (29.6 mg, 0.125 mmol) was dissolved in 2 mL of dmf, followed by layering of 1 ml of a MeOH solution of 2-methyl-1,10-phenanthroline (9.7 mg, 0.05 mmol). Slow evaporation over several weeks resulted in the formation of colorless crystals suitable for X-ray diffraction studies, which were filtered washed and dried to afford 7.9 mg of solid (15% yield). **EA** calc for $C_{117}H_{131}N_9O_{21}Cd_2$, C, 63.18; H 5.94; N, 5.67%. Found C, 65.27; H, 5.39, N, 3.50%. **IR** ν_{max} 3137 cm^{-1} (OH), 2949 cm^{-1} (C-H), 1650 cm^{-1} (C=O), 1611 cm^{-1} (C-O), 1538 cm^{-1} (C-C), 1383 cm^{-1} (C-H), 725 cm^{-1} (C-H). Due to inhomogeneity of the product PXRD experiments were not carried out. Discrepancy between theoretical and experimental results of elemental analysis solvent loss upon removal from mother liquor / drying.

Synthesis of 49: A mixture of **29b** (31.3 mg, 0.05 mmol) and $Zn(NO_3)_2.6H_2O$ (37.2 mg, 0.125 mmol) was dissolved in 2 mL of dmf, followed by layering of 1 ml of a MeOH solution of 3,4,7,8-tetra-methyl-1,10-phenanthroline (11.8 mg, 0.05 mmol). Slow evaporation over several weeks resulted in the formation of colourless crystals suitable for X-ray diffraction studies, which were filtered washed and dried to afford 11.6 mg of solid (18% yield). **EA** calc for $C_{138}H_{178}N_{14}O_{26}Zn_2$, C, 64.25; H 6.95; N, 7.60%. Found C, 67.84; H, 6.59, N, 4.91%. **IR** ν_{max} 3151 cm^{-1} (OH), 2963 cm^{-1} (C-H), 1652 cm^{-1} (C=O), 1619 cm^{-1} (C-O), 1540 cm^{-1} (C-C), 1378 cm^{-1} (C-H), 717 cm^{-1} (C-H). PXRD analysis revealed that the material becomes amorphous upon removal from the mother liquor / drying, which is consistent with the discrepancy between theoretical and experimental results of elemental analysis.

Synthesis of 50: A mixture of **29b** (31.3 mg, 0.05 mmol) and $Cd(NO_3)_2.6H_2O$ (29.6 mg, 0.125 mmol) was dissolved in 2 mL of dmf, followed by layering of 1 ml of a MeOH solution of 3,4,7,8-tetra-methyl-1,10-phenanthroline (11.8 mg, 0.05 mmol). Slow evaporation over several weeks resulted in the formation of colourless crystals suitable for X-ray diffraction studies, which were filtered washed and dried to afford 9.8 mg of solid (16% yield). **EA** calc for $C_{129}H_{157}N_{11}O_{23}Cd_2$, C, 63.13; H 6.45; N, 6.28%. Found C, 65.49; H,5.78, N, 4.921%. **IR** ν_{max} 3160 cm^{-1} (OH), 2959 cm^{-1} (C-H), 1677 cm^{-1} (C=O), 1629 cm^{-1} (C-O), 1561 cm^{-1} (C-C), 1360 cm^{-1} (C-H), 722 cm^{-1} (C-H). PXRD analysis revealed that the material becomes amorphous upon removal from the mother liquor / drying, which is consistent with the discrepancy between theoretical and experimental results of elemental analysis.

5.5.2. Crystallographic tables for compounds 44 - 50

Complex number	**44**	**45**	**46**
Formula	$C_{111}H_{121}N_9O_{22}Cd_2$	$C_{107}H_{118}N_6O_{23}Cd_2$	$C_{111}H_{119}N_9O_{21}Zn_2$
***M*r**	1933.25	1856.16	2045.99
Crystal system	*C*2/*c*	$P2_1/n$	*P*-1
Space group	Monoclinic	Monoclinic	Triclinic
T/K	100(2)	100(2)	100(2)
***a* /Å**	19.192(17)	19.2266(10)	16.2471(13)
***b* /Å**	24.95(2)	24.9668(14)	19.4535(11)
***c* /Å**	20.75(2)	20.7082(12)	20.9084(13)
***α* / °**	90.00	90.00	64.117(4)
***β* / °**	97.97(2)	98.402(4)	80.915(4)
***γ* /°**	90.00	90.00	69.740(4)
***U* /Å^3**	9840(16)	4651.2(3)	5577.5(7)
Z	4	4	2
***F*(000)**	4000	4328	1744
D_c / g cm^{-3}	1.307	1.406	0.998
μ / mm^{-1}	0.501	0.510	0.483
$2\Theta_{max}$ / °	54.7	62.4	41.6
Data collected	21576	71151	40784
Unique reflections	13455	24198	11645
R_{int}	0.0977	0.0447	0.0871
Obs data ($I > 2\sigma(I)$)	5437	16915	5683
Parameters	756	1132	994
Restraints	8	16	204
R_1 (observed data)	0.0846	0.0676	0.0873
ωR_2 (all data)	0.2061	0.1969	0.2236
GooF	0.888	1.102	0.912
Max/min residuals [eÅ^3]	0.783 / -1.176	2.036 / -2.874	0.685 / -0.496

Complex number	**47**	**48**
Formula	$C_{112}H_{120}N_0O_{20}Cd_2$	$C_{117}H_{131}N_9O_{21}Cd_2$
***M*r**	2029.00	2224.20
Crystal system	*P*-1	*P*-1
Space group	Triclinic	Triclinic
T/K	100(2)	100(2)
***a* /Å**	16.819(2)	17.4037(6)
***b* /Å**	18.499(2)	18.8062(7)
***c* /Å**	20.614(3)	21.2318(7)
***α* / °**	93.067(2)	89.389(2)
***β* / °**	100.8540(10)	73.509(2)
***γ* /°**	112.9180(10)	65.333(2)
***U* /Å^3**	5744.4(13)	6008.7(4)
Z	2	2
***F*(000)**	1976	2112
D_c / g cm^{-3}	1.088	1.126
μ / mm^{-1}	0.477	0.413
$2\Theta_{max}$ / °	54.5	67.4
Data collected	46598	93166
Unique reflections	24662	36511
R_{int}	0.0503	0.0439
Obs data ($I > 2\sigma(I)$)	13717	25633
Parameters	1164	1232
Restraints	13	51
R_1 (observed data)	0.0805	0.0574
ωR_2 (all data)	0.2276	0.1667
GooF	0.991	0.973
Max/min residuals [eÅ^3]	1.235 / -1.473	1.635 / -1.222

Complex number	**49**	**50**
Formula	$C_{138}H_{178}N_{14}O_{26}Zn_2$	$C_{129}H_{157}N_{11}O_{23}Cd_2$
***M*r**	2579.79	2454.55
Crystal system	*P*-1	*P*-1
Space group	Triclinic	Triclinic
T/K	100(2)	100(2)
***a* /Å**	17.75(2)	17.7359(10)
***b* /Å**	19.60(2)	19.8660(15)
***c* /Å**	21.227(19)	21.1162(12)
***α* / °**	78.88(4)	79.620(5)
***β* / °**	68.37(3)	74.012(3)
***γ* /°**	63.67(4)	63.599(3)
***U* /Å^3**	6150(12)	6392.0(7)
Z	2	2
***F*(000)**	2104	2176
D_c / g cm^{-3}	1.077	1.085
μ / mm^{-1}	0.449	0.390
$2\Theta_{max}$ / °	42.0	56.6
Data collected	38275	96639
Unique reflections	12866	31652
R_{int}	0.0727	0.0539
Obs data ($I > 2\sigma(I)$)	7328	22746
Parameters	1163	1229
Restraints	26	14
R_1 (observed data)	0.0721	0.0705
ωR_2 (all data)	0.1815	0.1915
GooF	0.948	1.017
Max/min residuals [eÅ^3]	1.029/ -1.116	3.447 / -1.074

5.6. References

[1] F. A. Cotton, P. Lei, C. Lin, C. A. Murillo, X. Wang, S.-Y. Yu and Z.-X. Zhang, *J. Am. Chem. Soc.*, **2004**, *126*, 1518.

[2] S. Pasquale, S. Sattin, E. C. Escudero-Adán, M. Martínez-Belmonte and J. de Mendoza, *Nat. Commun.*, **2012**, *3*, 785.

[3] P. P. Cholewa, C. M. Beavers, S. J. Teat and S. J. Dalgarno, *Chem. Commun.*, **2013**, *49*, 3203.

[4] C. A. Hunter and J. K. M. Sanders, *J. Am. Chem. Soc.*, **1990**, *112*, 5525.

[5] A. Spek, *Acta Crystallogr. Sect. D*, **2009**, *65*, 148.

[6] P. P. Cholewa, C. M. Beavers, S. J. Teat and S. J. Dalgarno, *Cryst. Growth Des.*, **2013**, *13*, 5165.

Chapter 6. Extension of the connectivity between calixarene-based coordination polymers

In the previous three chapters it was shown that di-*p*-carboxylatocalix[4]arenes can be utilised to construct a series of different supramolecular assemblies. It was also shown that di-*O*-alkoxy-calix[4]arene C_2 symmetry enables selective synthesis of a desired di-topic linker (**16a - b** or **29a – b**), which can then be used to synthesise either linear or spiral 1-D CPs. Furthermore, it became evident that some TM(II) ions form discrete MOCCs rather than spiral 1-D CPs when reacted with *alt*-di-*p*-CO_2[4] **29a - b** and phen (or its derivatives). Structural analysis of the materials synthesised reveals different amounts of solvent in the crystals; this varies from almost no solvent (**17** and **20**) to channels running in all dimensions (**46 - 50**). However, the PXRD analysis of the materials synthesised reveals that all become amorphous upon removal from mother liquor / drying. It is a property observed in all materials discussed in this thesis, regardless of the calixarene-based di-topic linker used, or the structural features exhibited in the solid state by these supramolecular assemblies.

The common denominator in all materials discussed so far is the absence of a 3-D connectivity which is observed in MOFs, as highlighted in Chapter 1. Given the loss of crystallinity upon drying in all synthesised materials, it became apparent that the non-covalent interactions in which solvent molecules participate, significantly contribute towards the overall solid-state stability in the supramolecular structures formed, as one might expect. It became evident that by increasing the connectivity in the solid state between formed CPs, it may be possible to improve the stability of synthesised materials to de-solvation. This has led to a search for new strategies that would enable synthesis of 3-D CPs. A substantial number of reported MOFs syntheses employ solvothermal reaction conditions.[17] Given this, and that this method often results in high reaction yields, it was decided to explore solvothermal synthesis as a strategy to construct of 3-D CPs with *p*CO_2[4]s.

6.1. Synthesis of a 3-D coordination polymer

During the investigation into the impact of phen derivatives on assembly it was found that reactions of TM(II) ions (Ni and Co) with di-*p*-CO_2[4] **16b** and 2-me-phen result in formation of linear CPs **24** and **25**. However, reaction of Cd(II) with di-*p*-CO_2[4] **16b** and t-me-phen results in a markedly different structure. Following synthesis, slow evaporation over a period of several weeks afforded crystalline material of formula [Cd_4(**16b**)$_4$(t-me-phen)$_4$]·5dmf (**51**).[88] The colourless single crystals of **51** are in a monoclinic cell and the crystal structure was solved in space group $P2_1$. The unit cell parameters are a = 19.5995(9) Å, b = 28.7424(12) and c = 20.4414(9) Å, and β = 91.627(3)º. The solution of the crystal structure reveals formation of a complex 3-D CP based on a binuclear Cd(II) SBU (Figure 6.1A). The asymmetric unit contains four Cd(II) ions, four di-*p*-CO_2[4]s **16b**, four t-me-phens and five dmf of crystallisation (Fig 6.1B). Within the asymmetric unit there are two SBUs, each comprising two Cd(II) ions (Cd(4) and Cd(2), and Cd(1) and Cd(3) respectively), four carboxylate moieties (one from each of the four symmetry unique di-*p*-CO_2[4]s **16b)** and two t-me-phen. Structural analysis reveals that each di-*p*-CO_2[4] **16b** acts as a linker between two SBUs.

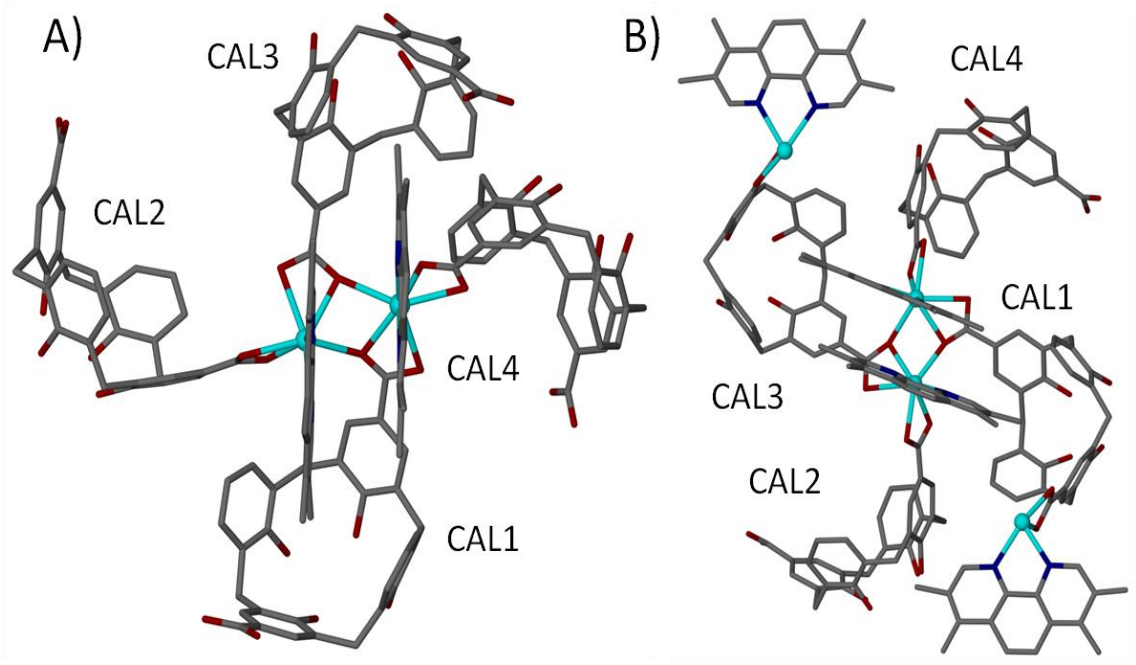

Figure 6.1 (A) Ball and stick representation of the SBU formed in **51**. (B) View of the asymmetric unit formed in **51**. Calixarene alkyl chains, dmf of crystallisation and all hydrogen atoms are omitted for clarity.

In the first SBU comprising Cd(4) and Cd(2) there are two carboxylate groups coordinated as bridging ligands: the O(7)-C(30)-O(8) group (CAL1) is coordinated to Cd(2) in a bidentate fashion and to Cd(4) *via* O(7) with respective bond lengths of 2.36(2), 2.50(2) Å and 2.42(3) Å, while the O(27)-C(130)-O(28) group (CAL3) is coordinated in a bidentate fashion to Cd(4) and to Cd(2) *via* O(27) with respective bond lengths of 2.38(2), 2.52(2) and 2.35(2) Å. The remaining two carboxylates that are forming the SBU are bonded in a bidentate fashion: the O(15)-C(69)-O(16) group (CAL2) is coordinated to Cd(2) with respective bond lengths of 2.41(2) and 2.33(2) Å, while the O(35)-C(159)-O(36) group (CAL4) is bonded to Cd(4) with respective bond lengths of 2.22(2) and 2.48(2) Å. The second SBU comprising Cd(1) and Cd(3) contains the remaining four carboxylate groups. The O(5)-C(29)-O(6) group (CAL1) is coordinated to Cd(1) and the O(25)-C(129)-O(26) group (CAL3) to Cd(3), both in a bidentate fashion, with respective bond lengths of 2.251(17), 2.44(2), 2.41(2) and 2.28(2)Å. The O(17)-C(70)-O(18) group (CAL2) is coordinated as a bridging ligand to s.e. Cd(1)' in a bidentate fashion and to s.e. Cd(3)' *via* O(17) with respective bond lengths of 2.318(19), 2.51(3) and 2.47(2) Å, while the O(37)-C(160)-O(38) group (CAL4) is bonded to a s.e. Cd(3)' (bidentate fashion) and to s.e. Cd(1)' *via* O(37) with respective bond lengths of 2.37(2), 2.464(19) and 2.36(2) Å. As expected the t-me-phens are coordinated to Cd(II) ions in a chelating fashion, restricting space around the metal centres, with Cd(1)-N(2), Cd(1)-N(2), Cd(2)-N(3), Cd(2)-N(4), Cd(3)-N(5), Cd(3)-N(6), Cd(4)-N(7) and Cd(4)-N(8) bond lengths of 2.36(3), 2.37(2), 2.35(2), 2.26(2), 2.32(2), 2.29(3), 2.34(3) and 2.36(3) Å respectively. All four di-*p*-CO_2[4]s adopt a partially pinched-cone conformation. In CAL1 the distances between diametrical arene *para* carbon atom pairs are 7.72 and 8.26 Å respectively. In CAL2, CAL3 and CAL4 these distances are 7.63 and 8.58, 7.63 and 8.60, and 7.65 and 8.37 Å respectively. In all four di-*p*-CO_2[4]s these parameters differ to those observed in di-*p*-CO_2[4]s in **17** - **25**, in which these distances range from 7.1 - 7.4 Å and 9.0 - 9.5 Å. In CAL1 angles ε and δ are measured to be 91.7° and 99.6° respectively. In CAL2, CAL3 and CAL4 angles ε and δ are 92.1° and 103.6°, 92.0° and 105.3°, and 92.8° and 101.3° respectively. For all four di-*p*-CO_2[4]s angles ε and δ are different to those observed in **17** - **25**, in which angle ε ranges from 87 - 89º and δ ranges from 108 - 118º. Structural analysis reveals that the cavity in all four di-*p*-CO_2[4]s is occupied by a t-me-phen methyl group located at 3-position and that all three methyl hydrogen form CH···π interactions with di-*p*-CO_2[4] aromatic rings (Fig. 6.2).

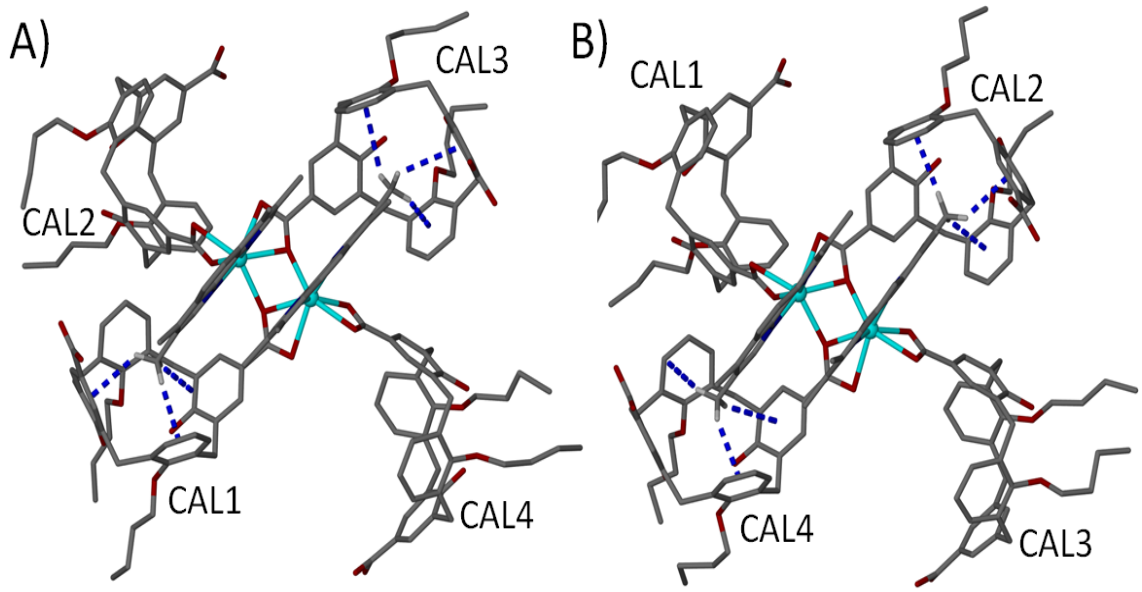

Figure 6.2 Views of the host-guest CH···π interactions (blue dashed lines) between the methyl group of t-me-phen and the di-*p*-CO_2[4] aromatic rings in (A) CAL1 and CAL2 and (B) CAL3 and CAL4. Hydrogen atoms except those of t-me-phen methyl groups are omitted for clarity.

In CAL1 this distance ranges from 2.86 - 2.95 Å, in CAL2 from 2.79 - 2.87 Å, in CAL3 from 2.73 - 3.08 Å and in CAL4 from 2.72 - 2.96 Å respectively. Further analysis of **51** shows that the pair of t-me-phens in each SBU is suitably positioned to facilitate π-stacking as shown in Figure 6.3. The closest contact distance between each pair of t-me-phens coordinated to Cd(1) and s.e. Cd(2)', and the pair bonded to Cd(3) and Cd(4) is 3.34 Å and 3.32 Å respectively. Analysis of the extended structure shows that each SBU is connected with four neighbouring SBUs through di-*p*-CO_2[4]s. As a result of such connectivity formation of a 3-D complex CP that conforms to adamantoid topology is observed, as shown schematically in Figure 6.4.

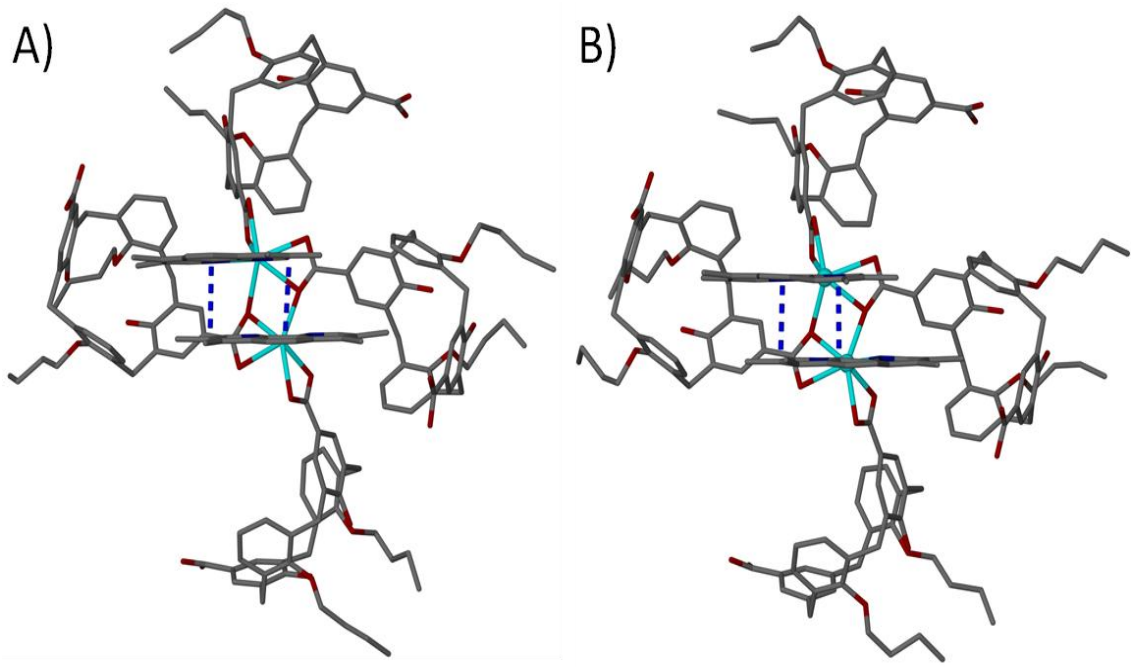

Figure 6.3 Section of the extended structure in **51** showing π-stacking between phens in both SBUs found in the asymmetric unit (blue dashed lines). All hydrogen atoms omitted for clarity.

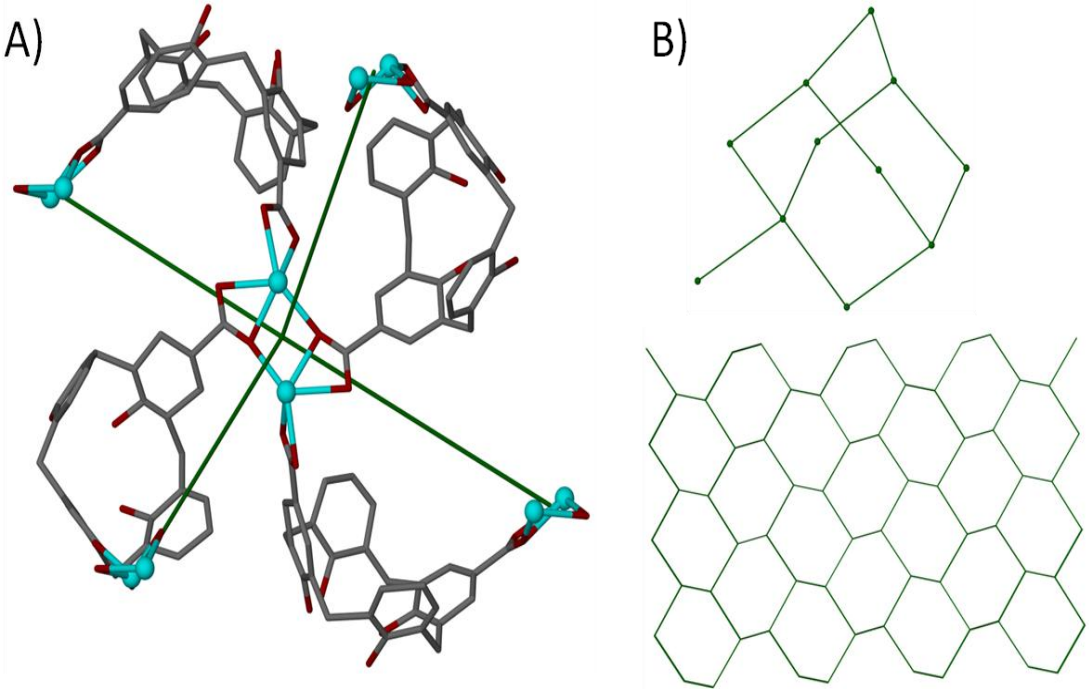

Figure 6.4 (A) The connectivity between neighbouring SBUs found in **51** (green line). (B) Adamantoid topology observed in **51**. Calixarene alkyl chains and all hydrogen atoms are omitted for clarity.

Inspection of the solid-state packing in **51** shows that there are solvent channels filled with dmf of crystallisation running along all three axes of the unit cell. Due to the interwoven nature of these channels, in order to better illustrate them, Mercury was used to calculate solvent accessible voids by removing dmf of crystallisation from the structure, as shown in Figure 6.5.[89] Unfortunately, attempts to isolate a homogeneous product were unsuccessful, making **51** unsuitable for subsequent sorption analysis.

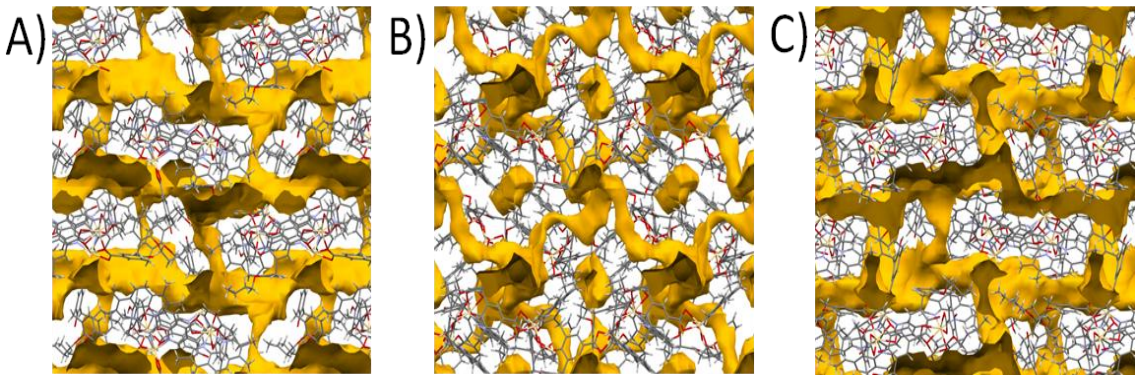

Figure 6.5 Solvent accessible voids in **51** generated using Mercury software along (A) *a* axis, (B) *b* axis and (C) *c* axis of the unit cell. Dmf of crystallisation removed for clarity.

In Chapter 3 it was shown that linear 1-D CPs (**18** and **19**) can be synthesised by reacting Cd(II) ions with di-*p*-CO_2[4]s **16a - b** and phen. The use of t-me-phen instead of phen to react with Cd(II) and di-*p*-CO_2[4] **16b** affords a material which possesses an increased connectivity between components in the solid-state (**51**). Analysis reveals that the synthesised material is a complex 3-D CP based on a binuclear SBU in which di-*p*-CO_2[4] acts as a di-topic linker. Unfortunately, due to inhomogeneity of the product it was not possible to study the stability of the material to de-solvation. Attempts to synthesise 3-D CPs using different TM(II) ions (Co, Ni, Cu and Zn) and di-*p*-CO_2[4]s did not yield crystalline material suitable for crystallographic analysis. As a result of this there is no evidence which would prove that the 3-D connectivity in the solid state in **51** improves the stability to de-solvation, an issue frequently observed in materials composed of di-*p*-CO_2[4]s or *alt*-di-*p*-CO_2[4]s that possess solvent channels. Nevertheless, solid-state structural features in **51** show that di-*p*-carboxylatocalix[4]arenes can be used to synthesise 3-D CPs.

6.2. Solvothermal synthesis of 3-D coordination polymers

Given that the synthetic strategy used to synthesise **17 - 25** and **30 - 51** afforded a 3-D CP in just one case (**51**), a search for a different approach that would enable construction of 3-D CPs using *p*-CO_2[4]s was undertaken. In **51** the synthesised material is composed of binuclear TM(II) SBUs and di-topic linkers (di-*p*-CO_2[4]s). These are structural features that often play a pivotal role when synthesising MOFs, further suggesting that *p*-CO_2[4]s can be potentially utilised to construct 3-D structures. This has led onto the exploration of solvothermal synthesis as a strategy enabling utilisation of di-*p*-carboxylatocalix[4]arenes to construct 3-D CPs.

As a starting point Cd(II) and Zn(II) ions were chosen as TMs that would aid the formation of SBUs. The choice of these two TM(II) ions was dictated by the structural features observed in **51** (Cd) and an abundance of MOF literature utilising Zn(II) ions.[20] Since di-*p*-CO_2[4] was successfully used to construct a 3-D CP (**51**), it was chosen as a candidate for the di-topic linker in this study. Given the shape and the composition of the SBU formed in **51**, phen-based co-ligands were also considered in the synthetic approach. As part of the ongoing study of the role and impact of phen-based co-ligands on the assembly, a series of reactions using only TM(II) ions and di-*p*-CO_2[4] were also carried out as a benchmark. In the course of the investigation the library of studied calixarenes was expanded to *alt*-di-*p*-CO_2[4]s.

One of the challenges in this part of the investigation was to optimise the reaction conditions, such as solvent, concentration, reaction temperature and cooling rate of the reaction mixture / vessel. Despite multiple efforts, none of the benchmark solvothermal reactions yielded crystalline product in which TM(II) ions and di-*p*-CO_2[4]s **16a - b** or *alt*-di-*p*-CO_2[4]s **29a - b** were reacted in the absence of a phen-based co-ligand. Syntheses using either TM ions, di-*p*-CO_2[4]s **16a - b** and phen-based co-ligands (phen, 2-, 3-me-phen and t-me-phen) also did not afford crystalline product. From the range of reagent combinations and reaction conditions that were studied, amongst reactions in which *alt*-di-*p*-CO_2[4]s **29a - b** were used, crystalline product was formed in only one case. Following a reaction at 120ºC for five days, cooling to room temperature at the rate of 12ºC per hour, crystalline material found to be of formula [Cd(**29a**)(phen)]·$(dmf)_2(H_2O)$ (**52**) formed.[88] The colourless single crystals of **52** are in a tetragonal cell and the crystal structure was solved in space group $P4_32_12$. The unit

cell parameters are $a = b$ =15.8642(4) Å and c = 42.9758(15) Å. The asymmetric unit contains one Cd(II) ion, one *alt*-di-*p*-CO_2[4]s **29a**, one phen, two dmf and one water of crystallisation (Fig 6.6A). The dmf and water of crystallisation were highly disordered and so were removed via the routine SQUEEZE.[74] The solution of the crystal structure reveals formation of a complex 3-D CP based on a binuclear Cd(II) SBU (Fig. 6.6B), similar to that found in **51**. Symmetry extension of the asymmetric unit reveals formation of a SBU comprising two Cd(II) ions, four carboxylate moieties and two phens. Each *alt*-di-*p*-CO_2[4]s **29a** is acting as a linker between two SBUs and the carboxylate group comprising atoms O(5)-C(29)-O(6) is coordinated as a bridging ligand to Cd(1) *via* O(5) and to s.e. Cd(1)' *via* O(6) with respective bond lengths of 2.270(10) and 2.195(11) Å. The second carboxylate group comprising atoms O(7)-C(30)-O(8) is coordinated in a bidentate fashion to the metal centre with respective bond lengths of 2.360(9) and 2.353(9) Å. As expected phen is coordinated to Cd(1) in a chelating fashion, restricting space around the metal centre, with Cd(1)-N(2) and Cd(1)-N(2) bond lengths of 2.317(19) and 2.350(14) Å respectively. The *alt*-di-*p*-CO_2[4] **29a** adopts a partially pinched-cone conformation. The distances between diametrical arene *para* carbon atom pairs are 7.71 and 8.43 Å and the angles ε and δ were found to be 93.0° and 101.9° respectively. These parameters are in good agreement with those observed in *alt*-di-*p*-CO_2[4] containing structures and similar to those of **51**.

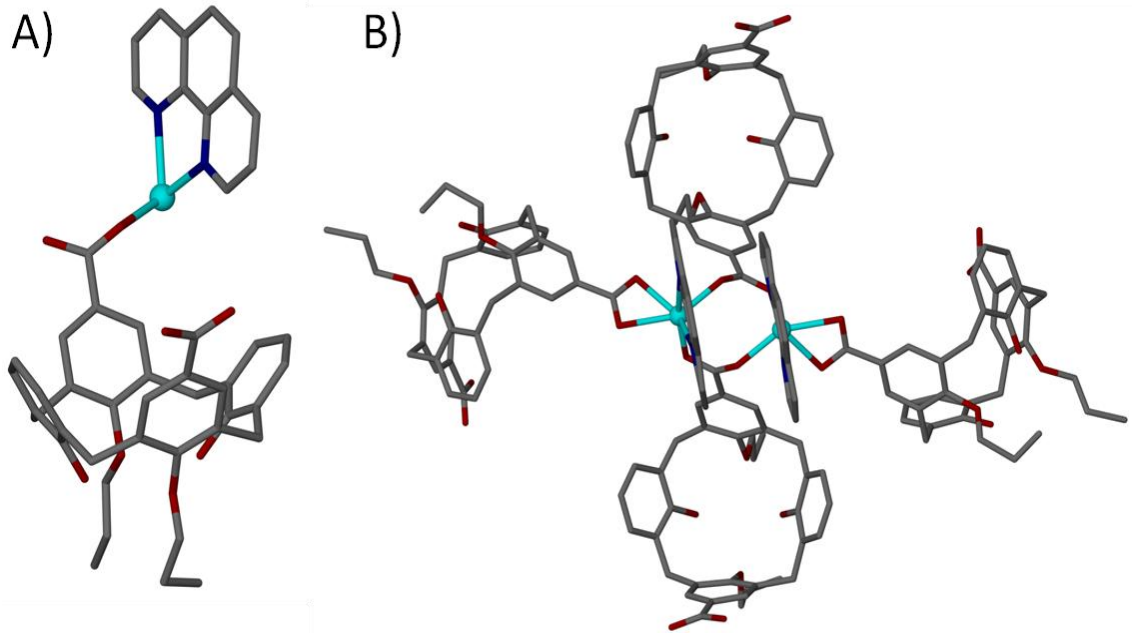

Figure 6.6 (A) Ball and stick representation of the asymmetric unit found in **52**. (B) View of the SBU formed in **52**. All hydrogen atoms omitted for clarity.

Structural analysis of **52** reveals that the cavity in *alt*-di-*p*-CO_2[4] is occupied by a disordered dmf of crystallisation, a feature different to that found in **51**, in which the interior of the calixarene is occupied by a methyl group of t-me-phen. Further analysis of **52** shows that the pair of phens in the SBU are suitably positioned to facilitate π-stacking, as shown in Figure 6.7. The closest contact distance between the pair of phens coordinated to Cd(1) and s.e. Cd(1)' is 3.44 Å. In **52** each SBU is linked to four others through the *alt*-di-*p*-CO_2[4]s, a structural feature observed in **51**. However, structural analysis shows a difference in the orientation of the calixarenes around the Cd(II) centres to that found in **51**. As a result there is a change of direction in which the carboxylate moieties are pointing, influencing the assembly of the 3D system, which is found to have a distorted adamantoid topology (Fig 6.8). Inspection of the solid-state packing in **52** shows that there are solvent channels filled with disordered dmf of crystallisation and water running along all three axes of the unit cell. Due to the interwoven nature of these channels, in order to better illustrate them, Mercury software was used to calculate solvent accessible voids by removing solvent molecules, as shown in Figure 6.9.[89]

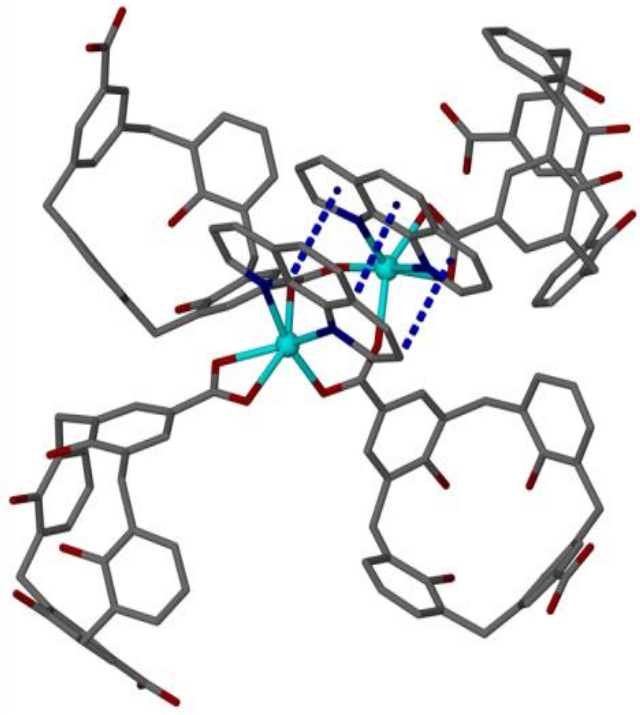

Figure 6.7 Section of the extended structure in **52** showing π-stacking between phens (blue dashed lines). Calixarene alkyl chains and hydrogen atoms omitted for clarity.

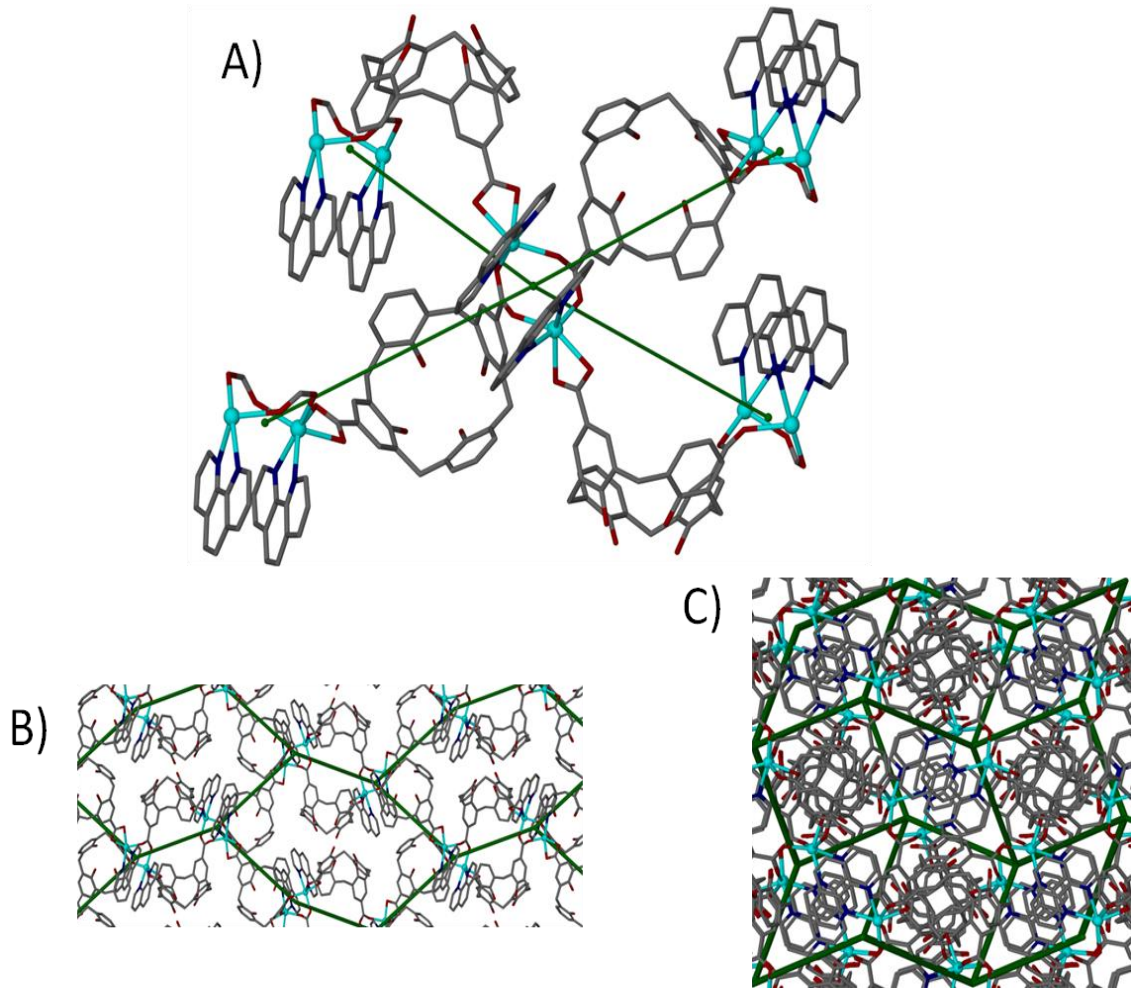

Figure 6.8 (A) The connectivity between neighbouring SBUs found in **52** (green line). (B) and(C) the distorted adamontoid topology observed in **52**. Calixarene alkyl chains and all hydrogen atoms are omitted for clarity.

The absence of methyl substituents on the phen-based co-ligand frees up the *alt*-di-*p*-CO_2[4] cavities, thereby increasing the overall of size of the solvent channels running through the crystal. These calculations revealed that in **51** solvent accessible voids occupy 25% of the volume of the unit cell volume, whereas in **52** they occupy 30%. Unfortunately, as in case of **51**, attempts to isolate a homogeneous product turned out unsuccessful, making **52** unsuitable for PXRD and subsequent sorption analysis.

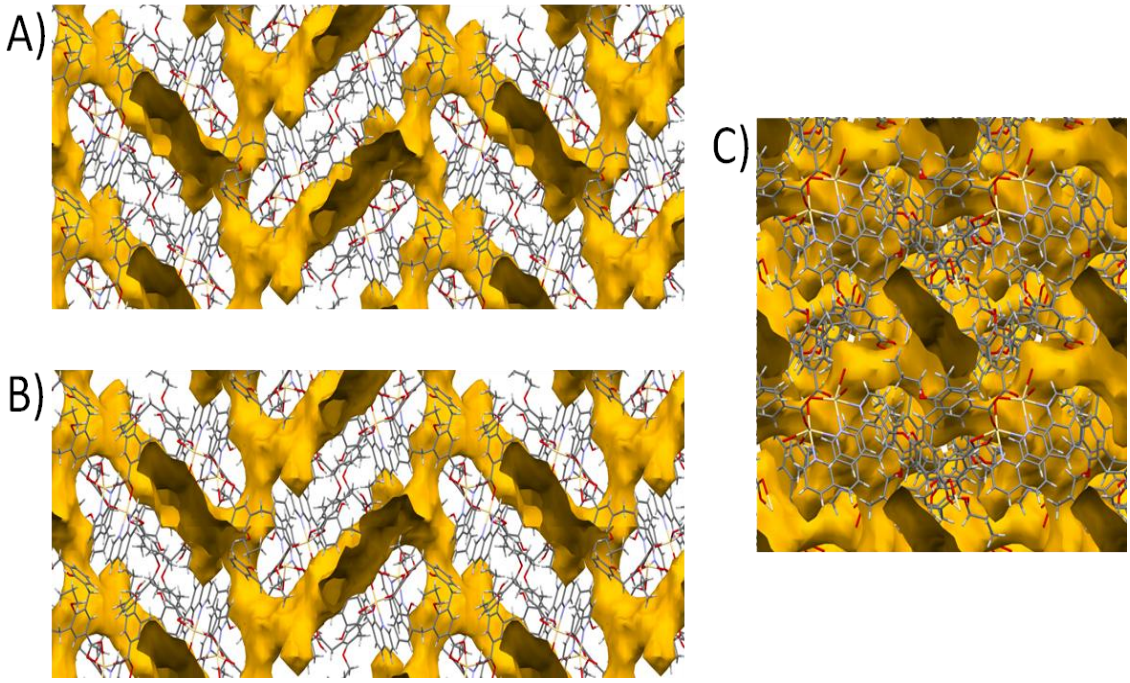

Figure 6.9 Solvent accessible voids in **52** generated using Mercury software along (A) *a* axis, (B) *b* axis and (C) *c* axis of the unit cell. Dmf of crystallisation removed for clarity.

The investigation exploring solvothermal reaction conditions as a method allowing for the synthesis of 3-D CPs did not provide enough evidence to arrive with unambiguous conclusions. None of the benchmark syntheses that were carried out afforded crystalline product, thus suggesting that the presence of a phen-based co-ligand may play an important role in the assembly and subsequent formation of a crystalline product. Attempts to synthesise a 3-D CP based on the binuclear TM(II) SBU using di-*p*-CO_2[4]s **16a - b** were unsuccessful. Interestingly, reaction of Cd(II) ions with *alt*-di-*p*-CO_2[4] **29a** and phen affords a 3-D CP based on binuclear TM(II) SBU (**52**), similar to that found in **51**. Structural analysis of **52** reveals that the use of unsubstituted phen results in *alt*-di-*p*-CO_2[4] cavity being freed up, increasing the overall size of the solvent channels within the crystal. Despite the 3-D connectivity present in the synthesised material, due to inhomogeneity of the reaction mixture, it was not possible to verify whether such connectivity improves the stability of the formed product to de-solvation.

6.3. Summary

In previous chapters it was shown that with the use of di-*p*-CO_2[4]s **16a - b** and *alt*-di-*p*-CO_2[4] **29a - b** it is possible to construct 1-D CPs and discrete MOCCs. However, all synthesised materials are exhibiting instability to removal from mother liquor / de-solvation. In order to overcome this obstacle an increase in the connectivity within the synthesised material was considered as a potential strategy that would improve this property. It was found that when reacting Cd(II) ions with di-*p*-CO_2[4] **16b** and t-me-phen formation of a material composed of complex 3-D CPs based on binuclear Cd(II) SBUs with di-*p*-CO_2[4] acting as di-topic linker is observed (**51**). As a result of such connectivity the formed 3-D complex CP conforms to an adamantoid topology. It is a significant increase in the connectivity compared to **18** and **19** which are synthesised using Cd(II), di-*p*-CO_2[4] **16a - b** and phen, and are constructed from 1-D CPs. Structural analysis shows that **51** possesses solvent channels running along all three axes of the unit cell, a desired feature when designing materials for potential application in gas storage. Unfortunately, due to inhomogeneity of the product it was not possible to study the stability of the material to de-solvation and carry out sorption analysis.

Solvothermal reaction conditions were explored as a synthetic method in the quest to improve the stability of the resulting material towards de-solvation. However, this investigation has not yet provided enough evidence to support this strategy as reliable method enabling synthesis of 3-D CPs. None of the solvothermal reactions in which di-*p*-CO_2[4]s **16a - b** were used afforded material suitable for crystallographic analysis. The investigation of the use of *alt*-di-*p*-CO_2[4] **29a - b** as a di-topic linker for construction of 3-D CPs afforded one result (**52**). The synthesised material was found to be a complex 3-D CP based on binuclear Cd(II) SBU, similar to that found in **51**. Due to the use of unsubstituted phen as a co-ligand to synthesise **52**, the *alt*-di-*p*-CO_2[4] cavity is no longer occupied by a methyl group, but instead by a dmf of crystallisation. Structural analysis reveals presence of solvent channels running along all three axes of the unit cell. Unfortunately, due to inhomogeneity of the reaction mixture, it was not possible to verify whether 3-D connectivity improves the stability of the formed product to removal from mother liquor / de-solvation.

Despite being unable to verify the stability to de-solvation or carry out sorption analysis of **51** and **52**, obtained results show that it is possible to synthesise 3-D CPs using di-*p*-carboxylatocalix[4]arenes as a di-topic linker. Binuclear SBUs are formed in both materials, a desired structural feature commonly present in MOFs. Furthermore, in both **51** and **52** there are solvent channels running through the crystal. This suggests that when utilising di-*p*-carboxylatocalix[4]arenes as building blocks for construction of 3-D structures, the resulting assemblies, given that they are stable to de-solvation, may possess promising structural features highly desired when synthesising materials for potential gas storage.

6.4. Experimental

General experimental procedures and specifications of analytical instruments used are provided in Chapter 8. The synthesis of di-*p*-CO_2[4] **16b** and *alt*-di-*p*-CO_2[4] **29a** is described in Chapter 3 and 4 respectively.

6.4.1. Synthesis of compounds 51and 52

Synthesis of 51: A mixture of **16b** (31.3 mg, 0.05 mmol) and $Cd(NO_3)_2.6H_2O$ (29.6 mg, 0.125 mmol) was dissolved in 2 mL of dmf, followed by layering of 1 ml of a MeOH solution of 3,4,7,8-tetra-methyl-1,10-phenanthroline (11.8 mg, 0.05 mmol). Slow evaporation over several weeks resulted in the formation of colorless crystals suitable for X-ray diffraction studies, which were filtered washed and dried to afford 3.1 mg of solid (6% yield). **EA** calc for $C_{231}H_{251}N_{13}O_{37}Cd_4$, C, 65.27; H 5.95; N, 4.28%. Found C, 66.28; H, 5.70, N, 3.49%. **IR** ν_{max} 3116 cm^{-1} (OH), 2952 cm^{-1} (C-H), 1649 cm^{-1} (C=O), 1617 cm^{-1} (C-O), 1537 cm^{-1} (C-C), 1380 cm^{-1} (C-H), 718 cm^{-1} (C-H). Due to inhomogeneity of the product PXRD experiments were not carried out. Discrepancy between theoretical and experimental results of elemental analysis suggest solvent loss from the material upon removal from mother liquor / drying.

Synthesis of 52: A mixture of **29a** (30.0 mg, 0.05 mmol) and $Cd(NO_3)_2.6H_2O$ (29.6 mg, 0.125 mmol) was dissolved in 2 mL of dmf, followed by addition of 1 ml of a dmf solution of 1,10-phenanthroline (9.0 mg, 0.05 mmol). Solvothermal reaction at 120ºC for five afforded colorless crystals suitable for X-ray diffraction studies, which were filtered washed and dried to afford 4.1 mg of solid (7% yield). **EA** calc for

$C_{57}H_{65}N_5O_{12}Cd_1$, C, 60.88; H 5.83; N, 6.23%. Found C, 62.53; H, 5.31, N, 4.47%. **IR** ν_{max} 3140 cm^{-1} (OH), 2939 cm^{-1} (C-H), 1657 cm^{-1} (C=O), 1630 cm^{-1} (C-O), 1527 cm^{-1} (C-C), 1380 cm^{-1} (C-H), 723 cm^{-1} (C-H). Due to inhomogeneity of the product PXRD experiments were not carried out. Discrepancy between theoretical and experimental results of elemental analysis suggest solvent loss from the material upon removal from mother liquor / drying.

6.4.2. Crystallographic tables for compounds 51 and 52

Complex number	**51**	**52**
Formula	$C_{231}H_{251}N_{13}O_{37}Cd_4$	$C_{57}H_{65}N_5O_{12}Cd_1$
*M*r	4251.24	1124.58
Crystal system	$P2_1$	$P4_32_12$
Space group	Monoclinic	Tetragonal
T/K	100(2)	100(2)
a /Å	19.5995(9)	15.8642(4)
b /Å	28.7424(12)	15.8642(4)
c /Å	20.4414(9)	42.9758(15)
α / ^{o}	90.00	90.00
β / ^{o}	91.627(3)	90.00
γ /^{o}	90.00	90.00
U /Å^3	11510.7(9)	10815.8(5)
Z	2	8
F(000)	4432	4688
D_c / g cm^{-3}	1.227	1.381
μ / mm^{-1}	0.434	0.471
$2\Theta_{max}$ / ^{o}	42.0	56.6
Data collected	100144	76809
Unique reflections	24417	10325
R_{int}	0.0833	0.0439
Obs data ($I > 2\sigma > (I)$	19001	9279
Parameters	2221	534
Restraints	311	18
R_1 (observed data)	0.1393	0.0687
ωR_2 (all data)	0.2668	0.1804
GooF	1.816	1.051
Max/min residuals [eÅ^3]	1.569 / -0.778	1.635 / -1.222

6.5. References

[1] T. R. Cook, Y.-R. Zheng and P. J. Stang, *Chem. Rev.*, **2012**, *113*, 734.

[2] P. P. Cholewa, C. M. Beavers, S. J. Teat and S. J. Dalgarno, *Cryst. Growth Des.*, **2013**, *13*, 5165.

[3] C. F. Macrae, P. R. Edgington, P. McCabe, E. Pidcock, G. P. Shields, R. Taylor, M. Towler and J. van de Streek, *J. Appl. Cryst.*, **2006**, *39*, 453.

[4] J. L. C. Rowsell and O. M. Yaghi, *Micropor. Mesopor. Mat.*, **2004**, *73*, 3.

[5] A. Spek, *Acta Crystallogr. Sect. D*, **2009**, *65*, 148.

Chapter 7. Summary and outlook

The main objective of this research was to design and develop CPs built from *p*-CO_2[4]s. In order to accomplish this a series of *p*-CO_2[4]s were synthesised as potential building blocks. A series of 1-3D CPs were synthesised through the use of various design strategies. In the course of this investigation it also emerged that these synthetic methods could also be used to assemble metal-organic calixarene capsules.

As a starting point for the rational design of CPs, using TMs as directing centres and *p*-CO_2[4]s as building blocks, two synthetic strategies were chosen based on the synthesis of target metal cluster motifs. The selection criteria for the target motifs were: 1) to provide the directionality in which the assembly could be extended and 2) be easily reproducible for a series of TMs. The first motif investigated was based on a binuclear TM cluster. Attempts to assemble this molecular panel using TM(II) ions (Co, Mn and Cd), mono-*p*-CO_2[4]s (**5a** - **c**) and pyridine were unsuccessful. However, the use of di-topic bipyridines instead of pyridine resulted in formation of 1D CPs (**6** - **11**) containing the target binuclear metal cluster. The orientation of mono-*p*-CO_2[4]s in the molecular panels formed confirmed that this design strategy could be potentially used to assemble CPs with *p*-CO_2[4]s. Selection of the second target motif was driven by an alternative design strategy that was based on the "directional bonding" approach. In order to obtain the desired directionality at the metal centre when coordinating mono-*p*-CO_2[4]s, a chelating co-ligand (1,10-phenanthroline, phen) was utilised in order to restrict the TM coordination sphere. Application of the "directional bonding" approach resulted in formation of the second target motif, a discrete coordination complex (**12** and **13**) constructed from a TM(II) ion (Mn, Cd), mono-*p*-carboxylatocalix[4]arene and phen.

The arrangement of discrete complexes found in **12** suggested that it may be possible to construct a linear CP using di-*p*-CO_2[4] as a di-topic linker and the TM as a node. Using the design strategy based on the "directional bonding" approach linear 1D CPs (**17** - **25**) were constructed from TM(II) ions (Co, Cd, Ni and Cu), di-*p*-CO_2[4]s **16a** -

b and phen. Structural analysis of **17 - 21** revealed that, despite all being linear 1D CPs, subtle differences in the coordination sphere and complementary host-guest interactions can have a profound effect on the final outcome of assembly. This variation in solid-state packing was found to coincide with variation of the guest residing within the calixarene cavity. It was also found that by using various phen derivatives in the synthesis of CPs, through steric hindrance, inclusion of the guest within the interior of the macrocycle could be influenced (**25**). By exploiting di-*O*-alkoxycalix[4]arene C_2 symmetry, *alt*-di-*p*-CO_2[4]s (**29a - b**) were synthesised and used as alternative di-topic building blocks. Using the same design strategy to that used in the synthesis of **17 - 25** spiral 1-D CPs (**30 - 43**) were constructed from TM(II) ions (Co, Ni and Zn), *alt*-di-*p*-CO_2[4]s (**29a - b**) and phen (or phen derivatives). As a result of a different bite angle of carboxylate moieties in *alt*-di-*p*-CO_2[4]s (**29a - b**) relative to that found for di-*p*-CO_2[4s] (**16a - b**), the CPs **30 - 43** were found to be spiral rather than linear (**17 - 25**). This difference has a concomitant effect on the solid-state packing as might be expected. The use of bulky phen derivative (t-me-phen) in the synthesis of spiral 1-D CPs (**40 - 43**) results in the disruption of π-stacking found between phens in **30 - 32**, 2-me-phens in **33 - 38** and 3-me-phens in **39**. Utilising the same reaction procedure, but using Cd(II) and Zn(II) ions (with the exception of **37** and **38**) as metal-directing centres, dimeric MOCCs (**44 - 50**) were constructed. It was found that MOCCs constructed from Cd(II) ions, *alt*-di-*p*-CO_2[4]s (**29a - b**) and phen adopt a tilted shape (**44** and **45**). By changing the metal-directing centre to a Zn(II) ion, formation of head-to-head rather than tilted MOCCs (**46** and **47**) was observed. It was found that the use of bulky phen derivatives in the synthesis of Cd(II)-directed MOCCs results in rearrangements in the coordination sphere which induce changes to the overall shape of the capsules formed and their solid-state packing (**48** and **50**). Unfortunately, linear and spiral 1-D CPs that were isolated as homogenous products exhibit instability to de-solvation, and as such sorption analysis could not be carried out. Similarly, in case of dimeric MOCCs it was found that assemblies in the solid state become amorphous upon removal from mother liquor / de-solvation. Using the same design strategy used to synthesise 1-D CPs and MOCCs, a 3-D CP constructed from Cd(II) ions, di-*p*-CO_2[4s] **16b** and t-me-phen was synthesised (**51**). Despite the material possessing 3-D connectivity, a feature that potentially could improve the stability of the product to de-solvation, attempts to isolate a homogenous product were unsuccessful. As a result sorption analysis was not carried out and this hypothesis has not yet been validated.

Finally, solvothermal reaction conditions were investigated as a potential synthetic strategy for the construction of 3-D CPs with di-*p*-carboxylatocalix[4]arenes. Despite multiple efforts, from the range of reagent combinations and reaction conditions that were studied, a crystalline product was isolated in only one case (**52**). Structural analysis revealed formation of a 3-D CP, however attempts to isolate a homogenous product were unsuccessful and further analysis was not carried out.

Within this thesis a focus was placed on the synthesis of 1-3D CPs constructed using *p*-carboxylatocalix[4]arenes as building blocks. The chosen design strategies have proven to be viable in enabling the construction of a range of different supramolecular assemblies. Although this is the case the issue of product stability towards de-solvation requires further scrutiny. Achieving 3-D connectivity may help in overcoming this obstacle, but as state above this hypothesis is yet to be proven for these systems. Considering that phen or its derivatives used in the synthesis has been shown to heavily influence solid-state packing, future work in this area may focus on the use of alternative co-ligands. Furthermore, solvothermal reaction conditions may also be fully explored for the synthesis of desirable CPs with these calixarene building blocks. Until now, relatively little attention has been paid to the synthesis of supramolecular assemblies constructed from *p*-carboxylatocalix[4]arenes. The results presented here show the enormous potential of these molecules for the construction of many new and interesting supramolecular systems that warrant further investigation.

Chapter 8. General Experimental

All precursors used for the synthesis of *p-tert*-butylcalix[4]arene, the chemical reagents used in subsequent syntheses and all solvents were purchased from Sigma-Aldrich, Acros Organics or Fisher Scientific, and were used as supplied without further purification. Analytical thin layer chromatography was performed on pre-coated silica gel plates (Merck, 60 F_{254}) and column chromatography was performed with silica gel (Merck).

^{1}H NMR and $^{13}C\{^{1}H\}$ NMR spectra were collected on Bruker Avance^{III} 300 or a Bruker Advance^{III} 400. All the chemical shifts are expressed in ppm. Electrospray ionisation mass spectra were recorded on Finnigan (Thermo) LCQ classic ion trap mass spectrometer. Elemental analyses were carried using EAI 440 Elemental Analyser. Infrared spectra were collected on a PerkinElmer Spectrum 100 FT-IR Spectrometer. SCXRD data were collected on a Bruker Apex II operating with graphite monochromated Mo-Kα radiation or a Bruker Apex II operating with a synchrotron radiation. PXRD patters were collected on a Bruker D8 Discover instrument operating with Cu-Kα radiation and analysed using EVA software.

X-Seed 2.0 software was used for crystal structure solution and refinement. All structures were solved by direct methods (SHELXS) and refined using least squares refinement routine (SHELXL). Disordered atoms were modelled by applying restraints and / or constraints on geometrical and displacement parameters. Structures containing severely disorder solvent molecules were treated with routine SQUEEZE.

All pictures of crystal structures were generated using POV-Ray 3.6. Solvent accessible voids and pictures illustrating them were generated using Mercury 3.5.1. Reaction schemes were generated using ChemBioOffice 14.